RESPONSIVE LANTHANIDE COMPLEXES FOR RECOGNITION OF BIO-SPECIES

YIP YUK WANG

Ph.D

The Hong Kong Polytechnic University

2017

The Hong Kong Polytechnic University

Department of Applied Biology and Chemical Technology

Responsive Lanthanide Complexes for Recognition of Bio-species

Yip Yuk Wang

A thesis submitted in partial fulfillment of the requirements for the degree of Doctor of Philosophy

APRIL 2017

Certificate of Originality

I hereby declare that this thesis is my own work and that, to the best of my knowledge and belief, it reproduces no material previously published or written, nor material that has been accepted for the award of any other degree or diploma, except where due acknowledgement has been made in the text.

Signature

Yip Yuk Wang

Name of Student

Abstract

The development of lanthanide complexes for recognition of various prevalent bio-species, including metal cations and anions, has received great attention. Such senors offer some benefits over conventional sensors: their long-lived luminescence enables time-resolved detection and sharp narrow emission line.

The work presented herein is divided into seven chapters, the first of which consists of a review of the general background, coordination properties and photophysical properties of lanthanides, along with a discussion of the classification of sensors, their signal transduction mechanisms and strategies on the designs of responsive lanthanide sensors.

1,4,7,10-tetraazacyclododecane and its derivatives, which are the marcrocyclic metal chelators, are recognized as a promising chelator for formation of highly stable complexes. To aid the development of stable lanthanide probes, a synthesis of a series of marcrocyclic derivatives has been executed and described in Chapter Two.

Chapter Three focuses on the synthesis and evaluation of new water-soluble europium(III) complexes for selective detection of hydrogen sulfide among other inorganic and organic sulphur compounds. In the binding of copper(II) ion, its luminescence is almost completely quenched but is recovered upon addition of hydrogen sulfide. Such alternate addition of copper(II) ion–hydrogen sulfide demonstrates an on–off–on type of luminescence, which allows it to be utilized as a monitoring system.

Chapter Four describes the synthesis and investigation of new reaction-based europium(III) complexes for selective detection of cysteine among other thiol derivatives and amino acids. A range of luminescence and kinetic studies have been performed to evaluate the photophysical properties, pH behavior, kinetic parameters

and confirmation of reaction mechanisms.

A series of europium(III) complexes bearing dipicolylamine as a receptor have been developed for selective detection of Zinc and this is shown in Chapter Five. Detailed luminescence studies have been carried out to investigate their photophycal properties, binding stoichiometry of a binding event and binding constants. In the binding of Zinc, **EuL5** exhibits selective response towards ATP over ADP and AMP and its binding study has also been performed.

Chapter Six presents work on the development of a series of copper(I) responsive probes. Through a series of titrations with various cations, the selectivity of the probes is assessed. Their photophysical studies have also been performed.

Chapter Seven describes the experimental procedures for the synthesis and general experimental procedures.

The complexes described in this dissertation demonstrate great promise in the detection of bio-species of interest.

Acknowledgements

I would like to fully express my gratitude for all of following. Without their support, the work described in thesis would not be possible.

My deepest gratitude goes first and foremost to my supervisor, Prof. Wing-Tak Wong, whose wisdom, guidance, encouragement, support and patience has been greatly valued. I am delighted and lucky to be his student to gain many knowledge regarding research and personal issue.

I grateful acknowledge Dr Ga-Lai Law for her support, guidance and patience. My thanks are also given to the former and current Wong's group members: Dr. Ka-Leung Wong, Dr. Ka-fu Yung, Dr. Chi-Tung Yeung, Dr. Yan-Juan Gu, Dr. Wai-Sum Lo, Dr Wei-wei Jin, Mr. Li-xiong Dai, Dr. Ho-Lun Yeung, Dr. Yuen-On Fung and Mr. Tik-Hung Tsoi and other Wong's group members for their constant help, support and precious advice.

I would like to express my appreciation to the scientific officer and technical staffs of Department of Applied Biology & Chemical Technology for their technical helps and suggestions

A very special thank to my Mum, Dad and girlfriend for their continued love, care, faith and support.

Table of Contents

Abbreviations

A	absorbance
AMP	adenosine monophosphate
ATP	adenosine triphosphate
BET	back energy transfer
br	broad
cm^{-1}	wave number
cyclen	1,4,7,10-tetraazacyclododecane
d	doublet
DCM	dichloromethane
dd	doublet of doublets
DMF	N,N-dimethylformamide
DO3A	1,4,7,10-tetraazacyclododecane-1,4,7,10-tetraacetic acid
DOTA	1,4,7,10-tetraazacyclododecane-1,4,7,10-tetraacetic acid
eqv.	equivalent
ES+	electrospray ionization with positive ion detection
ESI	electrospray ionization
g	gram
HEPES	4-(2-hydroxyethyl)-1-piperazineethanesulphonic acid
HOMO	highest energy occupied molecular orbital
h	hour
Hz	Hertz
IC	internal conversion
IR	Infrared
ISC	intersystem crossing
K	Kelvin
L	litre
Ln(III) ion	Lanthanide(III) ion
LUMO	lowest energy un-occupied molecular orbital
τ	lifetime
M	mol dm^{-3}
MeCN	acetonitrile
ε	molar extinction coefficient
MeOH	methanol
mM	millimolar

mmol	millimole
MS	mass spectrometry
NMR	nuclear magnetic resonance
^{o}C	degree Celsius
PBS	phosphate buffered saline
PET	Photoinduced electron transfer
PPi	Pyrophosphate
ppm	parts per million
q	quartet
Φ	quantum yield
Rf	radio frequency
s	singlet
s	second
t	triplet
TFA	trifluoroacetic acid
THF	tetrahydrofuran
TLC	thin layer chromatography
UV-vis	ultraviolet and visible region

CHAPTER 1

General Introduction

1 Introduction

This chapter will start with an introduction of the lanthanides in general and europium in particular and a discussion on their coordination, absorption and characteristic luminescence properties. Different kinds of sensors with their signal transduction mechanisms and corresponding reaction mechanisms will be briefly introduced. The aims for the work will also be presented.

1.1 Lanthanides

The Lanthanides, known as rare earth elements, comprise fifteen elements ranging from La to Lu with atomic numbers 57 through 71 located in the 4*f* block of the periodic table. Their colourful history started with the discovery of a black mineral yttria by Johann Gadolin in 1794.[1][2] In 1803, a new oxide ("ceria") which consisted of lanthanum, cerium, praseodymium, neodymium, and europium was isolated.[1][2] Later, Henry Moseley revealed by X-ray spectroscopy that there were 15 rare earth elements from lanthanum to lutetium.[1][2] Carl Auer Von Welsbach, an Austrian scientist, first developed a lanthanide based lighting device in 1891[3] and by now lanthanides have ever-increasing use in various research areas, such as luminescent sensing,[4]-[8] material science and [9]-[12] coordination chemistry[13][14], owing to their distinctive physical and chemical properties.

1.1.1 Coordination of lanthanides

In nature, the lanthanides almost exist in their trivalent oxidation state due to their specific electronic configurations and the low electronegativity. Owing to the good shielding provided by 5s and 5p orbitals, 4*f* orbitals contribute little in their bonding. As a result, the bonding in their complexes is exclusively ionic as well as non-directional and hence steric factors play a role in the determination of geometry of Ln(III) complexes. Their coordination number varies depending on the size of the ligands but is

usually between 6 to 12. In the aquo ions $[Ln(H_2O)_n]^{3+}$ this number is 9 for the earlier Ln(III) ions from La(III) ion to Eu(III) ion and 8 for Dy(III) ion to Lu(III) ion. As a hard donor, Ln(III) ions have their high preference to interact with hard Lewis bases (in the order of S< N < O) to form stable Ln(III) complexes. Based on this rationale, various linear and macrocyclic ligands, including linear polyamino carboxylates, macrocyclic analogues, calixarenes, schiff-base ligands have shown great utility for luminescent Ln(III) complexes, in which some pendant arms, such as carboxylates or amides are required to fulfil the coordination number. Their corresponding selective examples are shown below and their binding sites are labelled in bold red. (**Figure 1.1**)[13][15]-[17]

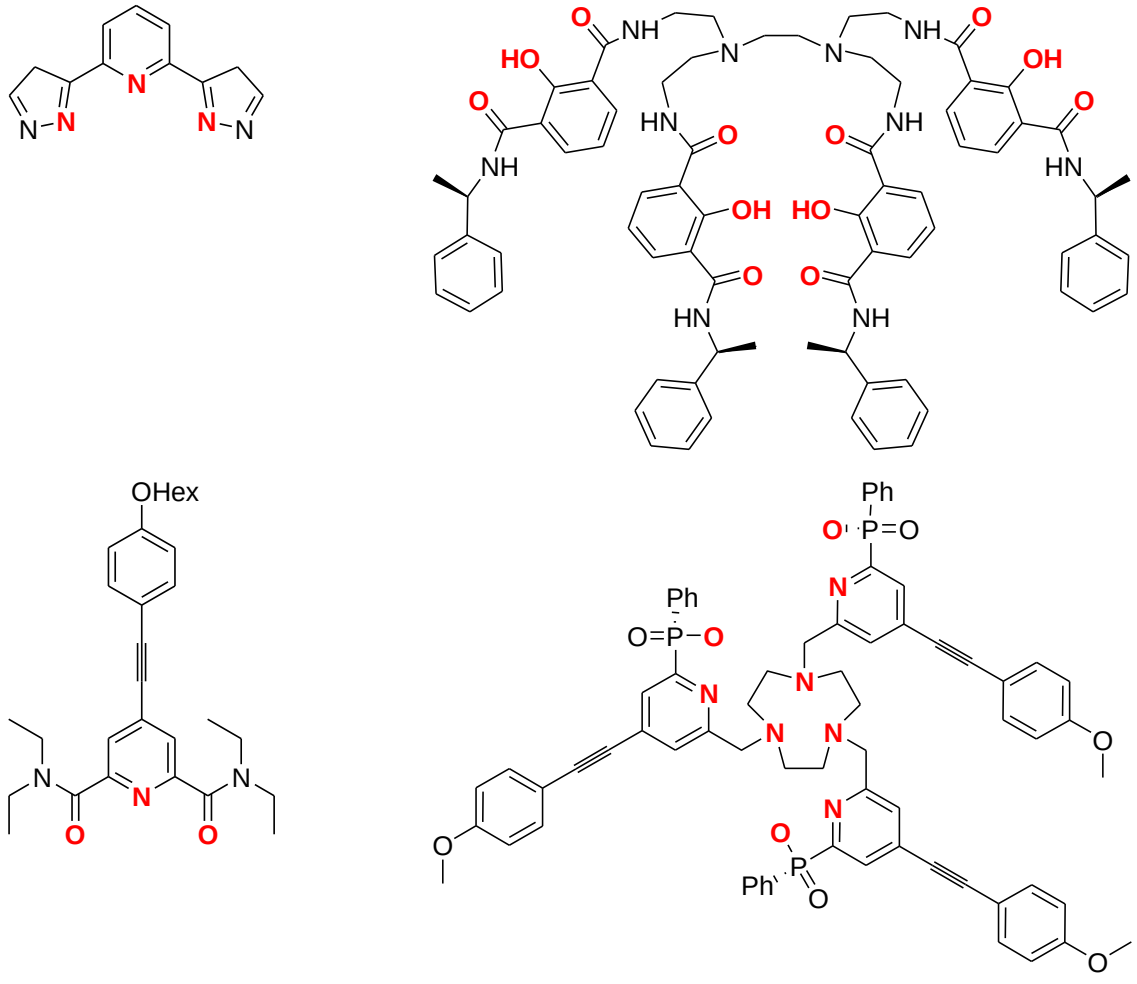

Figure 1.1 Selective examples of multidentate ligands for luminescent Ln(III) complexes.[13][15]-[17]

1.1.2 Absorption properties of the lanthanides

When lanthanides absorb UV or visible light, their absorption spectra display sharp peaks due to intraconfigurational $4f^N$ -$4f^N$ transitions (*f-f* transitions) that are electronic transitions in the 4*f* orbtials. However, not all lanthanides can absorb light, such as Y(III) ion, La(III) ion and Lu(III) ion due to their closed-shell configurations. The rest of the lanthanides have their corresponding characteristic absorption bands in the UV-Visible region.(**Figure 1.2**)[18] Generally speaking, such *f-f* transitions include electric and magnetic dipole. Electric dipole *f-f* transitions are formally 'forbidden' by the parity selection rule in which electronic transitions (e.g. electric-dipole) between energy levels with the same parity are not allowed. Electric dipole *f-f* transitions, therefore, do not obey the parity selection rule owing to the same parity of the initial and final states and transitions while magnetic dipole *f-f* transitions are allowed but have weak oscillator strengths (10^{-7} – 10^{-8}), leading to their very low molar extinction coefficients of Ln(III) ions ($\varepsilon \approx 1 - 10$ L mol^{-1} cm^{-1}).

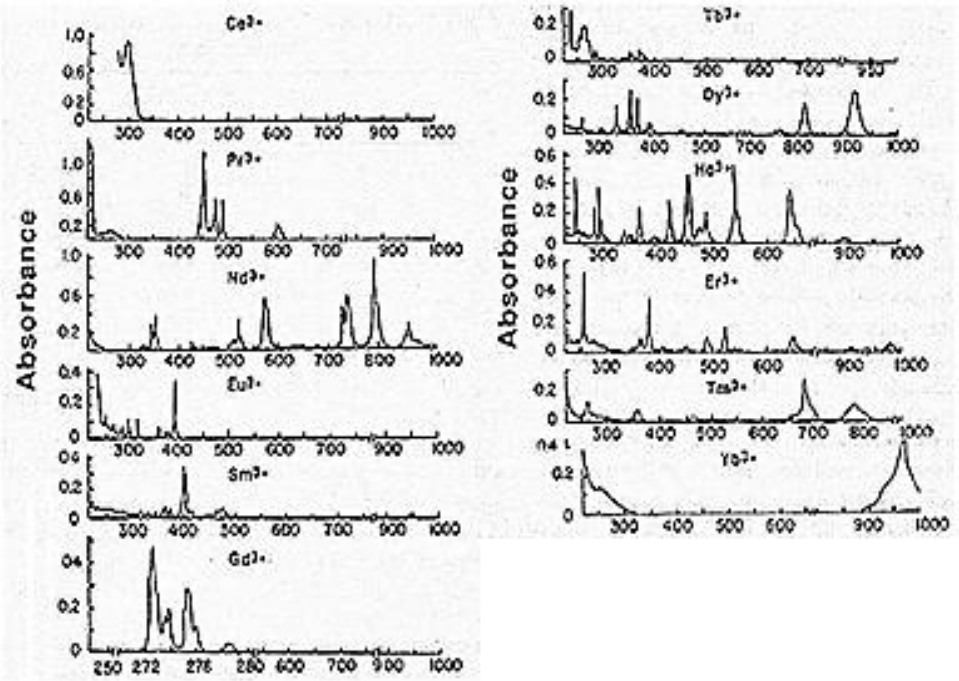

Figure 1.2 Absorption spectroscopy of Ln(III) ions.[18]

1.1.3 Luminescence properties of lanthanides

The luminescence from the Ln(III) ions is normally due to electronic transitions within the 4*f* energy levels of the Ln(III) ions which results in some characteristic narrow absorption and sharp emission bands. The narrow absorption and sharp emission bands are mainly due to the good shielding of the 4*f* orbitals by 5*s* and 5*p* orbitals, which causes the inter-nuclear distance of the molecule at the ground state to be very similar to that at the excited states. Negligible or small Stoke shift results. Since various Ln(III) ions have their own emissive state (**Figure 1.3**),[19] they emit different colors. For instance, Tb (III) ion has $^5D_0$ as its emissive state to emit a green color.

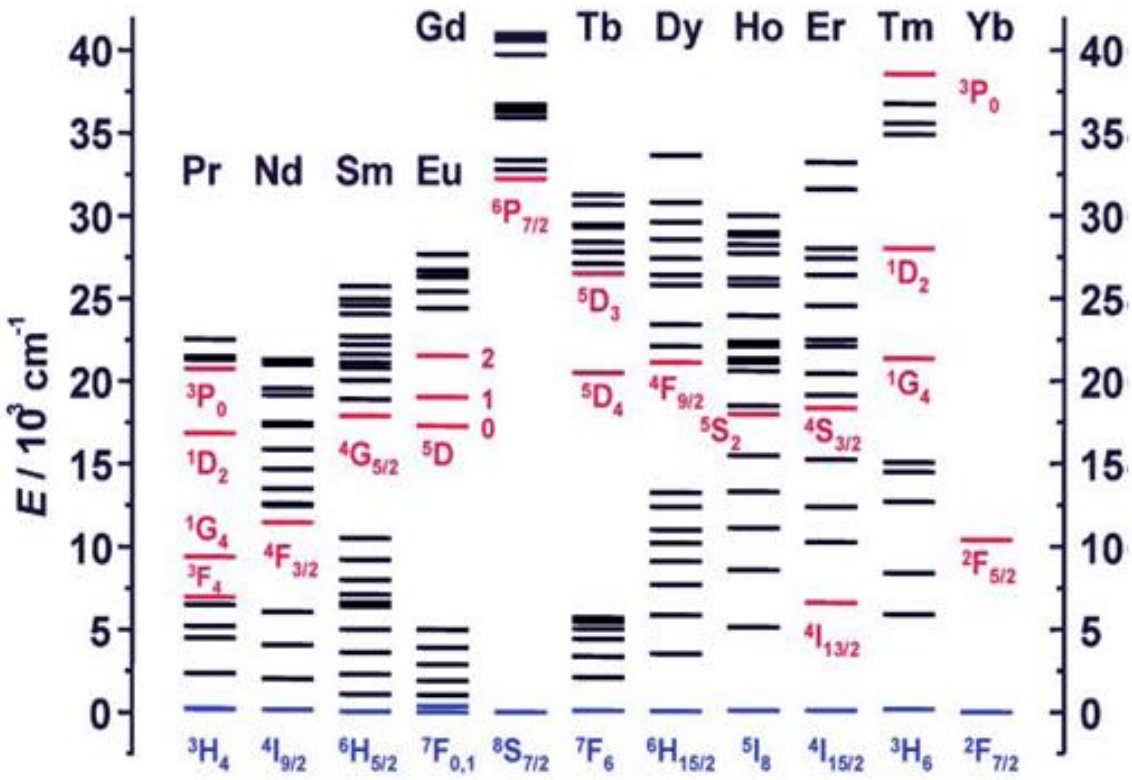

Figure 1.3 Partial energy diagrams for the Ln(III) ions. The main emissive states are in red, while the fundamental levels are in blue.[19]

Unlike d-d transition of transition metal complexes in which parity selection rule is relaxed by ligand field, *f-f* transitions of the Ln(III) ions should theoretically strictly be forbidden by the parity selection rule. For instance, ED transitions are forbidden by parity rules. (Laporte's rule: $\Delta l = \pm 1$) A number of studies regarding to electronic transitions within the 4*f* energy levels have been published.[20][21] Generally, there are three ways for emission of Ln(III) complexes- magnetic dipole (MD) transition, induced (or forced) electric dipole (ED) transition and quadrupolar transition.[22]

MD transitions are Laporte allowed in centrosymmetric and noncentrosymmetric point groups since its magnetic dipole operator has a g (gerade) symmetry and the *f* orbitals has a u symmetry. MD transitions are also not interfered with the environment around Ln(III) ion.[23] (**Table 1.1**)

As opposed to true ED transitions, induced ED transitions are partially allowed by relaxation of parity selection rule by the mixing of opposite parity wavefunctions (mixing between 5*d* orbital into 4*f* orbital). Such induced ED transitions "borrow" some intensity from parity allowed 4f-5d transitions with similar oscillator strength as MD transitions. Thus, induced ED can be seen in the spectra of Ln(III) ions.[24]

Transition	ΔS	ΔL	ΔJ
MD	0	0	0, ± 1, but 0→0 is forbidden
ED	0	≤ 6	$\leq 6$and =2,4,6 if J=0

Table 1.1 Selection rules for intraconfigurational f-f transitions.[25][26]

Even though 4*f* electrons are well shielded from the ligand field and not influenced significantly by coordination environment such as symmetry, some ED transitions appear to demonstrate their particular sensitivity towards their coordination environments,[24] including changes in shifts of peak, intensities of transitions and shape of bands. Judd and Jerrgensen described this phenomenon as hypersensitive transition.**(Table 1.2**)

Transitions	Ln(III) ion
Tb(III) ion	$^5D_4 \rightarrow {}^7F_5$
Eu(III) ion	$^5D_0 \rightarrow {}^7F_2$
Dy(III) ion	$^4F_{9/2} \rightarrow {}^6H_{13/2}$
Pr(III) ion	$^3D_0 \rightarrow {}^7F_2$

Table 1.2 Examples of some hypersensitive Ln(III) ion absorption and emission transition

1.1.4 Luminescence of europium

Emission of europium is in the red region from 577 nm to 840 nm due to electronic transitions (J = 0–6) from $^5D_0$ excited state to J levels of the ground term ^7F_j and its corresponding spectra are informative. Generally, except for $^5D_0 \rightarrow {}^7F_1$ transition, the rest of $^5D_0 \rightarrow {}^7F_j$ transition are ED. $^5D_0 \rightarrow {}^7F_{0,3,5}$ transition is forbidden by selection rule, but they can measured since they "borrow" their intensity from $^5D_0 \rightarrow {}^7F_2$ transition through higher order perturbations by the crystal field.[24][26] The presence of $^5D_0 \rightarrow {}^7F_0$ transition indicates C_n, C_{nv} or C_s symmetry of the coordination environment of Eu(III) ion, but it does not mean the symmetry is not C_n, C_{nv} or C_s in the absence of $^5D_0 \rightarrow {}^7F_0$ transition.[24] $^5D_0 \rightarrow {}^7F_1$ transition is MD and its corresponding intensity is normally independent of the coordination environment of the Eu(III) ion. $^5D_0 \rightarrow {}^7F_2$ transition is a hypersensitive transition and its intensity is affected by the coordination

environment of Eu(III) ion such as the nature of ligands and local symmetry and its intensity is sometimes used as a measure of the asymmetry of Eu(III) ion. For instance, Eu(III) diketonate complexes usually have a intense hypersensitive $^5D_0 \rightarrow {}^7F_2$ transition and some of them are 10 times more intense than $^5D_0 \rightarrow {}^7F_1$ transition. The high intensity can be explained by the low symmetry of Eu(III) ion and high polarizability of diketonate ligands for enhancing its intensity. $^5D_0 \rightarrow {}^7F_3$ transition is a weak transition due to the forbiddance by selection rule. It can be observed owing to the 'borrowed' intensity from $^5D_0 \rightarrow {}^7F_2$. $^5D_0 \rightarrow {}^7F_4$ transition has an intensity that is coordination environment-dependent, but it cannot be said it is hypersensitive. There are many examples that show $^5D_0 \rightarrow {}^7F_4$ transition is weaker than $^5D_0 \rightarrow {}^7F_2$ transition.[26] But if europium complex has D_{4d} symmetry, $^5D_0 \rightarrow {}^7F_4$ transition is more intense than $^5D_0 \rightarrow {}^7F_2$ since $^5D_0 \rightarrow {}^7F_4$ transition is stronger in the absence of a centre of symmetry while $^5D_0 \rightarrow {}^7F_2$ transition is forbidden.$^5D_0 \rightarrow {}^7F_5$ transition and $^5D_0 \rightarrow {}^7F_6$ transition are usually ignored since they are very weak and cannot be detected accurately by detector such as the blue-sensitive PMTs.[26]

1.1.5 Antenna effect

As mentioned in **Section 1.1.2**, Ln(III) ions have low molar absorption extinction coefficients ($\varepsilon \approx 1 - 10$ L mol^{-1} cm^{-1}) to populate excited energy states. Although they can be excited directly by laser or by the use of highly concentrated solutions, such excitation is not practical for application in fields such as biological studies since laser is harmful to cells. To make bright Ln(III) complex, a common way is utilization of a chromophore or sensitiser which works as an 'antenna' to capture light energy and transfer it to Ln(III) ion.(**Figure 1.4**) This antenna effect was first introduced by Weissman. The energy processes in this sensitisation can be described by Jablonski diagram. (**Figure 1.5**)

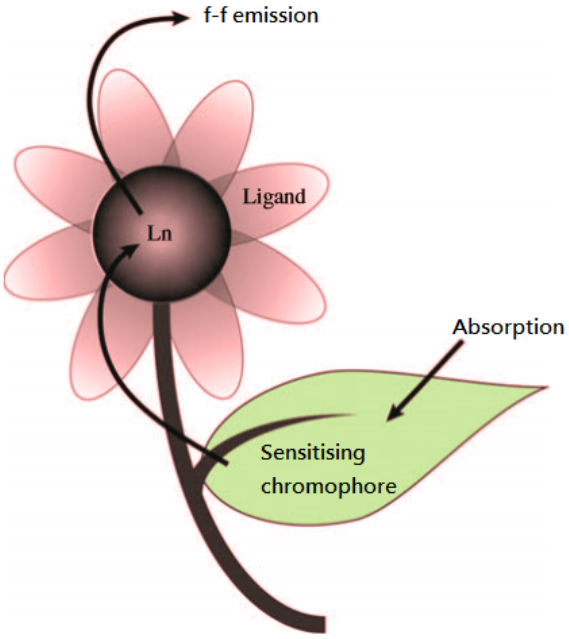

Figure 1.4 Ln(III) complexes can capture light energy using an organic chromophore as a sensitiser.[25]

The antenna effect' is brought about by the first excitation of chromophore from the ground state singlet state S_0 to the excited singlet state S_n by absorption of photon. Then, it undergoes either vibrational relaxation followed by heat releasing or fluorescence or intersystem crossing (ISC) from S_n to its triplet state T_1. Although such ISC is spin-forbidden, it can be relaxed by spin-orbit coupling of a heavy atom such as Ln(III) ion. There are three possible ways for energy transfer from T_1, including back–ISC to S_1, phosphorescence and energy transfer to the lanthanide excited state. According to Latva's empirical rule, the energy gap between T_1 and accepting lanthanide excited state (e.g. $^5D_0$) should be in the range of 2500 – 4000 cm^{-1}.[27] If the energy level of chromophore falls within this range, the energy transfer would be favourable.

Generally, this electronic energy transfer between chromophore and Ln(III) ion can be described by either the Förster[28] or Dexter mechanism. Förster mechanism expresses the energy transfer from a donor (D) to an acceptor (A) through dipole-dipole in which its transfer efficiency is based on how energy matches between A and D

ground and excited states. In **Equation 1**, the rate constant of energy transfer K_{et} is related to the distance between A and D and τ_0 is the lifetime of D in the absence of A. Dexter mechanism expresses that there is energy transfer when electron exchange interaction between A and D occurs at a short distance. In **Equation 2**, the rate constant of energy transfer K_{et} is directly proportional to the distance between D and A.

$$K_{et} = \left(\frac{1}{\tau_0}\right)\left(\frac{R_0}{r}\right)^6 \quad \phi A = \pi r^2 \qquad \textbf{Equation 1}$$

R_0, the critical distance for energy transfer, is defined as the intermolecular separation between donor and acceptor at which K_{et} is the rate of radiative decay

$$R_0 = 8.78(10^{-2})(k^2)(\phi_D)(n^{-4})\mathrm{J} \qquad \textbf{Equation 2}$$

Where k^2 is an orientation factor, ϕ_D is the quantum yield of the donor emission in the absence of A, n is the refractive index of the solvent, J is the spectral overlap integral of the absorption spectrum of the acceptor and the emission spectrum of donor.

$$K_{et} = K(J)exp\left(\frac{-2r}{L}\right)$$

Where K is specific orbital interactions, J is spectral overlap integral, R is the distance between D and A, and L is D-A separation relative to their vander Wasls radii.

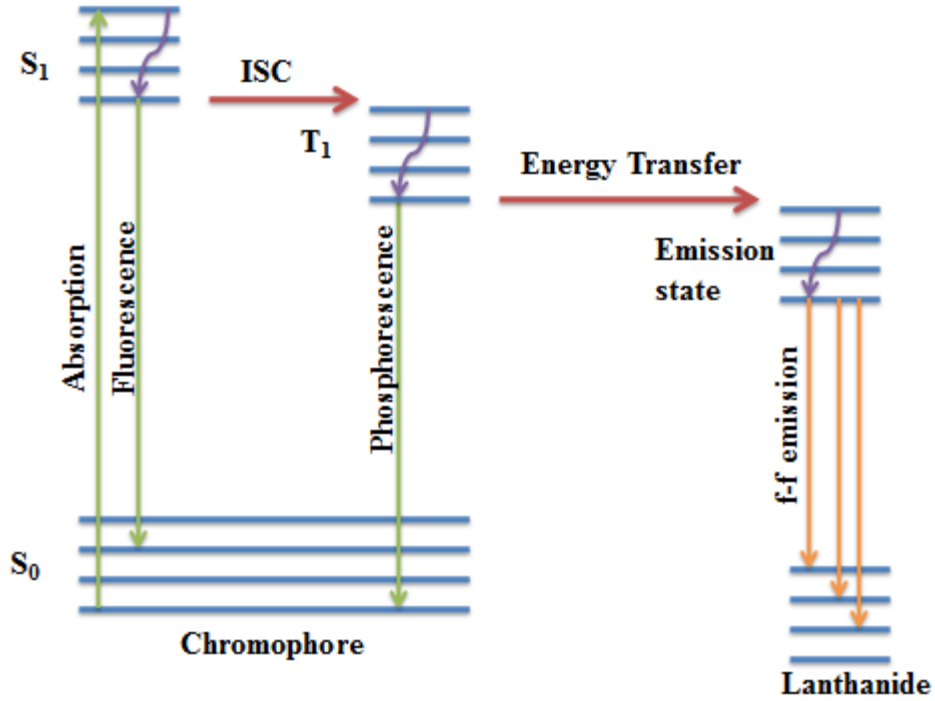

Figure 1.5 Simplified Jablonski diagram depicting the main processes involved in the 'antenna effect'. Wavy lines show vibrational relaxation processes.

1.2 The design of responsive probes

Recognition of biologically and environmentally important species has attracted much attention. Conventional detections are some of the methods such as Flame photometry,[28] atomic absorption spectrometry,[29] ion sensitive electrodes,[30] high performance liquid chromatography,[31] gas chromatography,[32] and inductively coupled plasma mass spectrometry[33] However, most of them require complicated sample pretreatment, sophisticated instruments and high cost. Development of luminescent responsive probes is therefore of great significance due to their advantages in terms of high selectivity, fast response time and good sensitivity.

Generally, there are two approaches for designing responsive probes and they are termed "recognition" and "reactivity". If response towards an analyte is based on recognition, it will be a chemosensor. If response towards an analyte is based on reactivity, it will be a chemodisometer. (**Figure 1.6**) This will be discussed in detailed below.

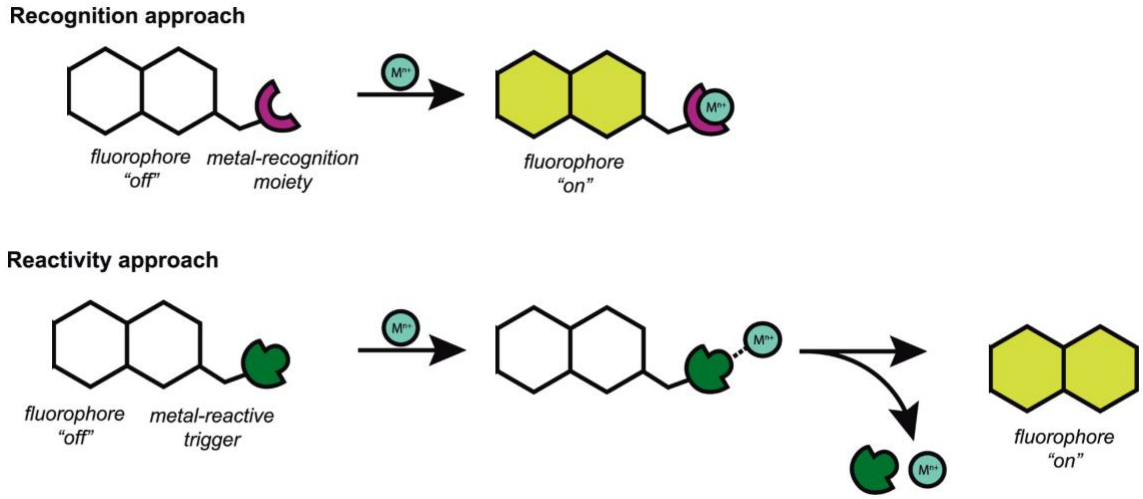

Figure 1.6 Recognition- and reactivity-based approaches for turn on fluorescent responsive probes.[34]

1.2.1 Chemosensor

A chemosensor is a compound that is able to have specific recognition of analyte by invoking changes in one or more of its properties, such as absorption, emission, and redox potential characteristics. In particular, detecting changes in fluorescence is one of effective ways for applications due to the ease in visualization, short response time for detection and high sensitivity.[35]

In general, a chemosensor consists of a receptor and a chromophore linked with or without a spacer.(**Figure 1.7**) A receptor is the recognition moiety and mainly determines the binding selectivity and sensitivity.[35] The specific interactions between receptor and analyts of interest often rely on coordination chemistry, electrostatic interactions hydrogen bonding, metal coordination, hard-soft acid-base theory and hydrophobic interaction. They are often affected by the characteristics of analyts, pH value, solvent environment, and temperature and are reversible. Such reversibility in the case of recognition of metal ions is demonstrated by reversal of the photophysical response by the addition of a strong chelating agent such as EDTA.

The chromophore serves as a signal transducer and converts detection of analyst into photophysical changes such as absorption, emission intensity, fluorescence quantum yield and lifetime. These changes are due to the perturbation of photoinduced processes including charge transfer, energy transfer, electron transfer and formation of excimer. Sometimes, it can participate into the recognition processes of analyte since a receptor can be a chromphore. Therefore, sensing sensitivity and selectivity are dependent on the whole structure of chemosensor and various principles utilized in chemosensors are important in the design of chemosensor.

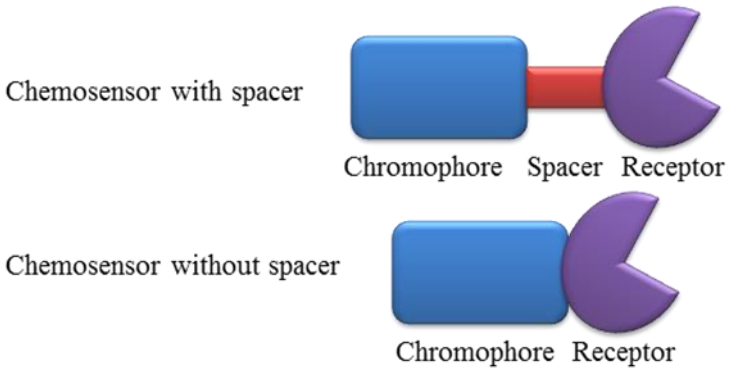

Figure 1.7 Structure of chemosensor.

1.2.2 Signal transduction mechanisms

The mechanism, by which probes recognize analyte, gives an observable signal and is known as signal transduction. Effective luminescent responsive probes can generate such signal upon selective binding to an analyte. It is important to realize how such modulation of signal happens for design of sensors. In general, the mechanisms of luminescent transduction involves manipulation of electron transfer on binding of the analyte by sensors such as photoinduced electron transfer (PET),[38] intramolecular charge transfer (ICT),[39] fluorescence resonance energy transfer (FRET),[40] and excited-state intramolecular proton transfer (ESIPT)[41] and so on.

1.2.2a Photoinduced Electron Transfer (PET) Principle

The first PET probe developed by de Silva et al. in 1985,[41] PET probe have been developed to detect a variety of analytes including anions, cations and molecules. PET sensor has a typical structure which is a receptor and a chromophore linked with a spacer. (**Figure 1.8**) PET describes an electron transfer from the HOMO of a donor (D) in a ground state to the vacancy in the HOMO of the acceptor (A) in an excited state and PET can also occur in the opposite sense: that is, from the donor in an excited state. If the electron transfer is between uncharged species of the same part of the same molecule and which leads to the formation of a radical ion pair, this is called primary electron transfer. If electron transfer is between two uncharged species of two individual components of a molecule, it will form a solvent separated ion radical pair after electron transfer where the distance between the two individual components can be up to 7˚A. The probability of electron transfer in PET is usually determined by an overall free energy of the system ($\triangle G_{ET}$) which can be estimated using the Rehm–Weller equation (below):[43]

$$\Delta G_{ET} = -E_s - E_{red.chromophore} + E_{oxo.receptor} - e^{-2}/(\varepsilon r)$$

where the chromophore is an electron acceptor and the receptor as an electron donor. E_S is the singlet energy of the excited chromophore, $E_{red.chromophore}$ is the reduction potential of the chromophore, and $E_{ox.receptor}$ is the oxidation potential of the receptor. The $e^{-2}/(\varepsilon r)$ term is the coulombic interaction energy between the chromophore and the receptor after an ion radical pair has been formed, which usually has a value of ~0.1 eV in acetonitrile.

Classical PET probes consist of three main parts: a chromophore, a spacer and a receptor. The roles of chromophore and receptor have been discussed before. The spacer is used to separate the chromophore and the receptor and minimizes any π–π* or n–π* interaction in the ground state between them. Generally, the rate of intermolecular PET

is usually of the second order and diffusion-rate-limited. It is usually increased if the chromophore and the receptor are held together at a fixed distance. Without this spacer, the electron transfer would depend on their colliding before this transfer takes place. Such collision will take place with several times before electron transfer occurs and is dependent on their concentration and on the solvent molecules. If their concentration is low, the rate of collision and probability of the electron transfer is decreased. Compared with those PET sensors with a spacer, such system has a low probability of electron transfer.

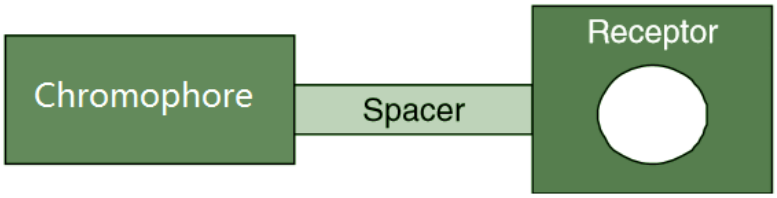

Figure 1.8 Structure of PET based sensor.

The process of PET can be discussed in terms of frontier orbital diagrams. When an electron is excited from its HOMO to its LUMO, the chromophore (C) becomes an excited state (C*). Then, there are three possible ways for PET to proceed. The first case is that if C has its HOMO lying below the HOMO of another ground state of the receptor (here referred to as R), then an electron transfer is energetically favorable to occur from R to C*and this leads to excited state quenching and formation of the radical ion species $C^{\bullet-}R^{\bullet+}$.

The previously excited electron left in LUMO cannot return to the previous HOMO by losing its excited state energy through fluorescence emission. This is called an off state, and is shown in **Figure 1.9**. The electron left in the former LUMO will deactivate by some ways other than fluorescence. For example, it can undergo thermal deactivation through external or internal molecular collisions. Therefore, the probe is not emissive.

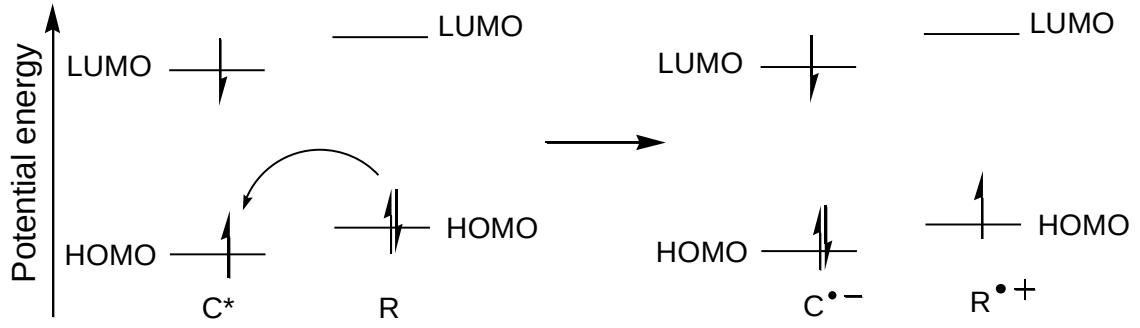

Figure 1.9 The electron transfer process of PET in a two component molecular system as an "off state."

The second case is that if the HOMO of C* lies above the HOMO of R on an energy scale, and the LUMO of C* lies above the LUMO of R, then an electron transfer occurs from the excited state of C of LUMO of C* to the LUMO orbital of R by forming an $C^{\bullet+}R^{\bullet-}$ ionic pair, which is shown in **Figure 1.10**.

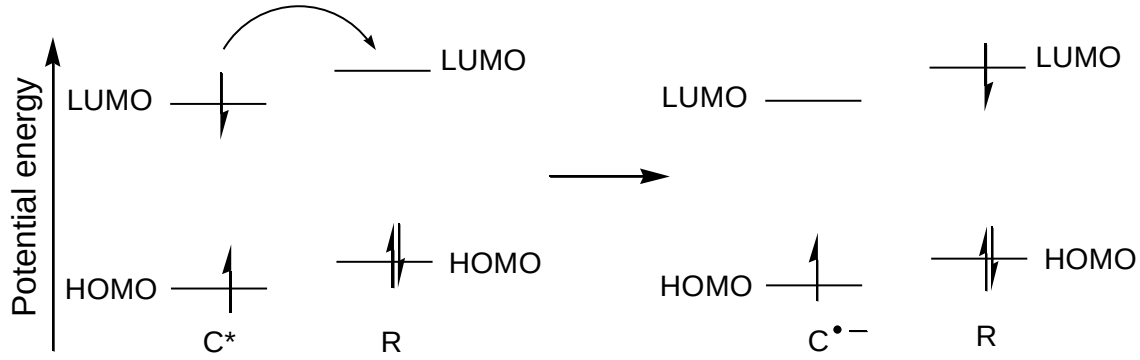

Figure 1.10 The electron transfer process of PET in a two component molecular system as an "off state."

The third case is that if LUMO and HOMO of R lie between LUMO and HOMO of C on an energy scale, there is a way for an electron transfer to take place from LUMO of C* to LUMO of R and from HOMO of R to HOMO of C*. This type of electron transfer is two simultaneous single-electron transfers and is referred to as an electron exchange mechanism, in which no ion radical species are formed and is shown in **Figure 1.11**.

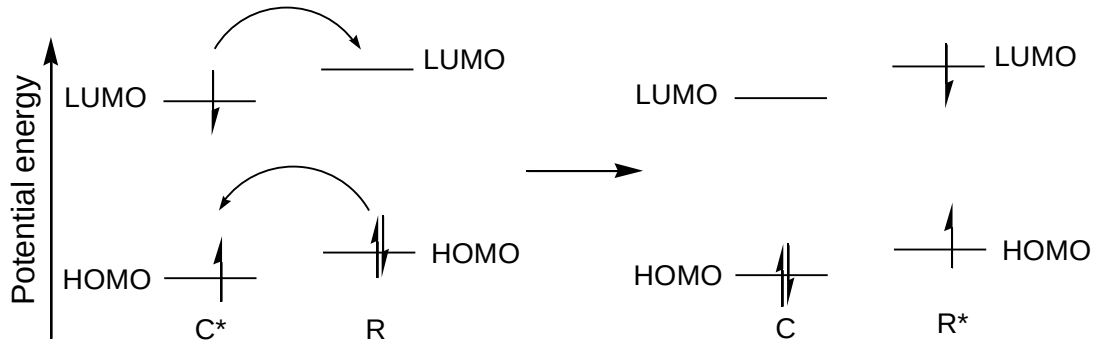

Figure 1.11 The electron transfer process through an electron exchange mechanism.

The PET-based sensor can recognize target analyte with observable signal by changing the energy level of orbital (HOMO or LUMO) of C or R. It is supposed to be a PET based metal sensor. In the absence of any analytes, it is non-emissive (in the "off-state") due to the PET process as discussed before. When it chelates target metal, this coordination produces an electrostatic attraction between the metal ion and an electron in the highest occupied molecular orbital (HOMO) of R. As a result, the oxidation potential of this analyte-receptor complex declines sufficiently to make thermodynamics of the PET process unfavourable.(**Figure 1.12**)[44][45] The sensor becomes emissive (in the "on-state"). The PET is a classical signal transduction mechanism and can have fine tune the photophysical properties of responsive luminescent probes by altering the reduction and oxidation potentials of their components and the excited state equilibrium energy when they detect target analytes.

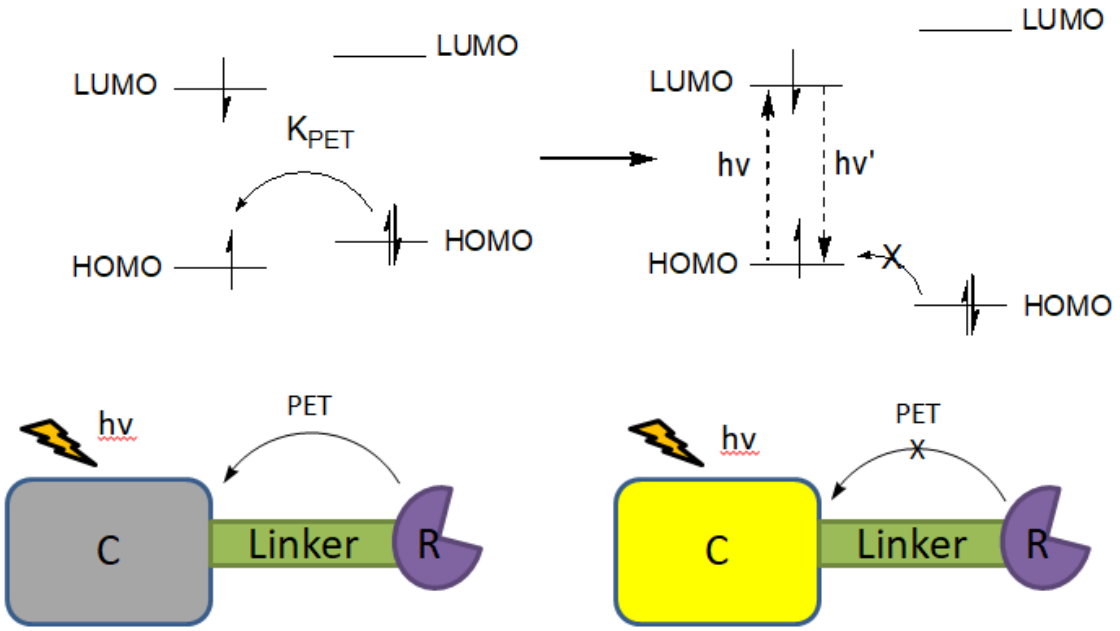

Figure 1.12 Energy level diagram (the frontier molecular orbital perspective) showing the PET process. (A) In the absence of any analytes, electron transfer from the electron-rich receptor to the photoexcited chromophore acceptor (A) is favourable to have quenching. (B) Complex formation with analyte decreases the HOMO level of receptor slows down electron transfer and restores luminescence.

1.2.2b Intramolecular charge transfer (ICT) Principle

Intramolecular charge transfer (ICT) is another signal transduction mechanism applied in sensing application. The chromophore of a probe has usually an electron-donating unit conjugated to an electron-accepting unit to give rise to a ‘‘push–pull’’ π-electron system in the excited state. The ICT-based sensors are usually solvatochromic; they are sensitive towards changes in solvent polarity. Typically, the dipole moment of chromophore in the excited state is larger than that in the ground state. Solvent dipoles can relax around the excited state and decrease the energy of the excited state. This effect is more pronounced for more polar solvents, resulting in emission at lower energies or longer wavelengths.

ICT is usually used for sensing, especially for cation. (**Figure 1.13**) When the electron donating group of a sensor chelates with cation, this electron donating character

of the probe decreases and leads to a blue shift in the emission spectrum. Conversely, when a cation is chelated by the electron accepting group of a sensor, this electron accepting character of the probe decreases and leads to a red shift in the emission spectrum.[35]

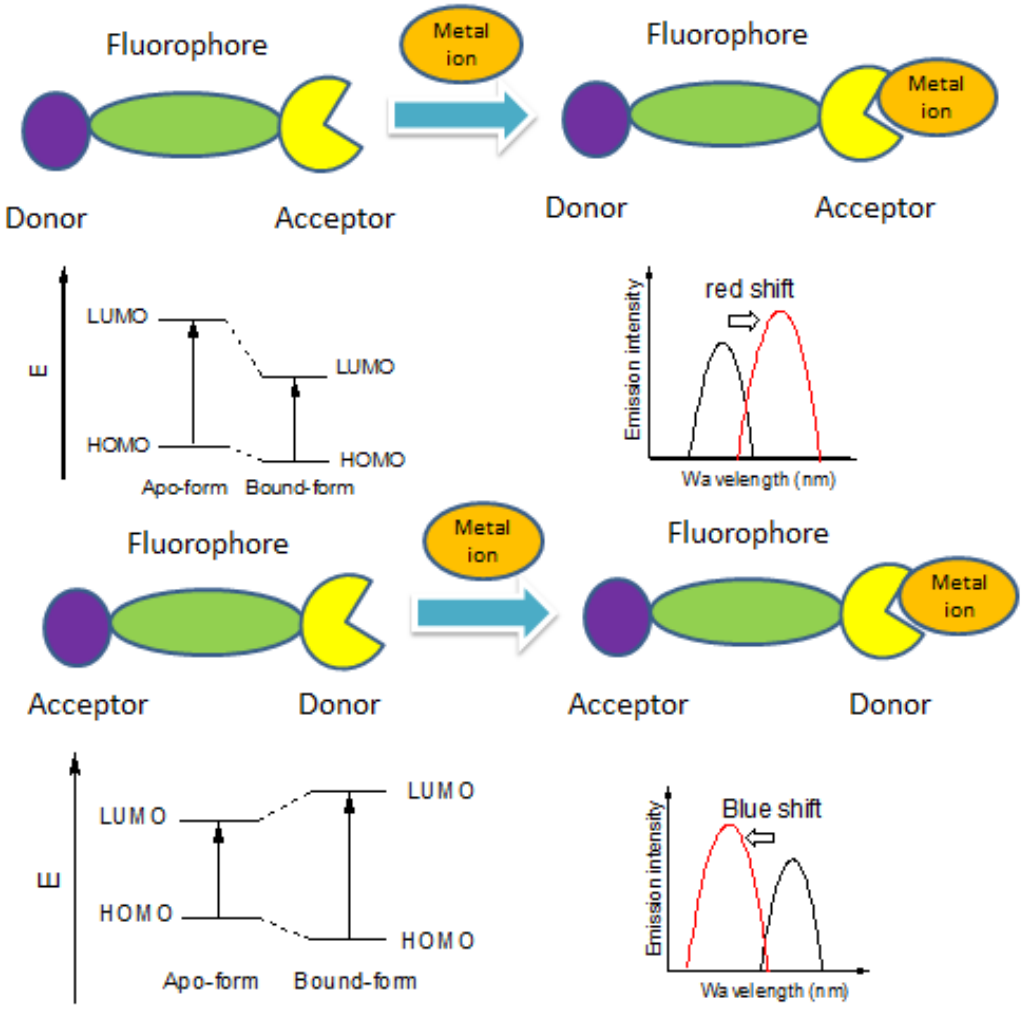

Figure 1.13 Energy level diagram (the frontier molecular orbital perspective) showing ICT process to changing photophysical properties of sensor.

1.2.2c Twist intramolecular charge transfer (TICT) Principle

Typical structure of TICT-based sensor is composed of an electron acceptor group which is in conjugation with an electron donor group through a network of alternating double and single bonds. (**Figure 1.14a**) At the ground state, the molecule has nearly planar lowest energetic conformation and the p-orbitals are aligned owing to extended conjugation within the molecule (**Figure 1.14b**)

When moleucle is photoexcited, intramolecular charge transfer occurrs from the donor to to acceptor within the molecule and the excited molecule has a planar locally-excited state (S_1^{LE}). The molecule has a rapid twist around a single bond which is intramolecular rotation around the σ-bonds that have electronically connection between the electron rich donor and the acceptor under the influence of the excited state charge separation.

Since the fluorescence deexcitation rate (k_{LE}) is usually lower than the intramolecular rotation rate (k_R), the quantum yield from the S_1^{LE} state is usually not high.(**Figure 1.15**) However, this quantum yield can be enhanced when intramolecular rotation is interrupted in the case of higher energy barrier between the planar and the twisted excited-state and K_r is reduced significantly and favours the emission from the planar and twisted excited-state. For instance, molecule cannot rotate at 77 K and thus it emits exclusively from the S_1^{LE} state.[46] Moreover, the energy gap between the ground and excited state in a twisted conformation is lower than that in the planar conformation, the emission from the S_1^{TICT} state is found to be red shifted.

TICT-based sensors are usually environmentally sensitive and are affected by two main factors, namely solvent polarity and microviscosity. First, they are solvatochromic since solvent polarity affects the stability of the polar excited state. More polar solvents can stabilize the S_1^{TICT} state over the S_1^{LE} state. Owing to the larger dipole moment of the excited TICT state, there will be a stronger bathochromic shift of the TICT emission as compared with the LE emission. Second, they are also affected by solvent microviscosity since solvent microviscosity affects the intramolecular twisting of the excited state and the intramolecular rotation rate k_R. More viscous solvents are usually found to have higher energy barrier between planar and twisted states, which declines the intramolecular rotation rate (k_R) and thus favours emission from the S_1^{LE} state

Figure 1.14 (a) General structure of a TICT chromophore. A is acceptor group and D is electron donor group. Intramolecular charge transfer takes place from the donor group to the acceptor group and is possible to have intramolecular rotation of the acceptor with respect to the donor group. (b) Chemical structure of DMABN has the two different planes of the donor group and the acceptor group. When the benzene and dimethylamino plane are approximately parallel, it is in the lowest-energy ground-state conformation. When the benzene and dimethylamino plane are perpendicular to each other by rotation around the nitrogen–benzene single bond, it is in a higher-energy twisted conformation.

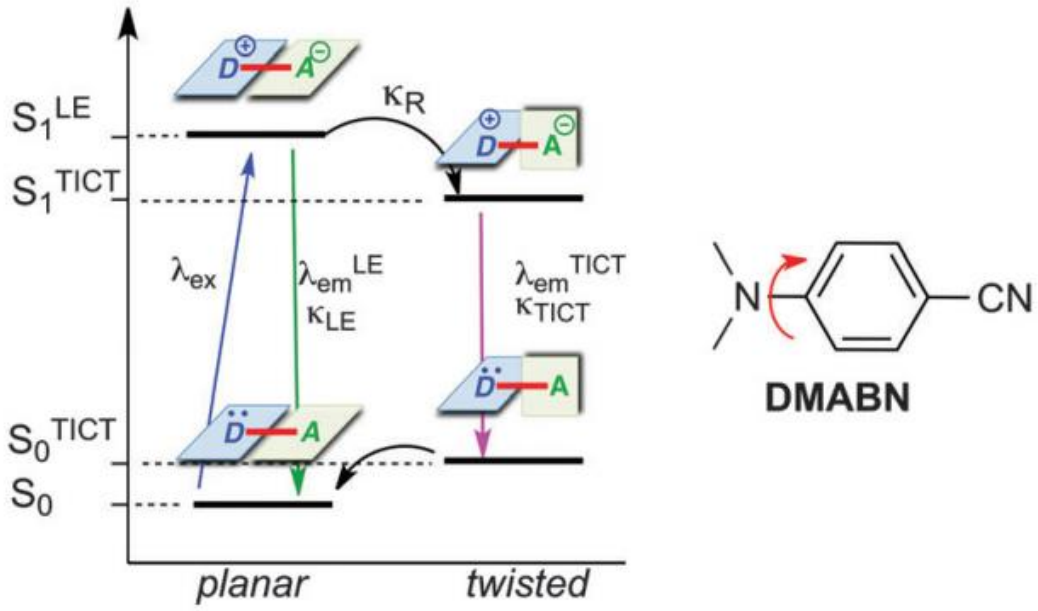

Figure 1.15 Jablonski diagram demonstrates TICT states and kinetics for DMABN. Photoexcitation with λ_{ex} (blue arrow) leads to a locally-excited planar state (S_1^{LE}) from where fluorescent relaxation occurs with deexcitation rate k_{LE} and λ_{em}^{LE} (green arrow). Molecule can have an intramolecular twisting with rate k_R to enter a twisted excited state (S_1^{TICT}) from where it can relax by photon emission with a deexcitation rate k_{TICT}

and a red-shifted $\lambda_{em}{}^{TICT}$ (red arrow)

1.2.2d Excimer and exciplex emission

When a chromophore has a flat aromatic surface and has photoexcition. This aromatic surface of the chromophore in the excited state interacts with the other aromatic surface of the chromophore in the ground state through π–π stacking to form a complex. This complex is called an excimer.

Figure 1.16 shows that the complex formed between C* and C, [C*···C], emits at a longer wavelength than the chromophore owing to the smaller energy gap in [C*···C]. The formation of such excimer complexes is solvent-dependent; it also depends on the ability of the two chromophores to adopt conformations that successfully allow such orbital overlap to occur. Formation of complexes between two different kinds of chromophore is possible. This is referred to as an exciplex formation.

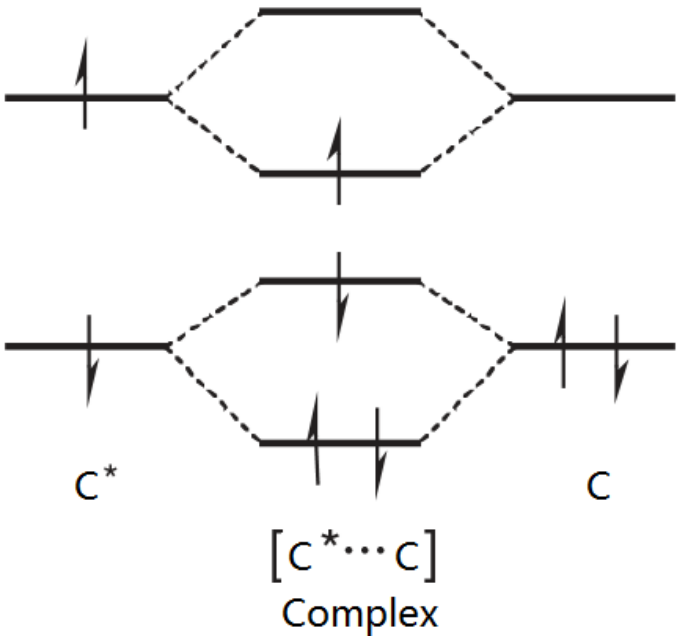

Figure 1.16 The formation of an excimer achieved upon formation of a complex between an excited stated fluorophore (C*) and a ground state fluorophore (C) of the same nature.

1.2.3 Chemodosimeter

The term “chemodosimeter”, [34] which was first coined by Czarnik and Chae, refers to an abiotic molecule utilized to detect target analyte with a concomitant irreversible transduction of an observable signal.[36] This type of sensor is based on specific reaction with analyte to have significant chemical transformation such as breaking and forming of covalent bonds that results in the formation of products different from the initial chemodosimeter concomitantly with various photophysical properties. Owing to the chemical transformations that involve bonding breaking and formation of covalent, there are very few examples of the regeneration of chemodosimeter. However, only specific reaction can take place between chemodosimeter and target analyte. Chemodosimeter therefore has relative high selectivity and is not easily interfered with the environment.

There are some common mechanisms for luminescent chemodosimeter, including bond-cleavage reactions and oganic addition approach.(**Figure 1.17**) In the bond-cleavage reaction approach, reaction sites and chromophore are both appended in the same molecule by a covalent bond. When a target analyte is bound to the reaction site and triggers a specific reaction within chemodosimeter, there is a photophysical change within chemodosimeter that indicates the detection of an analyte. For instance, 2,4-dinitrophenyl sulfonate group is a reaction site easily cleaved by neucleophile such as thiol groups. It can be used to detect thiol derivatives. In the organic addition nucleophilic approach, there is an addition reaction that allows the analyte to react with reaction site, resulting in a change in the photophysical properties of chromophore. For instance, Michael addition reaction[37] is applied in this type of chemodiometer. If an electrophilic α,β-unsaturated acrylate methyl ester functional group is positioned in proximity to the aldehyde, the trapped thiol can subsequently undergo an intramolecular Michael addition to form a stable thioacetal product.

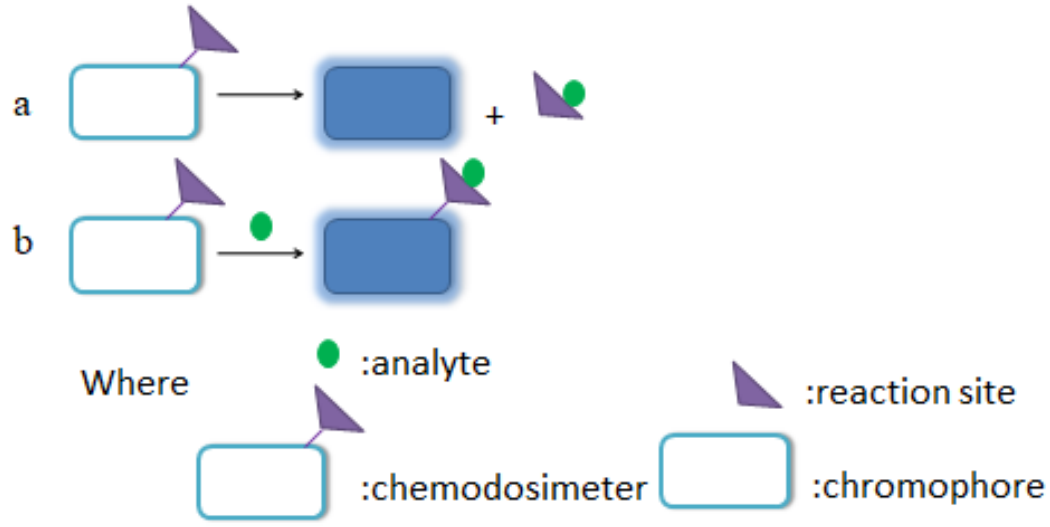

Figure 1.17 Representative mechanisms for luminescent chemodosimeter. a.Bond -cleavage reactions (cleavage of bond between reaction site and chromphore); b. Organic addition/ metal-ligand substitution approach (nucleophilic addition reaction and metal-mediated fluorescent fluoride probes). The blue "rectangular" shape is used to represent a generic chromphore.

1.2.4 Selective reaction mechanisms used in chemodiometer

The selection of suitable reaction mechanisms is a key to design reaction-based sensors for detection of specific analyte. In this section, we highlight some examples classified according to the reaction types used for fluorescence sensing of nucleophilic anions and neutral species.

1.2.4a Nucleophilic addition

Nucleophilic addition reaction is an addition reaction in which an electron-deficient functional group in a molecule such as double or triple bond reacts with an electron-rich nucleophile to give a new saturated molecule. Carbonyl addition and Conjugate addition are usually applied. In carbonyl addition, it is common to use senors with electrophilic centers such as carbonyl carbons to detect anions or neutral species such as amines (RNH_2) and bifunctional compounds such as amino-thiols ($H_2N–R–SH$) and other thiols derivatives which are nucleophiles having lone pair

electrons and that are like Lewis bases to donate their electron pairs to the electrophilic centers to form adducts. For instance, cyanide (CN^-) is usually found solvated in water weakly but has a strong affinity toward carbonyl carbon. Therefore, if the nucleophilic addition approach is used, it can distinguish CN^- ion from other anions such as F^- ion in the sensing studies. Utilizing this feature of CN^- ion, Hong's group reported a turn-on fluorescent sensor using Ahn's concept of intramolecular H-bonding stabilization of cyanohydrin adducts.(**Figure 1.18**) [48]

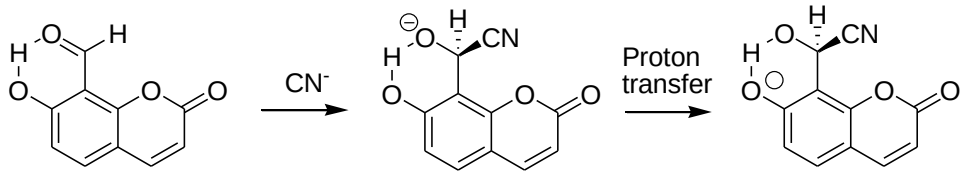

Figure 1.18 Detection of CN^- ion through formation of the cyanohydrin adduct.[48]

Moreover, the Michael addition to α,β-unsaturated carbonyl compounds is a common reaction for the development of fluorescent probes, especially for thiol derivatives. Commonly, Carbon-carbon double bond with an electron-withdrawing group such as carbonyl group and conjugate with chromophore such as coumarins, BODIPY can have Michael addition selectively with thiol derivatives and give observable signals.[49]-[52]

1.2.4b Nucleophilic substitution

Nucleophilic substitution, which is a reaction in which nucleophile selectively attacks the positive or partially positive charge of an atom or a group of atoms to replace a leaving group, is commonly used in chemodiometer. For instance, dinitrobenzenesulfonate is commonly used in nucleophilic substitution in the design of chemodiometer since it is prone to deprotection by nucleophiles. Dinitrobenzenesulfonate contains two strong electron-withdrawing nitrogroups that is weak luminescent due to PET. Therefore, a senor can be turn on after removing dinitrobenzenesulfonates. For example, Maeda's group has developed a fluorescein based probe for detection of thiols in which there is a nucleophilic substitution of dinitrobenzenesulfonates by thiols to turn on senor.(**Figure 1.19**) [53]

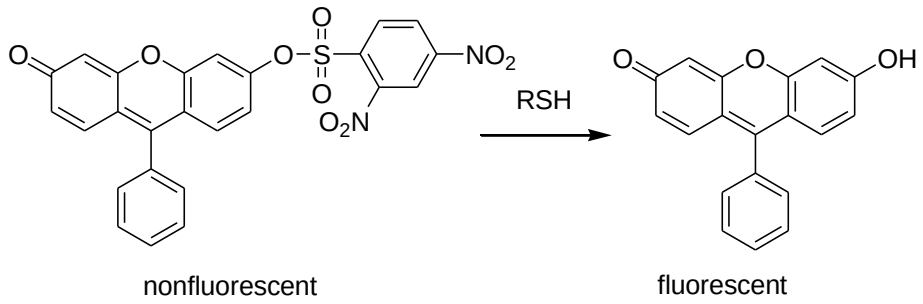

Figure 1.19 Sensing of thiols through substitution to sulfonates.[53]

1.2.4c Tsuji–Trost type reaction

The Tsuji–Trost reaction, which was first introduced by Jiro Tsuji in 1965, is a palladium-catalyzed substitution reaction for a compound with a leaving group in an allylic position and is usually used to detect Pd(II) ion.[54][55] Koide's group has developed a fluorescein-based sensor for detection of Pd(II) ion. It is based on allylic oxidative insertion to cleave the allylic C–O bond of an allylic ether into a fluorescein compound. The conversion of allylic fluorescein into a fluorescein compound without any allylic functional group is particularly efficient with Pd. This sensor can do quantitative detection of Pd of less than 50ng of Pd with a good linear relationship (R^2 =

0.993) between the fluorescence intensity and Pd concentrations of 0.95 to 95ng. It can be used in Pd(II) ion analyses of pharmaceutical products and Pd detection in rock samples.(**Figure 1.20**) [56]

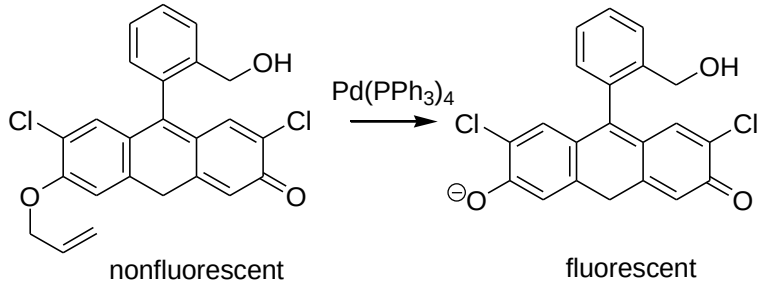

Figure 1.20 Scheme for the reaction-based detection of Pd by chemodosimeter.[56]

1.2.4d Ion-induced hydrolysis reactions

Metal ions, including Cu(II) ion, Fe(II) ion, Hg(II) ion and Au(II) ion, can be catalysts to hydrolyze ester groups, schiff bases and acylsemicarbazide groups. If chemodosimeters have these functional groups, they can be used to detect those cations. The hydrolysis does not go far beyond a single turnover due to the stronger binding of corresponding hydrolysis products towards the target analytes. For instance, Cu(II) ion can hydrolyse α-amino acid esters at a rate much faster than other metal ions. This strategy used in chemodosimeter was first suggested by Czarnik's group in 1997 in which a rhodamine derivative with α-amino acid esters was used for Cu(II) ion detection.(**Figure 1.21**) [57]

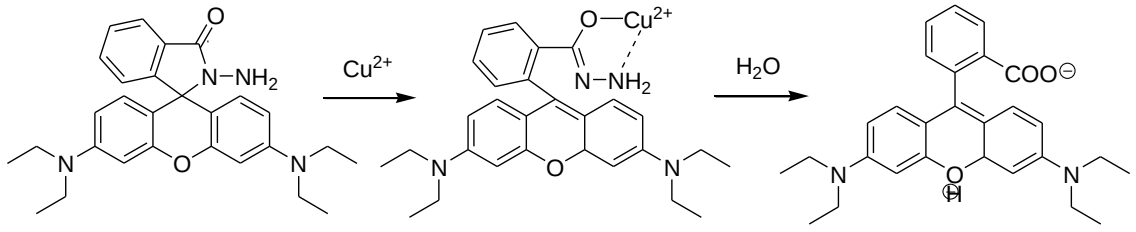

Figure 1.21 for the reaction-based detection of Cu(II) ion by chemodosimeters.[57]

1.3 Lanthanide based responsive probes for sensing

Development of lanthanide based responsive complexes has attracted much interest due to their large stoke shift and long lived lifetimes. Generally, there are several ways

to modulatetheir signal in the presence of the analyte, including changing the coordination environment of lanthanide ion or pendant arm structure and changing the chromophore via reaction. Selected strategies applied in the design of such responsive probe will be shown below.

1.3.1 Strategy 1: Varying the distance between chromophore and lanthanide ion

The distance between chromophore and Ln(III) ion is one of the main keys to affect the energy transfer from chromophore to lanthanide since the energy transfer from chromophore to Ln(III) ion is usually Förster type. The Förster type energy transfer efficiency is usually affected by the distance between chromophore and Ln(III) ion hence the signal of Ln(III) complex is changed for variation in distance There are three ways to do this. First, a receptor is connected between chromophore and Ln(III) ion. In the absence of analyte, the receptor keeps the chromophore and Ln(III) ion far away from each other and the energy transfer is small. When the receptor binds to an analyte, such binding can bring the chromophore in close proximity to the Ln(III) ion, thereby increasing the luminescence of Ln(III) ion.(**Figure 1.22**) In **Figure 1.23**, a lariat crown ether is used to connect the azaxanthone chromophore and terbium complex. Before addition of potassium ion, the azaxanthone chromophore and terbium ion are kept far away from each other to have weak luminescence. After addition of potassium ion, the ethylene bridge between phenyl and the crown ether allows concomitant complexation of the potassium ion by cation–π interaction with the arene and bring the azaxanthone chromophore in close proximity to the terbium ion, leading to enhancement in luminescence.[58]

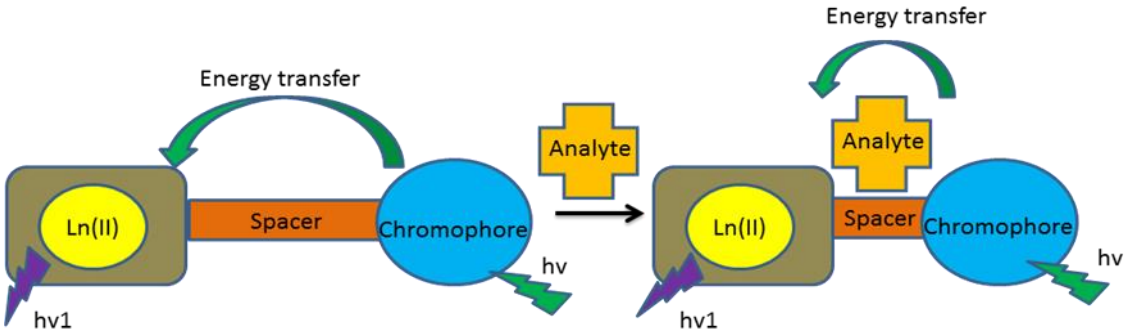

Figure 1.22 Spacer acts as receptor which chelates analyte and brings the chromophore in close proximity to the Ln(III) ion.

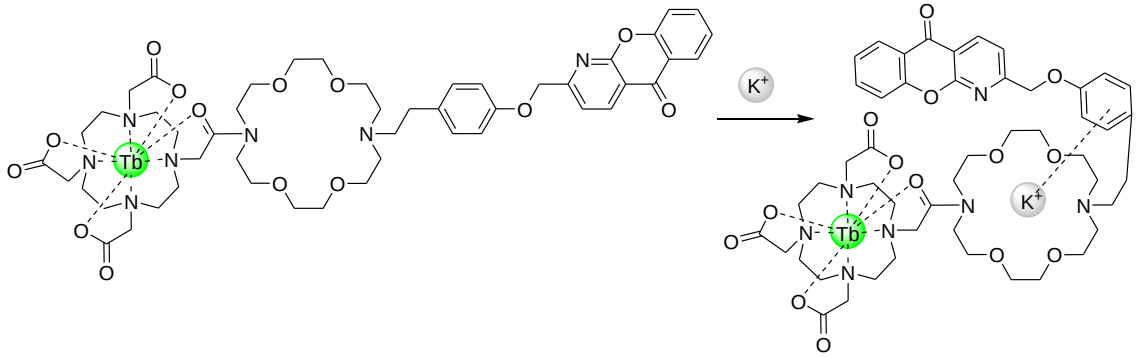

Figure 1.23 Example of lanthanide responsive probe which use receptor as space for sensing.[58]

Second, if the sensor is used for detection of some analyts which has has ability to catalyse specific reaction, the sensor can recognize them by incorporation of that specific functional group and allows analyte to catalyse the reaction in sensor and gives out some observable response. In **Figure 1.24**, in the absence of analyte, lanthanide complex and chromophore are separated. But in the presence of analyte, there is a specific reaction taken place between chromophore and lanthanide complex since analyte catalyses the conjugation of lanthanide complex to chromophore to have observable signal. In **Figure 1.25**, Hulme's group develops lanthanide based sensor for detection of Cu(I) ion. In the absence of Cu(I) ion, Eu-DOTA complex and azideterminated dansyl chromophore are not covalent bonded, so there is not any energy transfer between them. In the presence of Cu(I) ion, there is Huisgen 1,3-dipolar cycloaddition ("click" reaction) catalyzed by analyte copper(I) ions between Eu-DOTA

complex and azideterminated dansyl chromophore. As a result, they are connected together and emit strongly.[59]

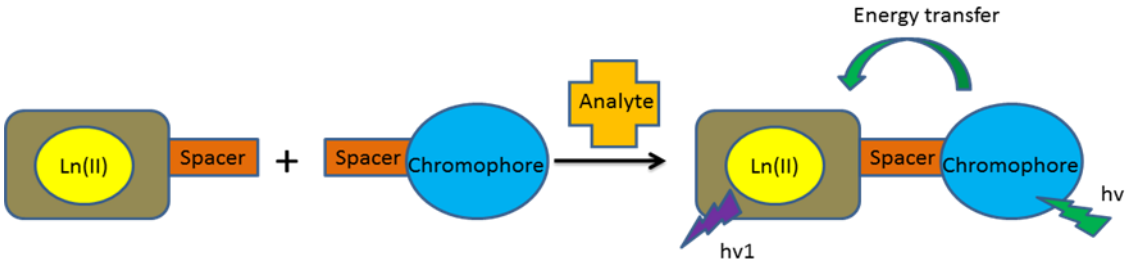

Figure 1.24 Analyte catalyses the conjugation of lanthanide complex to chromophore to have observable signal.

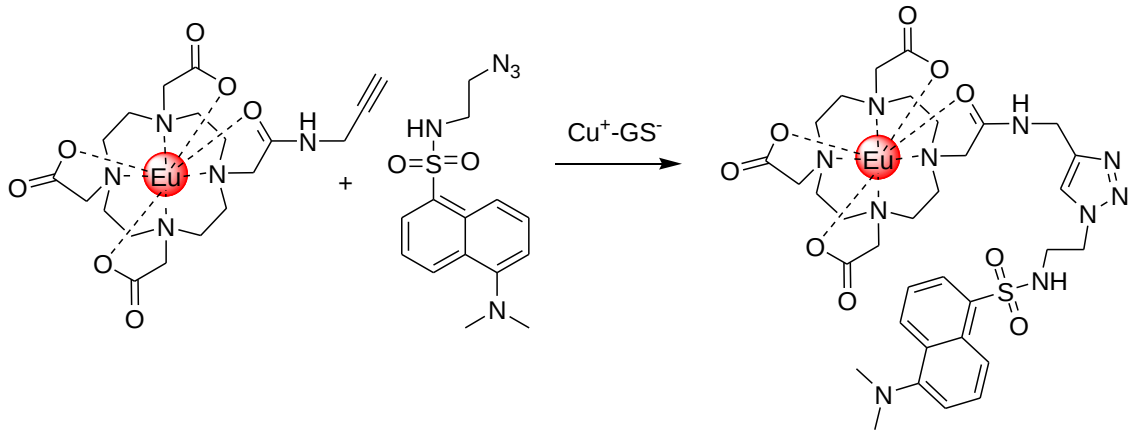

Figure 1.25 Example of responsive luminescent lanthanide sensors shows Cu(I) ion catalyses the conjugation of lanthanide complex to chromophore.[59]

Third, some analyte has strong chelating properties towards the Ln(III) ion. If the sensor coordinates weakly with chromophore, analytes then can displeace a weakly coordinated chromophore and lanthanide's luminescence is turned off. (**Figure 1.26**)

In **Figure 1.27**, Gunnlaugsson's group developed a ternary luminescent europium complex for detection of HCO^- ion through a displacement assay.[8] In the absence of HCO^- ion, naphthyl chromophore coordinated towards Eu(III) ion through a labile β-diketonate functional group. In the presence of HCO^- ion, β-diketonate functional group is displaced by a stronger chelating HCO^- ion and therefore the luminescence intensity of the europium decreases.[60]

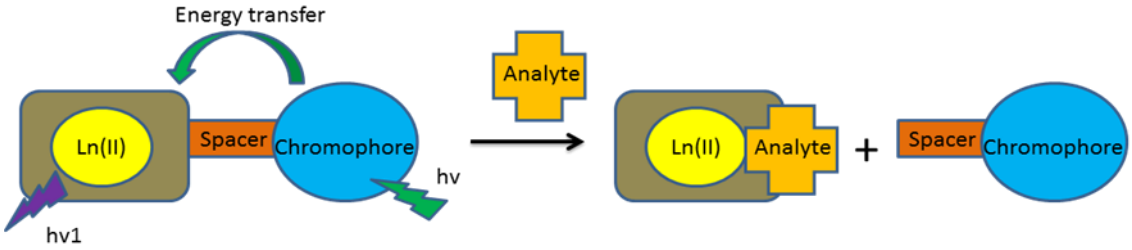

Figure 1.26 analyte has direct coordination lanthanide by displacement of a weakly coordinated chromophore.

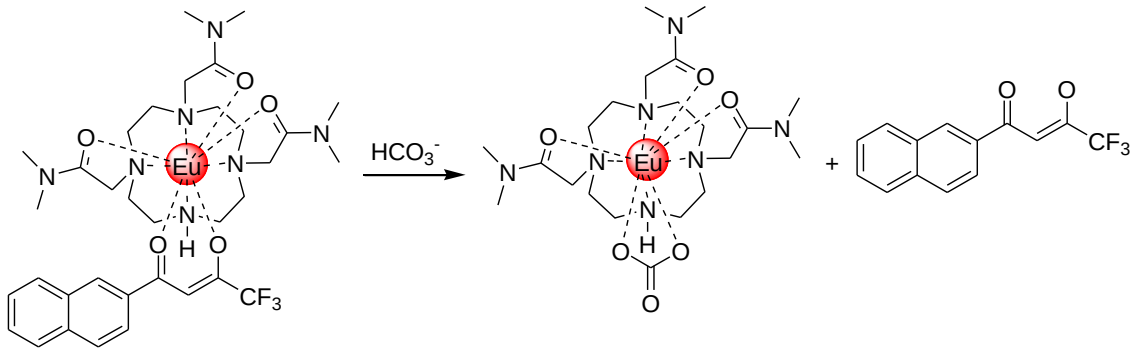

Figure 1.27 Example of responsive luminescent lanthanide sensors in which the signal is turned off due to displacement of weak coordinated chromophore caused by analyte.[60]

1.3.2 Strategy 2: Varying the coordinated water molecules

Luminescence of lanthanide complexes such as Eu(III) and Tb(III) complexes is easily quenched through O–H and N–H oscillators of lower energy, especially for quenching by fourth overtone of the O–H oscillator of water which is slightly lower in energy than the excited $^5D_0$ states of Eu(III) ion and $^5D_4$ of Tb(III) ion. The quenching efficiency is always dependent on the number of water molecules coordinated to the Ln(III) ion and the distance between O–H oscillator and the Ln(III) ion. In the design of lanthanide based responsive probes, control of the number of water molecules coordinated to the Ln(III) ion is more common and easier than the control of the distance between O–H oscillator and the Ln(III) ion. Addition of the analyte as an chromophore or ligand towards lanthanide complex is a common approach. In the absence of analyte, the lanthanide complex has one or more open coordination sites and

therefore water molecules will fill these open sites and quench the luminescence of the lanthanide complex. In the presence of analyte, the analyte can remove the water molecules and bind to lanthanide ion. And the lanthanide complex can be turned on.(**Figure 1.28**) In **Figure 1.29**, Gunnlaugsson's group has developed a sensor for detection of salicylic acid and other benzoic acid derivatives using this strategy. After addition of salicylic acid, two inner-sphere water molecules of Tb(III) ion can be readily displaced and the sensor turned on.[61]

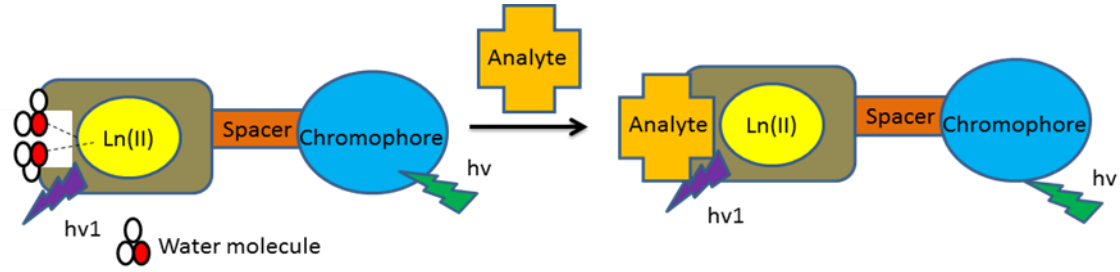

Figure 1.28 The luminescence of lanthanide sensors is modulated by direct coordination of chromophore.

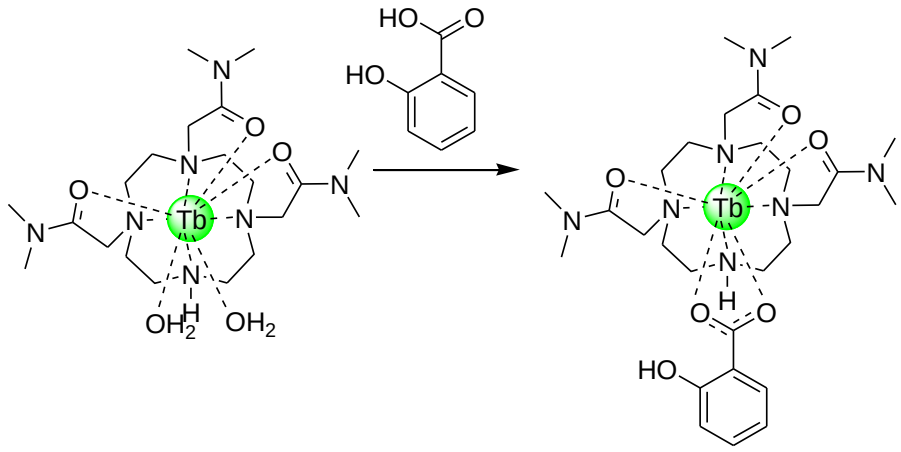

Figure 1.29 Example of responsive luminescent lanthanide sensors which modulate the luminescence of lanthanide sensors by direct coordination of chromophore.[61]

1.3.3 Strategy 3: Changing chromophore via reaction

This strategy is to change the structure of the chromophore through reaction with analyte and hence alter the triplet state of the antenna and then the luminescence of a complex. Therefore, a sensor should contain a reactive site that can react selectively

with a desired analyte to give a product that has a triplet state of substantially different energy than the previous one.(**Figure 1.30**) In **Figure 1.31**, Eu(III) complex uses N-methylphenanthridinium as the reactive site for recognition of hydroxide at the 6 position. The absorption spectrum of Eu(III) complex after addition of hydroxide is different from that of the initial phenanthridinium and significantly affects the quantum yield of the corresponding europium complex.[62]

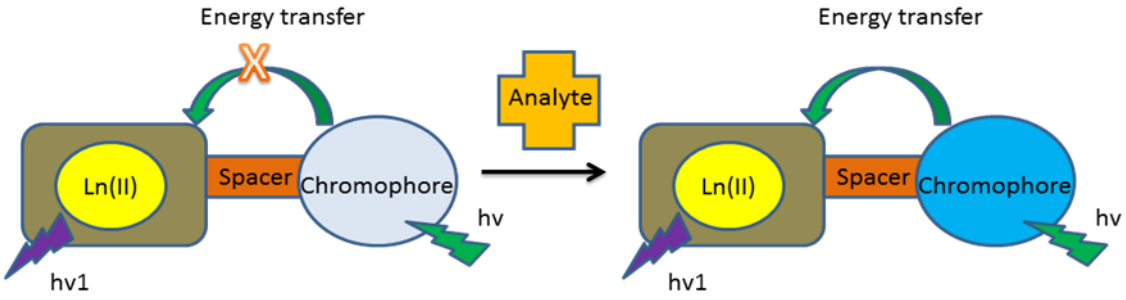

Figure 1.30 Variation of luminescence of lanthanide sensors via reaction.

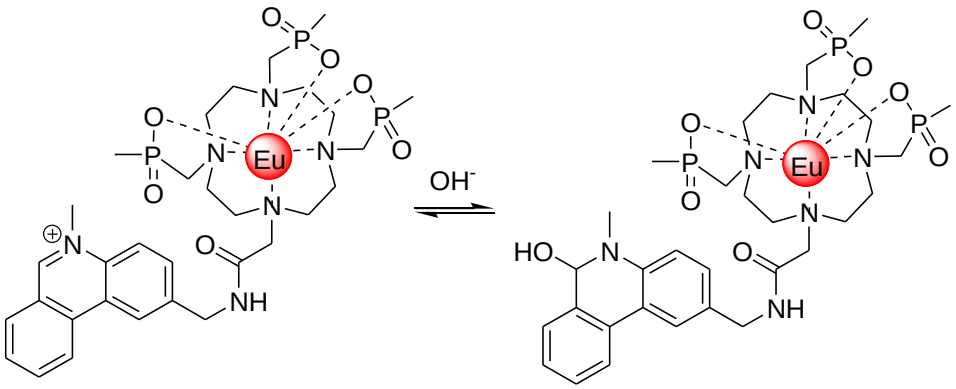

Figure 1.31 Example of responsive luminescent lanthanide sensors which detect OH^- ion through Strategy 3. [62]

1.4 Objective

This thesis describs the development of a new class of responsive Ln(III) based probes for detection of Cu(II) ion, H_2S, cysteine, Cu(I) ion, Zn(II) ion. The probes must meet a number of criteria:

- The probe must be water soluble and fully functional in aqueous solution for detection of desired analytes.

- The probe must have good selectivity for the desired analytes. For instance, there are many other cations present and selectivity for desired analyte is required against a competing background of these.
- The probe should be thermodynamically stable under physiological condition.
- The probe should have a saturated coordination environment of the Ln(III) ion, so the process of non-radiative process can be reduced and the probe is highly luminescent.

1.5 References

[1] T. Moeller, *The Chemistry of the Lanthanides*, Reinhold Publishing Corporation, 1965.

[2] N. Kaltsoyannis, P. Scott, *The f-Elements*, Oxford University Press, 1999.

[3] R. M. Macfarlane and R. M. Shelby, *Spectroscopy of solids containing rare earthions*, North-Helland, 1987.

[4] Y.W. Yip, G. L. Law and W. T. Wong, *Dalton Trans*., 2016, **45**, 928-935.

[5] Z. Liang, T. H. Tsoi, C. F. Chan, L. Dai, Y. Wu, G. Du, L. Zhu, C. S. Lee, W. T. Wong, G. L. Law and K. L. Wong, *Chem. Sci*., 2016, **7**, 2151-2156.

[6] A.R. Lippert, T. Gschneidtner, and C.J. Chang, *Chem. Commun*., 2010, **46**, 7510–7512.

[7] E. Pershagen, J. Nordholm, and K.E. Borbas, *J. Am. Chem. Soc*., 2012, **134**, 9832–9835.

[8] J.P. Leonard, C.M.G. DosSantos, S.E. Plush and T. Gunnlaugsson, *Chem. Commun*., 2007, 129–131.

[9] P. W. Roesky and Z. Anorg. *Allg. Chem*., 2003, **629**, 1881-1894.

[10] S. Harder and D. Naglav, *Eur. J. Inorg. Chem*., 2010, 2836-2840.

[11] W.-S. Lo, W.-T. Wong, G.-L. Law, *RSC Adv*., 2016, **6**, 74100-74109.

[12] R. Litlabø, H. S. Lee, M. Niemeyer, K. W. Törnroos and R. Anwander, *Dalton Trans*., 2010, 6815-6825.

[13] Y. W. Yip, H. Wen, W. T. Wong, P. A. Tanner and K. L. Wong, *Inorg Chem*., 2012, **51**,7013-7015.

[14] G. L. Law, K. L. Wong, K. K. Lau, S. T. Lap, P. A. Tanner, F. Kuo and W. T. Wong, *J. Mater. Chem*., 2010, **20**, 4074-4079.

[15] S. Petoud , G. Muller, E. G. Moore, J. Xu , J. Sokolnick , J. P. Riehl, U. N. Le, S. M. Cohen and K. N. Raymond, *J. Am. Chem. Soc*., 2007, **129**, 77–83.

[16] P. Alexandre, M.Floriane, L. G. Boris, P. L. Baldeck, J. A. G. Williams, C.Andraud, and O. Maury, *Inorg. Chem*., 2007, **46**, 2659−2665.

[17] S. J. Butler, M. Delbianco, L. Lamarque, B. K. McMahon, E. R. Neil, R. Pal, D. Parker, J. W. Walton and J. M. Zwier, *Dalton Trans*., 2015, **44**, 4791-4803.

[18] C. H. Evans, *Biochemistry of the Lanthanides*, Plenum Press, 1990.

[19] J. P. Hessler and W. T. Carnall, *Abstr. Pap. Am. Chem. S*. 1979, 231-231.

[20] P. Franzen, J. P. M. Woudenberg, C. J. Goiter, *Physica*., 1943, **10**,365-367.

[21] J. Hoogschagen, *Physica*, 1946, **11**,513-518.

[22]Geschneider and Eyring, *Handbook on the Physics and Chemistry of the Rare Earths*, North-Holland Publishing Company, 1979.

[23] K. Binnemans, K. Herck, C. G.Walrand, *Chem Phys. Lett*., 1997, **23**,297-302.

[24] M. H. V. Werts, R. T. F. Jukes and J. W. Verhoeven, *Phys. Chem. Chem. Phys*., 2002, **4**, 1542–1548.

[25] T. Storr, *Ligand Design in Medicinal Inorganic Chemistry*, John Wiley & Sons, 2014.

[26] K. Binnemans, *Coord. Chem. Rev*., 2015, **295**, 1-45.

[27] M. Latva, H.Takalo, V. M..Mukkala, C. Matachescu and R. U. J. C.Kankare, *J.Lumin*. 1997, **75**, 149–169.

[28] Th. Förster, *Discuss. Faraday Soc*. 1959, **27**, 1-6.

P.J.Slevin, E. G. Szebe´nyi, G. Svehla, *Talanta*., 1972, **19**, 307– 315.

[29] A. Tong, Y. Akama, and S. Tanaka, *Analyst*., 1990, **115**, 947–949.

[30] T. Poursaberi, L. H. Babaei, M. Yousefi, S. Rouhani, M. Shamsipur, M. K. Razi, A. Moghimi, H. Aghabozorg and M. R. Ganjali. *Electroanal*., 2001, **13**, 1513–1517.

[31] A. Atanassova, R. Lam and D.B. Zamble, *Anal Biochem*., 2004, **335**,103-111.

[32] S.F. Shepherd, N.D. McGuire, B.P. Costello, R .J.Ewen, D.H.Jayasena, K. Vaughan, I. Ahmed, C.S. Probert and N.M. Ratcliffe,*J Breath Res*. 2014, **8**,1-13.

[33] G.Jarzynska and J. Falandysz., *J Environ Sci Health A*, 2011, **46**, 569–573.

[34] J. Chan, S. C. Dodani and C. J. Chang, *Nature Chemistry*., 2012, **4**, 973–984.

[35] Z. Liu, W. He and Z. Guo, *Chem. Soc. Rev*., 2013, **42**, 1568-1600.

[36] M.Y. Chae and A.W. Czarnik, J. Am. Chem. Soc., 1992, **114**, 9704-9705.

[37] Y. Qian, J. Karpus, O. Kabil, S. Y. Zhang, H. L. Z., R. Banerjee, J. Zhao and C. He, *Nature Commun*., 2011, **2**, 495-502.

[38] M. Yuan, Y. Li, H. Liu and Y. Li, *Sci China Ser B*., 2009, **52**, 715-730.

[39] N. Boens, V. Leen and W. Dehaen, *Chem Soc Rev*., 2012, **41**, 1130-1172.

[40] K. Kikuchi, *Chem Soc Rev*., 2010, **39**, 2048-2053.

[41] J. Zhao, S. Ji, Y. Chen, H. Guo and P. Yang, *Phys Chem Chem Phys.*, 2012, **14**, 8803-8817.

[42] R.A.Bissell, A. P. Silva, H. Q. N. Gunaratne, P. L. M. Lynch, G. E. M. Maguire and K. R. A. S. Sandanayake, *Chem. Soc. Rev*., 1992, **21**, 187-195.

[43] A. Weller, *Pure Appl. Chem.*, 1968, **16**, 115-124.

[44] N. Boens, V. Leen and W. Dehaen, *Chem. Soc. Rev*., 2012, **41**, 1130-1172.

[45] S. Doose, H. Neuweiler and M. Sauer, *ChemPhysChem*., 2009, **10**, 1389-1398.

[46] R. O. Loutfy and K. Y. Law, *J. Phys. Chem*., 1980, **84**, 2803-2808.

[47] M. A. Haidekker and E. A. Theodorakis, *J. Mater. Chem. C*, 2016, **4**, 2707-2718.

[48] K. S. Lee, H. J. Kim, G. H. Kim, I. Shin and J. I. Hong, *Org. Lett*., 2008, **10**, 49-51.

[49] Y. Zeng, G. Zhang, D. Zhang and D. Zhu, *Tetrahedron Lett*., 2008, **49**, 7391- 7394.

[50] W. Lin, L. Yuan, Z. Cao, Y. Feng and L. Long, *Chem. Eur. J*., 2009, **15**, 5096-5103

[51] H.S. Jung, K.C. Ko, G. H. Kim, A. R. Lee, Y. C. Na, C. Kang, J.Y. Lee and J. S. Kim, *Org. Lett*., 2011, **13**, 1498- 1501.

[52] H. Kwon, K. Lee, H. J. Kim, *Chem. Commun*., 2011, **47**, 1773- 1775.

[53] H. Maeda, H. Matsuno, M. Ushida, K. Katayama, K. Saeki and N. Noth, *Angew.*

Chem. Int. Ed., 2005, **44**, 2922-2925.

[54] B. M. Trost and T. J. Fullerton, *J. Am. Chem. Soc*., 1973, **95**, 292–294.

[55] B. M. Trost and D. L. Van Vranken, *Chem. Rev*., 1996, **96**, 395–422.

[56] F. L. Song, A. L. Garner and K. Koide, *J. Am. Chem. Soc*., 2007, **129**, 12354–12355.

[57] V. Dujols, F. Ford and A. W. Czarnik, *J. Am. Chem. Soc*., 1997, **119**, 7386–7387.

[58] A. Thibon and V.C. Pierre, *J. Am. Chem. Soc*., 2009, **131**, 434–435.

[59] R. F. H. Viguier and A. N. Hulme, *J. Am. Chem. Soc*., 2006, **128**, 11370–11371.

[60] J.P. Leonard, C.M.G. dos Santos, S.E. Plush, T. McCabe and T. Gunnlaugsson, *Chem. Commun*., 2007, 129–131

[61] T. Gunnlaugsson, A.J. Harte, J.P. Leonard and M. Nieuwenhuyzen, *Chem. Commun.*, 2002, 2134–2135

[62] D. Parker, K. Senanayake and J.A.G. Williams, *Chem Commun*, 1997, 1777–1778.

CHAPTER 2

Synthetic Aspects: Macrocyclic Compounds

2.1 Introduction

Macrocycle, a promising metal ligand widely applied in lanthanide chemistry, is a cyclic polydentate ligand containing donor atoms to form stable complexes. Unlike open-chain ligands, it usually forms higher theromodynamic and kinetic stable complexes. This phenomenon can be explained by macrocyclic effect which was first proposed by Cabiness and Margerum.[1] Ligand usually requires preorganization to have good complexation with metal ions.[2][3] In other words, conformation in the free state should be similar to complex conformation and conformation rearrangement energy can be minimized. Generally, the extent of preorganization within a macrocycle is higher than that within an open-chain derivative.

Among the various macrocycles, 1, 4, 7, 10-teraazacyclododecane (cyclen) is widely used as a lanthanide ligand. It consists of four secondary amine groups which allow chelation and incorporate pendant arm by simple organic reactions such as neuclophilic substitution reaction.There are various possible pendant arms used, such as carboxylic groups (-RCOOH), amide groups (-RCONH-, RCONR-), amine groups ($-NH_2R$, $-NHR_2$, $-NR_3$), alkyl groups and phosphorus moieties (ex. $-PO(OH)(R)_2$). Such ligand can provide a number of coordination sites to form stable lanthanide complex. For instance, one of the most commonly used macrocyclic derivatives is 1,4,7,10-tetraazacyclododcane-1,4,7,10-tetraacetic acid (DOTA) (**Figure 2.1**). It can form highly theromodynamically and kinetically stable complexes. Its thermodynamic metal-ligand stability constants (K_{ML}) are summaried in **Table2.1**.[4] Generally, K_{mL} of lanthanide complexes are larger than that of other biological cations such as Ca(II) ion and Mg(II) ion, lanthanide DOTA complexes are therefore stable in biological condition. It is very important to choose a suitable ligand for biological application since free lanthanides are toxic to human [5][6] and their values of LD_{50} are usually about 0.1 $mmolkg^{-1}$. One reason is that lanthanides are similar to Ca(II) ion and are able to replace

Ca(II) in biological processes.

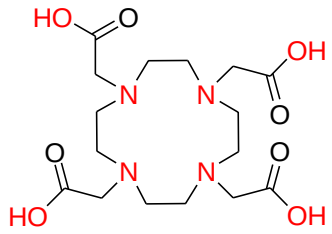

Figure 2.1 The structure of DOTA and donors are labelled in red.

Metal ion	Ce(III) ion	Nd(III) ion	Eu(III) ion	Gd(III) ion	Yb(III) ion	Y(III) ion	Ho(III) ion	Mg(II) ion	Ca(II) ion
Log K_{ML}	23.39	22.99	26.2	24.67	25.00	24.3	24.54	11.92	17.23

Table 2.1 Summary of metal-ligand stability constants of DOTA and cations.[4]

In this work, the macrocyclic ligands developed were derived from cyclen, which had three pendant arms for chelating with lanthanide and the remaining secondary amine is used for connection to the chromophore. As shown in **Figure 2.2**, **DO3A** has seven donor atoms and one from chromophore since chromophore in this thesis is designed to have one donor atom for chelation with lanthanide. Therefore, **DO3A** and chromophore can provide eight coordination environments. However, there is one water molecule to chelate lanthanide in this situation especially for Eu(III) ion. As discussed in Chapter 1, the water molecule in the inner coordination environment can lead to a non-radiative process. Therefore, **DO3A-M** is necessary to be synthesized since one of the pendant arms is an ethoxyacetic acid derivative which can provide one more donor. Therefore, **DO3A-M** and the chromophore can provide nine coordination environments. There are no water molecules in the inner coordination of Eu(III) ion and Eu(III) complex should be brighter than the case of **DO3A**. To have an easy synthesis, the protected forms are first synthesized and depicted in **Figure 2.3**. Tert-butyl ester group and ethyl ester group are used to protect of carboxylic group. The protected carboxylic group can be easily deprotected by a simple method such as acid or basic

deprotection.

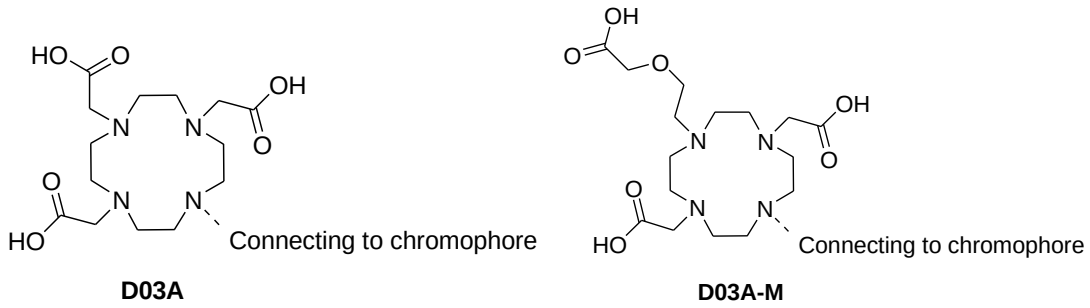

D03A **D03A-M**

Figure 2.2 The marcrocyclic ligands used in this thesis.

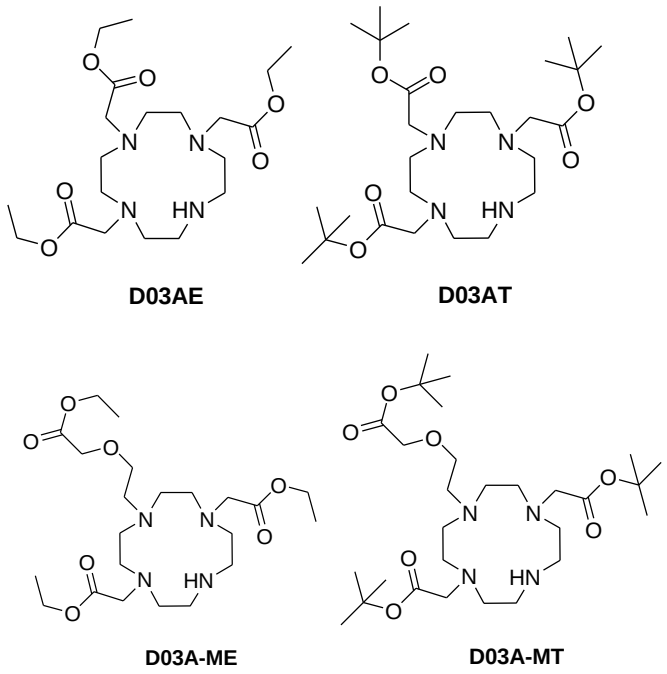

D03AE **D03AT**

D03A-ME **D03A-MT**

Figure 2.3 The protected marcrocyclic ligands used in this thesis.

2.2 Synthesis of marcocyclic compounds

Synthesis of DO3AT

The general synthetic scheme for the preparation of **DO3AE** and **DO3AT** ligands involved the tri-alkylation of cyclen at 1,4,7 positions with their ester side arm, as illustrated in **Scheme 2.1**. **DO3AE** or **DO3AT** were prepared by a reaction between cyclen and an appropriate amont of ethyl bromoacetate/tert bromoacetate under mild basic conditions ($NaHCO_3$) at room temperature for two days. A long reaction time would ensure the completed reaction to yield trisubstituted desired product. High

temperature or stronger bases such as cesium carbonate led to majority of the side product tetra-substituted analogue. For **DO3AE**, the product was isolated by purification using column chromatography over silica gel (MeOH in DCM) with yield 40%. For **DO3AT**, the product was isolated by hot filtration from hot diethyl ether. Yield was 61%

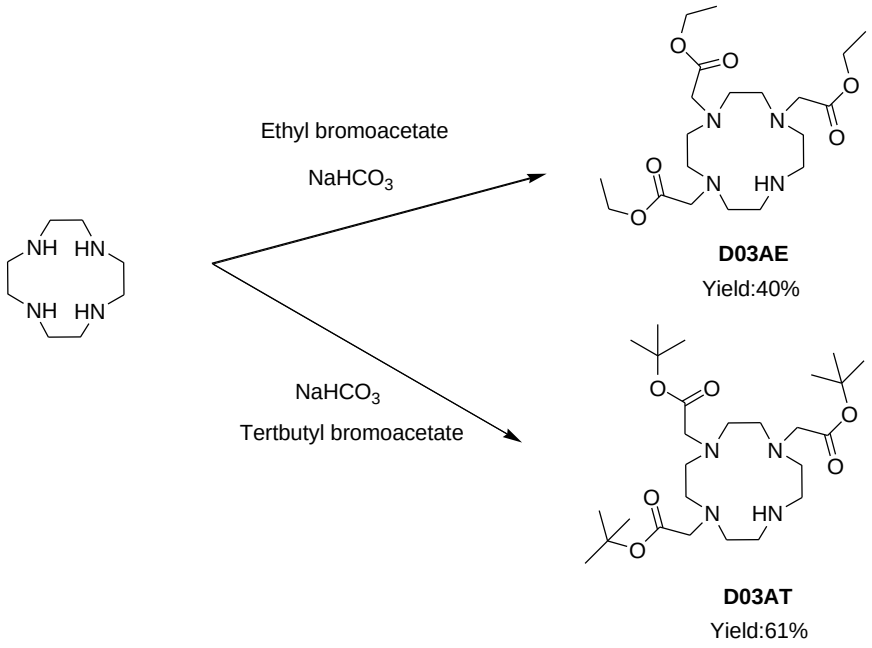

Scheme 2.1 General synthetic procedure for **DO3AE** and **DO3AT**.

Synthesis of pendant arms tert-butyl 2-(2-chloroethoxy)acetate and ethyl 2-(2-chloroethoxy)acetate

The synthesis of pendent arms was shown in **Scheme 2.2**. Tert-butyl 2-(2-chloroethoxy)acetate is an intermediate of synthesis of ethyl 2-(2-chloroethoxy)acetate. First, bromoacetate was mixed with chloroethanol with sodium hydroxide to afford tert-butyl 2-(2-chloroethoxy)acetate. (Yield:72%) Then, the basic deprotection afforded 2-(2-chloroethoxy)acetic acid with a yield of 84%. The final step was esterification catalyzed by a few drops of concentrated sulphuric acid. The reaction was reflux overnight and purified through solvent extraction with DCM. The yield was 70%.

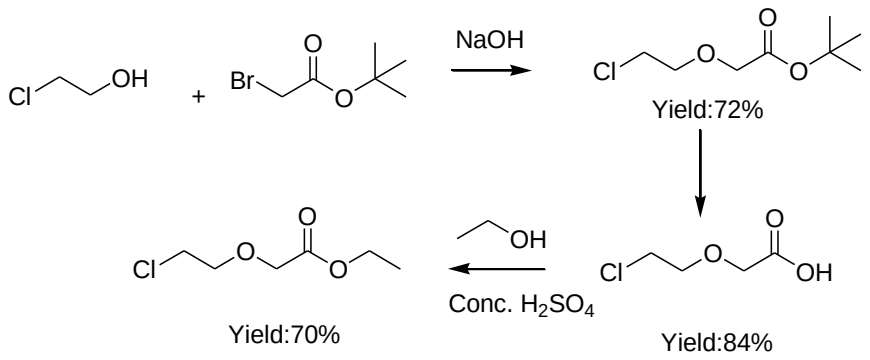

Scheme 2.2 Synthetic procedure for tert-butyl 2-(2-chloroethoxy)acetate and ethyl 2-(2-chloroethoxy)acetate.

Synthesis of DO3A-ME and DO3A-MT

The synthesis of **DO3A-ME** is illustrated in **Scheme 2.3**. 1,4,7,10-tetraazacyclododecane has selective alkylation at 1,4 postion by benzyl chloroformate (CbzCl) in the phosphate buffer (pH 3) to afford **2A** with a yield of 51%. **2B** was prepared by mixing **2A** and alkyl bromoacide and allowed to react at room temperature overnight. The desired product could be isolated through column chromatography. Heterogeneous dehydrogenation was performed to remove Cbz protecting groups to regenerate secondary amine in 1, 4 postion. In this reaction, **2B** was stirred with a catalytic amount of Pd/C under hydrogen balloon. The final step was the nucleophilic substitution. A dropwise addition of ethyl 2-(2-chloroethoxy)acetate into the reaction mixture of **2C** and potassium carbonate was needed since the dropwise addition could prevent the formation of the tetra-substituted analogue. The desired product was isolated through column chromatography.

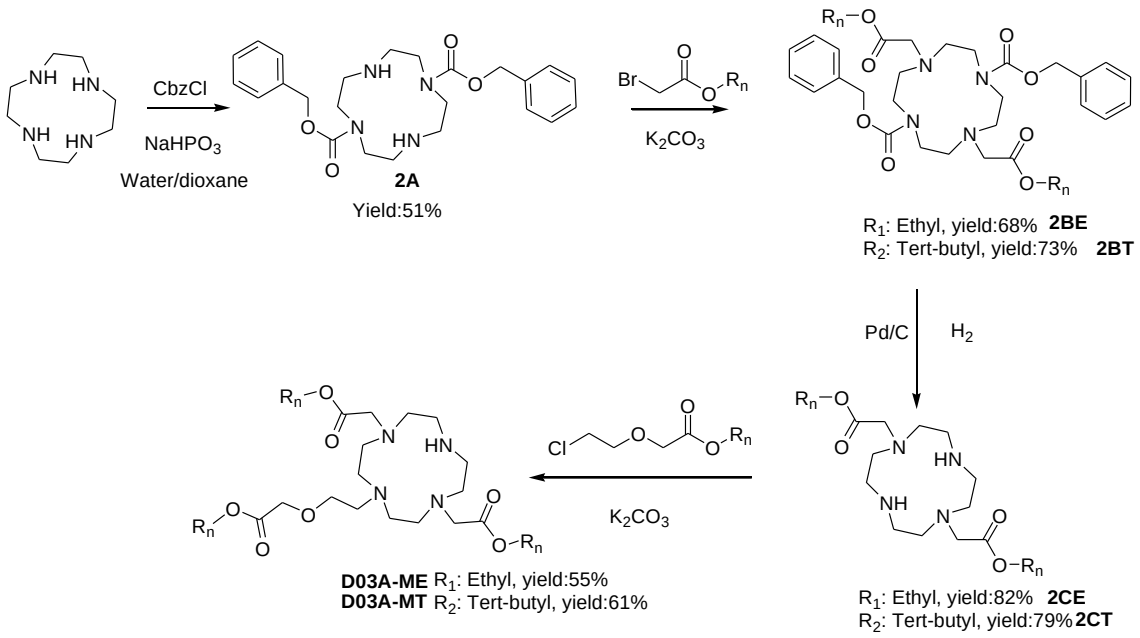

Scheme 2.3 Synthetic procedures for **DO3A-ME** and **DO3A-MT**.

To conclude, a series of macrocyclic ligands **DO3AE**, **DO3AT**, **DO3A-ME** and **DO3A-MT** were successfully synthesized with reasonable yields and used in the synthesis of sensors.

2.3 References

[1] D.R. Cabiness and D.W. Margerum, *J.Am. Chem. Soc*., 1969, **91**, 6540-6541.

[2] D.J. Cram, *Angew. Chem*., 1986, **98**, 1041-1060.

[3] D.H. Busch, *Chem. Rev*., 1993, **93**, 847-860.

[4] G. Tircso, Z. Kovacs and A.D. Sherry, *Inorg Chem*., 2006, **23**, 9269–9280.

[5] V. S. Khoo, D. P. Dearnaley, D. J.bFinnigan, A.bPadhani, S. F. Tanner and M. O. Leach, *Radiother Oncol*., 1997, **42**, 1-15.

[6] H. Ersoy and F. J. J. Rybicki, Magn. *Reson. Imaging*, 2007, **26**, 1190-1197.

CHAPTER 3

Development of lanthanide complexes for detection of H_2S

3.1 Introduction

Hydrogen sulfide (H_2S), first discovered by Carl Wilhelm Scheele [1] in 1777, is a colourless, flammable and toxic gas with a characteristic odour like that of a rotten egg. H_2S is also the third recognized endogenous gasotransmitter after NO and CO, a gaseous molecule which is synthesized and released in a biological system and can do signal transduction. Generally, gasotransmitters should have the following features. First, it should be a gas endogenously and enzymatically produced in a regulated manner. Second, it should have specific interaction with cellular targets and should utilize a specific mechanism of inactivation.

The production and metabolism of H_2S are catalyzed by enzymes such as cystathionine β-synthase (CBS), cystathionine γ-lyase (CSE) and 3-mercaptopyruvate sulfurtransferase (MST). There are four possible routes for its generation. [2] First, cystathionine that is derived from homocysteine (Hcys) is converted to cysteine (Cys) by CSE. Both CBS and CSE convert this Cys into H_2S. Second, H_2S is produced by conversion of α-ketobutyrate in the presence of CSE. Third, Asp aminotransferase (AAT) catalyzes the conversion of 3-mercaptopyruvate. Then, H_2S is released from the reaction of 3-mercaptopyruvate and MST. Fourth, Cys can be converted into pyruvate by CSE and H_2S is released. So far, it is still unclear which main pathway is responsible for H_2S biosynthesis in mammalian. Some literatures have showed that CSE is the dominant source of H_2S in peripheral tissues [3], while CBS may be mainly responsible for H_2S formation in the brain.(**Figure 3.1**)

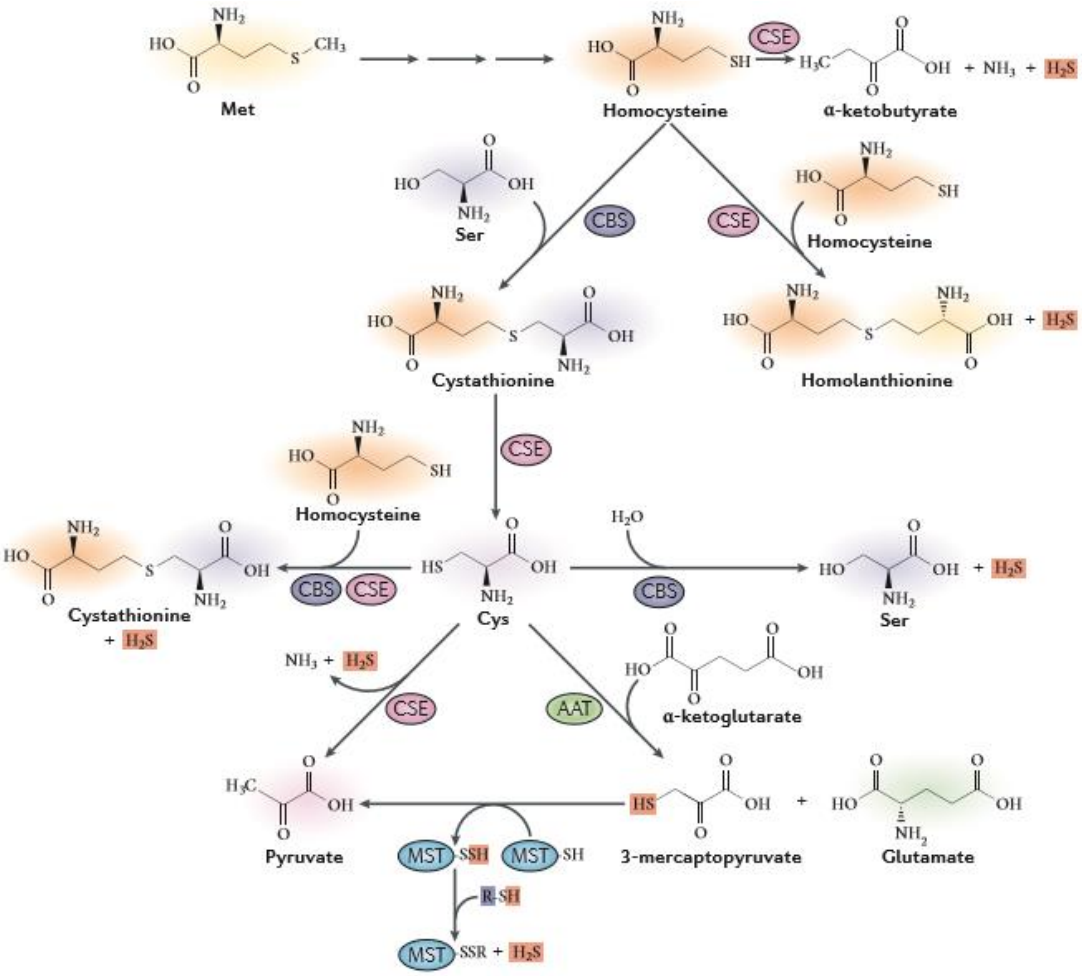

Figure 3.1 Pathways of H_2S metabolism.

H_2S is recognized as a crucial biological molecule with important physiological functions in diverse fields.[4]-[8] In cardiovascular system, H_2S dilates blood vessels, modulates the flow of blood in mircrocirculation and regulates blood pressure by controlling the opening of ATPsensitive potassium (KATP) channels in the vascular smooth muscle cells.[9][10] In neurobiology, H_2S plays as a neuromodulator and an intracellular messenger which regulates the intracellular concentration of calcium.[11] H_2S enhances N-methyl-Daspartic acid (NMDA) receptor-mediated responses[12] and detection of NMDA receptor by H_2S may be related to pain sensation.[13] In inflammation research, H_2S has both pro-inflammatory and anti-inflammatory properties to regulate inflammatory responses. When the concentration of H_2S is low, H_2S is predominantly anti-inflammatory. When the concentration of H_2S is high, H_2S promotes inflammation.

There are some classical techniques for detection of H_2S, including the methylene blue method[14] and the sulfide ion-selective electrode method.[15] Some methods are listed in the **Table 3.1**.

Method	Advantages	Disadvantages	References
Methylene blue assay	Easy protocol, performed in most reported studies of H_2S	Limited detection sensitivity; low-mid μM Prone to contamination from acid labile sulfur pools Possible color interference	[14], [16],[17]
Ion chromatography	Sensitive detection (around 30 ppb)	Poor conductivity Limited throughput	[18]
Gas chromatography/flame photometric detector (FPD	Sensitive/selective detection (ppb)	Multiple steps needed for measurement Difficult to determine different forms	[19]
Fluorescent detection of H_2S	Easy protocol Direct visualization of production Moderate detection sensitivity (μM)	Possible substance interference	[20]

Table 3.1 Comparisons of dıfferent H_2S detection methods.

Among these methods, fluorescent detection is one of the most common methods for recognizing of H_2S since it is simple, non-invasive, selective and sensitive. To date, there are three main approaches for the detection of H_2S

The first approach is reduction of azides to amines. H_2S is the reducing agent and ready to reduce N_3 into NH_2 functional group. Their electronic properties are very different.

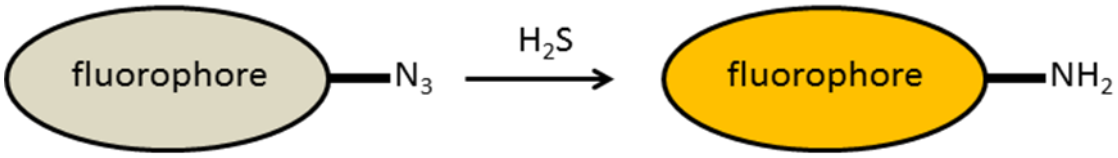

Figure 3.2 The first approach of H_2S sensing approach based on reduction of azides to amines.

The second approach is nucleophilic reaction such as aryl nitro thiolysis. H_2S can functıon as neucleophile to attack some labile group such as 2,4-dinitrophenyl (DNP) ether moiety. H_2S has pKa values of about 6.9,[21] while other typical free thiols such as Cys or GSH have higher pKa values of about 8.6.[22] So the thiolysis of 2,4-dinitrophenyl (DNP) ether moiety is more favorable to be used for detection of H_2S in physiological condition.

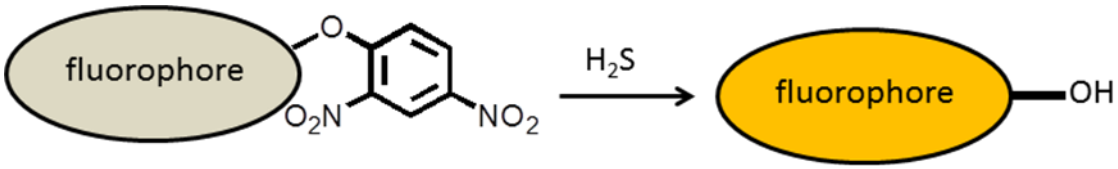

Figure 3.3 The second approach of H_2S sensing approach based on aryl nitro thiolysis.

The third approach is CuS precipitation between copper complex and H_2S. In the absence of H_2S, Cu(II) ion is chelated and affects the photophyscial properties of sensor. In the presence of H_2S, Cu(II) ion leaves and CuS is formed. Hence, the photophysical properties of sensor will be changed.

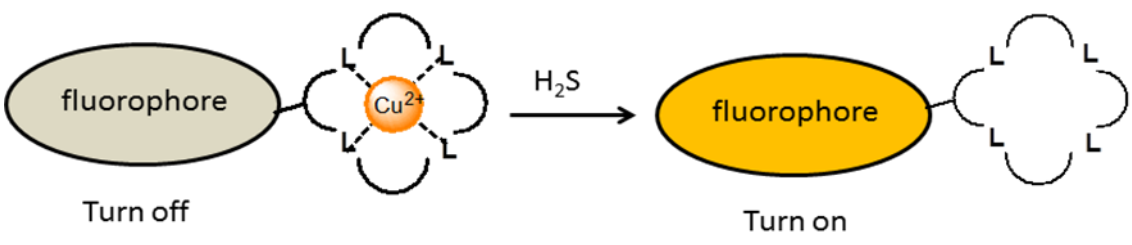

Figure 3.4 The third approach of H_2S sensing approach based on CuS precipitation.

3.2 Design of probe

The structure of the H_2S sensor **EuL1Cu** is depicted in **Figure 3.5**. It consists of three main parts, namely a reaction site for recognizing H_2S, a chromophore for sensitization of Eu(III) ion and an Eu chelator. The reaction site is a diphenylamine-Cu(II) ion complex that allows CuS precipitation after addition of H_2S. The chromophore is benzenamide, a 4-[2-(4-pyridinyl)ethynyl]derivative in which pyridine is used for direct coordination towards Eu(III) ion. The Eu chelator is a macrocycle that provides nine coordination environments for Eu(III) ion. This Eu chelator has one ethoxyacetic acid as a side arm to make the overall complex more hydrophilic and hence more water soluble.

The sensitisation mechanism of **EuL1Cu** is shown in **Scheme 3.1**. It is based on copper sulfide precipitation. In the presence of Cu(II) ion, **EuL1** uses dipicolylamine for chelation with Cu(II) ion to form **EuL1Cu** with almost completely quenched luminescence. On the addition of H_2S ($NaHS$ was used as H_2S source), Cu(II) ion is removed from dipicolylamine to form CuS and therefore the luminescence of **EuL1** is recovered.

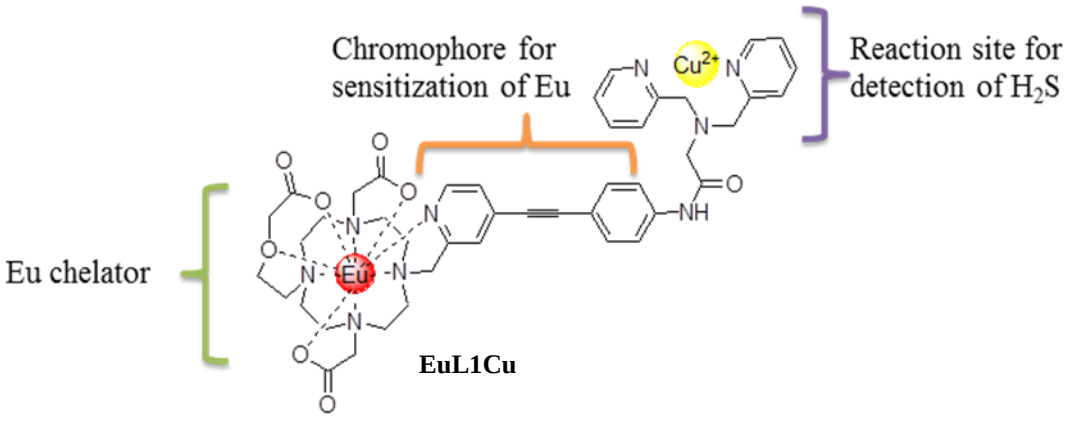

Figure 3.5 Structure of H_2S sensor **EuL1Cu**.

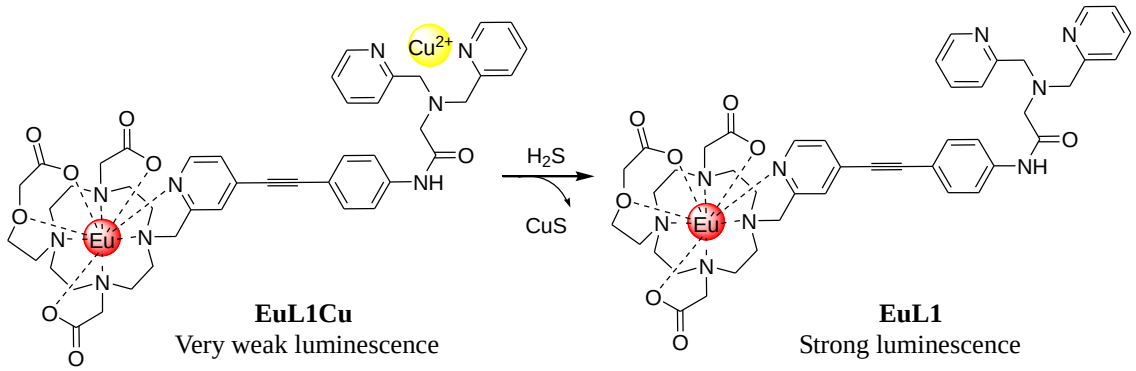

Scheme 3.1 Reaction mechanism for luminescence response of **EuL1Cu** towards H_2S.

3.3 Results and Discussion

3.3.1 Synthesis of EuL1

The synthetic routes to form complex **EuL1** are shown in the Schemes below. The seven-step synthesis of **EuL1** can be divided into four main parts, namely synthesis of the chromophore, followed by connection between the chelator and chromophore, connection with receptor bis(pyridin-2-ylmethyl)amine and deprotection of the side arm of the chelator and final metal complexation.

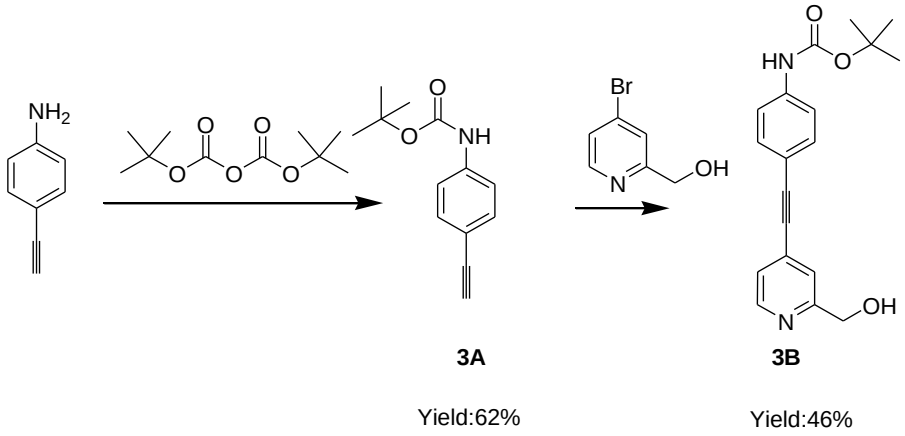

Scheme 3.2 Synthetic Routes to **3B**.

Reaction of 1.1 eqv of $(Boc)_2$ and 4-ethynylaniline was stirred under reflux and gave protected **3A** in 62% yield. This protection was crucial since protection can prevent some side reaction with amine compounds in the following reaction and decline the polarity of product to have easy purification. **3B** was prepared by the Sonogashira coupling **3A** and (4-bromopyridin-2-yl)methanol which were stirred with catalytic

amount of $PdCl_2(PPh_3)_2$, triphenylphosphine and copper(I) iodide at 70°C. After column purification, a desired yellow solid was obtained with yield 46%.

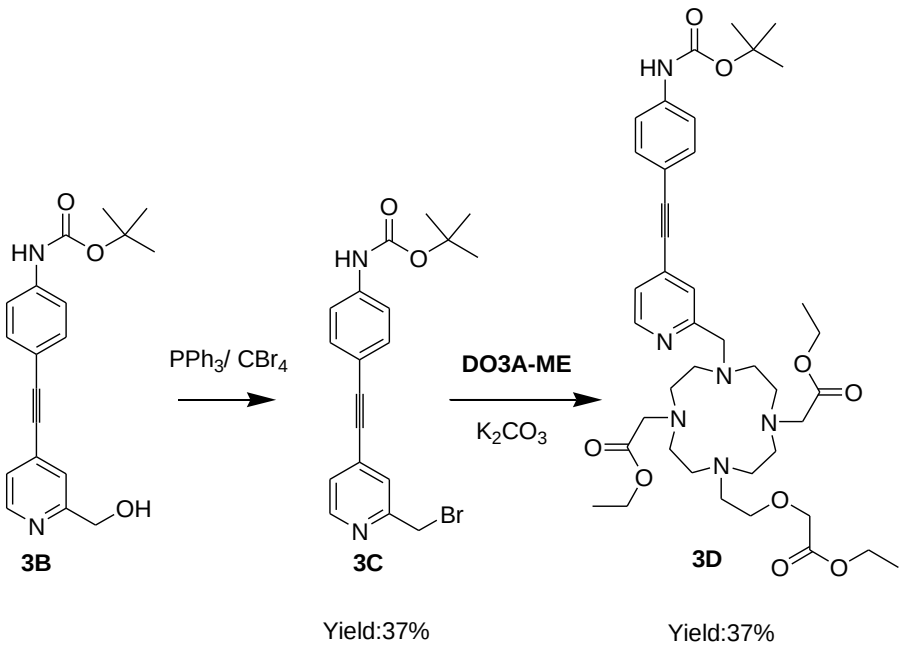

Scheme 3.3 Synthetic Routes to **3D**.

After obtaing **3B**, the next step was conversion of hydroxy functional group into some labile groups such as bromine group to allowed nucleophilic substitution with **DO3A-ME**. In this step, some synthetic methods were tried. First, some common bromination reagents such as phosphorus tribromide (PBr_3) and phosphorus pentabromide (PBr_5) were used. However, a lower yield was obtained due to the higher reactive bromination reagent and hence more side products were formed. The second method used methanesulfonyl chloride (MsCl) which can convert alcohol group into more labile OMs to allow nucleophillic substitution. However, crude OMs product was rather unstable during the column separation and it was observed that it would decompose into the starting material **3B** during column chromatography. Therefore, this method was not chosen. The final method was a mild appel reaction in which triphenylphosphine (PPh_3) and tetrabromomethanes (CBr_4) were reagents to convert alcohols into the corresponding alkyl bromine derivative under mild conditions. **3B** and

PPh_3 were mixed and CBr_4 was added to the reaction mixture and stirred for three hours at room temperature. After purification, a yield of 37% of **3C** was obtained. Bromine derivative **3C** had nucleophillic substitution with **DO3A-ME** in the presence of potassium carbonate. In this case, ethyl ester protecting group was used instead of tert-butylester protection group because the next step would be the acidic deprotection by trifluoroacetic acid (TFA). Ethyl ester protecting group would be stable in such acidic condition while tert-butylester protection group was labile in such acidic condition reaction. The isolated yield of **3D** was 37%.

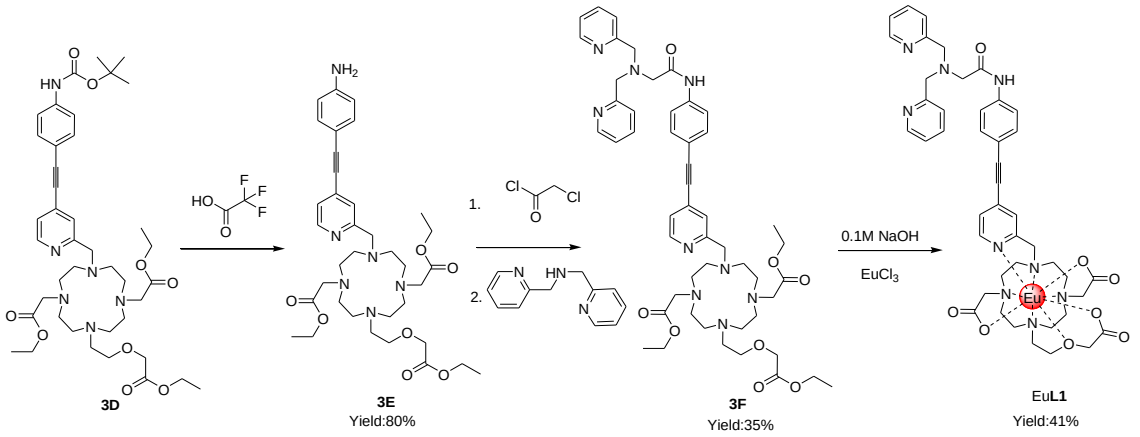

Scheme 3.4 Synthetic Routes to **EuL1**.

3E was prepared by acidic deproptection of the amine protected boc group in the presence of trifluoroacetic acid (TFA) and CH_2Cl_2 (v/v=1:1) with a yield of 85%. Then, **3F** was prepared by first reaction between **3E** and 2-chloroacetyl chloride in the presence of triethylamine. Exactly 1 eqv amount of 2-chloroacetyl chloride was added in order to eliminate any unreacted 2-chloroacetyl chloride. After confirmation of completion of reaction, 1 eqv of dipicolylamine (DPA) was added to the reaction mixture with stirring overnight. The crude product was purified through several times by column chromatography and the yield was 30%. Deprotection of tris-ethylester was done by mixing with 0.1M NaOH. Then, the pH of the solution was maintained at pH 7 and equimolar $EuCl_3.6H_20$ was added into the aqueous reaction mixture. The reaction mixture was refluxed overnight and the desired products could be obtained by

recrystallization in a mixture of the MeOH and diethyl ether or chloroform. **EuL1Cu** was prepared by mixing **EuL1** and 1 eqv of $CuCl_2$ at room temperature. The high-resolution mass spectra (ESI+) showed peaks corresponding to the double protonated Eu(III) complexes **EuL1** and **EuL1Cu** with characteristic Eu(III) isotopic pattern entities which confirmed the formation of the desired Eu(III) complexes.(**Figure 3.6** & **3.7**)

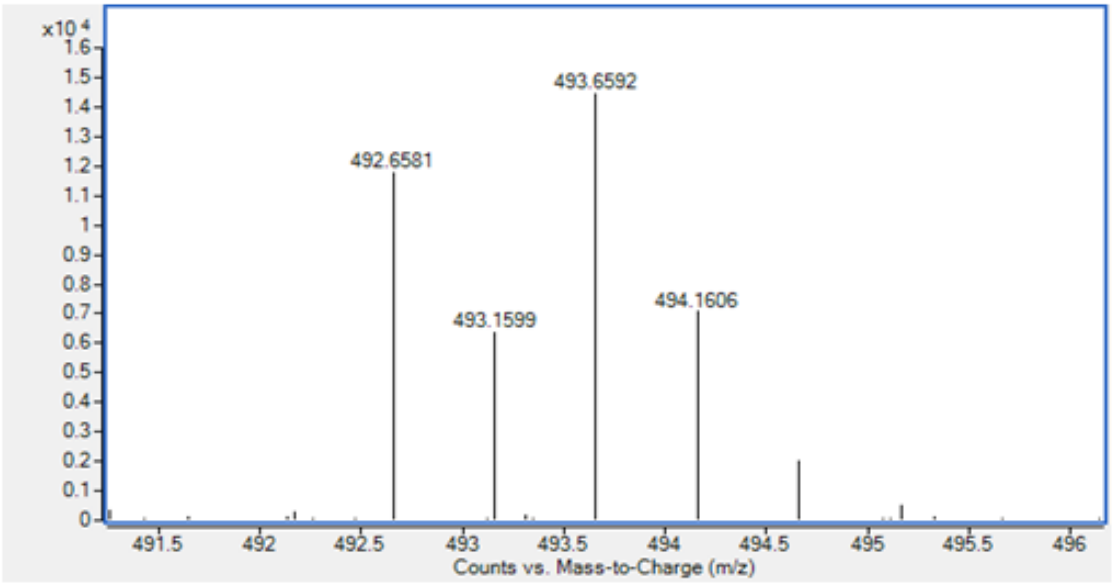

Figure 3.6 High resolution mass spectrum of **EuL1**.

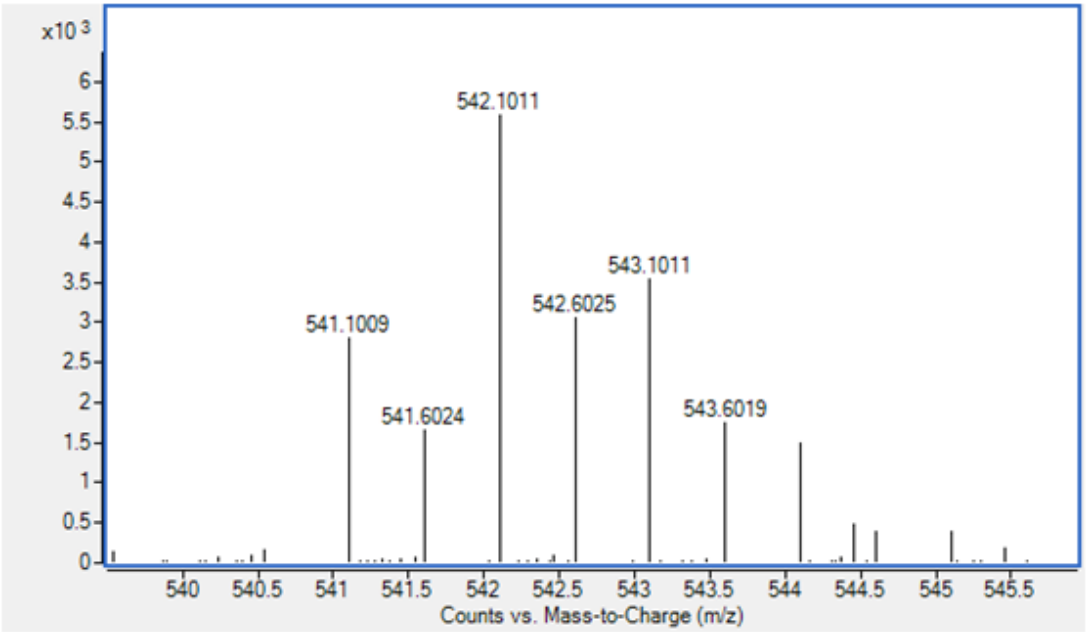

Figure 3.7 High resolution mass spectrum of **EuL1Cu**.

3.3.2 Photophysical Study

Absorption and Excitation Spectra

The photophysical properties of **EuL1** and **EuL1Cu** were studied. The UV-vis spectra of **EuL1** and **EuL1Cu** were shown in **Figure 3.8**. Their absorption bands were similar and the peak maxima centred at 325 nm which corresponded to π to π* transitions of the aromatic moieties. Their corresponding molar extinction coefficients were calculated as 11994 (**EuL1**) and 11374 (**EuL1Cu**)M^{-1} respectively. Their absorption spectra were very similar to their excitation spectra, suggesting that there was an energy transfer from the aromatic chromophore moieties to Eu(III) ion metal centres.

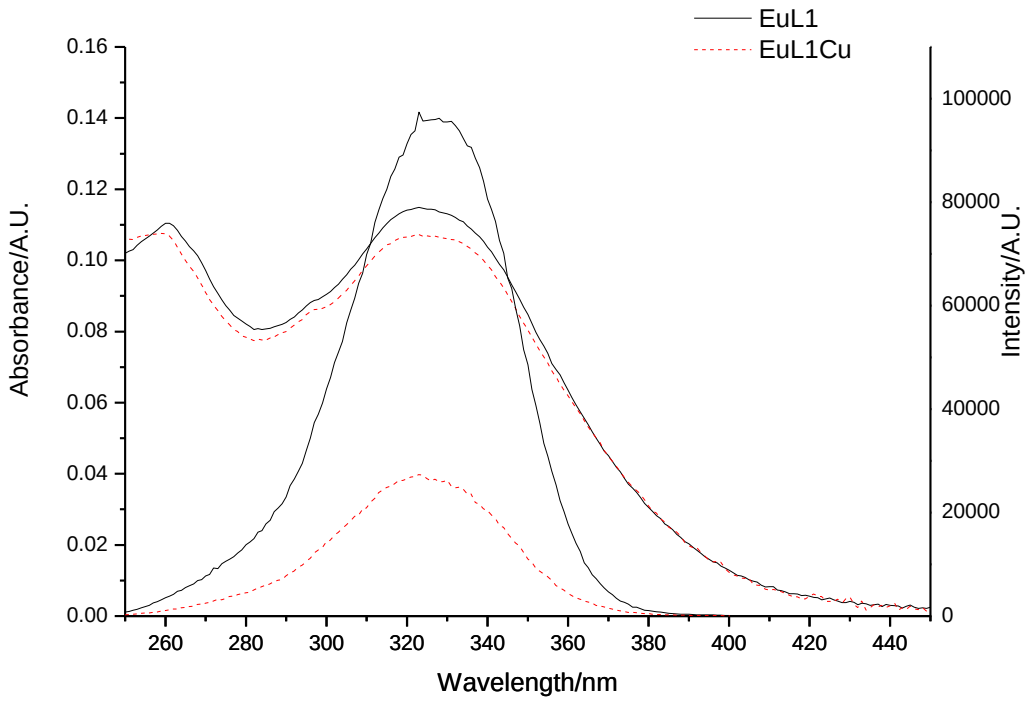

Figure 3.8 UV/Vis absorption spectra (solid line), excitation spectra (dotted lines, Eu, λ_{em} =616 nm) (black line: **EuL1** red line: **EuL1Cu** (0.01M HEPES, pH 7.4)).

Titration Emission Spectra and Job's plot

On the addition of Cu(II) ion (0-2 eqv Cu (II) ion) and upon excitation at 350 nm, there were some narrow structured emission patterns of $^5D_0 \rightarrow ^7F_J$ (J=0-4) transitions

characteristic of Eu (III) ions.(**Figure 3.9**) The luminescence of **EuL1** was gradually decreased upon the formation of Cu(II)-dipicolylamine complex moiety. During the titration with Cu(II) ion, there was one sharp component centred at 580 nm corresponding to the $^5D_0 \rightarrow {}^7F_0$ transition of Eu(III) complexes, indicating there was only one single species in solution.

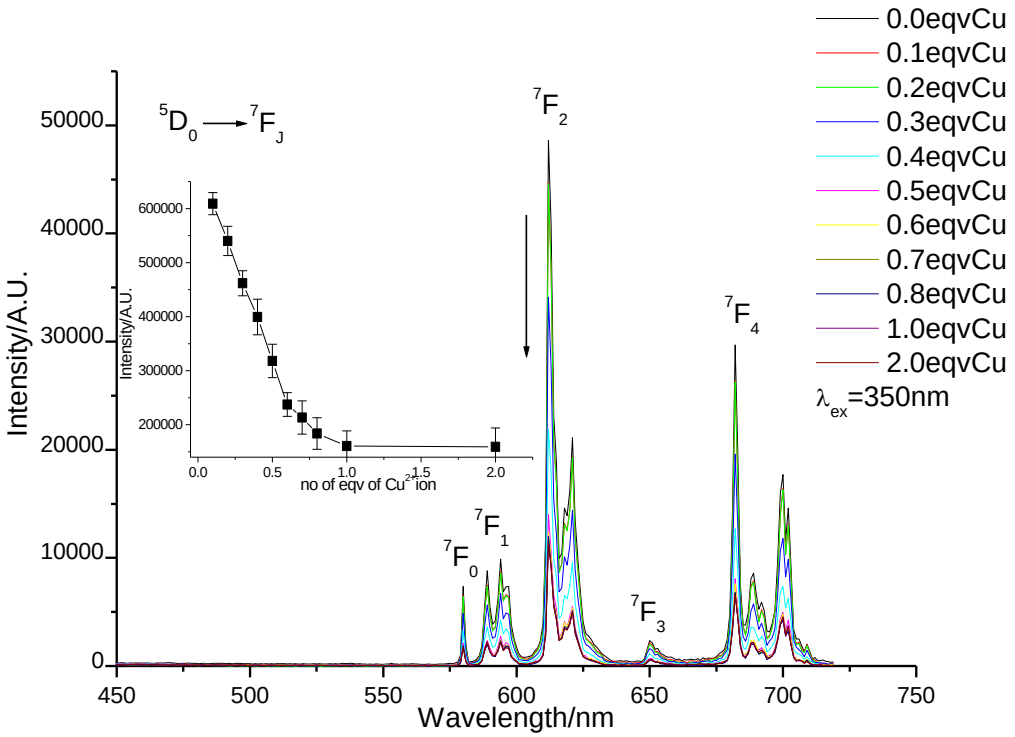

Figure 3.9 Emission spectra of 10 µM aqueous solution upon addition of aliquots of various eqv of Cu(II) ions with respect to **EuL1** (0.01M HEPES, pH=7.4, λ_{ex}=350nm). Inert: Luminescence response of europium emission intensity (λ= 612 nm) to changing Cu(II) ion.

$^5D_0 \rightarrow {}^7F_2$ transition (I_{ED}) is the electric dipole and hypensensitive and its intensity is affected by local symmetry of the Eu (III) ions and ligand. This splitting of hypersensitive $^5D_0 \rightarrow {}^7F_2$ transition did not change significantly during the titration. Therefore, Cu(II) ion did not affect the coordination environment of Eu(III) ion significantly. $^5D_0 \rightarrow {}^7F_1$ (I_{MD}) is magnetic dipole transition whose intensity is

independent of the crystallographic site of the Eu (III) ions. The I_{ED} /I_{MD} ratios, which usually gives information of the chemical environments and symmetries of Eu(III) ions, were 3.78 (**EuL1Cu**) and 3.70 (**EuL1**), indicating that symmetries of the Eu(III) ions were not be influenced by titration of Cu(II) ion. Job's plot was used to determine the stoichiometry of a binding event between Cu(II) ion and **EuL1**. In **Figure 3.10**, there was a peak at 0.5 of Cu(II) ion/Cu(II) ion and complex, indicating that the optimal binding mode between **Eu L1** and Cu(II) ion was 1:1.

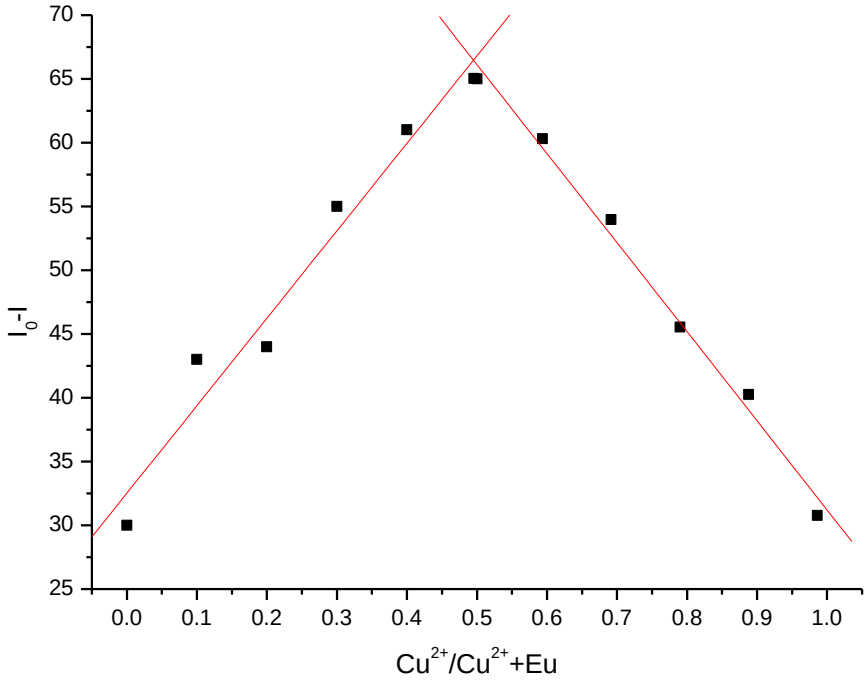

Figure 3.10 Job's plot of **EuL1** and Cu(II) ion.

Quantum yield

The quantum yield was the ratio of the amount of absorption of photons to the amount of emission of photons from the Eu(III) ion centre through luminescence. It can be calculated by two methods, including a comparative method and an absolute method. Herein, the comparative method was used to measure the relative quantum yields of **EuL1** against quinine sulfate (Φ = 0.577)[23] at excitation of 350 nm. By keeping the

constant excitation wavelength of 350 nm and absorbance of sample and standard solution below 0.1, the relative quantum yields were calculated as 6.40% (**EuL1**) and 0.68% (**EuL1Cu**) respectively.

Binding constant

Moreover, the binding constant (K) of **EuL1** towards Cu(II) ion calculated from luminescence titration data was 74026±2899.0M^{-1}.(**Figure 3.11**) It was larger than the binding constants towards other cations inculding Fe(II) ion (7951±936.0M^{-1}), Co(II) ion (16713±3342.0M^{-1}) and Ni(II) ion (15210±3042.0M^{-1}).(**Figure 3.12-3.14**) Therefore, **EuL1** had better interaction with Cu(II) ion than the other cations.

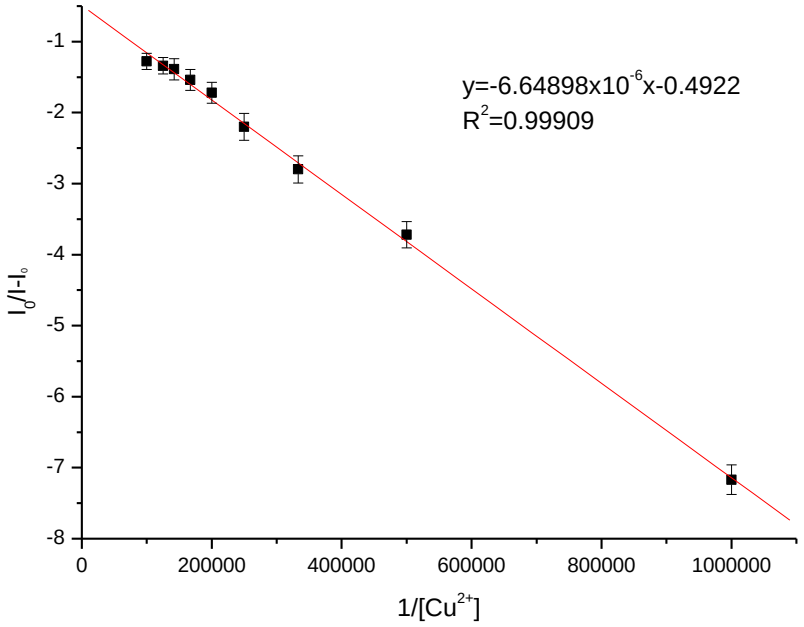

Figure 3.11 Fitting of fluorescence Cu(II) ion titration curve of **EuL1**.

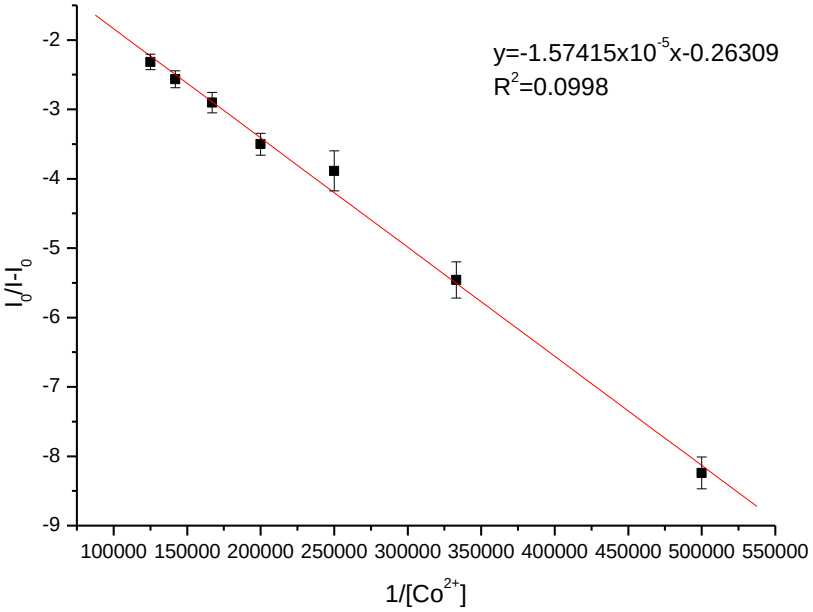

Figure 3.12 Fitting of fluorescence Co(II) ion titration curve of **EuL1**.

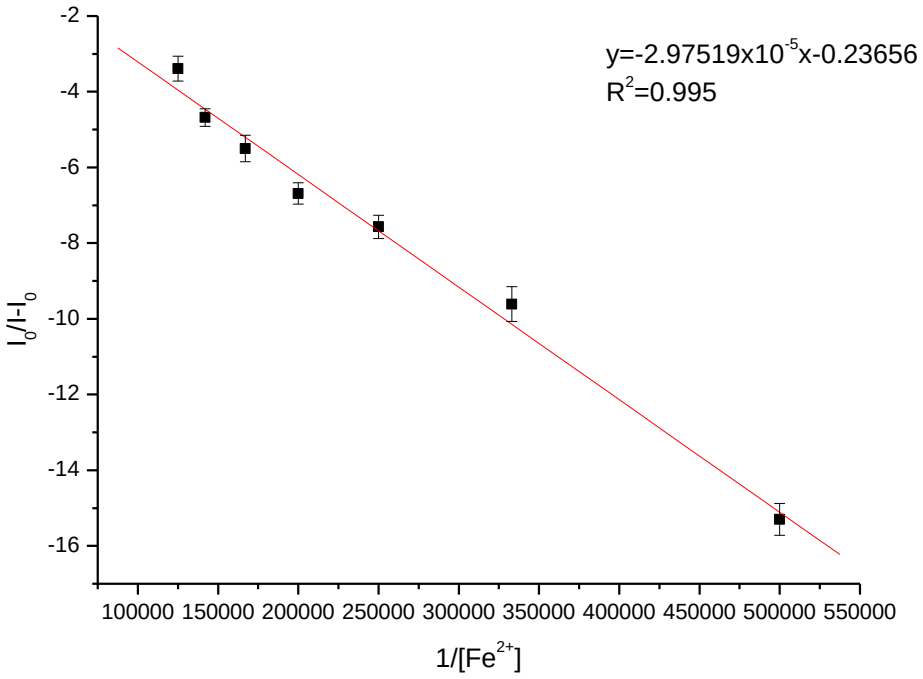

Figure 3.13 Fitting of fluorescence Fe(II) ion titration curve of **EuL1**.

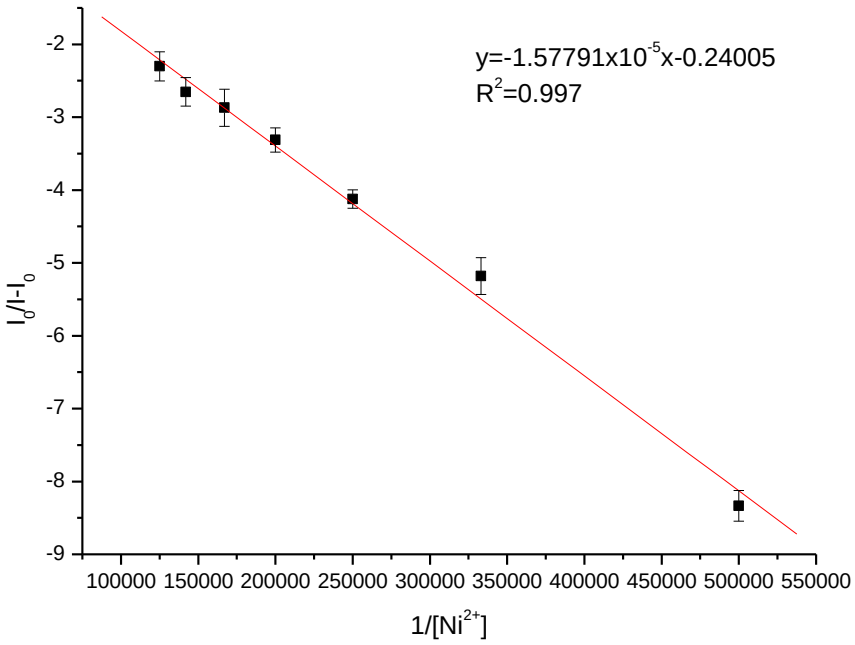

Figure 3.14 Fitting of fluorescence Ni(II) ion titration curve of **EuL1**.

Lifetime time and q value

Knowing the number of water molecules coordinated to a Eu(III) ion is important in understanding the nature and coordination environment of Eu(III) complexes in solution. The q value is a value that allows the prediction of the number of water molecules in the first coordination sphere of a Eu(III) ion. The q values of **EuL1** and **EuL1Cu** were determined by the measuring the luminescence lifetimes in H_2O and D_2O upon emission at 612 nm. The lifetime of Eu(III) complexes in H_2O was 0.97 ms which was shorter than that in D_2O (1.3ms). The lifetime in H_2O was similar to the lifetime in HEPES. All the lifetime data were fitted by mono-exponential dacays, indicating the presence of only one species in solution state. Based on their lifetimes in H_2O and D_2O, the q value was calculated as zero in the absence or presence of Cu(II) ion, suggesting there was no water molecule in the first coordination sphere of a Eu(III) ion before or after addition of Cu(II) ion.

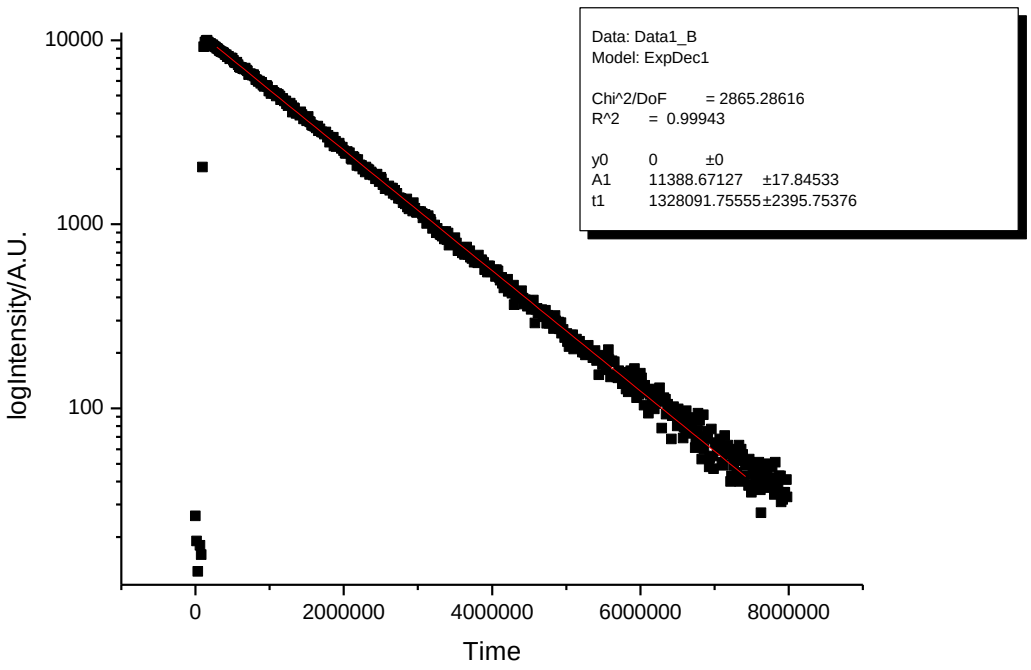

Figure 3.15 Decay curve of luminescence lifetime measurement of **EuL1Cu** in D_2O.

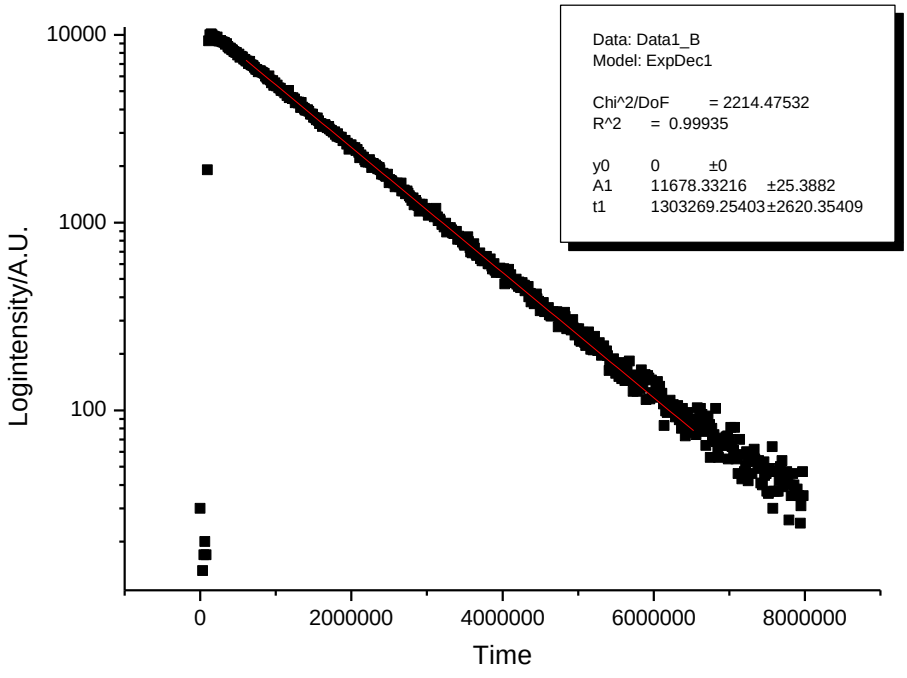

Figure 3.16 Decay curve of luminescence lifetime measurement of **EuL1** in D_2O.

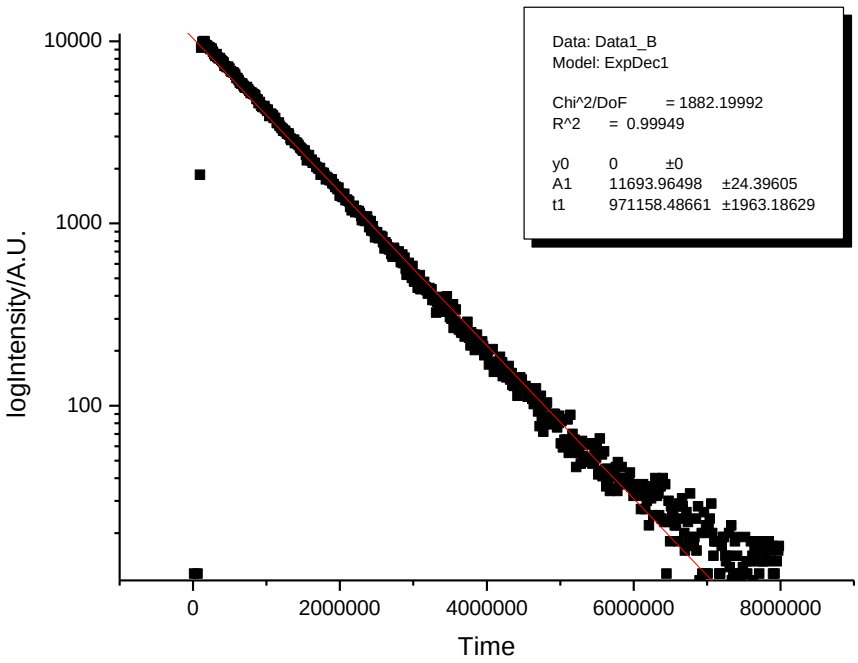

Figure 3.17 Decay curve of luminescence lifetime measurement of **EuL1** in H_2O.

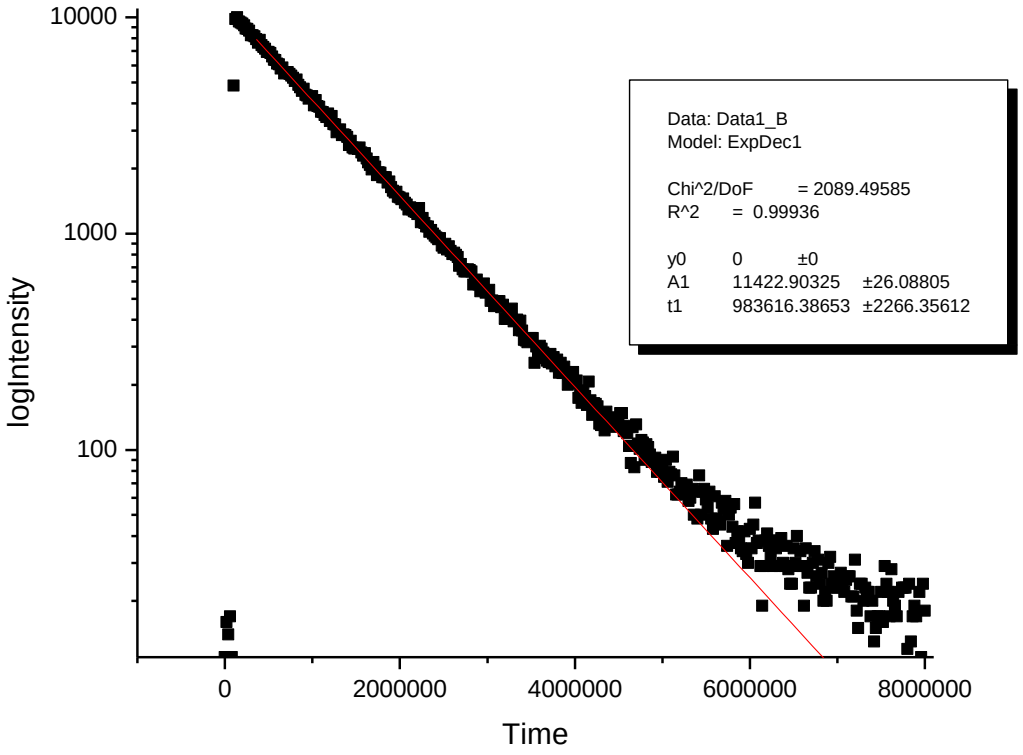

Figure 3.18 Decay curve of luminescence lifetime measurement of **EuL1Cu** in H_2O.

Selectivity test of EuL1 towards cations

The luminescent response of **EuL1** towards various cations was evaluated in 10 mM HEPES buffer (pH 7.4) **(Figure 3.19**) Upon the addition of important alkali and alkaline earth cations such as 0.1M Na(I) ion, 0.1M K(I) ion, 0.1mM Ca(II) ion, 0.1mM Mg(II) ion and 1 eqv of Ba(II) ion, there were no significant changes in the luminescent response of **EuL1**. The addition of 1eqv of transition metal ion such as Zn(II) ion, Hg(II) ion and Cd(II), Mn(II) ion, Fe(II) ion displayed negligible quenching luminescence of **EuL1**. Upon addition of Co(II) and Ni(II) ion, there was only slight quenching of signal of **EuL1**. The addition of Cu(II) ion can quench the luminescence of **EuL1** due to coordination of paramagnetic Cu(II) ion centre to dipicolylamine. The highest quenching efficiency for chelation of Cu(II) ion (I_0-I)/I_0x100%=76%) resulted. Moreover, **EuL1** can distinguish Cu(II) ion from Cu(I) ion and other anions such as ATP, GSH, cysteine, and BSA. Those anions did not affect luminescent response of **EuL1** significantly.

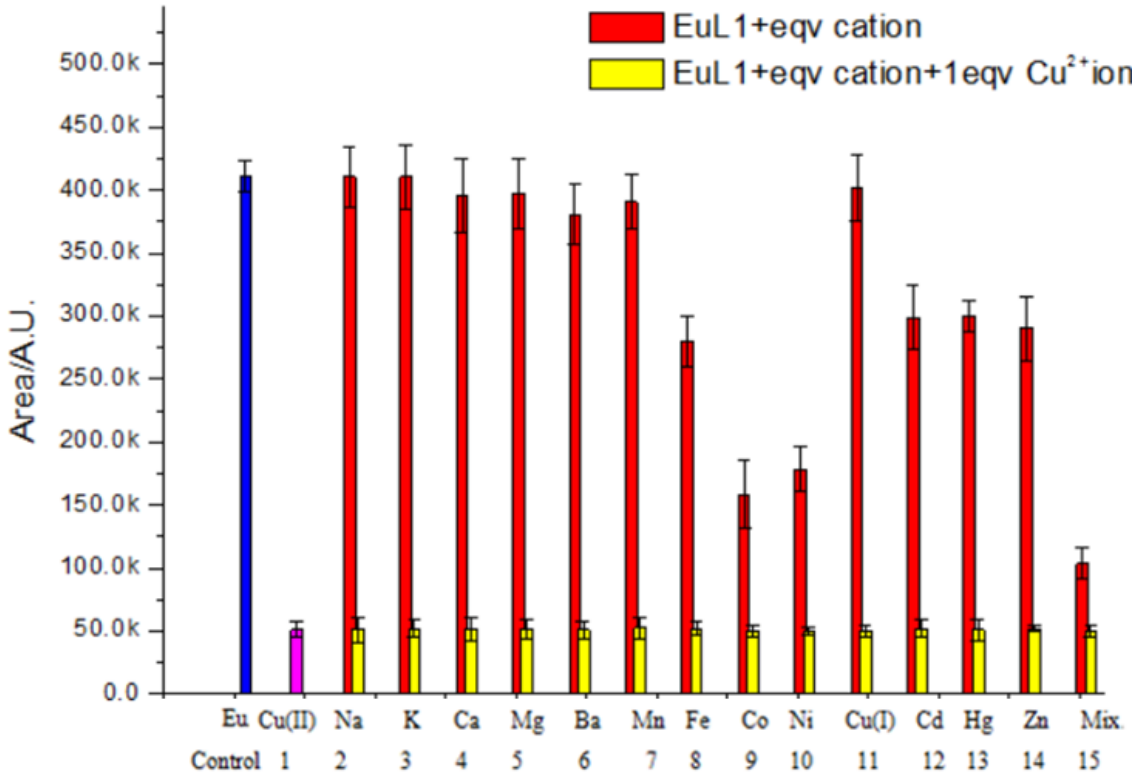

Figure 3.19 The luminescence intensity changes of [**EuL1**] (10 μM) in 10 mM HEPES with/without Cu(II) ion (excitation: 350 nm). Control 1: **EuL1 only**, 1: **EuL1**+1eqv Cu(II) ion only, 2: 0.1M Na(I) ion, 3: 0.1M K(I) ion, 4: 0.1mM Ca(II) ion, 5: 0.1mM Mg(II) ion, 6: 1eqv Ba(II) ion, 7. 1eqv Mn(II) ion, 8. 1eqv Fe(II) ion, 9. 1eqv Co (II) ion, 10. 1eqv Ni (II) ion, 11: 1eqv Cu(I) ion, 12: 1eqv Cd(II) ion, 13: 1eqv Hg(II) ion, 14: 1eqv Zn(II) ion, 15 (red bar): mixture of cations from 2 to 14, 15 (yellow bar): mixture of cations from 2 to 14 +1eqv Cu(II)ion.

Cations/Anions	Titration range	Effect
Na(I) ion	0 eqv to 5 eqv	No significant change
K(I) ion	0 eqv to 5 eqv	No significant change
Ca(II) ion	0 eqv to 5 eqv	No significant change
Mg(II) ion	0 eqv to 5 eqv	No significant change
Ba(II) ion	0 eqv to 5 eqv	No significant change
Mn(II) ion	0 eqv to 5 eqv	No significant change
Fe(II) ion	0 eqv to 5 eqv	Slightly quenched
Co(II) ion	0 eqv to 5 eqv	quenched
Ni(II) ion	0 eqv to 5 eqv	quenched
Cu(I) ion	0 eqv to 5 eqv	No significant change
Cd(II) ion	0 eqv to 5 eqv	Slightly quenched
Hg(II) ion	0 eqv to 5 eqv	Slightly quenched
Zn(II) ion	0 eqv to 5 eqv	Slightly quenched
BSA	0 eqv to 5 eqv	No significant change
ATP	0 eqv to 5 eqv	No significant change
GSH	0 eqv to 5 eqv	No significant change
Cysteine	0 eqv to 5 eqv	No significant change

Tabele 3.1 Summary of titration result of **EuL1** with various cations/anions.

Reverse titration had been performed.(**Figure 3.20**) In this titration, **EuL1** was first mixed with the 1 eqv of Cu(II) ion, followed by addition of other cations. The aim of this titration was to confirm whether the signal of **EuL1** towards Cu(II) ion would be altered once **EuL1** had been chelated with Cu(II) ion. The result showed that response of **EuL1Cu** was not significantly affect by the presence of various cations, including Na(I) ion, K(I) ion, Ca(II) ion, Mg(II) ion, Hg(II) ion, Cd(II) ion, Mn(II) ion and Fe(II) ion. Moreover, when NaHS was added into the solution of **EuL1Cu** and heavy cations,

the emission was recovered. In this case, the sensing of H_2S could not be affected by the presence of common metal cations.

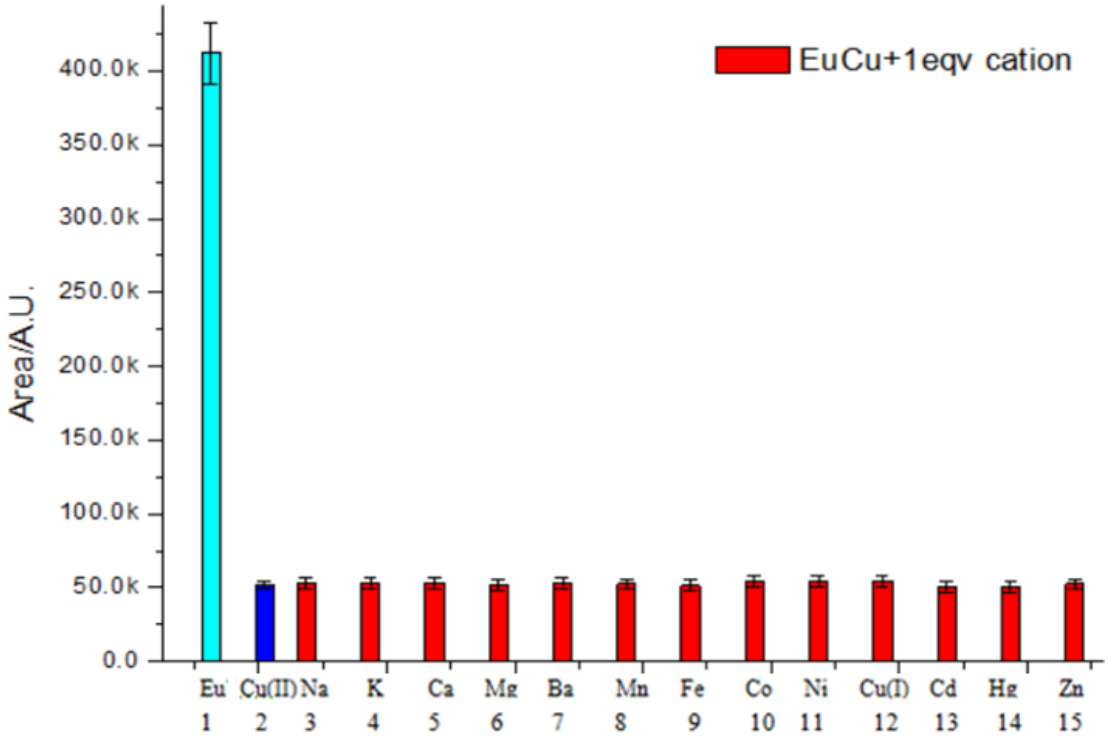

Figure 3.20 The luminescence intensity changes of [**EuL1Cu**] (10 μM) in 10 mM HEPES (reverse titration for 1 to 14: Cu(II) ion was first added to **EuL1**, then cation was added) (excitation: 350 nm). Control: **EuL1 only**, 1: **EuL1**+1eqv Cu(II) ion, 2: 0.1M Na(I) ion, 3: 0.1M K(I) ion, 4: 0.1mM Ca(II) ion, 5: 0.1mM Mg(II) ion, 6: 1eqv Ba(II) ion,7: 1eqv Mn(II) ion,8. 1eqv Fe(II) ion, 9. 1eqv Co(II) ion, 10. 1eqv Ni(II) ion, 11. 1eqv Cu(I) ion, 12: 1eqv Cd(II) ion, 13: 1eqv Hg(II) ion, 14: 1eqv Zn(II) ion.

Titration emission spectra of EuL1Cu with H_2S

Since there is strong affinity of H_2S with Cu(II) ion, the luminescence of **EuL1Cu** could be gradually recovered during titration from 0.0 eqv to 3.0 eqv of H_2S. (**Figure 3.21**) There were eight folds enhancement in terms of quantum yield before and after addition of 1eqv of H_2S into **EuL1Cu**. The shapes of splitting of hypersensitive $^5D_0 \rightarrow {}^7F_2$ transition were very similar, indicating that the coordination environment of Eu(III) ions was similar during H_2S titration. Several control experiments were also performed to show the selectivity for H_2S, such as GSH, cyteine. However, no

significant observation would be obtained. Moreover, there were not any significant changes in the signal of **EuL1** if H_2S (even in excess amount) was added into **EuL1**, suggesting **EuL1** did not respond towards H_2S significantly. Some thiol derivatives such as glutathione and cyteine had similar results.

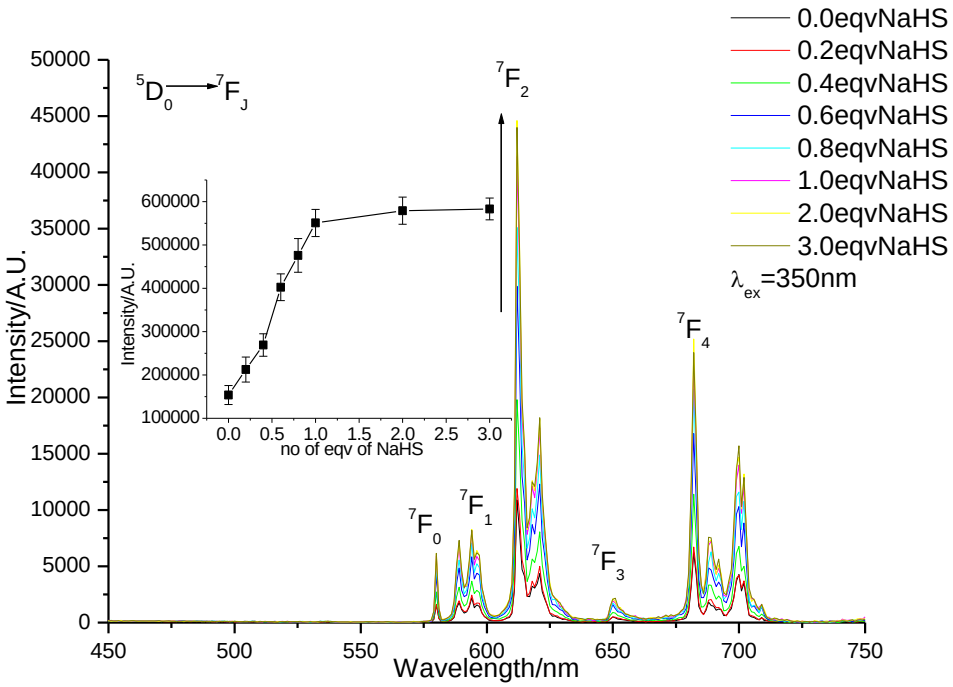

Figure 3.21 Emission spectra of 10 μM aqueous solution upon addition of aliquots of various equiv of NaHS with respect to **EuL1Cu** (0.01M HEPES, pH=7.4, λ_{ex}=350nm). Inert: Luminescence response of europium emission intensity (λ= 612 nm) to changing H_2S.

Selectivity test of EuL1Cu towards other anions

The luminescence response of **EuL1Cu** towards various anions, including sulfur species such as $NaHSO_3$, Na_2SO_4, $Na_2S_2O_3$, glutathione (GSH), cysteine and other important biological anions such as Na_2HPO_4, $NaHCO_3$, sodium citrate, sodium ascorbate, KI, KBr, pyrophospate, potassium acetate, was measured in 10 mM HEPES buffer (pH 7.4) upon excitation of 350nm.(**Figure 3.24**) Upon addition of 10 eqv of sulfur compounds such as $NaHSO_3$, Na_2SO_4, $Na_2S_2O_3$, glutathione (GSH), cysteine,

there were negligible changes in the luminescence of **EuL1Cu**. Cysteine and GSH which had SH group but did not interfere with the signal of **EuL1Cu** so much. Dipicolylamine could chelate with Cu(II) ion strongly to form a very stable complex.

Upon addition of H_2S to the solution which contained **EuL1Cu** and other anions, there was a recovery of luminescence, indicating that H_2S was the only one to remove Cu(II) ion from dipicolylamine and form precipitation of copper sulfide (CuS) and regenerated **EuL1**. Moreover, the addition of other important biological anions including Na_2HPO_4, $NaHCO_3$, sodium citrate, sodium ascorbate, KI, KBr, pyrophospate, potassium acetate, led to no observable luminescence changes of **EuL1Cu** due to the high stability of the Cu(II) ion-dipicolylamine complex. Based on the above results, **EuL1Cu** could detect H_2S selectively in the presence of other anions.

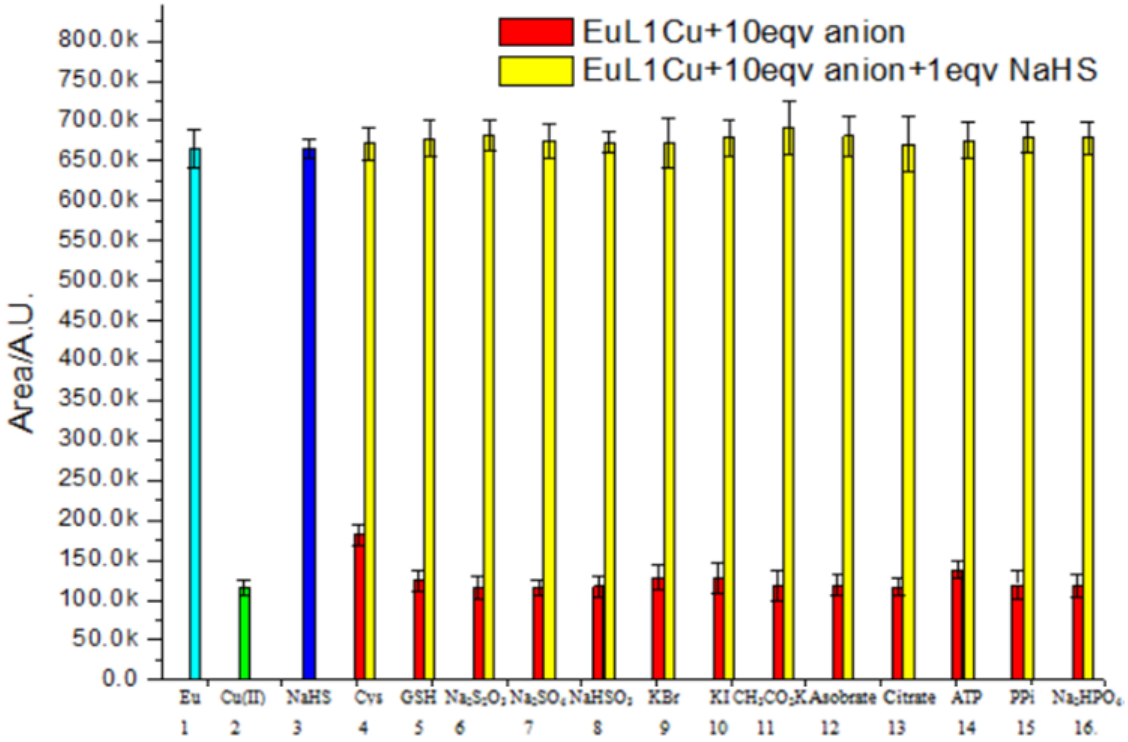

Figure 3.22 The luminescence intensity changes of [**EuL1Cu**] (10 μM) in 10 mM HEPES with/without (excitation: 350 nm). 1: **EuL1** only, 2: **EuL1** + 1eqv Cu(II) ion, 3. **EuL1** + 1eqv Cu(II) ion+1 eqv NaHS, 3: cysteine (Cys), 5: glutathione (GSH), 6: $Na_2S_2O_3$, 7: Na_2SO_4, 8: $NaHSO_3$, 9: KBr, 10: KI, 11: potassium acetate, 12: sodium ascorbate, 13: sodium citrate, 14: ATP, 15: pyrophosphate(PPi), 16: Na_2HPO_4.

Anions	Titration range	Effect
Cysteine	0 eqv to 10 eqv	No significant change
GSH	0 eqv to 10 eqv	No significant change
$NaHSO_3$	0 eqv to 10 eqv	No significant change
$NaSO_4$	0 eqv to 10 eqv	No significant change
$Na_2S_2O_3$	0 eqv to 10 eqv	No significant change
ATP	0 eqv to 10 eqv	No significant change
pyrophosphate	0 eqv to 10 eqv	No significant change
Na_2HPO_4	0 eqv to 10 eqv	No significant change
KI	0 eqv to 10 eqv	No significant change
KBr	0 eqv to 10 eqv	No significant change
Potassium acetate	0 eqv to 10 eqv	No significant change
Sodium citrate	0 eqv to 10 eqv	No significant change
Sodium asorbate	0 eqv to 10 eqv	No significant change

Tabele 3.2 Summary of titration result of **EuL1Cu** with various anions.

Reverse titration was performed. In this titration, NaHS was first added to **EuL1Cu** to regenerate **EuL1**, then other anions were added. The aim of this titration was to confirm whether the signal of **EuL1Cu** towards H_2S would be altered after addition of other anions. Based on the result (**Figure 3.23**), the luminescence after addition of anions was similar to the luminescence of **EuL1Cu** with H_2S. This revealed that after the regeneration of **EuL1,** the luminescence intensity of **EuL1** did not interfere with the other anions. Therefore, **EuL1Cu** could respond to the target H_2S in the presence of other anion.

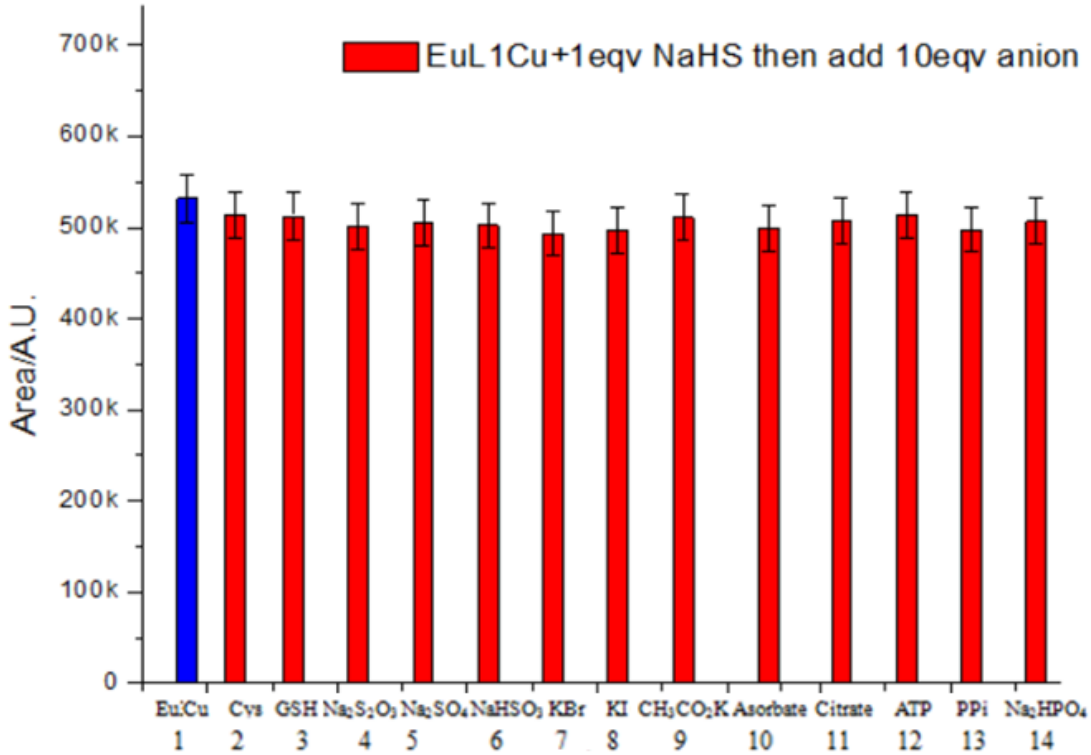

Figure 3.23 The luminescence intensity changes of [**EuL1Cu**] (10 μM) in 10 mM HEPES (excitation: 350 nm). 1: **EuL1Cu** + 1eqv NaHS, 2: cysteine, 3: glutathione (GSH), 4: $Na_2S_2O_3$, 5: Na_2SO_4, 6: $NaHSO_3$,7: KBr, 8: KI, 9: potassium acetate, 10: sodium ascorbate, 11: sodium citrate, 12: ATP, 13: pyrophospate, 14: Na_2HPO_4.

On-off-on type luminescence

It was observed that there was an on-off switchable change in the luminescence of the complex upon alternative addition of Cu(II) ion and H_2S to solution of **EuL1**. **Figure 3.24** demonstrates that such reversible interconversion can be repeated in at least four cycles by alterative addition of Cu(II) ion and H_2S, indicating that **EuL1** could be a good candidate for development of on-off-on probe for detection of Cu (II) ion and H_2S.

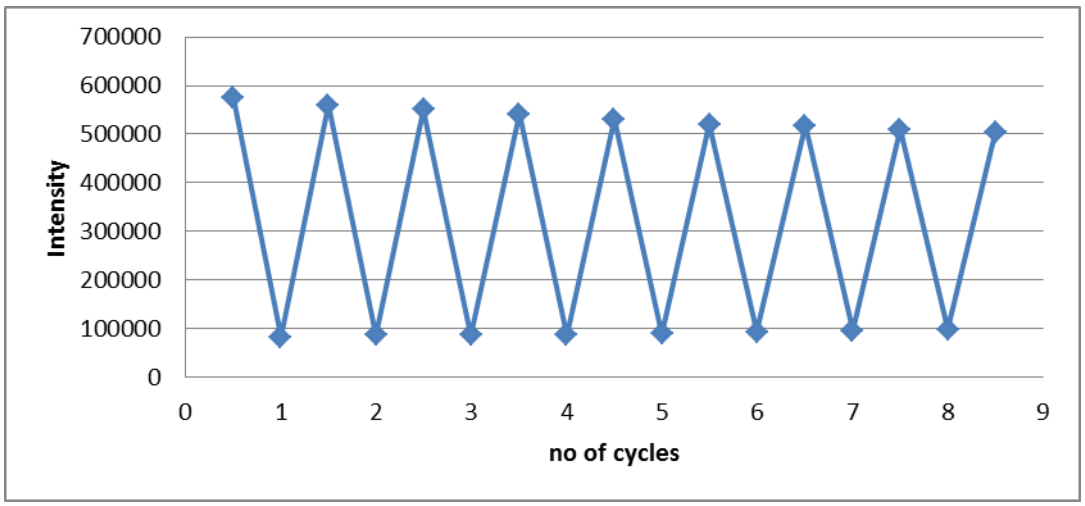

Figure 3.24 Luminescence intensity of **EuL1** (10μM) in 10mM HEPES (pH 7.4) on alternate addition of Cu(II) ion and H_2S. Each measurement was done after 60 min of an equilibrium from addition of each Cu(II) ion or H_2S.

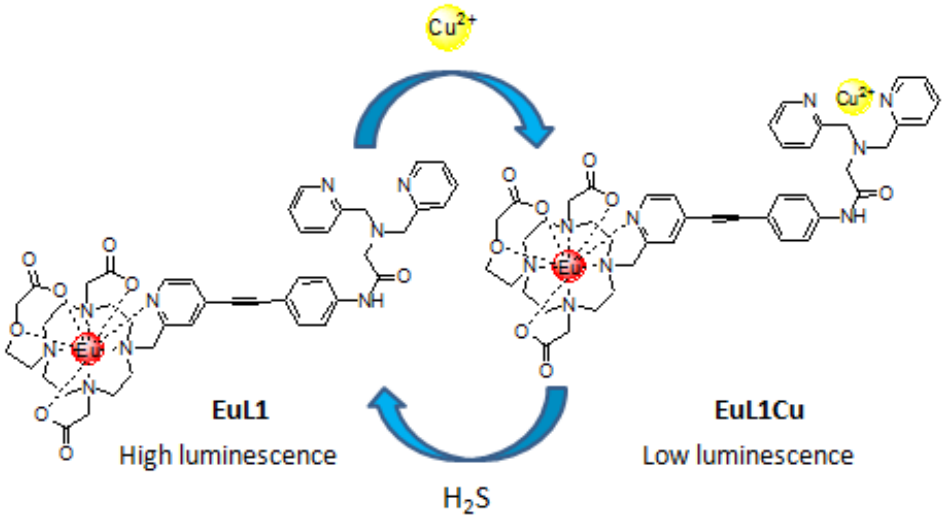

Scheme 3.5 Reaction mechanism for luminescence response of **EuL1** towards Cu(II) ion and **EuL1Cu** towards H_2S.

Low temperature mesearment

The emission spectrum of Gd(III) complex was measured at low temperature at 350 nm excitation to estimate the phosphorescence band and reveal the energy transfer process of **EuL1**. The singlet was estimated by referring to the UV−vis upper absorption edge of the Gd(III) complexes. The singlet ($^1\pi\pi^*$) energy level was determined to be approximate 410 nm (24390 cm^{-1}). Theoretically, the triplet energy

level was not affected significantly by Ln(III) ion, and the lowest lying excited level of Gd(III) ion was located at 32150 cm^{-1}. Based on this, the phosphorescence spectra had shown a red shift peak 507nm (19723 cm^{-1}).(**Figure 3.25**) According to the experimental results, the schematic energy level diagram and energy transfer process are shown in **Figure 3.26**. The triplet energy levels were higher than the $^5D_0$ level (17200 cm^{-1}) of Eu(III) ion and their energy gaps between $^5D_0$ level and triplet level was 2523 cm^{-1}. According to Latva's empirical rule, if the energy gaps between $^5D_0$ level and triplet level are within 2100–4500 cm^{-1},[24] there should be an optimal ligand to metal transfer process for Eu(III) ion.

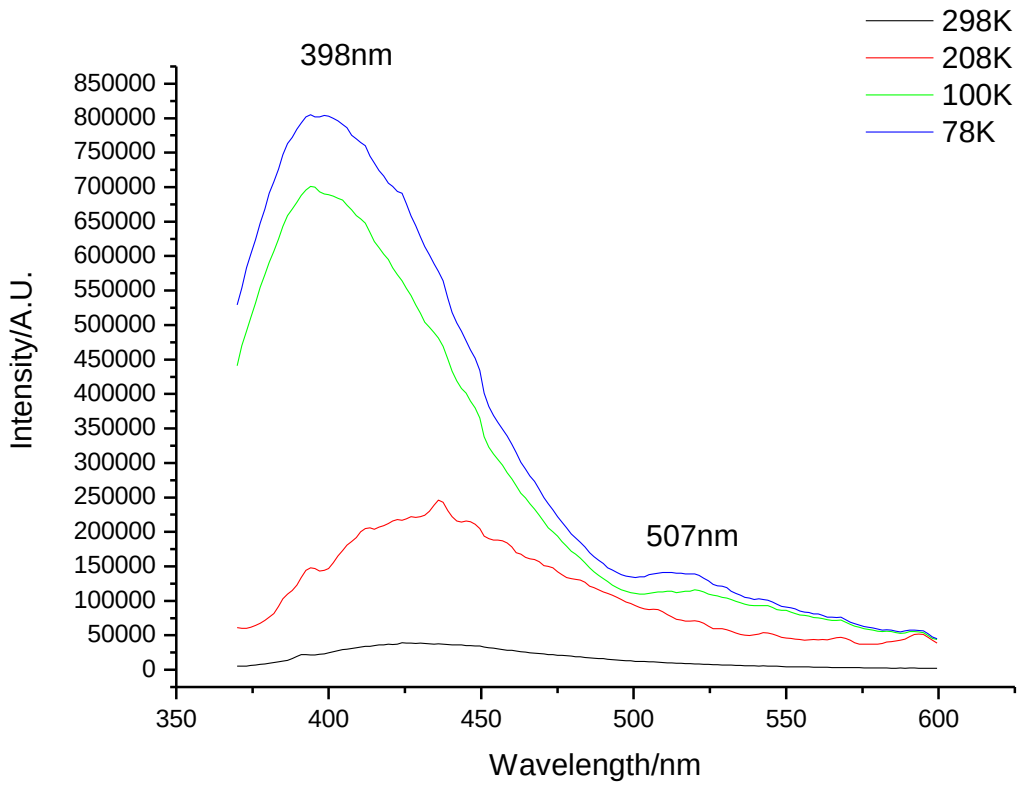

Figure 3.25 Phosphorecent spectra of Gd(III) complex.

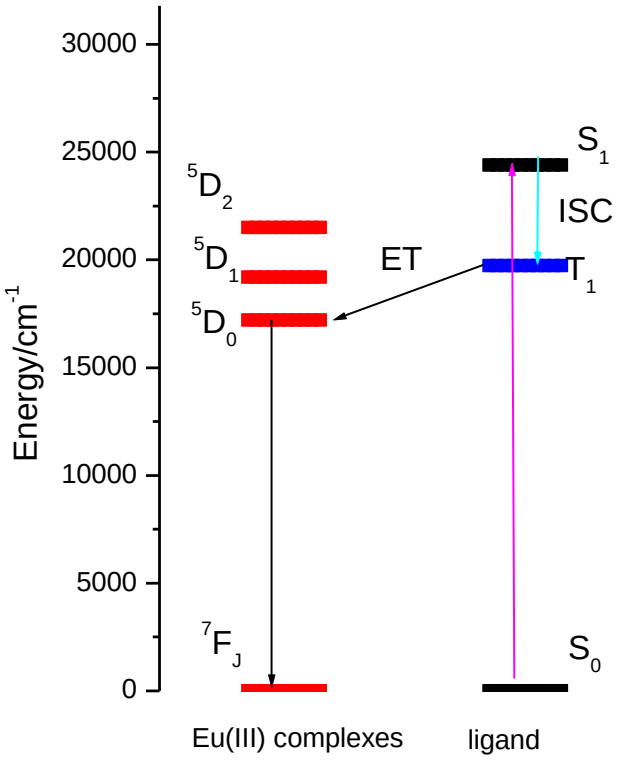

Figure 3.26 Schemaic energy level diagram and energy transfer process of **EuL1**.

3.4 Conclusion

A water soluble Eu(III) complex **EuL1** was designed and developed. It uses dipicolylamine as a receptor and demonstrated a high selectivity and sensitivity for Cu(II) ion. The binding constant was 74026±2899.0M^{-1} and larger than the binding constants towards other cations inculding Fe(II) ion (7951±936.0M^{-1}), Co(II) ion (16713±3342.0M^{-1}) and Ni(II) ion (15210±3042.0M^{-1}).

Photophysical solution studies were performed in detailed. **EuL1** and **EuL1Cu** complexes showed similar absorption bands with the peak maxima centred at 325 nm and their corresponding molar extinction coefficients were 11994 and 11374 M^{-1}. The relative quantum yields were calculated as 6.40% (**EuL1**) and 0.68% (**EuL1Cu**). The q value was calculated as zero, suggesting there are no water molecules in first coordination environment. The emission spectrum of the Gd(III) complex at low

temperature was measured and indicated that the energy gaps between the $^5D_0$ level and triplet level was 2523cm^{-1}.

Upon **EuL1** binding with Cu(II) ion, **EuL1Cu** becomes selective towards H_2S among other organic and inorganic sulfur compounds. The reversible binding between **EuL1** and Cu(II) ion or **EuL1Cu** and H_2S showed an on-off-on type of luminescence, allowing this probe to be used as a monitoring system.

3.5 References

[1] R. L. Myers, *The 100 Most Important Chemical Compounds: A Reference Guide*, Greenwood Press: Westport, 2007.

[2] B. D. Paul and S. H. Snyder, *Nat. Rev. Mol. Cell. Biol*., 2012, **13**, 499-507.

[3] G.Yang, L.Wu, B. Jiang, W. Yang, J. Qi, K. Cao, Q. Meng, A.K. Mustafa, W. Mu, S. Zhang, S.H. Snyder and R. Wang, *Science*., 2008, **322**, 587-590.

[4] L. Li and P.K. Moore, *Trends Pharmacol Sci*., 2008, **29**, 84-90.

[5] L. Li, P. Rose and P.K. Moore, *Annu Rev Pharmacol Toxicol*., 2011, **51**, 169-187.

[6] R. d'Emmanuele di Villa Bianca, R. Sorrentino, P. Maffia, V. Mirone, C. Imbimbo, F. Fusco, R. De Palma, L.J. Ignarro and G. Cirino, *Proc Nat Acad Sci*, 2009, **106**, 4513-4518.

[7] K.H. Kilburn, J.D. Thrasher and M.R. Gray, *Toxicol Ind Health*., 2010, **26**, 387-405.

[8] T.W. Miller, E.A. Wang, S. Gould, E.V. Stein, S. Kaur, L. Lim, S. Amarnath, D.H. Fowler and D.D. Roberts, *J Biol Chem*., 2012, **287**, 4211-4221.

[9] G. Yang, L. Wu, B. Jiang, W. Yang, J. Qi, K. Cao, Q. Meng, A.K. Mustafa, W. Mu, S. Zhang, S.H. Snyder and R. Wang, *Science*., 2008, **322**,587-90.

[10] M. Whiteman and P.K. Moore, *J Cell Mol Med*., 2009, **13**, 488-507.

[11] K. Qu, S.W. Lee, J.S. Bian, C.-M. Low and P.T.-H. Wong, *Neurochem. Int*., 2008, **52**, 155–165.

[12] H. Kimura, *Biochem Biophys Res Commun*., 2000, **267**, 129-133.

[13] A. Kawabata, T. Ishiki, K. Nagasawa, S. Yoshida, Y. Maeda, T. Takahashi, F. Sekiguchi, T. Wada, S. Ichida and H. Nishikawa, *Pain*., 2007, **132**, 74-81.

[14] V. Kuban, P. K. Dasgupta and J. N. Marx, *Anal. Chem.*, 1992, **64**, 36–43.

[15] N. S. Lawrence, R. P. Deo and J. Wang, *Anal. Chim. Acta*., 2004, **517**, 131–137.

[16] M.S. Budd and H.A. Bewick, *Anal. Chem*., 1952, **24**, 1536–1540.

[17] J.K. Fogo and M. Popowsky, *Anal. Chem*., 1949, **21**, 732–734.

[18]L.R. Goodwin, D. Francom, F.P. Dieken, J.D. Taylor, M.W. Warenycia, R.J. Reiffenstein and G. Dowling, *J. Anal. Toxicol*., 1989, **13**, 105–109.

[19] M.D. Levitt, M.S. Abdel-Rehim and J. Furne, *Antioxid. Redox Signal*., 2011, **15**, 373–378.

[20] B.H. Zhang, F.Y. Wu, Y.M. Wu and X.S. Zhan, *J. Fluoresc*., 2010, **20**, 243–250.

[21] J. C. Mathai, A. Missner, P. Kügler, S. M. Saparov, M. L. Zeidel, J. K. Lee and P. Pohl, *Proc. Natl. Acad. Sci. U. S. A*., 2009, **106**, 16633–16638.

[22] M. P. Lutolf, N. Tirelli, S. Cerritelli, L. Cavalli and J. A. Hubbell, *Bioconjugate Chem.*, 2001, **12**, 1051–1056.

[23] A. N. Fletcher, *Photochem. Photobiol*., 1969, **9**, 439-444.

[24] M. Latva, H.Takalo, V.-M. Mukkala, C. Matachescu, J.C. Rodriguez-Ubis and J. Kankare, *J. Lumin*., 1997, **75**, 149-169.

3.6 Appendix

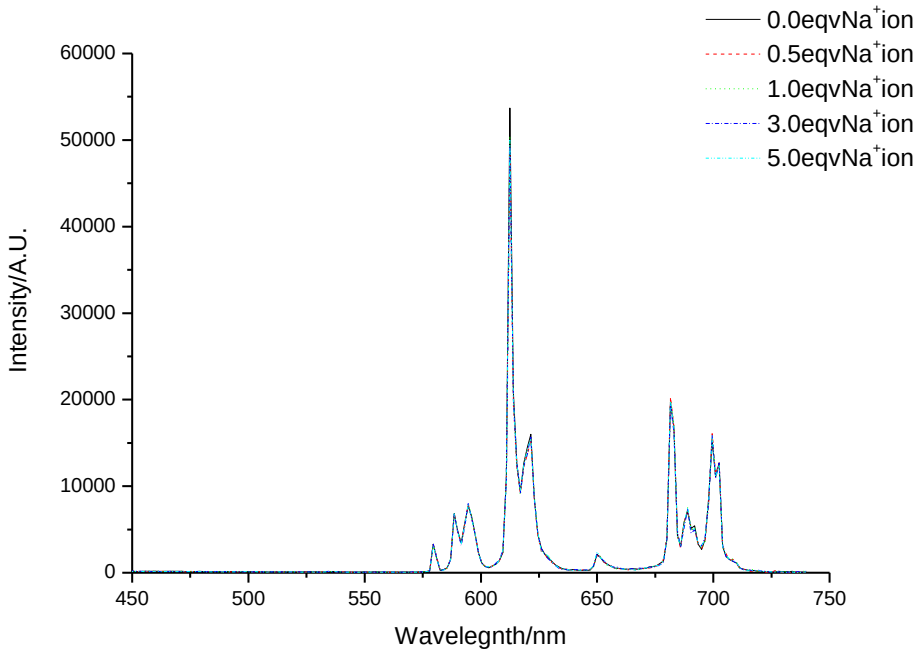

Figure 3.27 Emission spectra of 10 µM aqueous solution upon addition of aliquots of various equiv of Na(I) ions with respect to **EuL1** (0.01M HEPES, pH=7.4, λ_{ex}=350nm) .

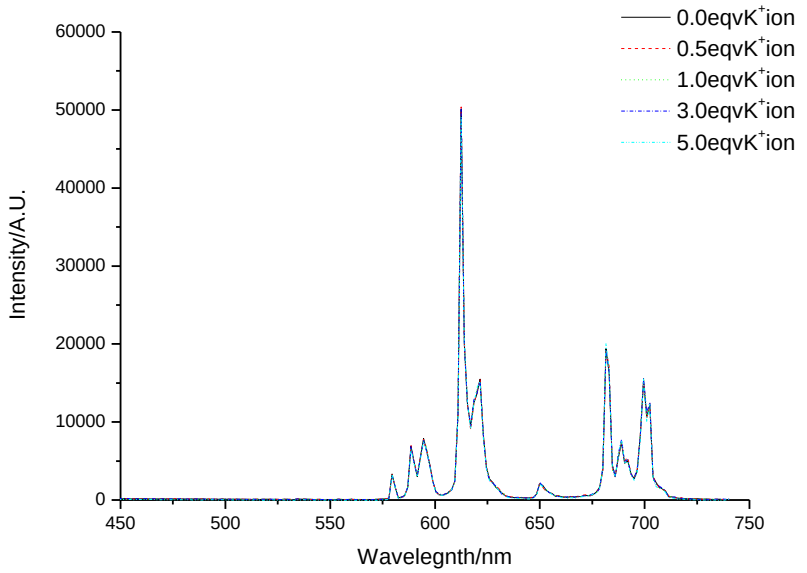

Figure 3.28 Emission spectra of 10 µM aqueous solution upon addition of aliquots of various equiv of K(I) ions with respect to **EuL1** (0.01M HEPES, pH=7.4, λ_{ex}=350nm) .

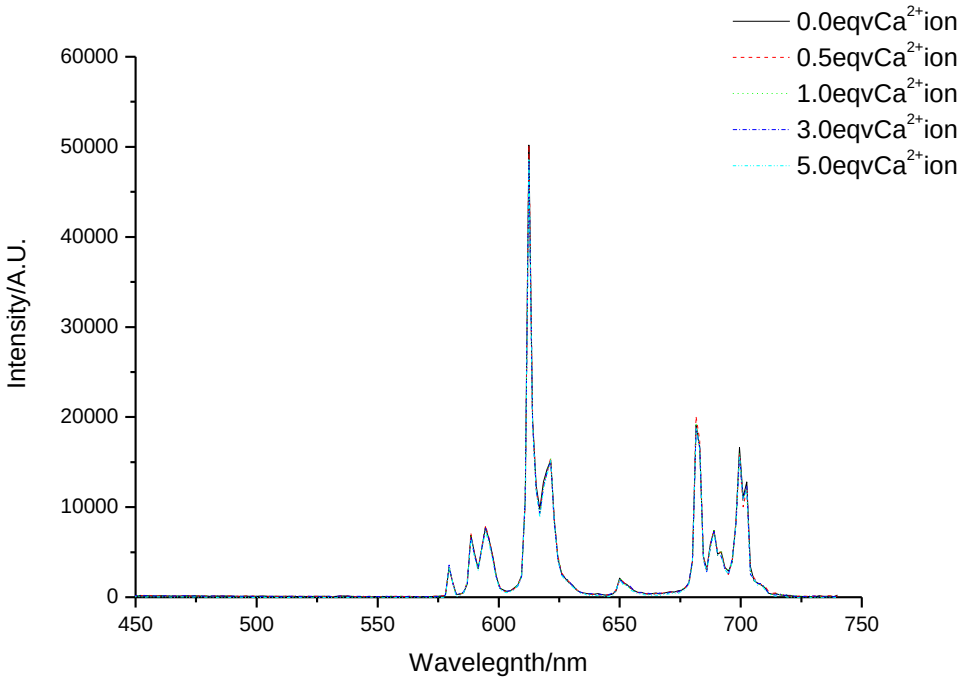

Figure 3.29 Emission spectra of 10 µM aqueous solution upon addition of aliquots of various equiv of Ca(II) ions with respect to **EuL1** (0.01M HEPES, pH=7.4, λ_{ex}=350nm) .

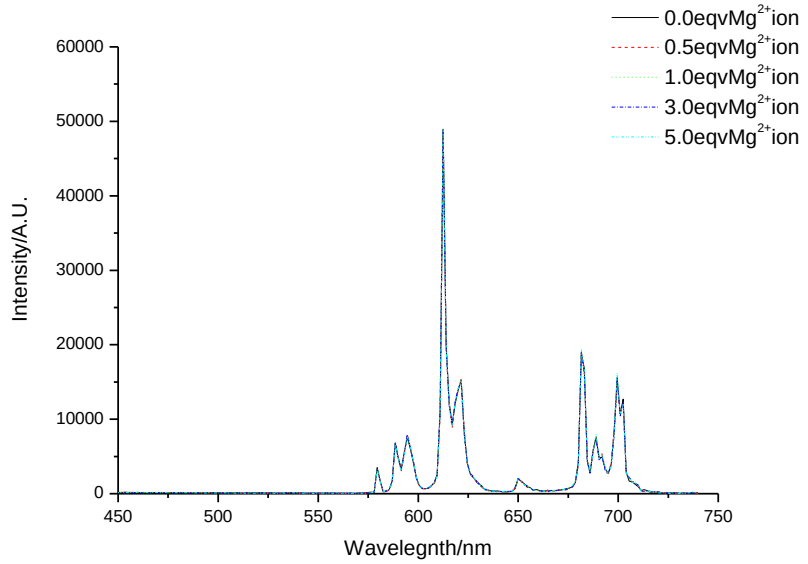

Figure 3.30 Emission spectra of 10 µM aqueous solution upon addition of aliquots of various equiv of Mg(II) ions with respect to **EuL1** (0.01M HEPES, pH=7.4, λ_{ex}=350nm) .

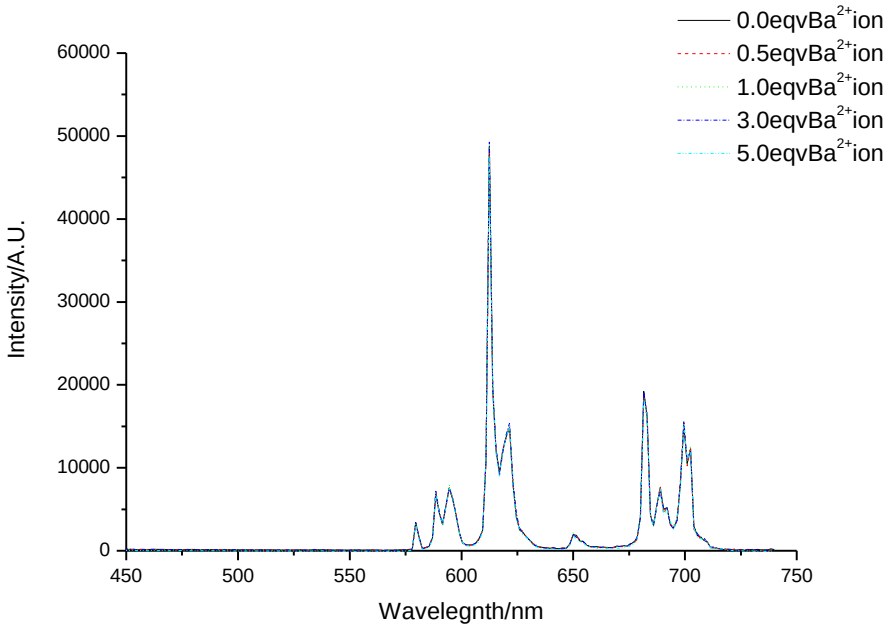

Figure 3.31 Emission spectra of 10 µM aqueous solution upon addition of aliquots of various equiv of Ba(II) ions with respect to **EuL1** (0.01M HEPES, pH=7.4, λ_{ex}=350nm) .

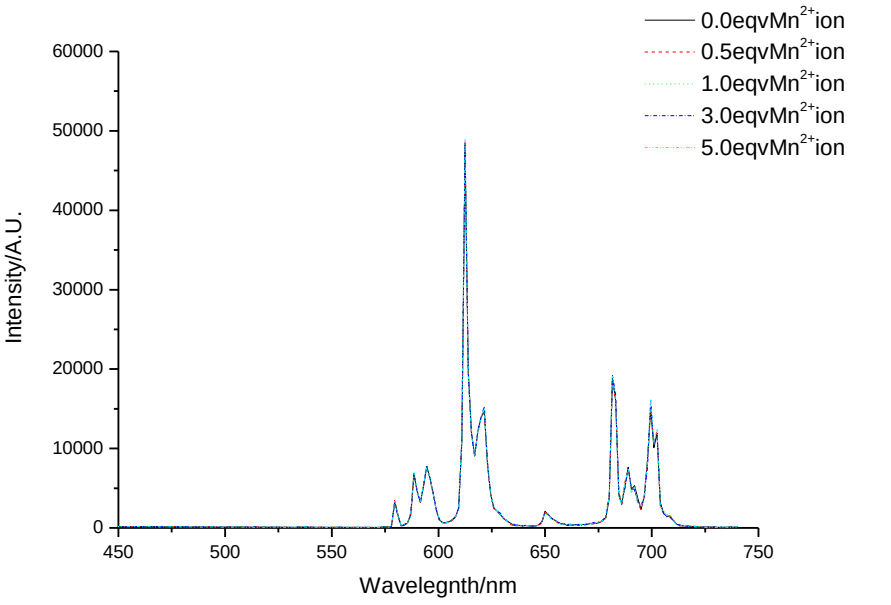

Figure 3.32 Emission spectra of 10 µM aqueous solution upon addition of aliquots of various equiv of Mn(II) ions with respect to **EuL1** (0.01M HEPES, pH=7.4, λ_{ex}=350nm) .

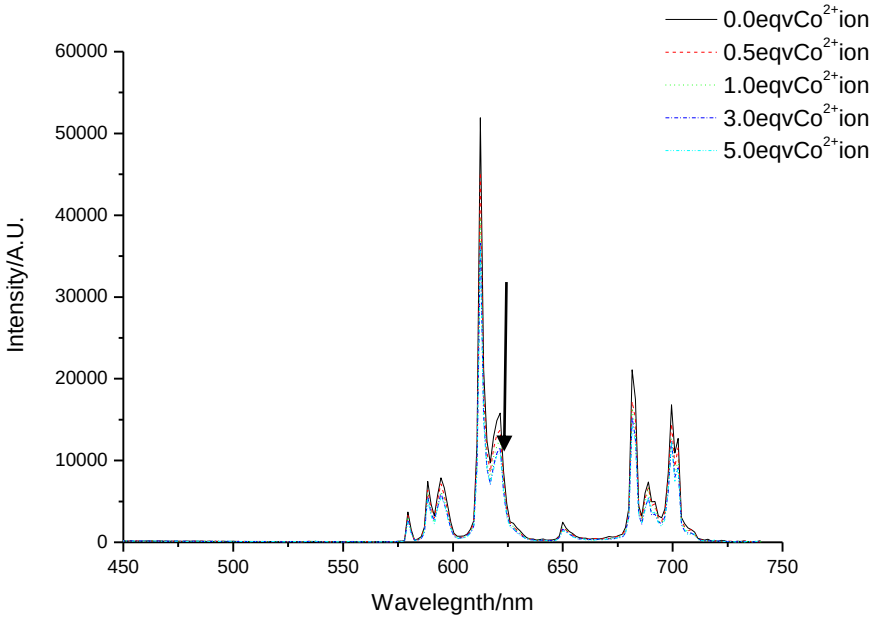

Figure 3.33 Emission spectra of 10 µM aqueous solution upon addition of aliquots of various equiv of Co(II) ions with respect to **EuL1** (0.01M HEPES, pH=7.4, λ_{ex}=350nm) .

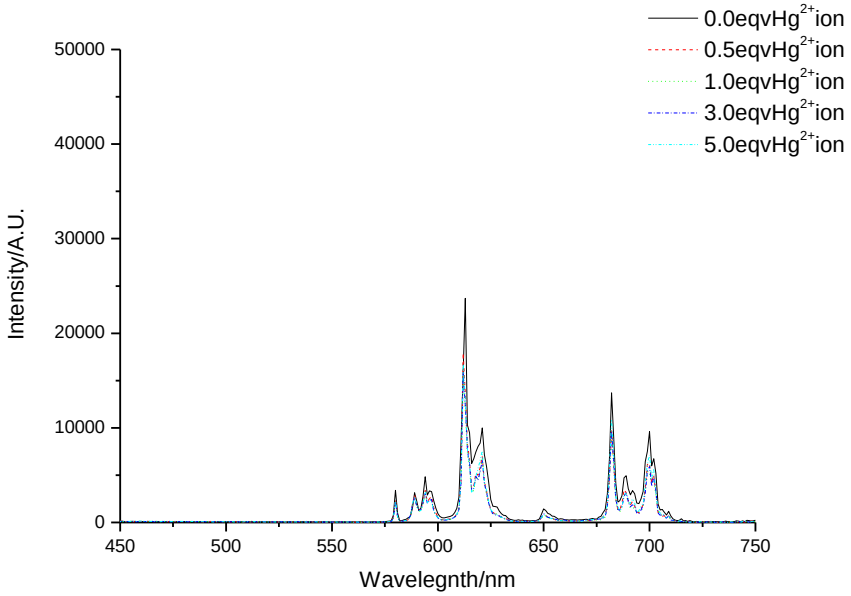

Figure 3.34 Emission spectra of 10 µM aqueous solution upon addition of aliquots of various equiv of Hg(II) ions with respect to **EuL1** (0.01M HEPES, pH=7.4, λ_{ex}=350nm) .

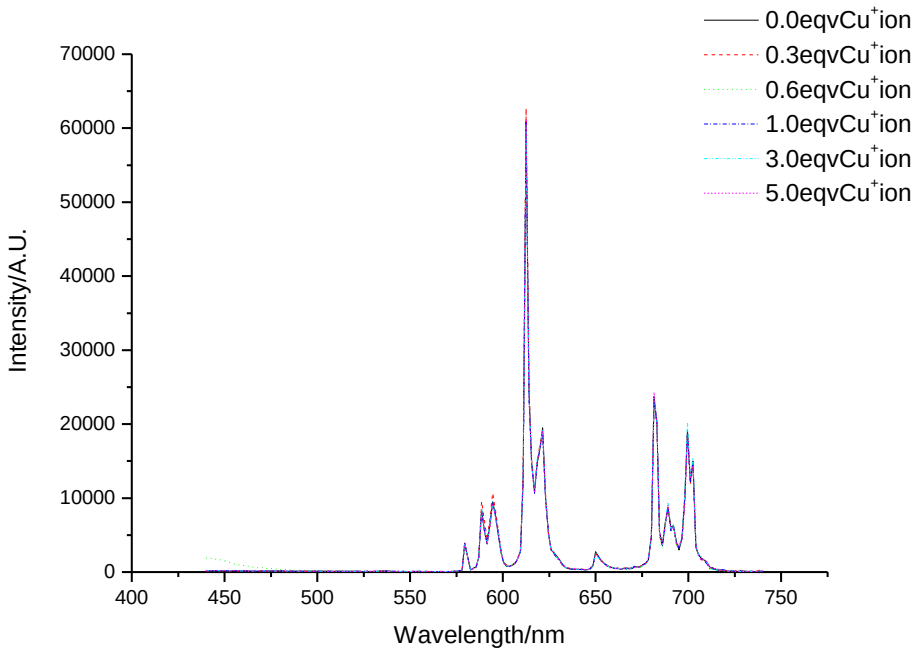

Figure 3.35 Emission spectra of 10 µM aqueous solution upon addition of aliquots of various equiv of Cu(I) ions with respect to **EuL1** (0.01M HEPES, pH=7.4, λ_{ex}=350nm) .

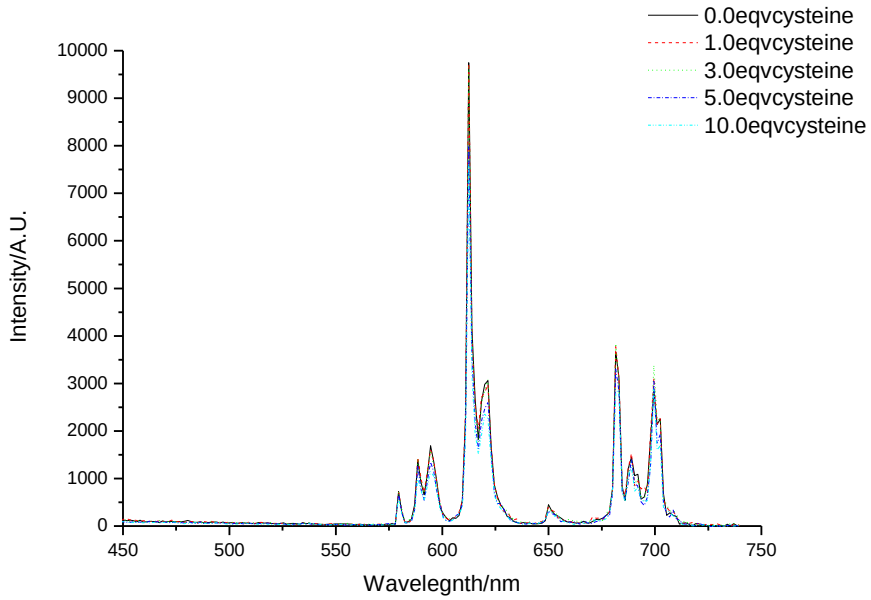

Figure 3.36 Emission spectra of 10 µM aqueous solution upon addition of aliquots of various equiv of Cysteine with respect to **EuL1Cu** (0.01M HEPES, pH=7.4, λ_{ex}=350nm) .

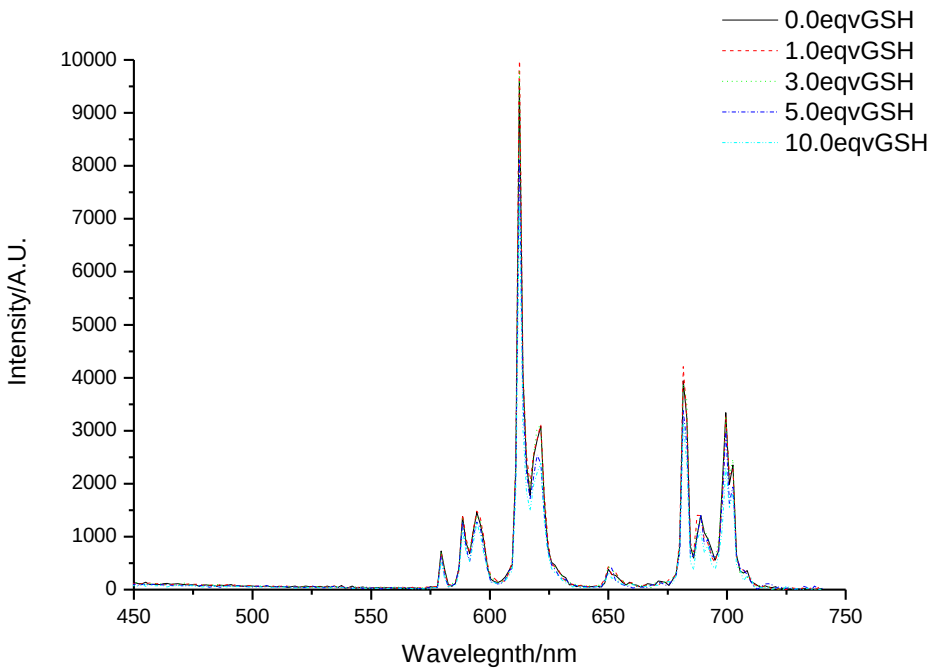

Figure 3.37 Emission spectra of 10 μM aqueous solution upon addition of aliquots of various equiv of GSH with respect to **EuL1Cu** (0.01M HEPES, pH=7.4, λ_{ex}=350nm) .

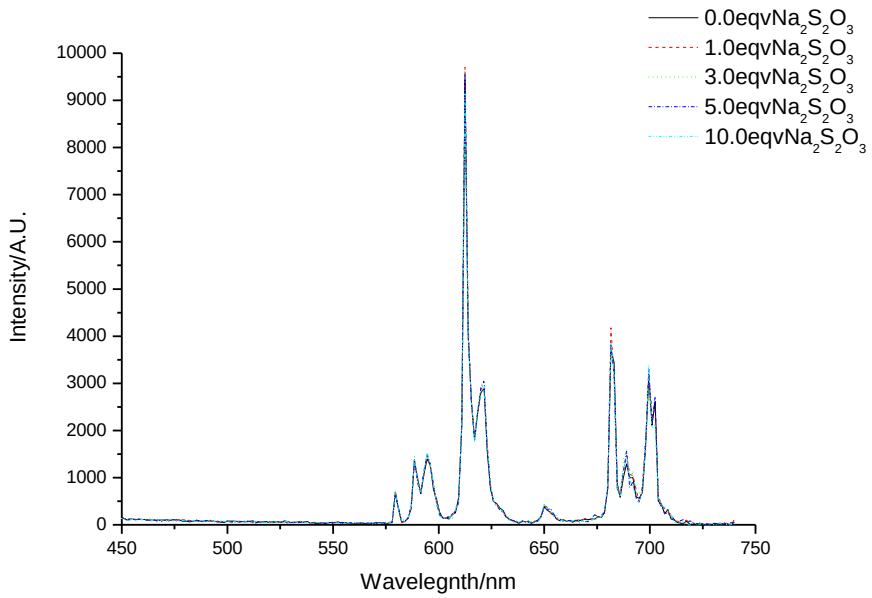

Figure 3.38 Emission spectra of 10 μM aqueous solution upon addition of aliquots of various equiv of $Na_2S_2O_3$ with respect to **EuL1Cu** (0.01M HEPES, pH=7.4, λ_{ex}=350nm) .

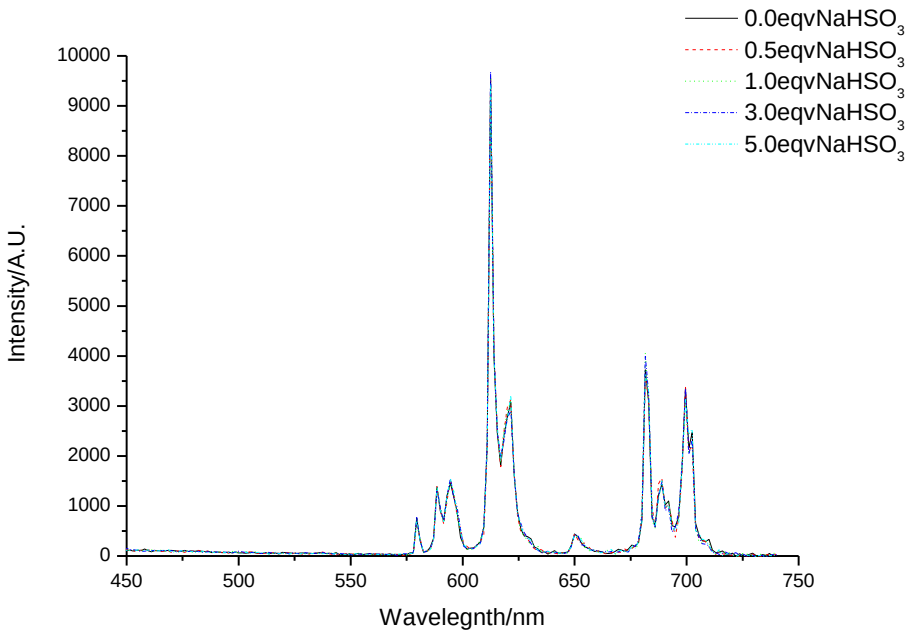

Figure 3.39 Emission spectra of 10 μM aqueous solution upon addition of aliquots of various equiv of $NaHSO_3$ with respect to **EuL1Cu** (0.01M HEPES, pH=7.4, λ_{ex}=350nm) .

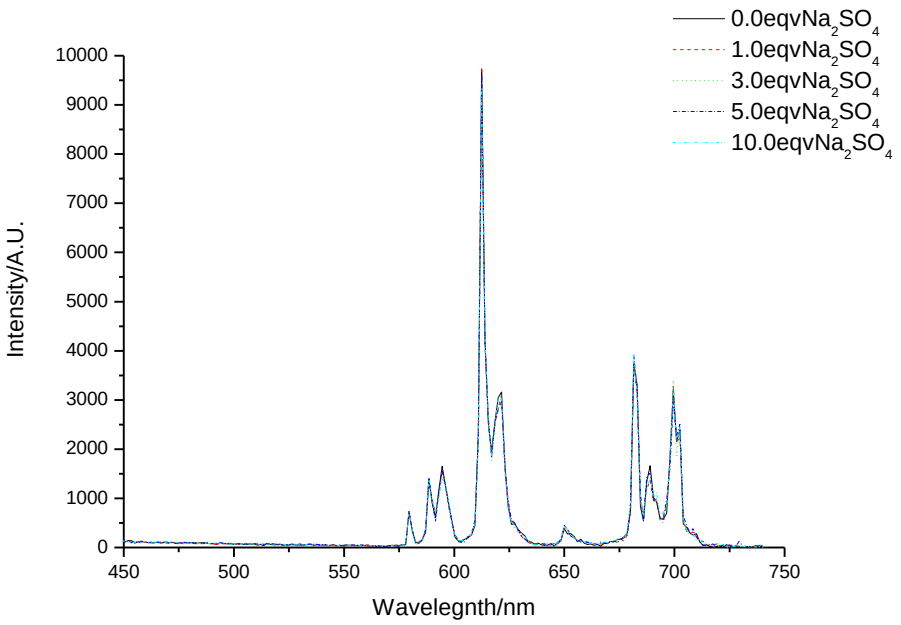

Figure 3.40 Emission spectra of 10 μM aqueous solution upon addition of aliquots of various equiv of Na_2SO_4 with respect to **EuL1Cu** (0.01M HEPES, pH=7.4, λ_{ex}=350nm) .

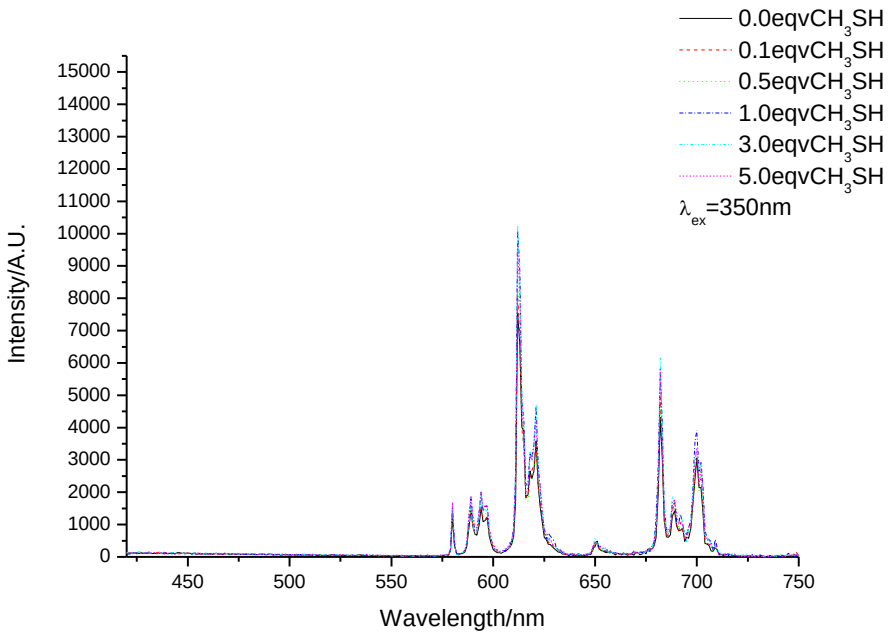

Figure 3.41 Emission spectra of 10 μM aqueous solution upon addition of aliquots of various equiv of CH_3SH with respect to **EuL1Cu** (0.01M HEPES, pH=7.4, λ_{ex}=350nm) .

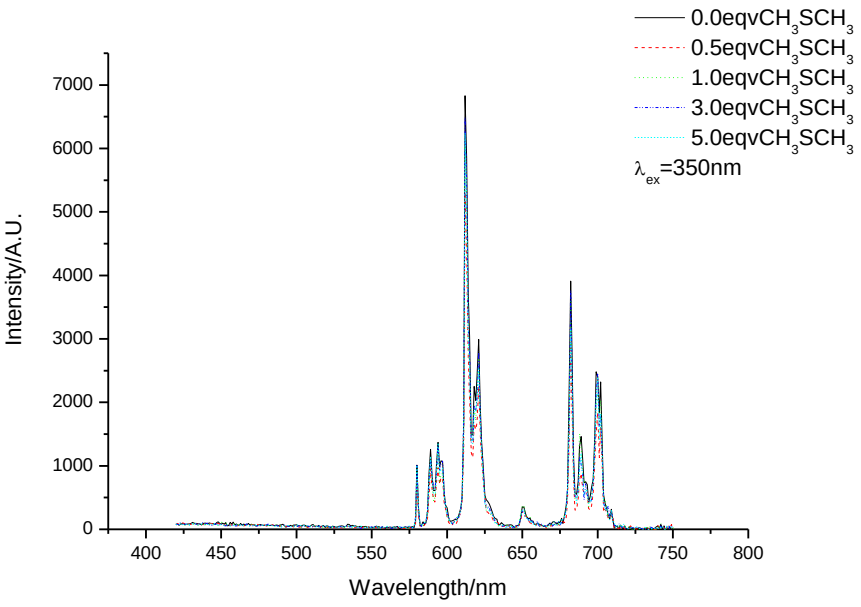

Figure 3.42 Emission spectra of 10 μM aqueous solution upon addition of aliquots of various equiv of CH_3SCH_3 with respect to **EuL1Cu** (0.01M HEPES, pH=7.4, λ_{ex}=350nm) .

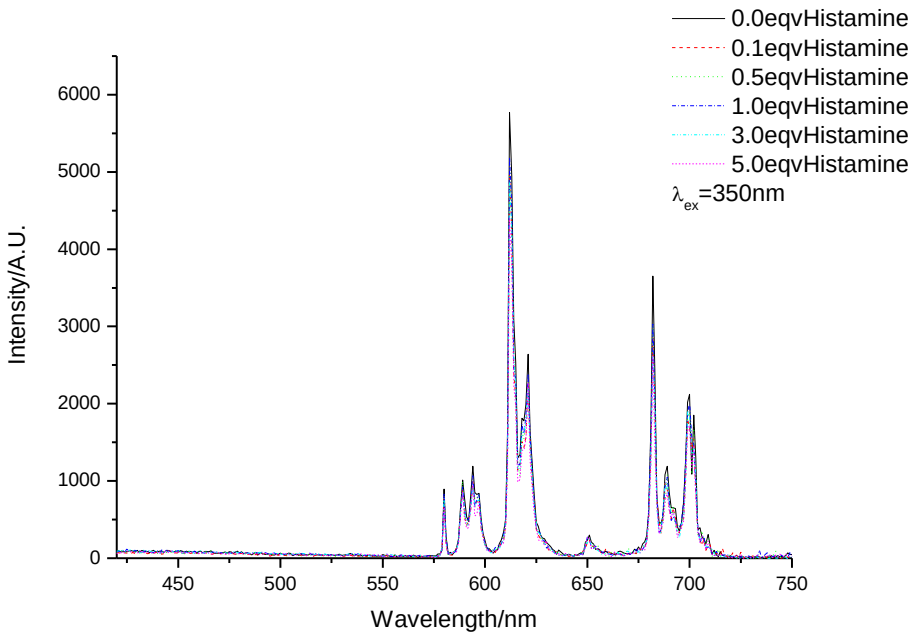

Figure 3.43 Emission spectra of 10 μM aqueous solution upon addition of aliquots of various equiv of Histamine with respect to **EuL1Cu** (0.01M HEPES, pH=7.4, λ_{ex}=350nm) .

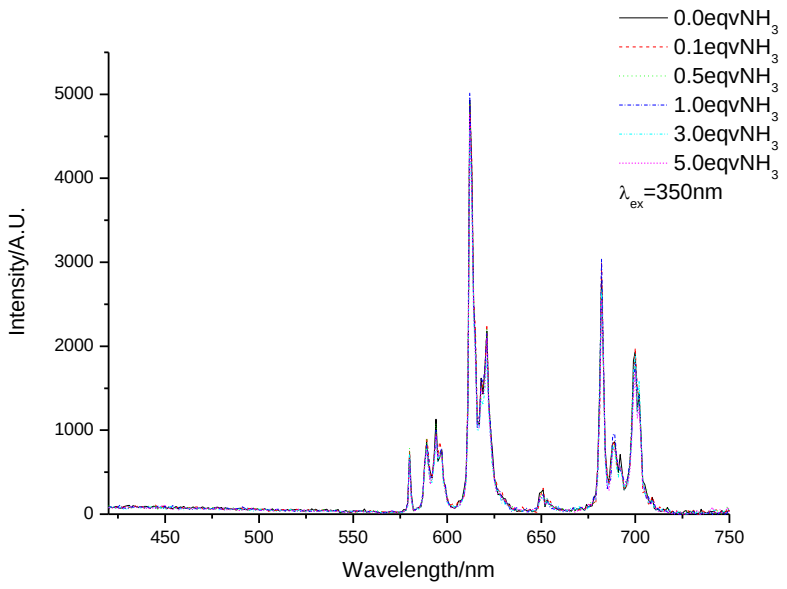

Figure 3.44 Emission spectra of 10 μM aqueous solution upon addition of aliquots of various equiv of NH_3 with respect to **EuL1Cu** (0.01M HEPES, pH=7.4, λ_{ex}=350nm) .

CHAPTER 4

Development of lanthanide complexes for detection of Cysteine

4.1 Introduction

Amino acids, a key component of proteins, are small molecules with different functional groups in side chains, which result in various roles in physiological processes. In family of amino acids, cysteine (Cys) is a semi-essential amino acid and an analogue of serine with the substitution of hydroxy functional group by a thiol functional group. Cys can do both nucleophilic and redox-active functions (low redox potential (-0.2~-0.3V))[1] owing to its low dissociation energy of S-H bond as well as a large, polarizable, and electron rich sulfur atom. Based on this special property, Cys plays a crucial role in biological processes. For instance, Cys uses its thiolate group as an effective nucleophile to attack the fifth position of dopamino-quinone to form 5-cysteinyl-dopamine[2], which is a crucial component of neuromelanin in the progression of Parkinson's disease.(**Figure 4.1**) For example, cysteine is oxidized into cysteine sulfinate through non-haeme mono-iron enzyme cysteine dioxygenase in the brain of a healthy person. (**Figure 4.2**) However, the oxidation of cysteine will be blocked in Parkinson's disease patients. Therefore, the concentration of cysteine would be higher in the brain of a Parkinson's disease patient. Moreover, its concentration is related to some diseases. For instance, a low level of Cys is related to liver damage, skin lesions, lethargy, edema and hair depigmentation.

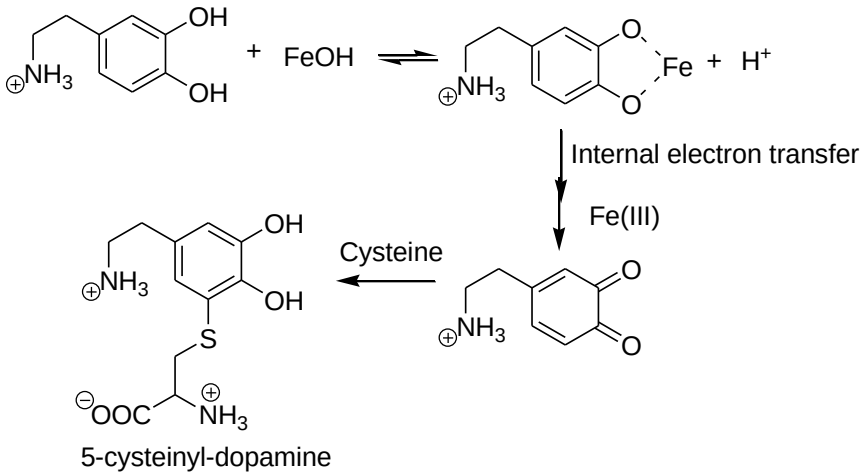

Figure 4.1 Synthetic pathway for 5-cysteinyl-dopamine in which cysteine acts as a nucleophile to attack dopamino-quinone.[2]

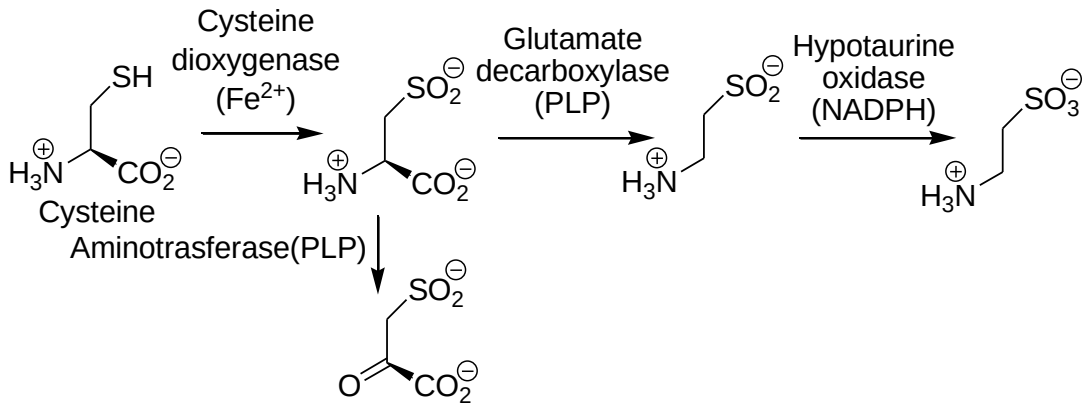

Figure 4.2 The pathway where cysteine is oxidized into cysteine sulfinate in the brain of a health person.[2]

In mammals, Cys can be synthesized through the transulfuration pathway (**Figure 4.3**). Methionine is first converted to S-adenosyl-L-methionine. It is subsequently demethylated to produce S-adenosyl-L-homocysteine, which is then hydrolyzed to homocysteine (Hcy). Hcy undergoes an irreversible reaction with serine to form cystathionine. Then, cystathionine is converted into Cys.[3]

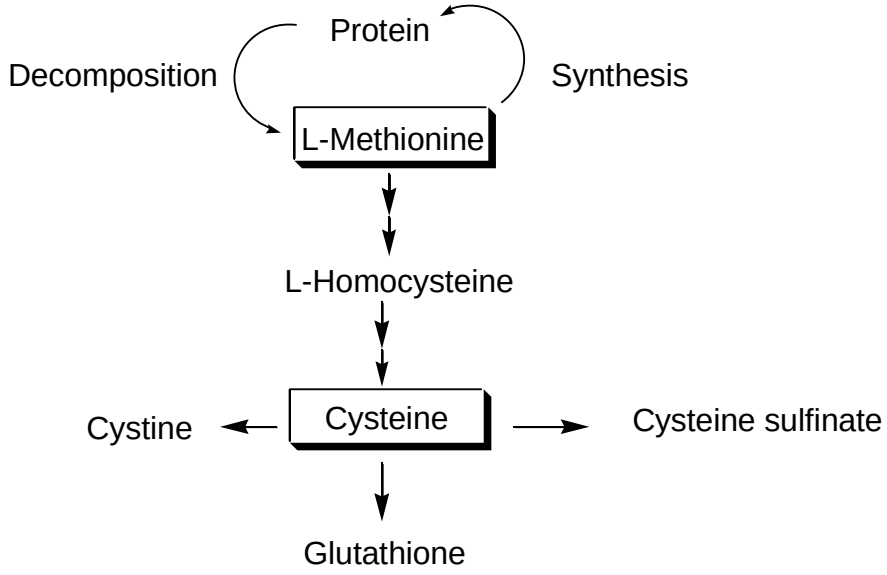

Figure 4.3 The pathway of Cys metabolism.[3]

There are some classical analytical methods for detecting of Cys such as high-performance liquid chromatography (HPLC),[4]-[7] potentiometry[8][9] and capillary electrophoresis.[10][11] However, they have some disadvantages such as sophisticated instrumentation, complex procedure, laborious pretreatment procedures

and expensive instrumentation. Optical detection is one of powerful methods for detecting cysteine since it is a simple, non-invasive, sensitive, selective, convenient and low-cost detection method. To date, there are several approaches to design Cys probe.

First, as it is discussed above, the sulfhydryl group has strong nucleophilicity and is ready to react with and deprotect electron withdrawing liable moieties such as sulphonamide, sulfonate ester and alkylating agents.[12] Therefore, some probes for cysteine are incorporated with such liable moiety conjugated to a chromophore. As a result, the probe allows nucleophilic substitution with thiols and photophysical properties of the probe will change. For instance, probe **4A** contained dinitrobenzenesulfonates that had two strong electron-withdrawing nitro groups that could quench fluorescence by Photoinduced electron transfer (PET) as reaction site. Thiols such as Cys deprotect dinitrobenzenesulfonates and large fluorescent enhancement was observed upon the addition of GSH or Cys.[13]

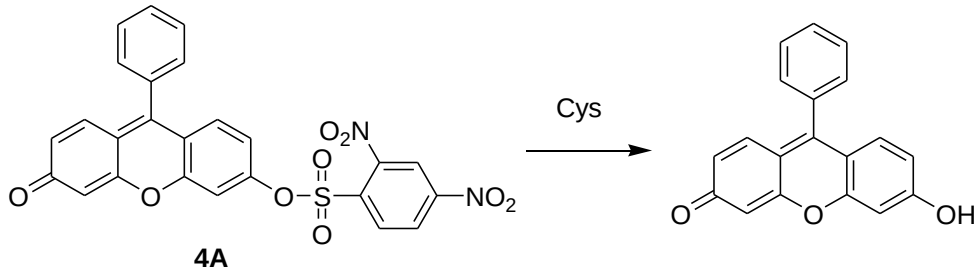

4A

Figure 4.4 Structure of probe **4A** and its reactions with thiols.[13]

Second, some probes contained aldehydes conjugated with suitable fluorophores with which cyclic reaction with thiols could take place. For instance, **4B** contained aldehyde coupled with benzene chromophore. When Cys attacked aldehyde, it would undergo cyclic reaction and change the photophysical properties of **4B**.

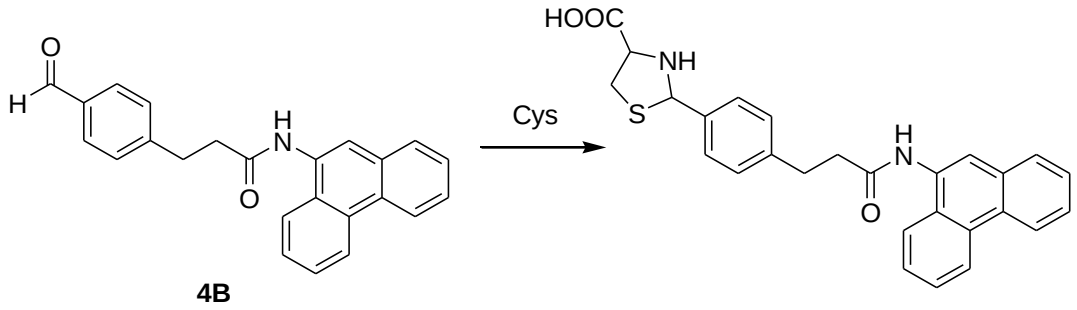

Figure 4.5 Structure of probe **4B** and its reactions with thiols.[14]

Third, probe contained α,β-unsaturated carbonyl moiety for thiols to react and this reaction is called Michael addition. For example, probe **4C** incorporated maleimide group which fluorescence of the probe was quenched by PET. Upon addition of a thiol, maleimide reacted with thiol and the luminescence was recovered.[15]

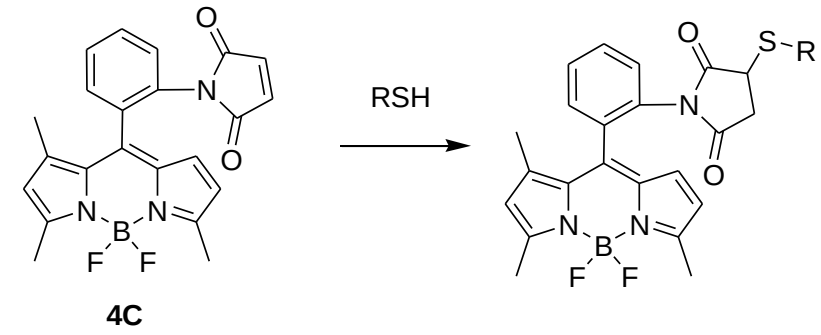

Weakly fluorescent Highly fluorescent

Figure 4.6 Structure of probe **4C** and its reactions with thiols.[15]

Fourth, probes were designed to have Se-N bond for detecting thiols, since strong nucleophilicity of the sulfhydryl group can cleave the Se-N bond of probes and trigger changes of optical signals of probes. For instance, probe **4D** incorporated Se-N bond connecting the strongly electron withdrawing 2-nitrophenylselane and its fluorescence was quenched by PET. Upon addition of thiol, 2-nitrophenylselane left **4D** upon cleavage of Se-N bond and PET was ineffective. Hence, fluorescence of **4D** was recovered.[16]

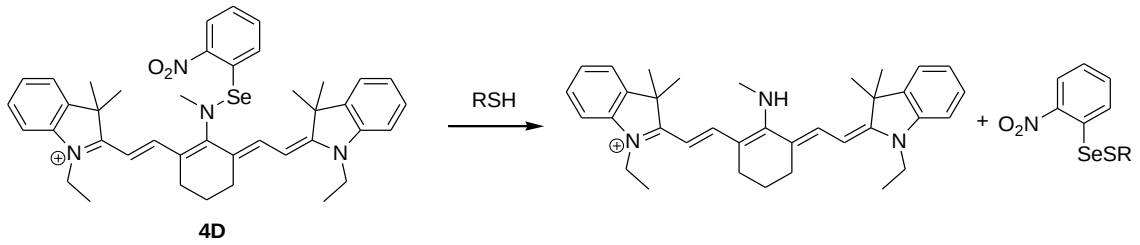

4D

Figure 4.7 Structure of probe **4D** and its reactions with thiols. [16]

4.2 Design of probe

The structure of the Cys sensor **EuL2** is shown in **Figure 4.8**. It consists of three main parts, including a reaction site for recognizing Cys, a chromophore for sensitization of Eu(III) ion and an Eu chelator. The reaction site is acrylate group. It is a selective reaction site for Cys and can distinguish Cys from other similar analogues such as homocysteine (Hcys) and glutathione (GSH). Its selectivity is due to intramolecular cyclization in which formation of a seven-membered ring with Cys is usually more kinetically favored than formation of an eight-membered ring with Hcy while such cyclization reaction for GSH is often hindered by its bulkiness. The chromophore is 4-(2-(naphthalen-2-yl)ethynyl)pyridine derivative in which pyridine is used for direct coordination towards Eu(III) ion for better energy transfer. Eu chelator is a macrocycle in which Eu(III) ion experienced a nine coordination environment and therefore there should not be any water molecule in the first inner coordination environment theoretically. There is one ethoxyacetic acid as a side arm in the Eu chelator and the overall complex will be more hydrophilic and hence more water soluble.

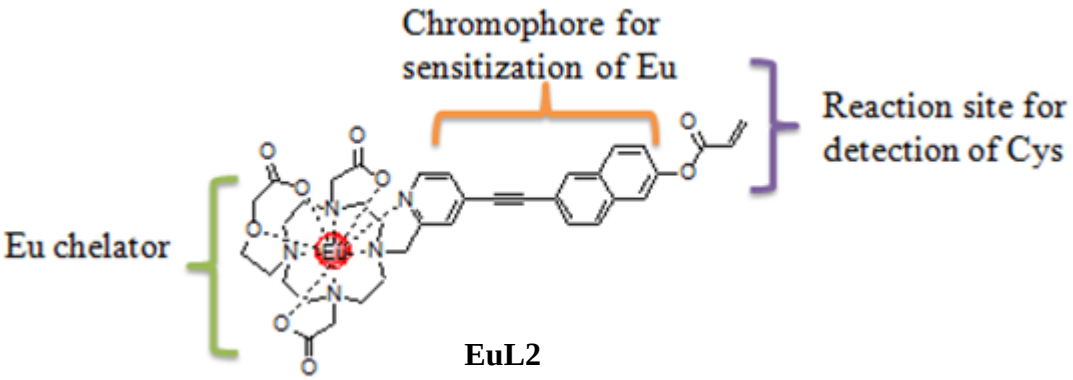

Figure 4.8 Structure of Cys sensor **EuL2**.

The sensitisation mechanism of **EuL2** is shown in **Scheme 4.1** and it is based on intramolecular cyclization. In the presence of Cys, Michael addition of Cys to the acryloyl group affords a seven-membered ring, which is followed by cleavage of the ester bond to form **4J** with changes in luminescence while Michael addition of **EuL2** with Hcy affords an eight member ring and the formation of eight member ring is less kinetically favored than the formation of the seven member ring. Reaction with GSH is often hindered by its bulkiness. Therefore, **EuL2** can distinguish Cys from Hcys and GSH.

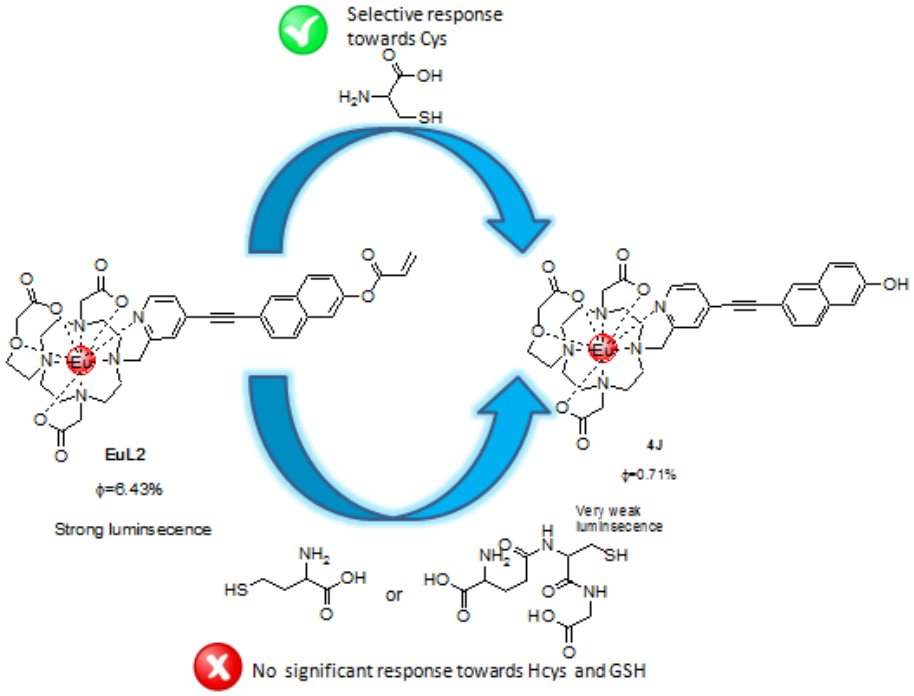

Scheme 4.1 Reaction mechanism for luminescent response of **EuL2** towards Cys, Hcys

and GSH.

4.3 Results and Discussion

4.3a Synthesis of EuL2

There were seven steps in the synthetic pathways of **EuL2** and they were depicted below. The seven steps synthesis can be divided into four main parts:- 1) the chromophore synthesis, 2) incorporation of **4G** into chromophore, 3) basic deprotection and Eu(III) ion complexation, 4) acylate functional group attachment. Since the acrylate was labile in basic condition, incorporation of acrylate group would be the last step.

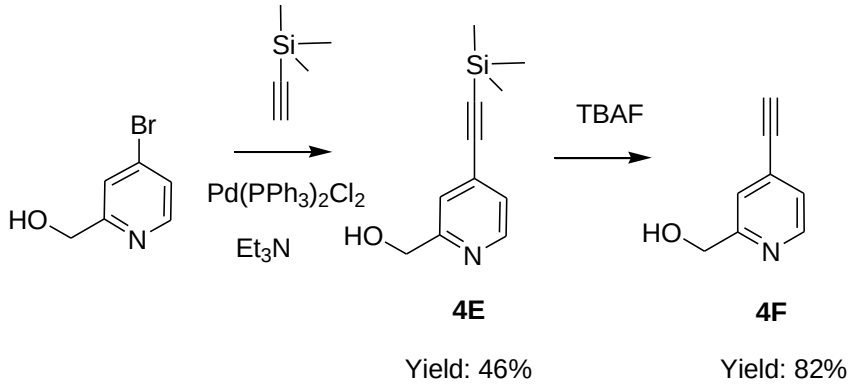

Scheme 4.2 Synthetic Routes to **4F**.

4E was prepared by Sonogashira coupling between ethynyltrimethylsilane and (4-bromopyridin-2-yl)methanol in the presence of a trace amount of $PdCl_2(PPh_3)_2$ catalysis to give the product in 64 % yield. **4E** was mixed with 1.5 eqv tetra-n-butylammonium fluoride (TBAF) in THF for five hours to have deprotection of the trimethylsiliane protecting group. The yield was 82%.

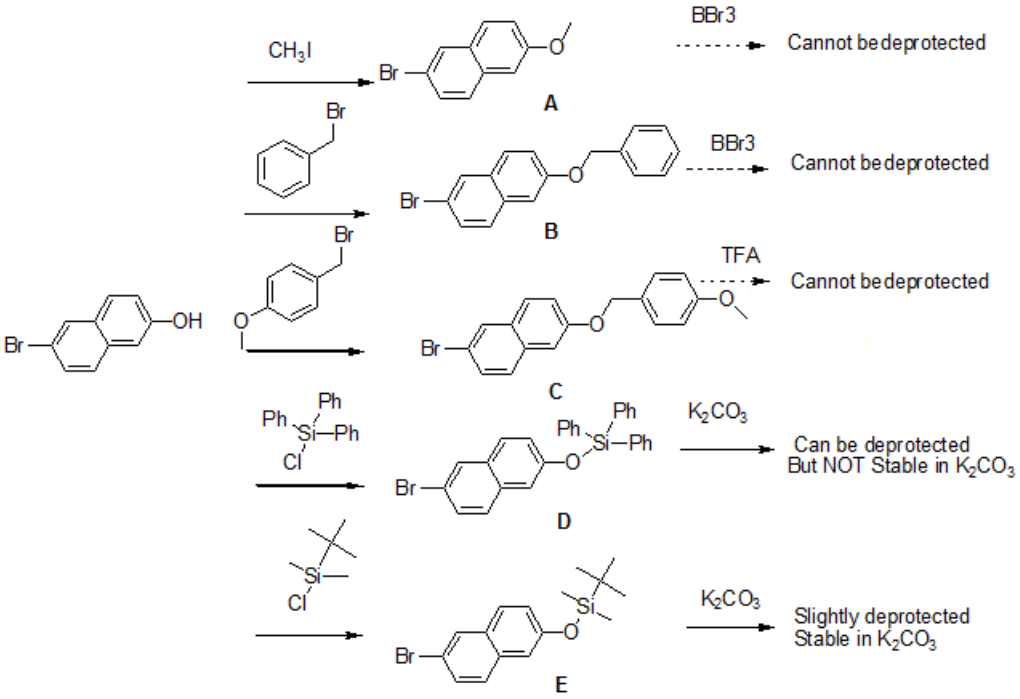

Scheme 4.3 Different protection methods for alcohol on naphthalene.

The next step was the synthesis of other parts of the chromophore. Protection of alcohol on naphthalene had to carry out first since alcohol would take part in the remaining steps. The protection method has to meet some requirements. First, it should be easy to do protection. Second, the protection group should be easily deprotected. Third, the protecting group should be stable in the basic reaction condition since some bases such as basic potassium carbonate (K_2CO_3) were used in the remaining steps.

Several protection methods have been attempted. The first was the conversion of alcohol group into methoxy group, a common alcohol protecting group. However, boron tribromide, which was a common reagent for deprotecting methoxy group to make compound **A**, would not deprotect methoxy group under reflux. The second protecting method tried was the converting of alcohol group into C_6H_5O group to make compound **B** since C_6H_5O group should be more easily deprotected than methoxy group. But the deprotection was not successful. Third was the converting of alcohol into p-$OMeC_6H_4CH_2$ to make compound **C**. However, compound **C** could not be deprotected by TFA, Therefore, silane type of protecting groups were used. But one of

disadvantage in synthesis was that they are very labile in base such as K_2CO_3. Since K_2CO_3 was a very common base to do connection between metal chelator and chromphore, it was so important to test stability of silane type of protecting groups in K_2CO_3. For triphenylsilane, it was not stable in K_2CO_3 while tert-butyldimethyl silane seemed to be stable in in K_2CO_3 after 2 days stirring in ACN. Therefore, tert-butyldimethyl silane was selected as the alcohol protection group.

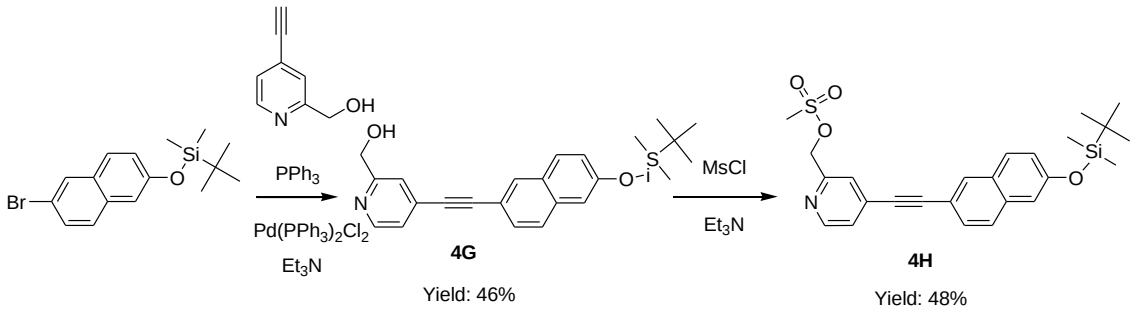

Scheme 4.4 Synthetic Route to **4H**.

4G was prepared from Sonogashira coupling reaction between **4F** and (6-bromonaphthalen-2-yloxy)(tert-butyl)dimethylsilane in the presence of a trace amount of $PdCl_2(PPh_3)_2$ to afford **4G**. (yield: 46 %) Then, **4G** was stirred with 1.2 eqv methanesulfonyl chloride with 2.0 eqv of triethylamine at room temperature overnight to yield **4H**. It was found that **4H** was stable in silica gel column and therefore the purification of **4H** was done by column chromatography. (yield: 48 %)

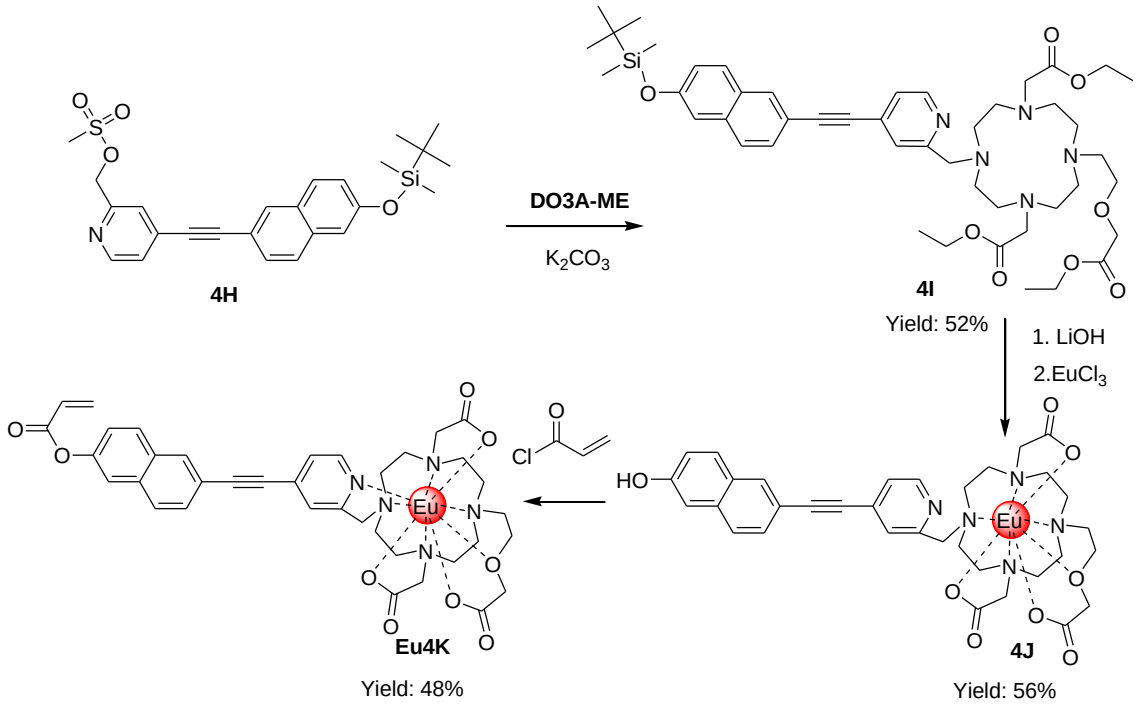

Scheme 4.5 Synthetic Route to **EuL2**.

4H was stirred with **DO3A-ME** with 2 eqv of K_2CO_3 overnight (yield: 52 %). The compound **4I** was mixing with LiOH and then tune pH value to 7 and then was refluxed with 1.0 eqv of $EuCl_3.6H_2O$ formed **4J**. (yield: 56 %) In the final step, **4J** was reacted with acryloyl chloride to yield **EuL2**. (yield: 48 %) The product was characterized by high-resolution mass spectrometry using positive electrospray ionisation (ESI+) with the main peak corresponding to the protonated **EuL2** complex and confirmed by the Eu(III) isotopic pattern.

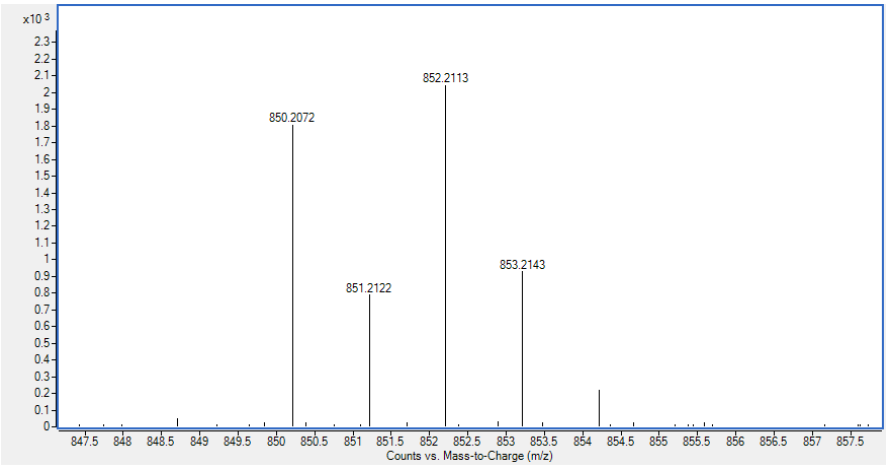

Figure 4.9 High resolution mass spectrum (+ve mode) of **EuL2**.

4.3b Photophysical Study

UV-vis and excitation spectra

The photophysical properties of **EuL2** were studied. There was no obvious difference in its UV-vis spectra before and after addition of Cys. (**Figure 4.10**) The absorption peak maximum was located at 323nm, which was related to π to π* transitions associated to the aromatic chromophore moieties. The molar extinction coefficients were calculated as 14439 M^{-1} (no Cys) and 15090 M^{-1} (add Cys). The excitation spectra were similar to the corresponding excitation spectra, suggesting that there was an energy transfer occurring from the chromophore moieties to Eu(III) ion centre.

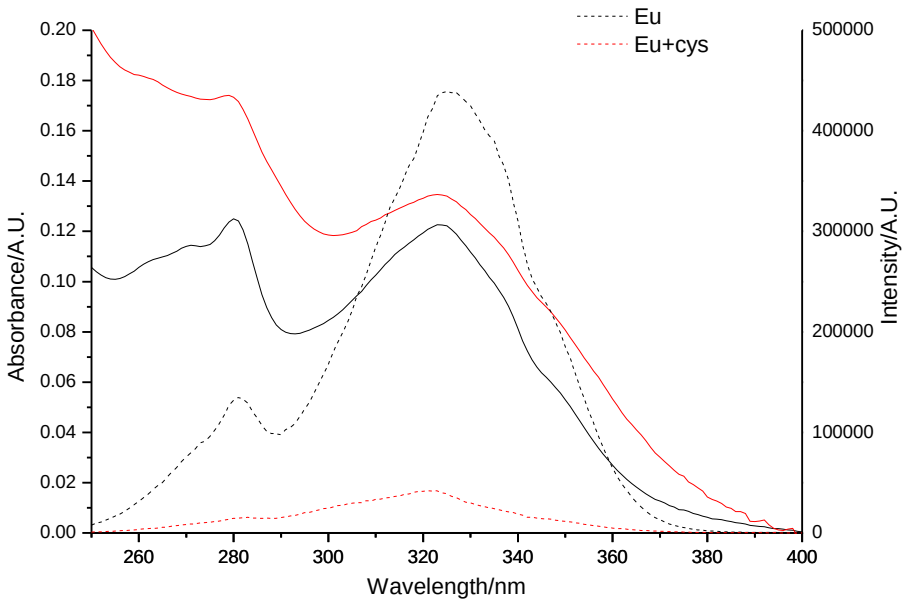

Figure 4.10 UV/Vis absorption spectra (solid line), excitation spectra (dotted lines, λ_{em} =612 nm) (Black line: **EuL2** red line: **EuL2**+10 eqv Cys (0.01M HEPES, pH 7.4).

Titration of EuL2 and its linear response with Cys

When Cys (0 to 20 eqv) was added to aqueous solution of **EuL2**, it demonstrated gradual quenching of the narrow structured emission patterns $^5D_0 \rightarrow {}^7F_J$ (J=0-4) transitions, which were characteristic of the Eu (III) ion. In **Figure 4.11**, there was one sharp peak at the $^5D_0 \rightarrow {}^7F_0$ transition centred at 580 nm, which indicated that there was a single species in solution. The electric dipole transition $^5D_0 \rightarrow {}^7F_2$ (I_{ED}) was hypersensitive and its corresponding splitting showed the coordination environment of Eu(III) ion. During titration, its hypersensitive splitting did not change significantly. Moreover, the ratio of the electric dipole transition $^5D_0 \rightarrow {}^7F_2$ (I_{ED}) and magnetic dipole transition $^5D_0 \rightarrow {}^7F_1$ (I_{MD}) generally provides information of the chemical environments and symmetries of the Eu (III) ion since I_{MD} is independent of the crystallographic site of the Eu (III) ions while I_{ED} is hypensensitive towards the Eu (III) ion. The I_{ED} /I_{MD} ratio was calculated as 4.86 (add Cys) and 4.96 (no Cys), indicating chemical environment of the Eu (III) ion was not significantly influenced by the presence of Cys. Titrations had also been done with the Hys and GSH and their extent of quenching was smaller than that of Cys. (**Figures 4.12** & **4.13**) The titration also showed a linear relationship between the luminescent intensity and concentration of Cys (5 μM to 80 μM). (**Figure 4.14**)

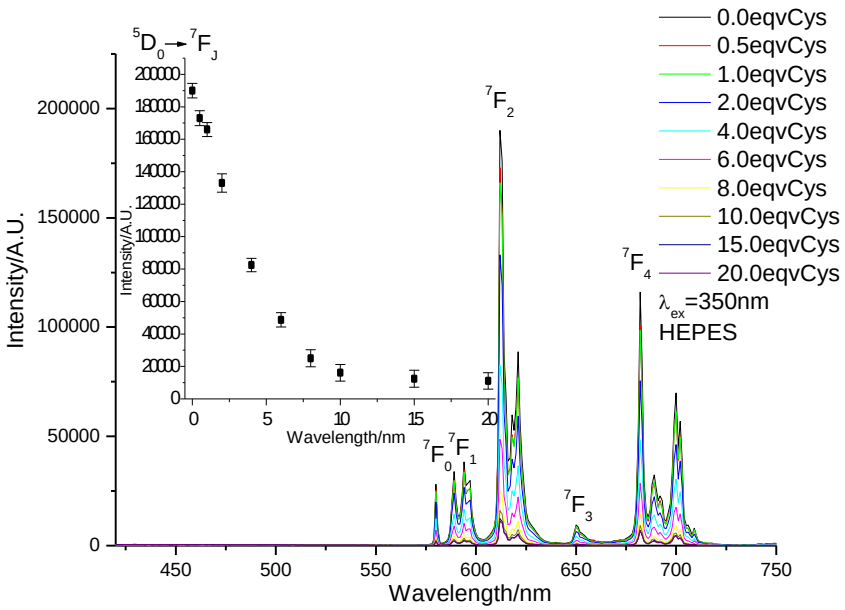

Figure 4.11 Emission spectra of 10 μM aqueous solution upon addition of aliquots of various equiv of Cys with respect to **EuL2** (0.01 M HEPES, pH=7.4, λ_{ex}=350 nm). Insert: Luminescence response of europium emission intensity (λ= 612 nm) to changing Cys.

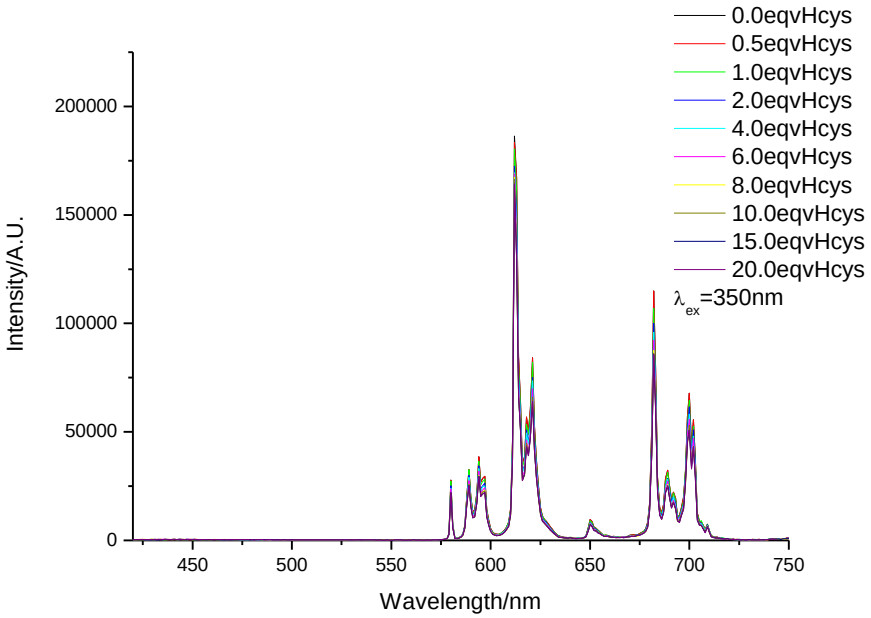

Figure 4.12 Emission spectra of 10 μM aqueous solution upon addition of aliquots of various equiv of Hcys with respect to **EuL2** (0.01 M HEPES, pH=7.4, λ_{ex}=350 nm).

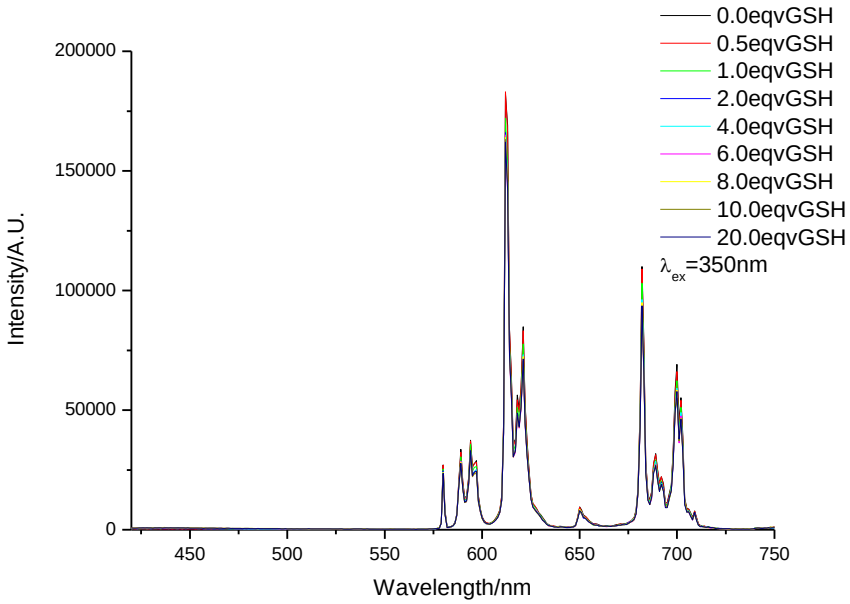

Figure 4.13 Emission spectra of 10 µM aqueous solution upon addition of aliquots of various equiv of GSH with respect to **EuL2** (0.01 M HEPES, pH=7.4, λ_{ex}=350 nm).

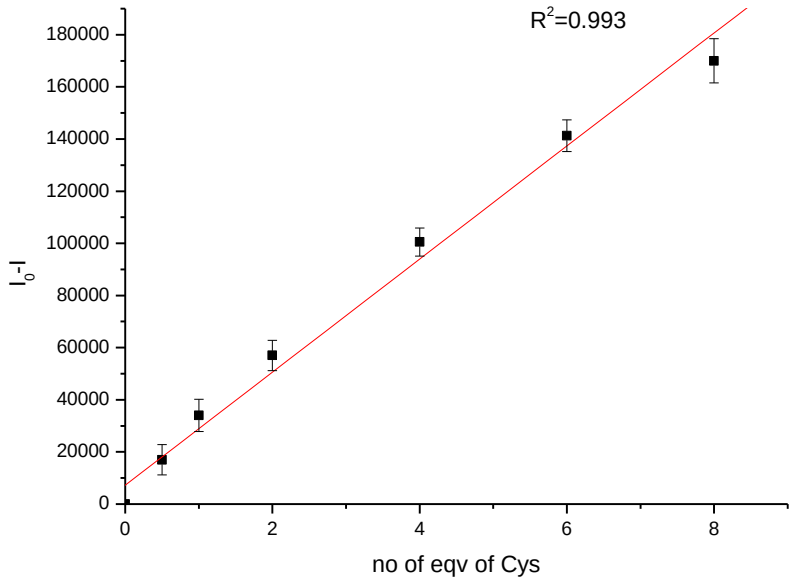

Figure 4.14 Linear luminescence response of 10 µM aqueous solution upon addition of aliquots of various equiv of Cys with respect to **EuL2** (0.01M HEPES, pH=7.4, λ_{ex}=350 nm)

Quantum yield

The quantum yield is the ratio of the amount of photons being absorbed to the amount of photons being emitted from Eu(III) ion centre through luminescence. It could be measured by two methods, the comparative method and the absolute method. In this case, the comparative method was used. By keeping the same excitation wavelength and slit bandwidths, the relative quantum yields of **EuL2** before and after addition of 10 eqv of Cys, 10 eqv of Hcys and 10 eqv of GSH were determined relative to a quinine sulfate of known quantum yield (Φ = 0.577) in 0.1 M sulfuric acid. The relative quantum yields were 6.43±0.04 % (without Cys), and 0.71±0.01 % (with Cys), 5.72±0.08 % (with Hcys) and 6.20± 0.06 % (with GSH). In view of the quantum yields, it could be concluded that the extent of quenching of luminescent intensity by Cys at around 89 % was much higher than that of Hcys (10.5 %) and GSH (3.6 %). Their quantum yields were summarized in **Table 4.1**.

	Quantum Yields
EuL2	6.43±0.04%
EuL2+Cys	0.71±0.11%
EuL2+Hcys	5.72±0.08%
EuL2+GSH	6.20±0.06%

Table 4.1 Summary of quantum yields.

Lifetime and q value

Sometimes, the luminescence intensity was quenched since there were the presence of O-H (such as water molecules) oscillators directly bound to the Eu(III) ion which provided an efficient pathway for radiationless decay via energy transfer from electronic to vibrational levels. Therefore, the quenching mechanism of **EuL2** was necessary to be confirmed to be solely reaction-based. The average hydration states of **EuL2** with and without the analytes should be calculated to confirm that there was no coordinating

water molecule within **EuL2**.

The hydration states were determined by measuring the luminescence lifetimes in H_2O and D_2O upon emission at 612 nm. The lifetime of **EuL2** without Cys in D_2O was 1.24 ms, which was longer than that in H_2O (0.92 ms) while the lifetime of **EuL2** with 10 eqv of Cys in D_2O was 1.16 ms, which was much longer than that in H_2O (0.87 ms). The measurements with analytes were done after 80min. The lifetimes were also measured in HEPES which were similar to the values in H_2O. Based on the lifetimes in D_2O and H_2O, the q value was calculated as zero in the presence and absence of Cys, indicating that there was no bound water molecule coordinating directly with Eu (III) ion and that the geometric coordination/complex was stable during the Cys titrations with no anion or solvent exchange.

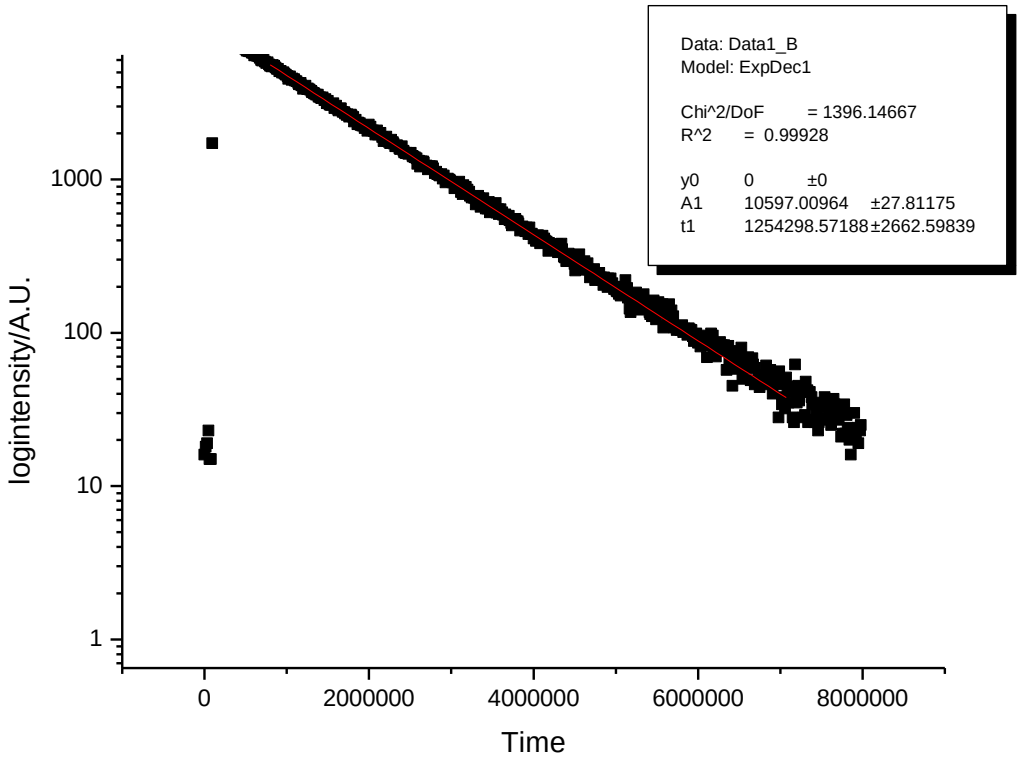

Figure 4.15 Decay curve of luminescence lifetime measurement of **EuL2** in D_2O.

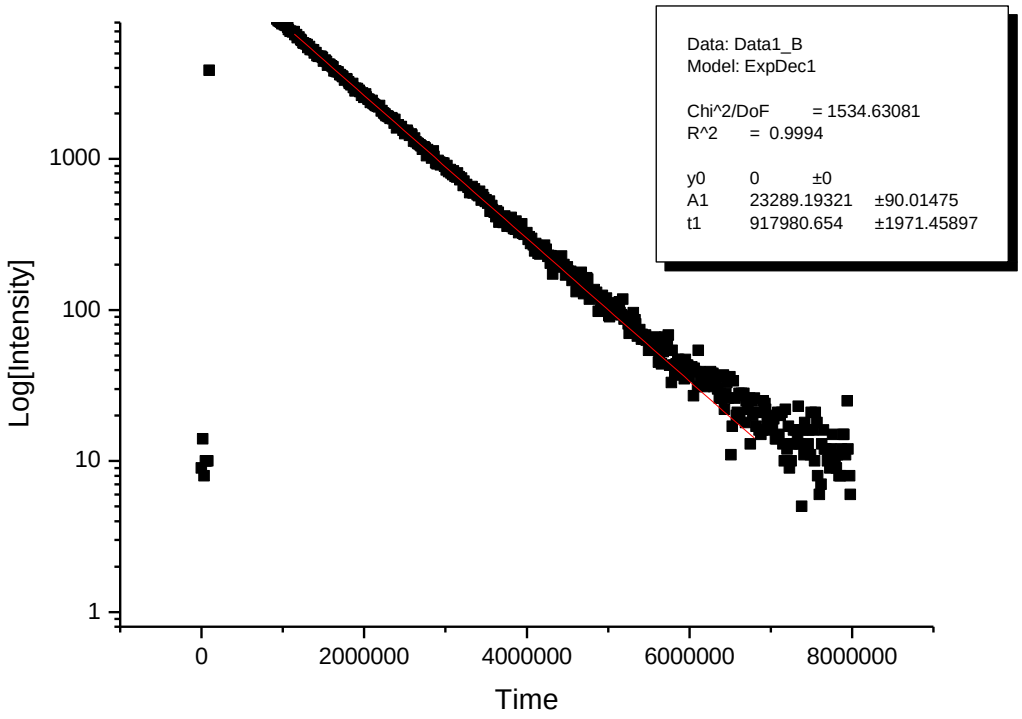

Figure 4.16 Decay curve of luminescence lifetime measurement of **EuL2** in H_2O.

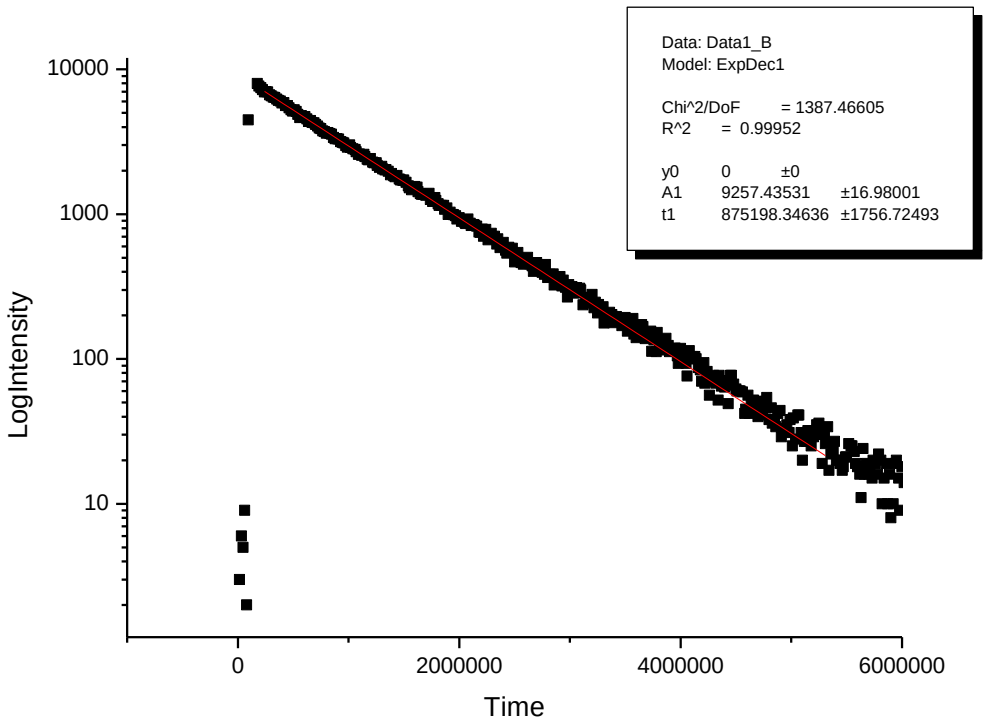

Figure 4.17 Decay curve of luminescence lifetime measurement of **EuL2** with Cys in H_2O.

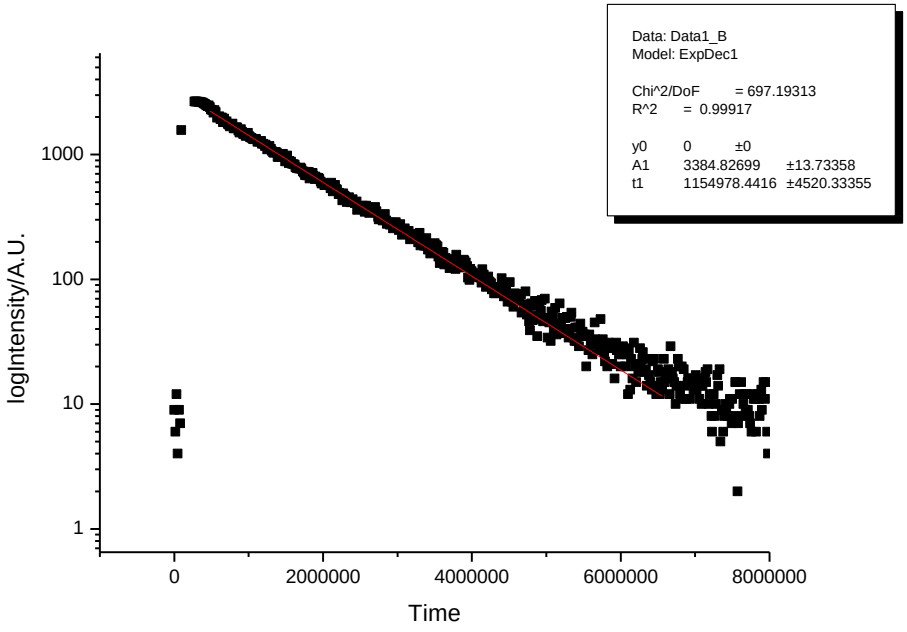

Figure 4.18 Decay curve of luminescence lifetime measurement of **EuL2** with Cys in D_2O.

Selectivity test of EuL2

The luminescent response of **EuL2** towards thiol derivatives and amino acids was investigated in 10 mM HEPES buffer (pH 7.4) at room temperature. (**Figure 4.19**) Upon addition of thiol derivatives such as cystine, CH_3SCH_3, N-Acetyl cysteine, H_2S, $NaHSO_3$, Na_2SO_4 and $Na_2S_2O_3$, the luminescent response of **EuL2** was not influenced significantly. **EuL2** did not respond towards some common amino acids such as valine (val), histidine (his), lysine (lys), isoleucine (Iso), arginine (arg), methionine (met), alanine (ala), asparagines (asp), aspartic acid (asc), serine (ser),

Moreover, **EuL2** could differentiate some Cys analogues including N-Acetyl cysteine and cystine. Upon the addition of Hcy and GSH, the luminescent intensity of **EuL2** was only slightly quenched. However, if Cys was added into the mixture of **EuL2** and other thiols or amino acids, the luminescent response of **EuL2** was quenched as in the case of a mixture of **EuL2** and Cys, indicating **EuL2** had good selective response towards Cys in the presence of other thiols or amino acids.

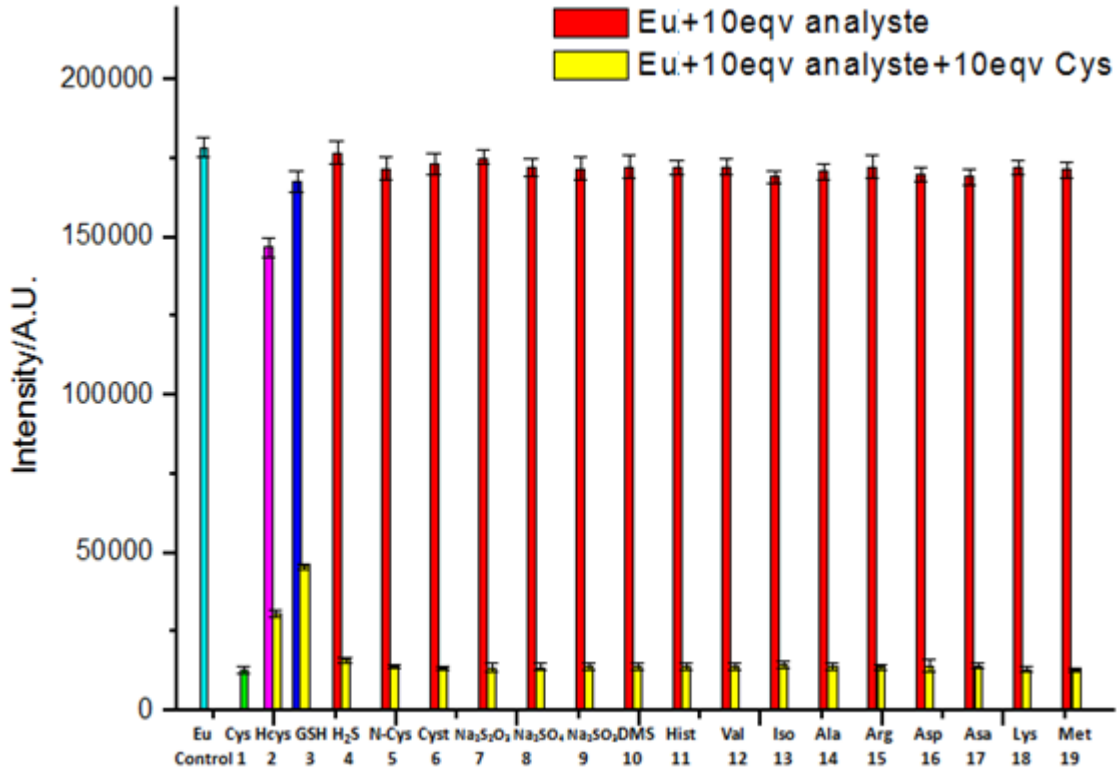

Figure 4.19 The luminescence intensity changes of [**EuL2**] (10 μM) in 10 mM HEPES with/without analytes (excitation: 350 nm). Control: **EuL2** only, 1: **EuL2**+10 eqv Cys, 2: 10 eqv Hcys, 3: 10 eqv GSH,4: 10 eqv H_2S, 5: 10 eqv N-acetyl cysteine, 6: 10 eqv Cystine,7: 10 eqv $Na_2S_2O_3$, 8: 10 eqv Na_2SO_4, 9: 10 eqv Na_2SO_3, 10: 10 eqv CH_3SCH_3, 11: 10 eqv histidine, 12: 10 eqv valine, 13: 10 eqv isoleucine, 14: 10 eqv alanine, 15: 10 eqv arginine, 16: 10 eqv asparagines, 17: 10 eqv aspartic acid, 18: 10 eqv lysine, 19: 10 eqv methionine, 20: mixture of Hcys, GSH and H_2S, (cyan point): mixture of analytes from 1 to 19 (red point): mixture of analytes from 1 to 19 +10 eqv Cys.

Reverse titration, in which Cys was first added to **EuL2** followed by addition of other thiols or amino acids, was also performed to confirm whether the signal of **EuL2** towards Cys would be altered after addition of other anions or amino acids. Based on the results showed in **Figure 4.20**, the luminescence response of **EuL2** was only quenched by the addition of Cys. After **EuL2** responded towards Cys, its luminescent

signal would not be further influenced significantly by the addition of other thiols or amino acids. This suggested that the response of **EuL2** towards Cys was specific and not altered by the presence of other thiols and amino acids.

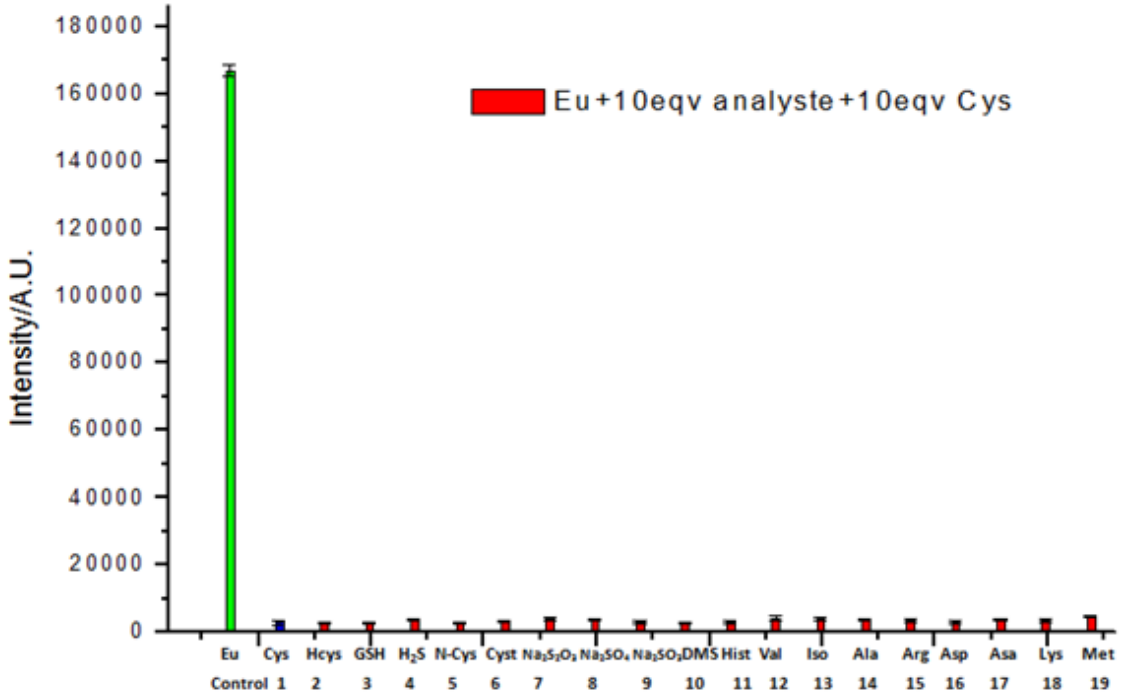

Figure 4.20 The luminescence intensity changes of [**EuL2**] (10 μM) in 10 mM HEPES with/without analytes (excitation: 350 nm). Control (green): **EuL2 only**, 1(blue): **EuL2**+10 eqv Cys only, (red) 2: 10 eqv Cys+10 eqv Hcys, 3: 10 eqv Cys+10eqv GSH,4: 10 eqv Cys+10 eqv H_2S, 5: 10 eqv Cys+10 eqv N-acetyl cysteine, 6: 10 eqv Cys+10 eqv Cystine,7: 10 eqv Cys+10 eqv $Na_2S_2O_3$, 8: 10 eqv Cys+10 eqv Na_2SO_4, 9: 10 eqv Cys+10 eqv Na_2SO_3, 10: 10 eqv Cys+10 eqv CH_3SCH_3, 11: 10 eqv Cys+10 eqv histidine, 12: 10 eqv Cys+10 eqv valine, 13: 10 eqv Cys+ 10 eqv isoleucine, 14: 10 eqv Cys+10 eqv alanine, 15: 10 eqv Cys+10 eqv arginine, 16: 10 eqv Cys+10 eqv asparagines, 17: 10 eqv Cys+10 eqv aspartic acid, 18: 10 eqv Cys+10 eqv lysine, 19: 10 eqv Cys+10 eqv methionine.

Kinetic study of EuL2

To evaluate of reactivity of **EuL2** towards Cys, Hcys and GSH, time-dependent luminescent spectra were analyzed by monitoring the luminescent changes of the reaction mixture in HEPES (pH 7.4). In the presence of 10eqv of Cys at room temperature, the luminescent intensity of **EuL2** reached a plateau, reaching its maximum within 80 min while Hcy and GSH demonstrated a smaller quenching of luminescent intensity in a slower rate. (**Figure 4.21a**) The pseudo-first-order-rate constant of reaction of **EuL2** with Cys was calculated as 0.061±0.00020 s^{-1}, which was higher than that of GSH (0.0025±0.00010 s^{-1}) and that of Hcys (0.0050±0.00030 s^{-1}). Based on these results, **EuL2** could have good selective detection of Cys over GSH and Hcys within 80 min. The faster reaction of **EuL2** with Cys could be rationalised by pKa values and the more favourable cyclisation with Cys. Firstly, pKa value of Cys (8.30) was smaller than that of Hcys (8.87) and GSH (9.20). Therefore, Cys was more reactive than Hcys and GSH since Cys is more easily deprotonated. Secondly, **EuL2** had an intramolecular cyclization reaction with Cys to form a seven-member ring which was generally more kinetically favoured than the formation of an eight-member ring such as with Hcy [15] while GSH had its natural bulkiness of the structure and could not have such intramolecular cyclization reactions easily. Therefore, based on the above reasons, **EuL2** demonstrated the advantageous discrimination of Cys over Hcys and GSH. The corresponding seven/eight-member ring intermediates with Cys/Hcys were characterized by high resolution mass spectra. (**Figures 4.22. & 4.23.)** (**Tables 4.2 & Table 4.3**)

a

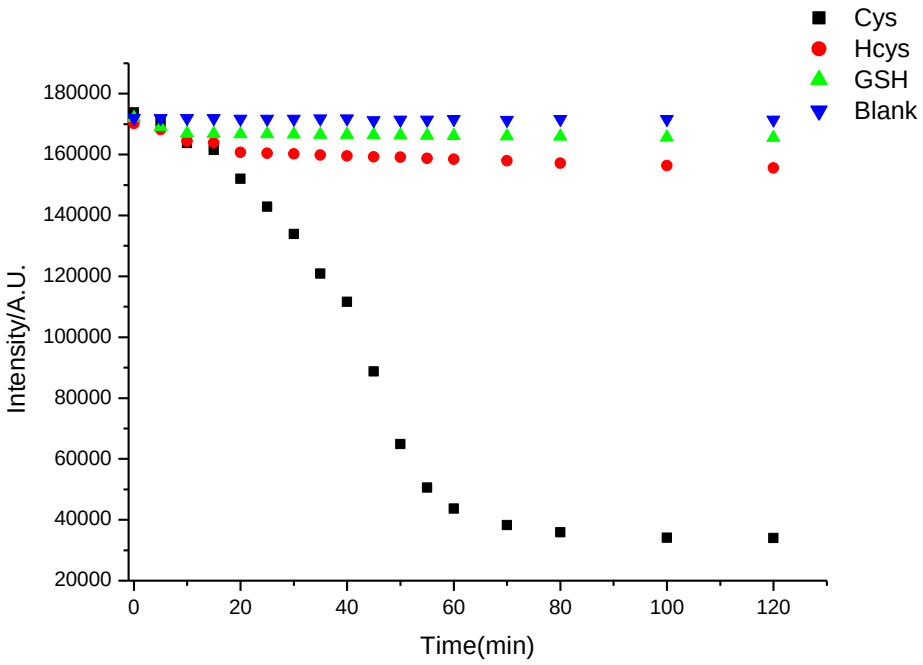
Cys
Hcys
GSH
Blank
Intensity/A.U.
Time(min)
180000
160000
140000
120000
100000
80000
60000
40000
20000
0
20
40
60
80
100
120

b

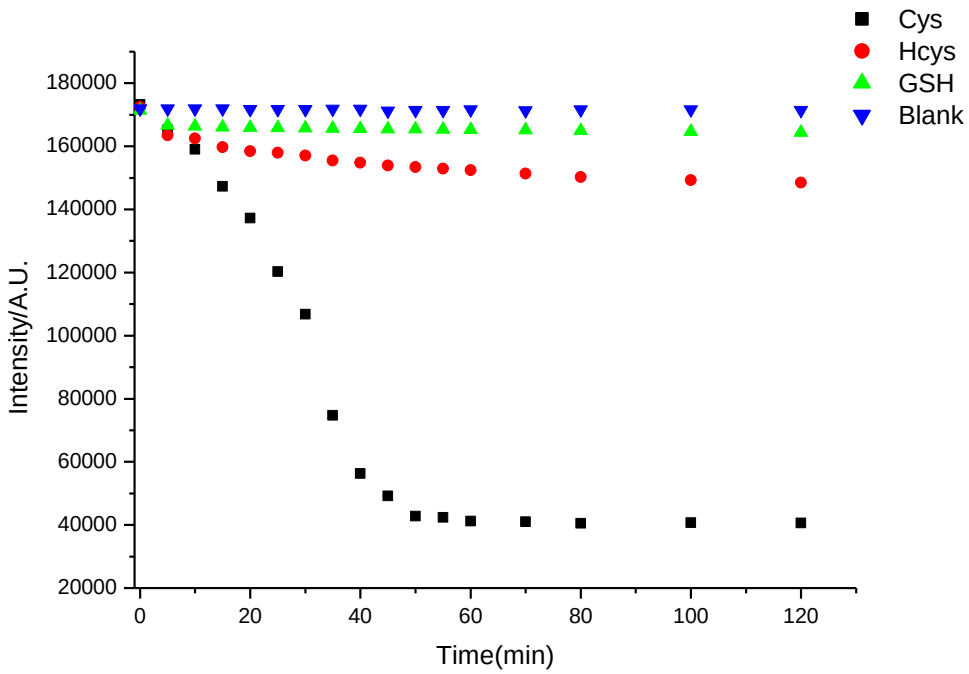
Cys
Hcys
GSH
Blank
Intensity/A.U.
Time(min)
180000
160000
140000
120000
100000
80000
60000
40000
20000
0
20
40
60
80
100
120

c

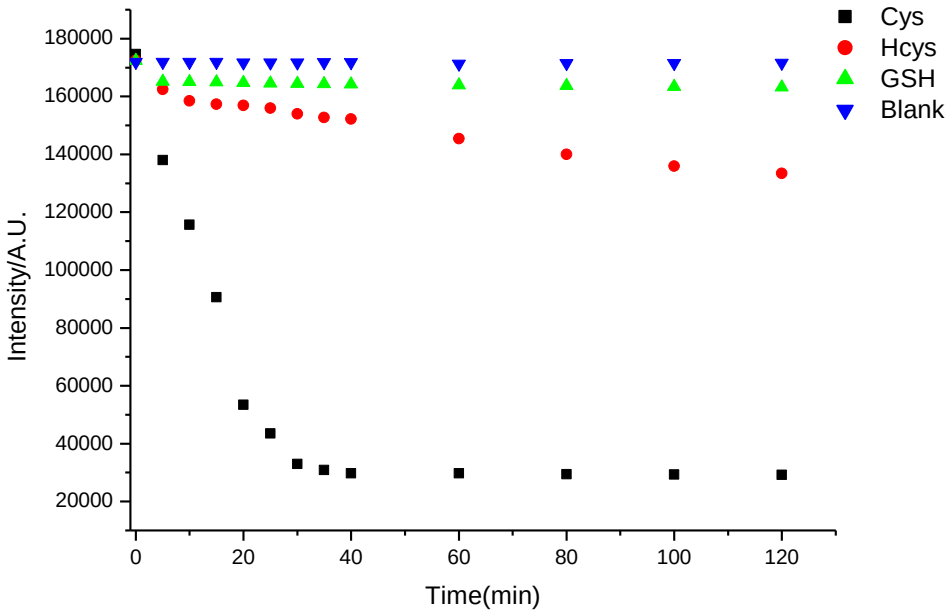

Figure 4.21 Plots of the luminescent intensity of **EuL2** (10 μM) as a function of time in the presence of Cys (10 eqv), HCys (10 eqv), GSH (10 eqv) in 0.01 M HEPES (pH 7.4) at **(a)** room temperature, **(b)** 37 ^{0}C and **(c)** 45 ^{0}C.

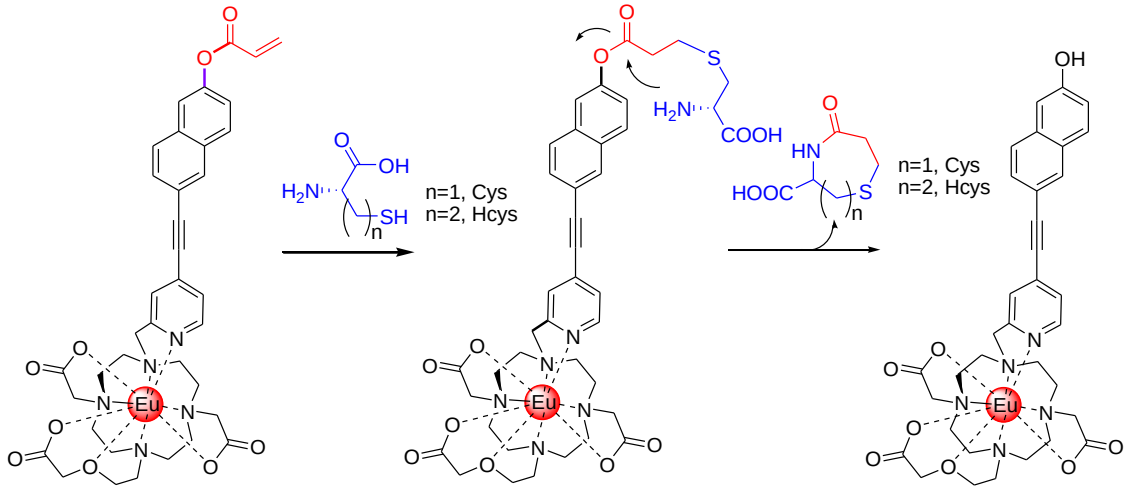

Scheme 4.4 Proposed response mechanism of **EuL2** towards Cys and Hcys.

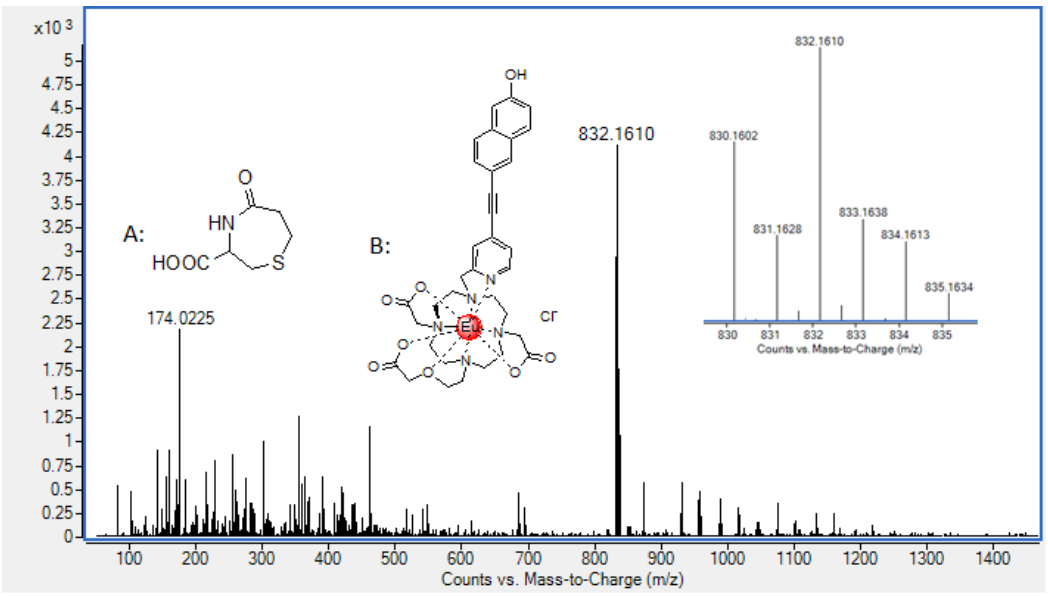

Figure 4.22 High resolution mass spectrum (-ve mode) of reaction between **EuL2** and Cys.

Name	Formula	Theoretical	Measured	Diff(mDa)	PPM
A	$C_6H_8NO_3S$	174.0230	174.0225	-0.5	-2.9
B	$C_{34}H_{38}ClEuN_5O_8$	830.1613	830.1602	-1.1	-1.3

Table 4.2 Summary of m/z of A and B from **Figure 4.21**.

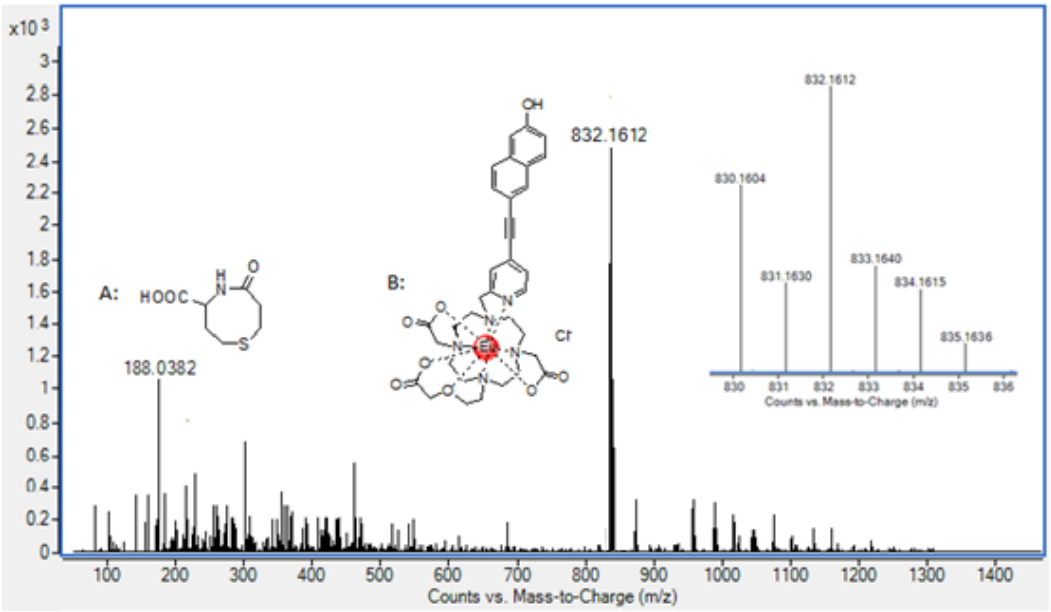

Figure 4.23 High resolution mass spectrum (-ve mode) of reaction between **EuL2** and Hcys.

Name	Formula	Theoretical	Measured	Diff(mDa)	PPM
A	$C_7H_{11}NO_3S$	188.0387	188.0382	-0.5	-2.7
B	$C_{34}H_{38}ClEuN_5O_8$	830.1613	830.1604	-0.9	-1.1

Table 4.3 Summary of m/z of A and B from **Figure 4.22**.

The time-dependent luminescent spectra at 37 ^{0}C and 45 ^{0}C were analyzed by monitoring the luminescent changes of the reaction mixture. (**Figure 4.21 b** and **c**) The luminescent intensity for reaction between **EuL2** and Cys achieved maximum quenching within 55 min (37 ^{0}C) and 40 min (45 ^{0}C). The pseudo-first-order-rate constants of reaction with Cys were 0.067±0.0003 s^{-1} (37 ^{0}C) and 0.070±0.0004 s^{-1} (45 ^{0}C) which were faster than that of Hcys (0.0088±0.0001 s^{-1} at 37 ^{0}C and 0.011±0.0002 s^{-1} at 45 ^{0}C) and that of GSH 0.0030±0.0001 s^{-1} at 37 ^{0}C and 0.0051±0.0002s^{-1} at 45 ^{0}C), indicating the pseudo-first-order-rate constants were enhanced with temperature. (**Table 4.4**)

	Cys(s^{-1})	**Hcys(s^{-1})**	**GSH(s^{-1})**
r.t.	0.061±0.00020	0.0050±0.00030	0.0025±0.00010
37 ^{0}C	0.067±0.00030	0.0088±0.00010	0.0030±0.00010
45 ^{0}C	0.070±0.00040	0.011±0.00020	0.0051±0.00020

Table 4.4 Comparison of pseudo first order rate constants of reaction of **EuL2** at room temperature, 37 ^{0}C and 45 ^{0}C.

Effect of pH value on reaction of EuL2 with Cys, Hcys and GSH

The pH value of reaction was monitored in order to know if pH value influenced the reaction between **EuL2** and Cys/ Hcys/ GSH and hence the quenching of luminescent intensity since ester group was easily attacked by thiol compounds in basic condition. In studies of the reaction between **EuL2** and Cys, the pH of the reaction medium was tuned to pH 8.4 or 8.0 or 7.4 and the quenching effect was the highest in basic regions, whereas there was little emission quenching in the acidic region such as pH 5.4 due to the less complete reactio in lower pH value. (**Figure 4.24**) In the case for Hcys and GSH, a similar phenomenon was also observed. (**Figures 4.25** & **4.26**)

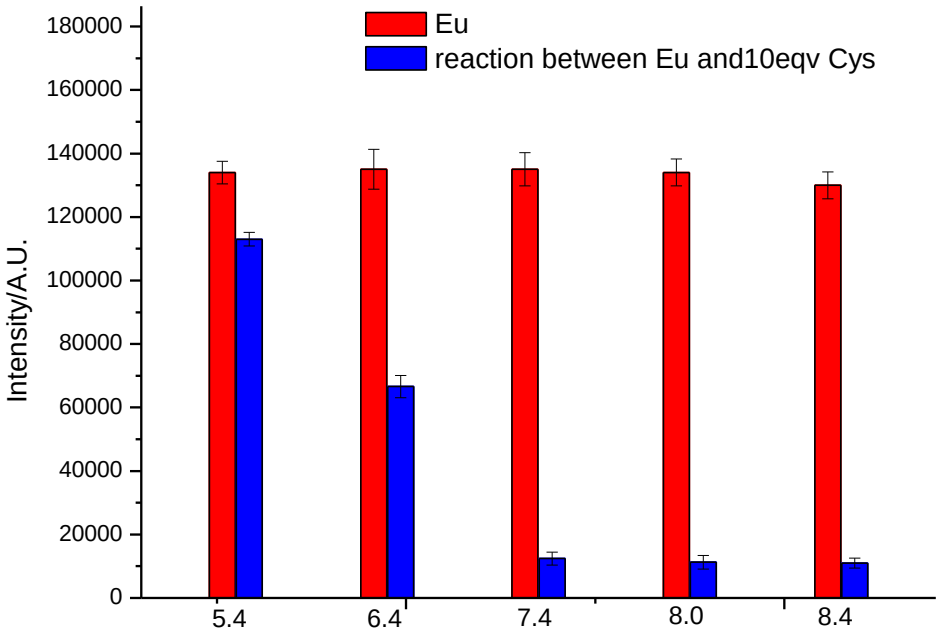

Figure 4.24. The luminescent intensity of (10μM) **EuL2** (red) and reaction of **EuL2** with 100 μM of Cys (blue) at different pH values in 80 min.

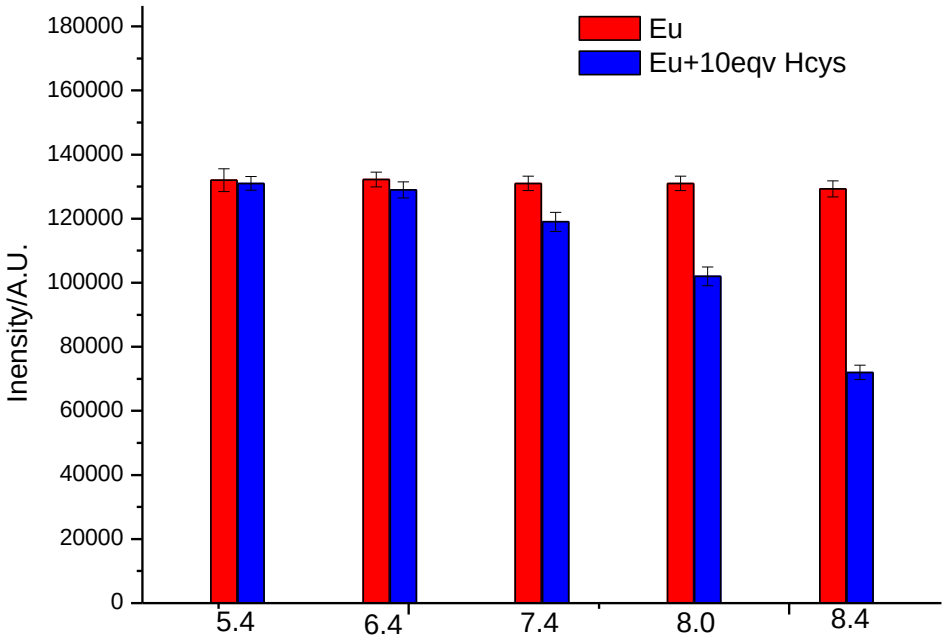

Figure 4.25 The luminescent intensity of (10 μM) **EuL2** (red) and reaction of **EuL2** with 100 μM of Hcys (blue) at different pH values in 80 min.

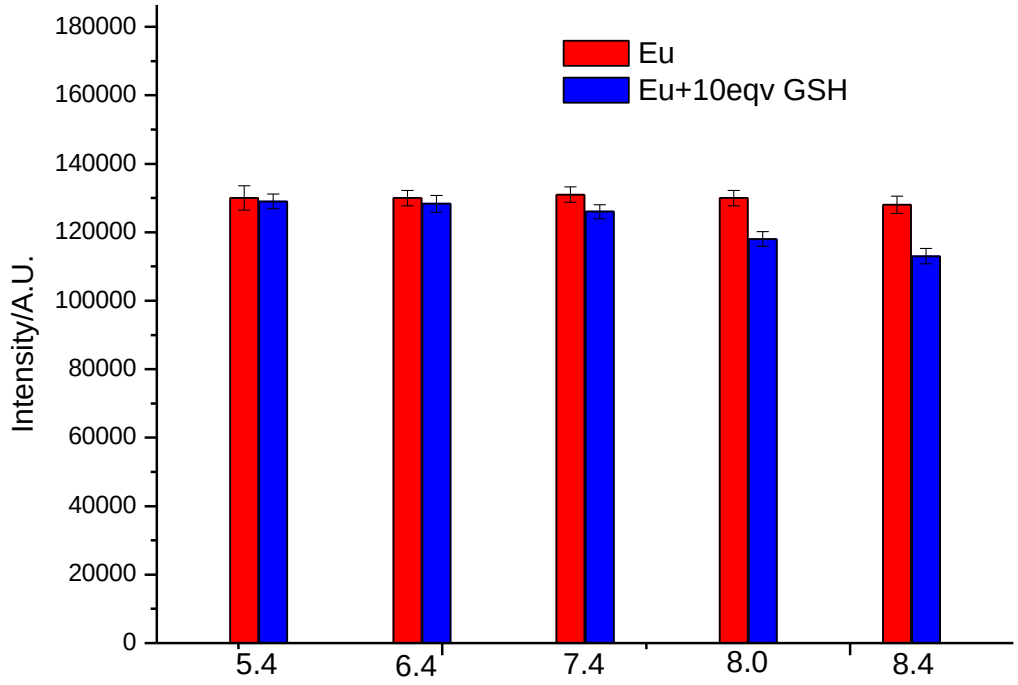

Figure 4.26 The luminescent intensity of (10 μM) **EuL2** (red) and reaction of **EuL2** with 100 μM of GSH (blue) at different pH values in 80 min.

Solution Stability of EuL2: pH dependent study

The luminescent intensities of **EuL2** and **4J** at various pH conditions were measured individually to demonstrate how pH variations influenced their luminescent intensities. The measurement was carried out after equilibrating for an hour. In **Figure 4.27**, the luminescent intensity of **EuL2** was stable from pH 4 to 8. After pH 8, its emission decreased owing to basic hydrolysis of the arcrylate group which was found in the MS spectrum. Luminescent responses of **4J** were stable from pH 4 to 7 and slightly quenched from pH 7 to 9.

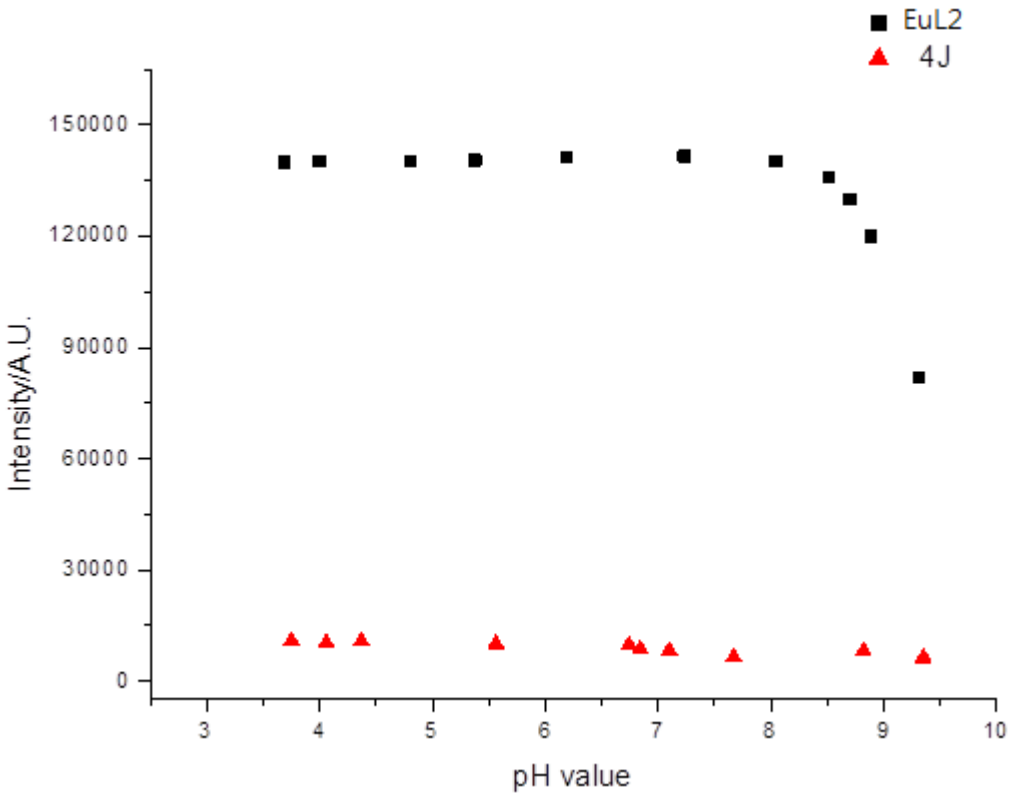

Figure 4.27 The luminescent intensity of **EuL2** (black) and **4J** (red) at different pH values.

Solution Stability of EuL2: DTPA Competition titrations

The stability of **EuL2** was investigated with diethylenetriaminepentaacetic acid (DTPA), a strong chelator and competitor with a pM value of 19.04.[16] In the study, **EuL2** and DTPA were mixed with incremental ratios of DTPA per Eu complex from 1:0 and 1: 900 and then shaken for seven days. The

luminescent intensities were measured. In **Figure 4.28**, there were around 20 % quenching, indicating **EuL2** had high stability and the Eu(III) ion was not easily decomplexed.

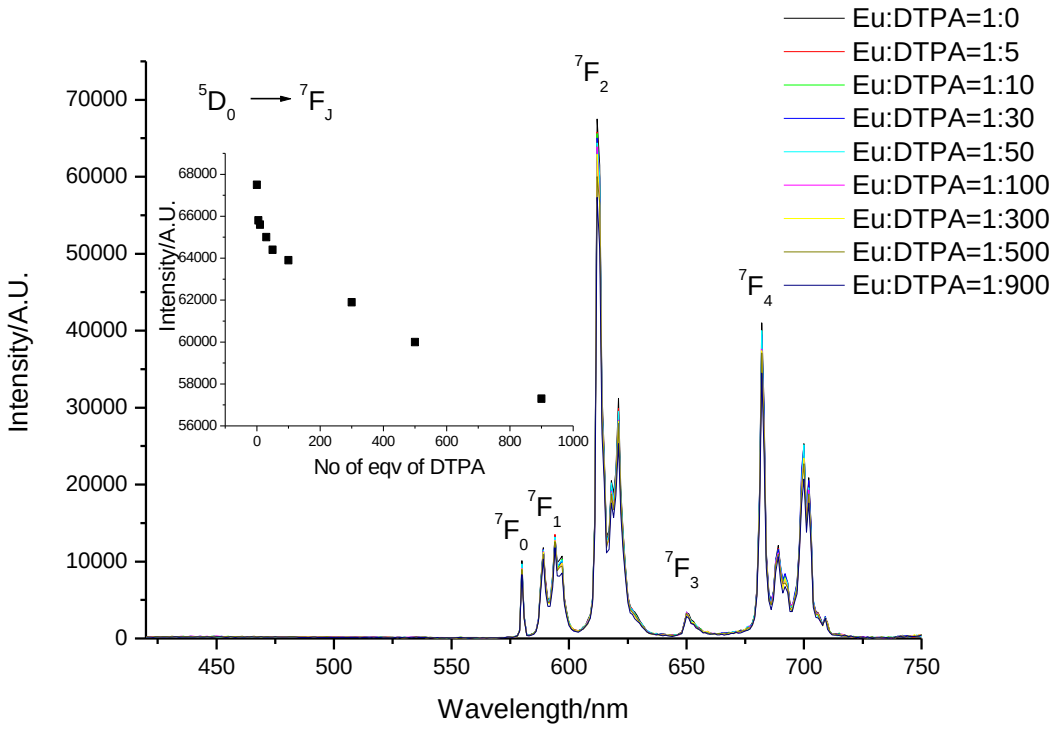

Figure 4.28 Emission spectra of the **EuL2** mixed with different amounts of the DTPA (0.1 M HEPES, pH=7.4)

4.4 Conclusion

A highly selective Cys probe, **EuL2**, was designed and developed. It utilized a Cys selective reactive site acrylate group which could distinguish Cys from other similar analogues such as homocysteine (Hcys) and glutathione (GSH). Its selectivity was due to an intramolecular cyclization in which formation of a seven-membered ring with Cys was usually more kinetically favoured than formation of an eight-membered ring with Hcy while such cyclization reaction for GSH was often hindered by its natural bulkiness. Apart from thiol derivative, other amino acids could not have interfered with its luminescent response.

Photophysical solution studies were carried out. There was significant quenching of around 90% with a linear relationship correlating to the luminescent intensity and the concentration of Cys (5μM to 80μM). The absorption maximum peak was located at 323nm and the molar extinction coefficients were calculated as 14439 M^{-1} (no Cys) and 15090 M^{-1}(add Cys). The relative quantum yields were 6.43±0.04 % (without Cys), and 0.71±0.01 % (with Cys), 5.72±0.08 % (with Hcys) and 6.20± 0.06 % (with GSH). The q value was calculated as zero both in the presence and absence of Cys, indicating that there was no bound water molecule directly coordinating with Eu (III) ion. **EuL2** was stable from pH 4 to 8. In kinetic studies, a higher pseudo first order rate constant with Cys was greater than for both Hcys and GSH.

4.7 References

[1]K. Wang, H. Peng, and B. Wang, *J. Cell. Biochem*., 2014, **115**, 1007–1022.

[2]G. N. L. Jameson, *Monatsh. Chem*., 2011, **142**, 325–329.

[3]D. M.Townsend and K. D.Tew, H.Tapiero, Biomed. Pharmacother., 2004, 58, 47–55.

[4] A.R. Ivanov, I.V. Nazimov and L.A. Baratova, *J. Chromatogr. A.*, 2000, **870**, 433–442.

[5] Y.V. Tcherkas and A.D. Denisenko, *J. Chromatogr. A*., 2001, **913**, 309–313.

[6] S. Ohmori, T. Kawase, M. Higashiura, Y. Chisaka, K. Nakata, Y. Yamasaki, *J. Chromatogr .B. Biomed. Sci Appl*., 2001,**762**, 25-32.

[7] J. D.H. Cooper, D.C. Turnell, *Methods Enzymol*., 1987, **143**, 141-143.

[8] S. Fei, J. Chen, S. Yao, G. Deng, D. He and Y. Kuang, *Anal. Biochem*., 2005, **339**, 29–35.

[9] W. Wang, L. Li, S. Liu, C. Ma and S. Zhang, *J. Am. Chem. Soc*., 2008, **130**, 10846–10847.

[10] T. Inoue and J.R. Kirchhoff, *Anal. Chem*., 2002, **74**, 1349–1354.

[11] G. Chen, L. Zhang and J. Wang, *Talanta.*, 2004, **64**, 1018–1023.

[12] I.V. Koval, *Russ. J. Org. Chem*., 2007, **43**, 319–346.

[13] H. Maeda, H. Matsuno, M. Ushida, K. Katayama, K. Saeki and N. Itoh, *Angew. Chem. Int. Ed*., 2005, **44**, 2922–2925.

[14] F. Tanaka, N. Mase and C. F. Barbas, *Chem. Commun*., 2004, 1762–1763.

[15] T. Matsumoto, Y. Urano, T. Shoda, H. Kojima and T. Nagano, *Org. Lett*., 2007, **9**, 3375–3377.

[16] R. Wang, L. Chen, P. Liu, Q. Zhang, and Y. Wang, *Chem. Eur. J*., 2012, **18**, 11343–11349.

[17] X. Yang, Y. Guo and R.M. Strongin, *Angew Chem Int Ed*., 2011, **50**, 10690–10693

[18] E. G. Moore, J. Xu, C. J. Jocher, E. J. Werner, and K. N. Raymond, *J. Am. Chem.*

Soc., 2006, **128**, 10648–10649

4.6 Appedix

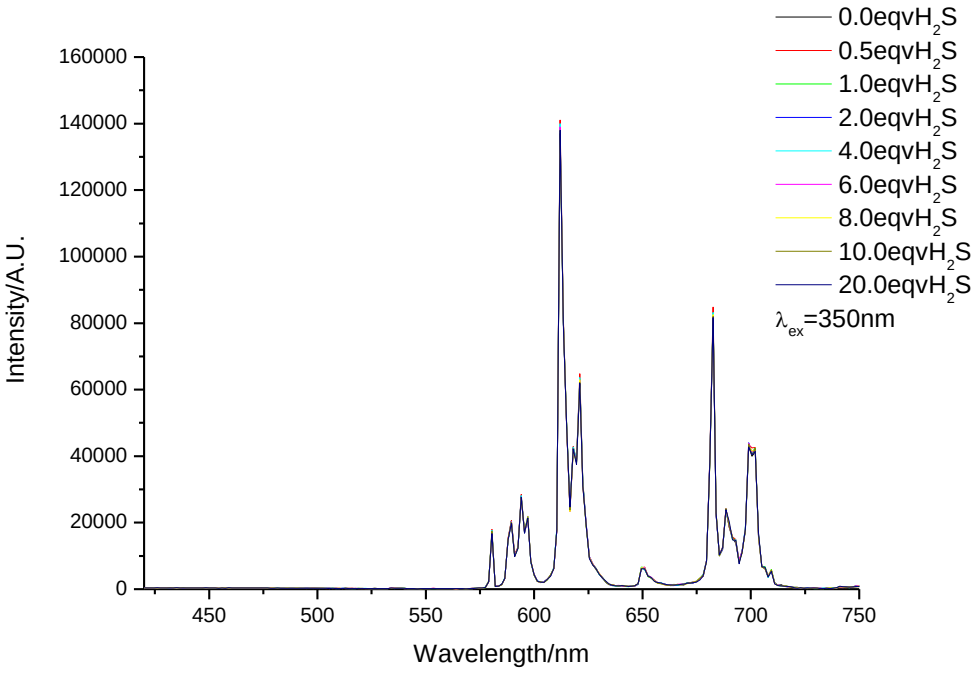

Figure 4.29 Emission spectra of 10 μM aqueous solution upon addition of aliquots of various equiv of H_2S with respect to **EuL2** (0.01 M HEPES, pH=7.4, λ_{ex}=350 nm).

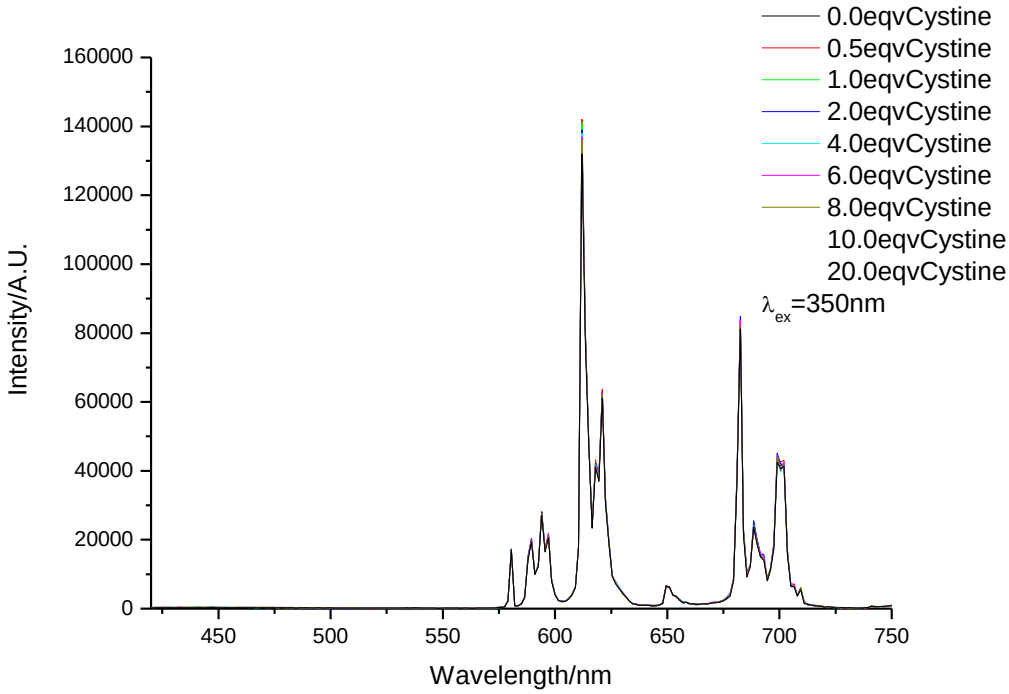

Figure 4.30 Emission spectra of 10 μM aqueous solution upon addition of aliquots of various equiv of cystine with respect to **EuL2** (0.01 M HEPES, pH=7.4, λ_{ex}=350 nm).

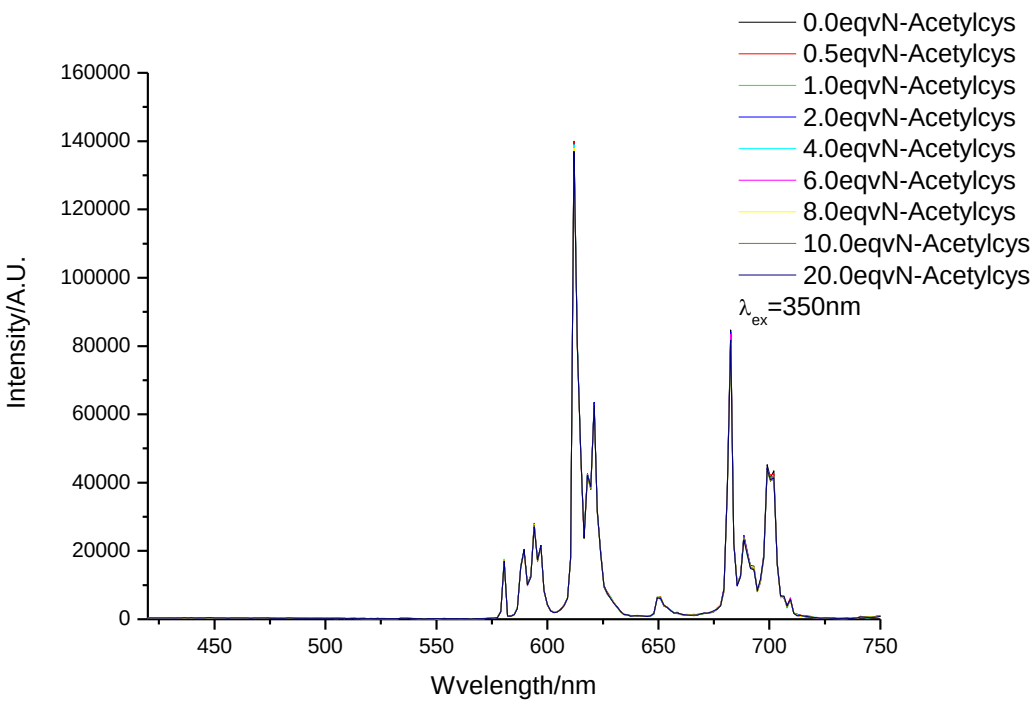

Figure 4.31 Emission spectra of 10 μM aqueous solution upon addition of aliquots of various equiv of N-Acetyl cysteine with respect to **EuL2** (0.01 M HEPES, pH=7.4, λ_{ex}=350 nm).

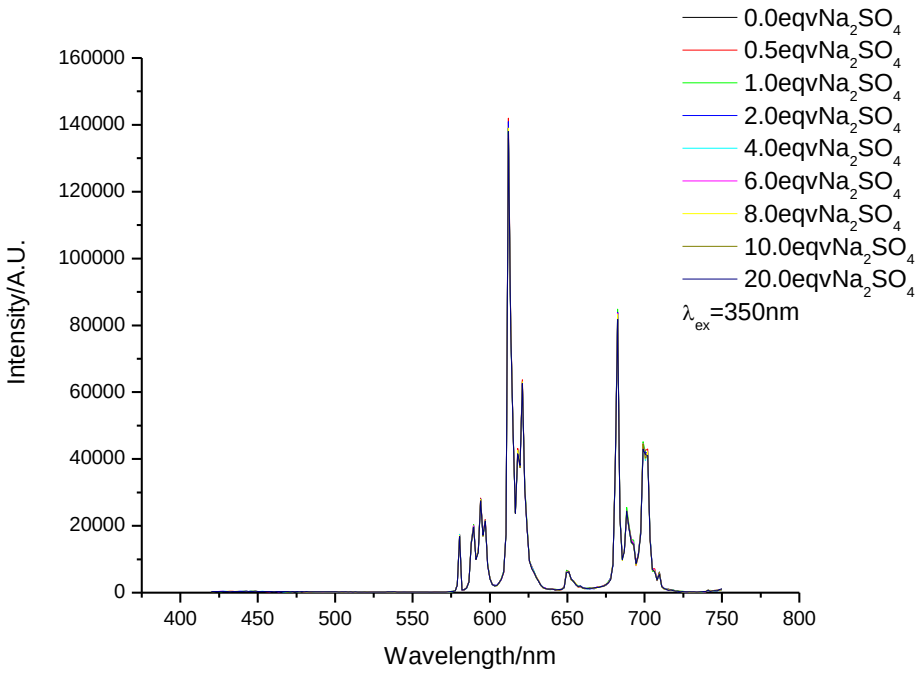

Figure 4.32 Emission spectra of 10 μM aqueous solution upon addition of aliquots of various equiv of Na_2SO_4 with respect to **EuL2** (0.01 M HEPES, pH=7.4, λ_{ex}=350 nm).

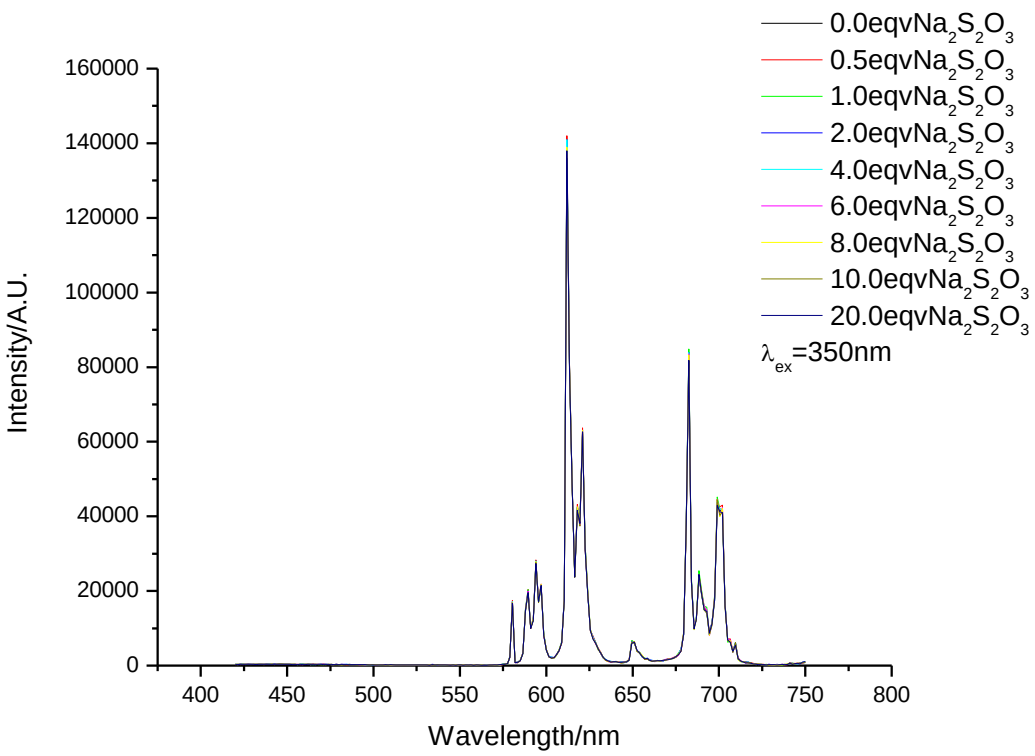

Figure 4.33 Emission spectra of 10 μM aqueous solution upon addition of aliquots of various equiv of $Na_2S_2O_3$ with respect to **EuL2** (0.01 M HEPES, pH=7.4, λ_{ex}=350 nm).

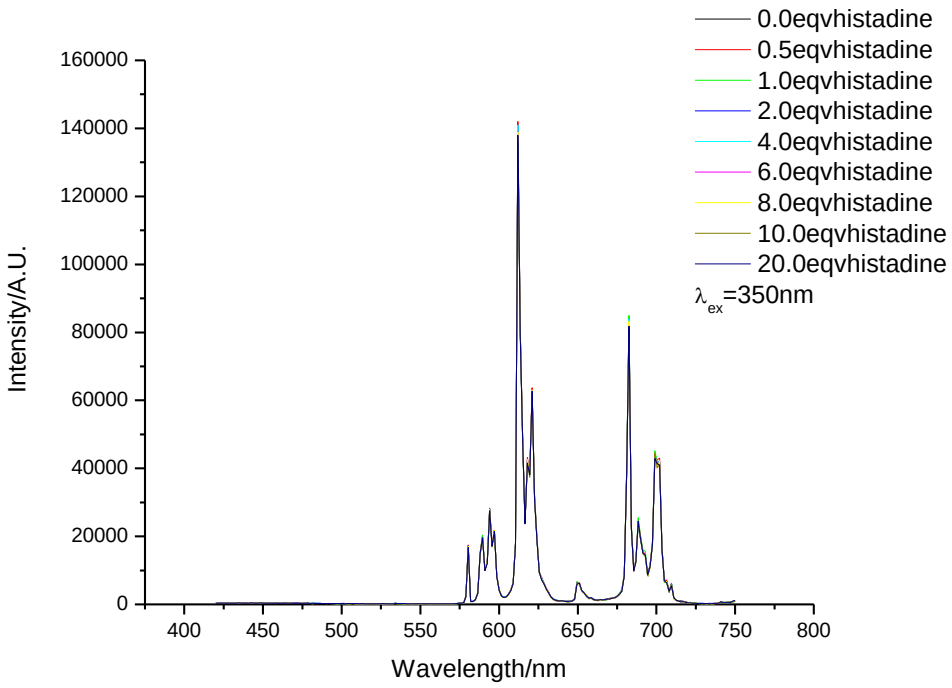

Figure 4.34 Emission spectra of 10 μM aqueous solution upon addition of aliquots of various equiv of histadine with respect to **EuL2** (0.01 M HEPES, pH=7.4, λ_{ex}=350 nm).

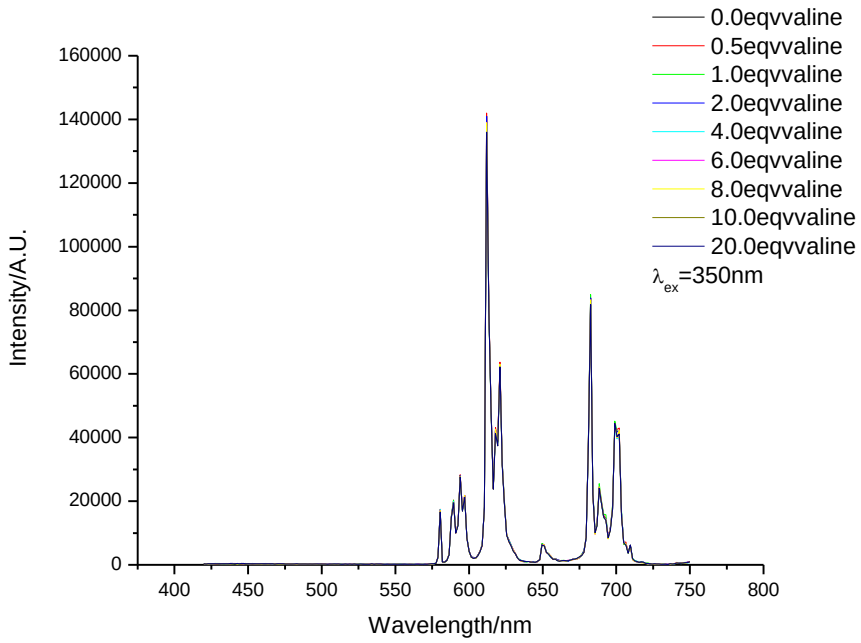

Figure 4.35 Emission spectra of 10 μM aqueous solution upon addition of aliquots of various equiv of valine with respect to **EuL2** (0.01 M HEPES, pH=7.4, λ_{ex}=350 nm).

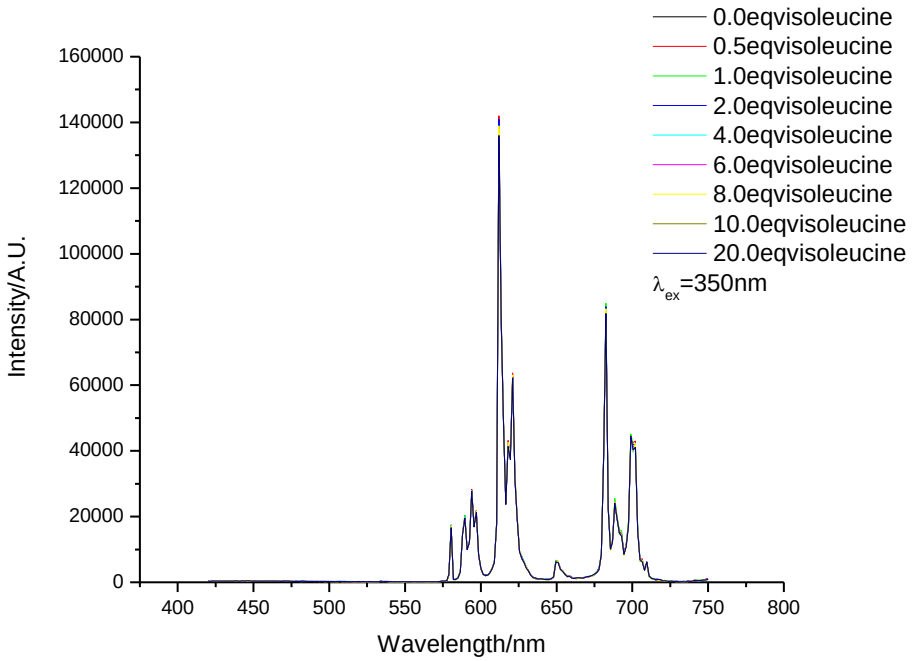

Figure 4.36 Emission spectra of 10 μM aqueous solution upon addition of aliquots of various equiv of isoleucine with respect to **EuL2** (0.01 M HEPES, pH=7.4, λ_{ex}=350 nm).

CHAPTER 5

Development of lanthanide complexes for detection of Zn(II) ion and ATP

5.1 Introduction

Zinc usually occurs in the +2 oxidation state in biological systems and is the second most abundant trace mineral in the human body after iron. [1] There is approximately 2g to 3g of zinc in total in an adult human. The majority of cellular zinc ions are chelated by proteins or enzyme peptides or amino acids strongly. The remaining zinc [2] is not chelated by protein or enzymes and exists in fluctuating labile pools for synthesis of new proteins or potential cell signalling functions. [3] The labile pools of zinc can be found in some tissues in organs such as the intestine, retina and brain.

The maintaining of zinc balance, zinc homeostasis, is important and is controlled by the coordinated actions of zinc transporters, which regulate the efflux and influx of zinc and maintain the extracellular and intracellular zinc distribution and concentration. A failure to maintain zinc homeostasis will lead to serious problems. For instance, zinc imbalance is related to various neurological diseases such as Alzheimer's disease. [4]-[6] Zinc deficiency causes growth retardation, dysfunction of cell-mediated immunity and increases the susceptibility to infection. [7]-[9]

As discussed before, zinc is the most common transition metal observed in proteins. This is due to its advantageous properties to perform structural and catalytic functions. First, it has good stability towards redox reactions since it is very stable only in the coordination number +2. Second, it has d^{10} electron configuration and is not susceptible to ligand field stabilization effects. Third, it is classified as a borderline Lewis acid and can have coordination of N, S, and O donor atoms. It is therefore found to be chelated by cysteines, glutamates, histidines and aspartates. Fourth, it is a Lewis acid and can activate coordinated substrates and maintain ligand nucleophilicity

Zinc plays diverse roles in biological processes. For instance, zinc plays a structural cofactor role in more enzymes or metalloproteins since zinc can maintain their

structures and shapes. Without zinc, their structures cannot be maintained to be recognized by substrates and protein cannot function well. Zinc is also important for development of the central nervous system since it is necessary for the formation of proteins, enzymes and growth factors that direct stem cell proliferation and differentiation during neurodevelopment. Zinc is essential for formation of enzymes in the development of brain including DNA polymerase, DNA synthesis enzyme. [10] Therefore, learning and memory will be abnormal if zinc is deficient. Apart from those functions, zinc also plays a role in cell division, wound healing and immune function [11]. The major functions of zinc are summarized in **Figure 5.1**.

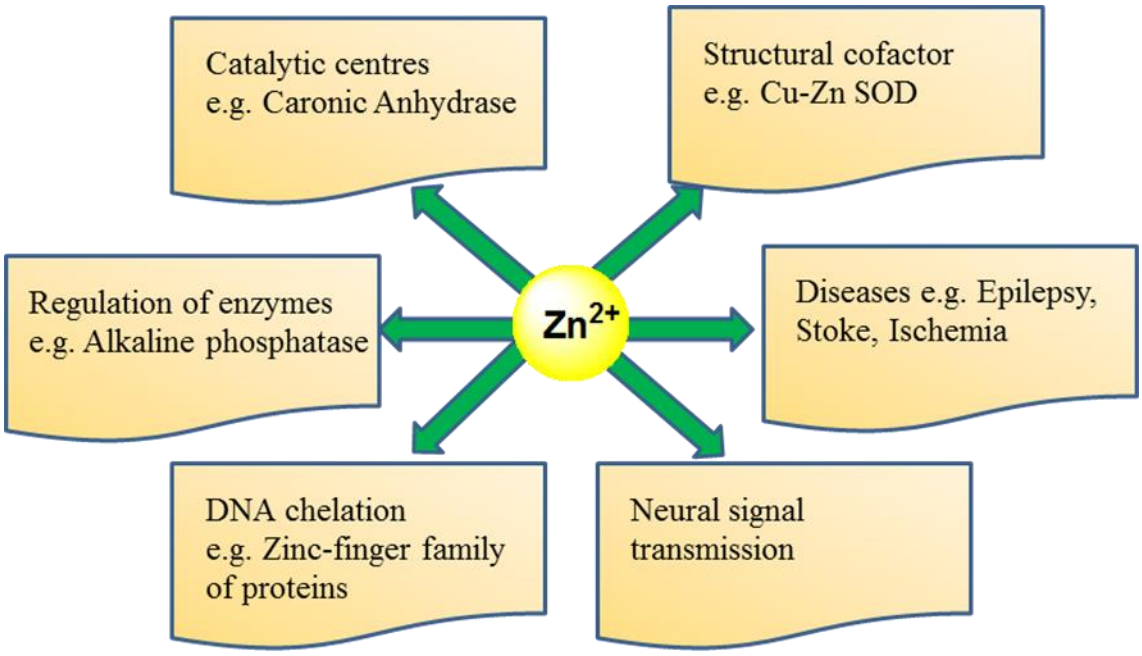

Figure 5.1 Major functions of zinc.

Unlike other transition metals such as copper, zinc is invisible to most spectroscopic methods due to d^{10} electronic configuration. Therefore, some analytic methods such as absorption spectroscopy and electron paramagnetic resonance spectroscopy used for studying copper and iron cannot be applied to measure zinc. However, there are still several common analytic techniques for measuring zinc such as s atomic absorption spectrometry, flow injection analysis, mass spectroscopies, x-ray fluorescence, electro-analytical techniques (e.g., stripping voltammetry) and neutron

activation analysis. (**Table 5.1**) For instance, inductively coupled plasma atomic emission spectroscopy (ICP-AES) is used for determination of zinc in urine, in tissue and blood samples. Detection limits in urine, tissue and blood are 0.1μg/sample, 0.2 μg/g are and 1 μg/100 g respectively.

Analytical method	Preparation method	Sample matrix	Sample detection limit
ICP-MS	Digest with HNO_3 using microwave digestion; dilute	Brain tissue	32mg/L
ICP-AES	Acid digestion with HNO_3/$HClO_4$, H_2SO_4, measure at 213.9 nm	Blood or tissue	1 μg/100 g
Flame AAS	Add Brij 35 to sample; mix	Serum	~0.6 μg/mL
EDXRF	Rinse sample with hexane; wet or dry ash with HNO_3	Hair	0.001 μg/L
Radiochemical NAA	Acid digestion with mixtures of different acids; distill volatile elements	Liver	/
GF-AAS	Microwave wet acid digestion	Semen	400 μg/L

Table 5.1 Summary of selected analytical methods for measurement of biological zinc. ICP is inductively coupled plasma spectroscopy; MS is mass spectrometry; AES is atomic emission spectroscopy; AAS is atomic absorption spectroscopy; Brij 35 is polyoxyethylene (35) lauryl ether; EDXRF is energy dispersive x-ray fluorescence;; NAA is neutron activation analysis.

However, the above methods usually involve complicated sample preparation. For instance, sample preparation in ICP-MS requires several steps of acid digestion with concentrated acids or some extraction of metals with polydithiocarbamate resin before digestion. Therefore, optical detection is one of the alternative methods for detection of zinc since it is convenient, non-invasive, simple, sensitive, selective and low cost. Based on the above advantages, the development of fluorescent probes for detection of zinc has drawn great attention.

To design a suitable chemical sensor for recognizing of zinc, it is crucial to realize the chemical properties of zinc and hence its coordination preference. Some factors such as donor atoms of ligands can be taken into consideration. Zinc is considered as a borderline Lewis acid that can interact with both hard and soft Lewis bases easily. The Irving-Williams series [12] generally shows the order which is related to smaller ionic radii across first row transition metal series leading to stronger metal to ligand interactions. This means copper is usually the one element to be chelated by ligand strongly. However, this order can be changed by preferred geometry of metal ion in ligand chelation. For instance, copper prefers to be chelated in a Jahn-Teller distorted or square planar geometry due to its high ligand field stabilisation energy. Zinc, having no ligand field stabilisation energy, prefers tetrahedral chelation by its ligands so as to minimise repulsion between donor groups. [13]

Over the past ten years, many zinc fluorescent probes have been developed and there are some common zinc receptors that have been used widely. Some common zinc receptors are introduced below.

Receptor for detection of Zn(II) ion

The zinc receptor dipicolylamine is one of the popular zinc chelators for constructing zinc binding domains with a 1:1 binding ratio to zinc. It is membrane-permeable owing to its structural similarity to the membrane-permeable

N,N,N9,N9-tetra(2-picolyl)ethylenediamine (TPEN). It is a typical electron donor in the photoinduced electron transfer (PET) zinc sensor. Upon binding with zinc, PET process from di-(2-picolyl)amino group to the chromophore is blocked and the luminescence is recovered. For instance, **5A** had selective detection of zinc with strong fluorescent enhancement. The binding ratio between **5A** and zinc was 1:1. The binding constant (K_a) of zinc binding to **5A** was 5.9×10^4 M^{-1}. [14]

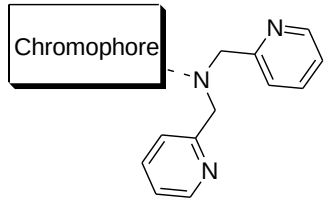

Figure 5.2 The structure of zinc receptor dipicolylamine.

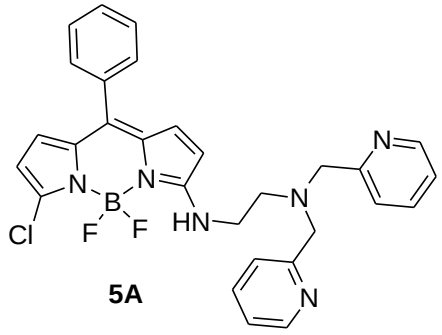

Figure 5.3 The structure of **5A**. [14]

Quinoline is another common receptor used to detect zinc. Many quinoline-based zinc sensors would incorporate the other receptor group in R_1 and R_5 group. (**Figure 5.4**) The withdrawing group or electron donating group is sometimes put in R_2, R_3 and R_4 groups. Different substituent groups R_1, R_2, R_3, R_4 and R_5 lead to variation in photophysical properties and selectivity towards zinc. One example of quinoline-based zinc sensors is shown in **Figure 5.5**. **5B** recognized zinc selectively with good luminescent enhancement. It showed 1:1 binding with zinc and the binding constant (K_a) was calculated to be 2.5×10^5 M^{-1}. [15]

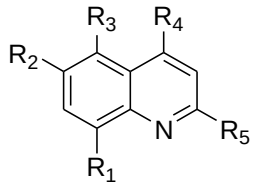

Figure 5.4 Structure of quinoline receptor.

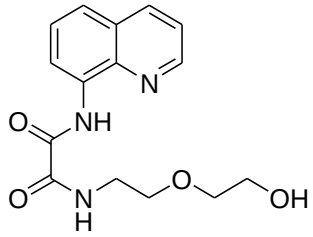

5B

Figure 5.5 Structure of **5B**. [15]

Schiff base is another common zinc receptor with a nitrogen atom for chelating zinc. Before binding with zinc, probe with Schiff base as receptor is nonfluorescent since C=N isomerization plays a predominant role in the decay process of the excited states with an unbridged C=N structure and the non-radiative process is predominant. Upon binding with zinc, the probe becomes fluorescent since binding of zinc by the C=N group would suppress non-radiative C=N isomerization in the excited states. For instance, **5C** had selective detection of zinc with good fluorescent enhancement. Binding with zinc led to rigidity, stopped C=N isomerization and the absorption band would shift to longer wavelength by 80 nm from 346 nm in a zinc-free environment to 426 nm. Association constant (Ka) was 3.9×10^4 M^{-1}.[16]

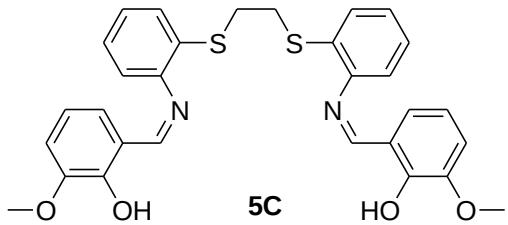

5C

Figure 5.6 Structure of **5C**.[16]

Receptor for detection of ATP

Adenosine triphosphate (ATP) is an important molecule which is responsible for the production and storage of energy in living cells.[17] Inspired by the good selectivity

for phosphate compounds exhibited by enzymes containing zinc at their active sites,[18]-[20] the detection of ATP can be achieved by the use of a zinc complex bearing one or two vacant coordination sites for ATP. Complex of zinc and dipicolylamine is the most common receptors for detection of ATP.[21]-[23] Dipicolylamine is a tridentate ligand with three nitrogen donors to bind with zinc and leaves coordination sites free for ATP binding. Zinc–dipicolylamine receptors demonstrate good selectivity for phosphate oxoanions over other anions in aqueous solution. For instance, **5D** showed selective binding towards ATP over other biological anions such as Adenosine diphosphate (ADP), Adenosine monophosphate (AMP) and phosphate under aqueous condition. It showed a 1:1 binding with ATP and binding constant was calculated as 5.62×10^5 M^{-1}.[24]

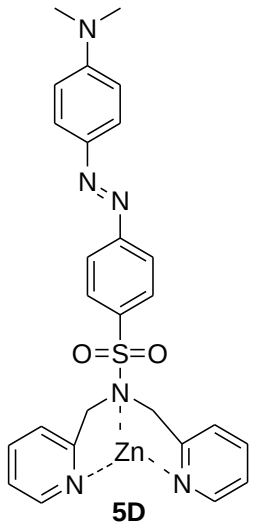

5D

Figure 5.7 Structure of **5D**.

5.2 Design of probes

The structures of the zinc sensors **EuL3**, **EuL4**, **EuL5** are depicted in **Figure 5.8**. They consist of three main parts, a selective receptor dipicolylamine for detection of zinc, a chromophore for sensitization of Eu(III) ion and an Eu chelator. As discussed before, dipicolylamine is a selective receptor for zinc. **EuL5** becomes an ATP sensor after chelation with Zn(II) ion. The chromophore is used for sensitization of Eu(III) ion.

Eu chelator is macrocycle in which there is no water molecule in the inner coordination environment due to nine coordination environment. It also makes the overall complex more hydrophilic and hence more water soluble.

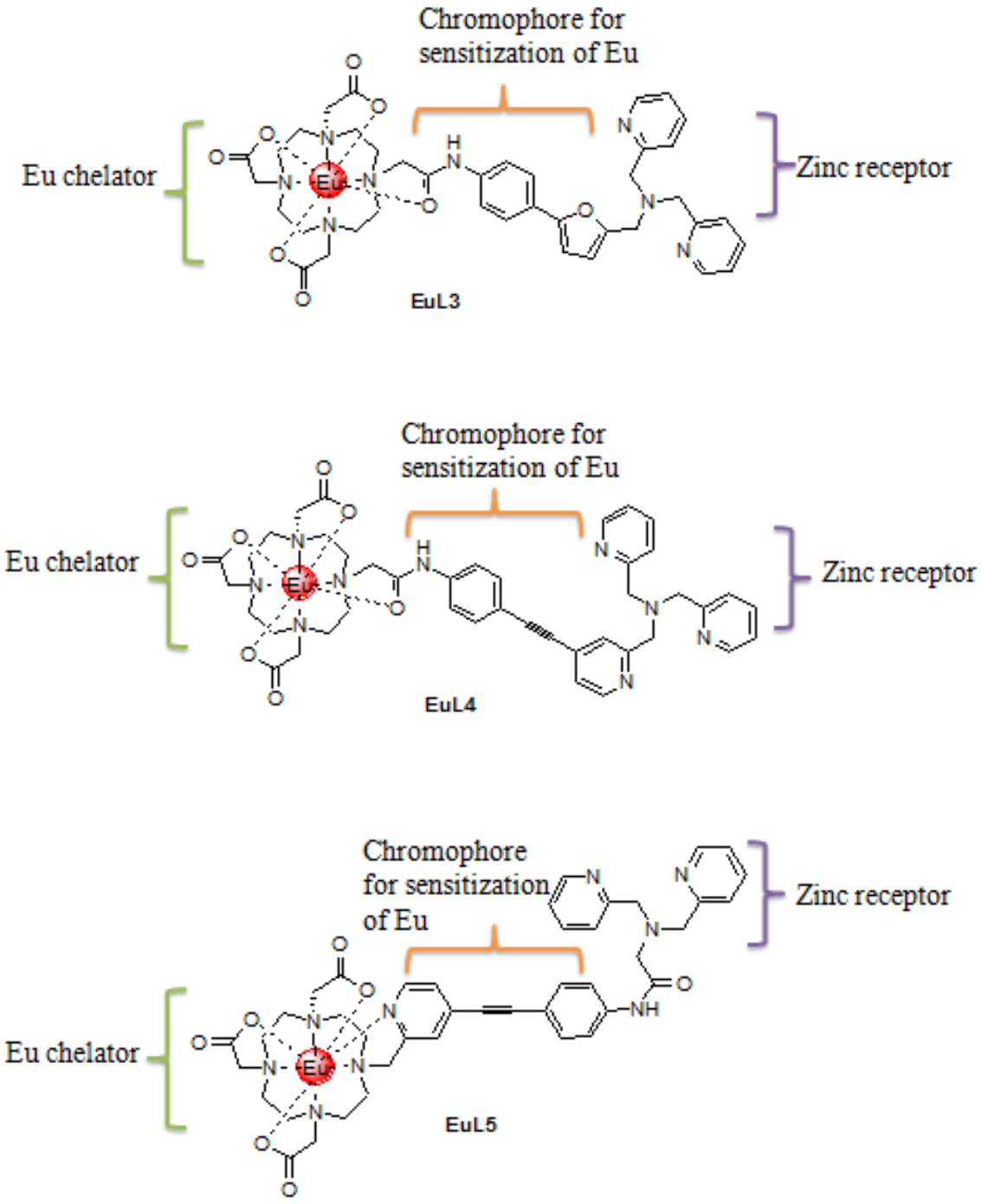

Figure 5.8. Structures of **EuL3**, **EuL4** and **EuL5**.

5.3 Result and discussion

5.3a Synthesis of probes

Synthesis of EuL3

The synthesis was started with reduction of 5-(4-nitrophenyl)furan-2-carbaldehyde. The reduction was simply done by the mixing starting material with excess amount of sodium borohydride and stirred for overnight. The yield was 78%. Other reducing agents such as lithium aluminium hydride were used, but the yield was lower than in the case of sodium borohydride. **5E** underwent bromination by mixing with phosphorus tribromide and the yield was 53%. Other bromination regents such as phosphorus pentabromide were used and the yield was similar as in the case of phosphorus tribromide.

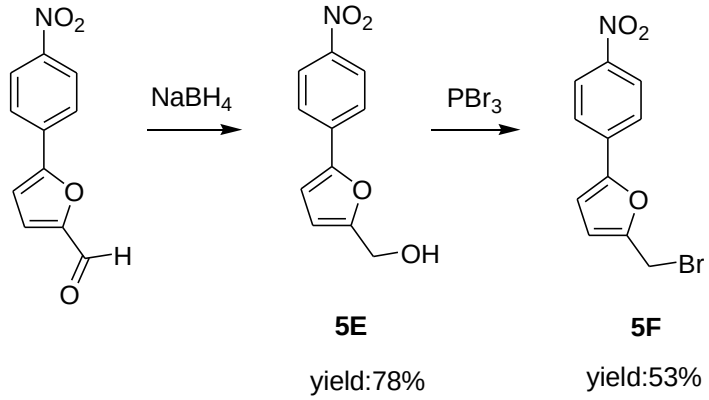

Scheme 5.1 Synthetic Routes to **5F**.

Receptor **5H** was synthesized in two steps. The first was reaction between pyridinecarboxaldehyde and 2-aminopyridine under refluxed overnight. The second was the reaction mixture reacting with sodium borohydride. The yield was 32%. **5I** was prepared from nucleophilic substitution between **5G** and **5H** in the presence of potassium carbonate. The yield was 45%.

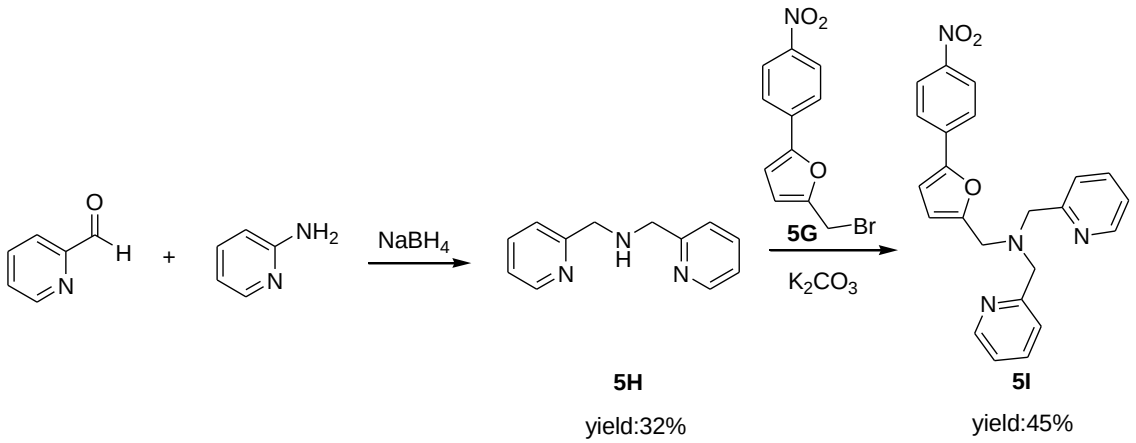

Scheme 5.2 Synthetic Routes to **5F**.

5J was prepared from reduction by zinc metal in acetic acid. The yield was 41%. Several reduction methods had been tried such as Pd/C heterogeneous dehydrogenation, Tin(II) chloride nitro reduction. They could not afford the desired products. The next step was reaction with chloroacetyl chloride in the prescence of triethylamine. Without further purification, **DO3A-ME** and potassium carbonate were added into the reaction mixture and refluxed overnight. The yield was 45%. Finally, deprotection of **5K** by mixing it with NaOH and then refluxed with 1.0 eqv of $EuCl_3.6H_2O$ was carried out to form **EuL3**. (yield: 56 %) The high-resolution mass spectra (ESI+) showed peaks corresponding to the protonated Eu(III) complexes **EuL3** with characteristic Eu(III) isotopic pattern entities which confirmed the formation of the desired Eu(III) complexes.(**Figure 5.9**)

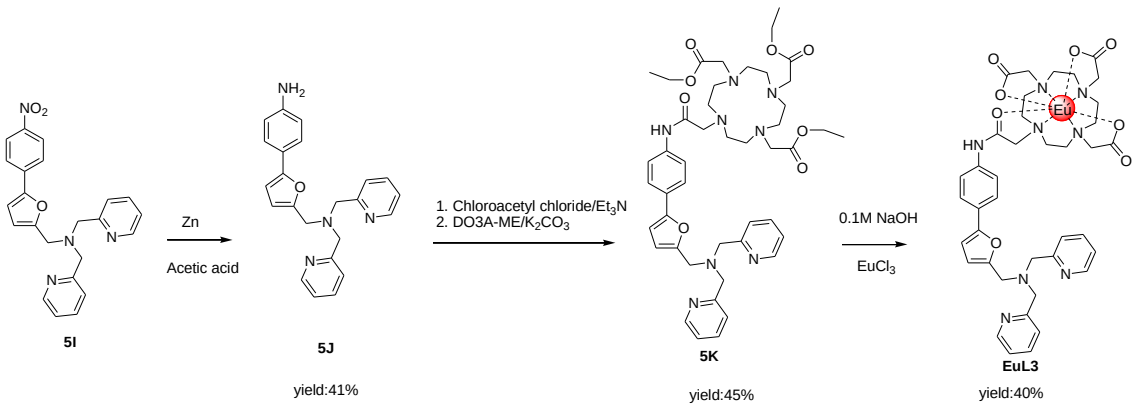

Scheme 5.3 Synthetic Routes to **EuL3**.

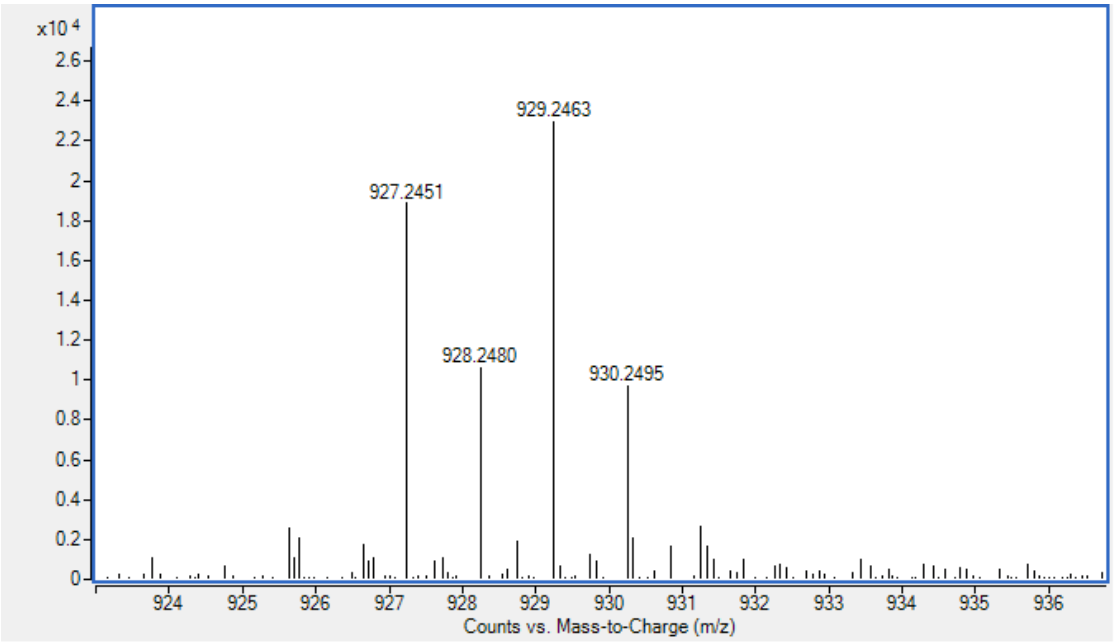

Figure 5.9 High resolution mass spectrum of **EuL3**.

Synthesis of EuL4

The synthesis of chromophore **3C** was mentioned in the synthesis in Chapter 3. **5L** was prepared from the nucleophilic substitution between **5H** and **3C** and the yield was 49%. Then, acidic deprotection of Boc protecting group was done by trifluoroacetic acid and the yield was 60%

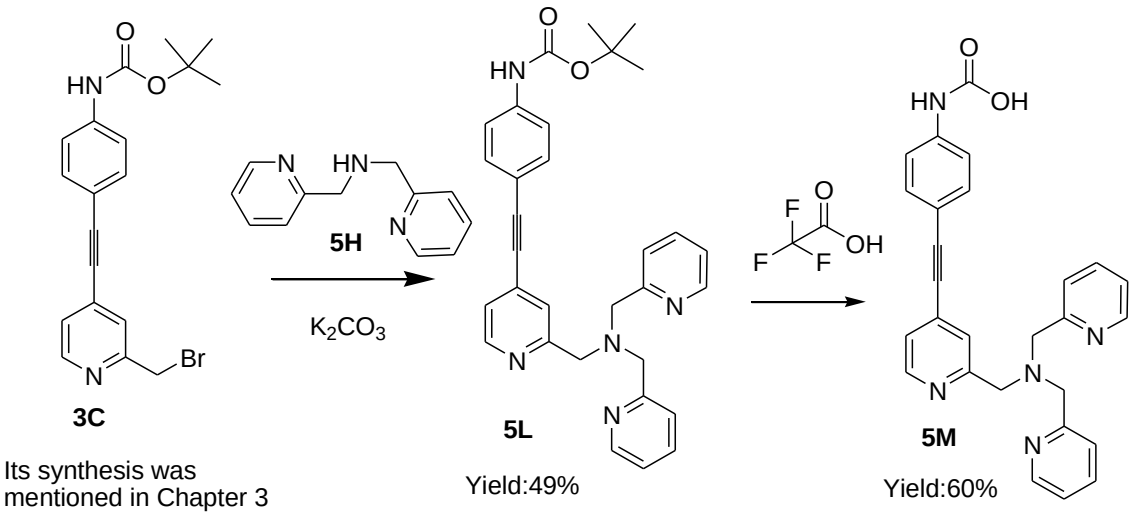

Scheme 5.4 Synthetic Routes to **5M**.

5M first reacted with chloroacetyl chloride and then further reacted with **DO3AE**. The yield was 57%. Finally, deprotection of **5N** by mixing with NaOH and then

refluxed with 1.0 eqv of $EuCl_3.6H_2O$ was carried out to form **EuL4**. (yield: 52%) The high-resolution mass spectra (ESI+) showed peaks corresponding to the protonated Eu(III) complexes **EuL4** with characteristic Eu(III) isotopic pattern entities which confirmed the formation of the desired Eu(III) complexes.(**Figure 5.10**)

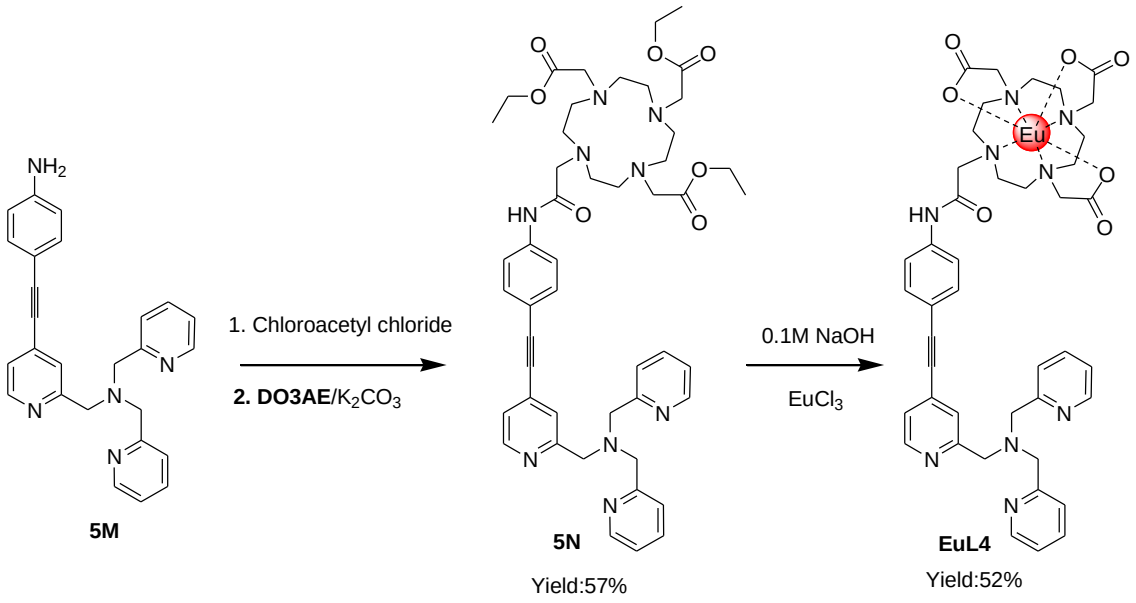

Scheme 5.5 Synthetic Routes to **EuL4**.

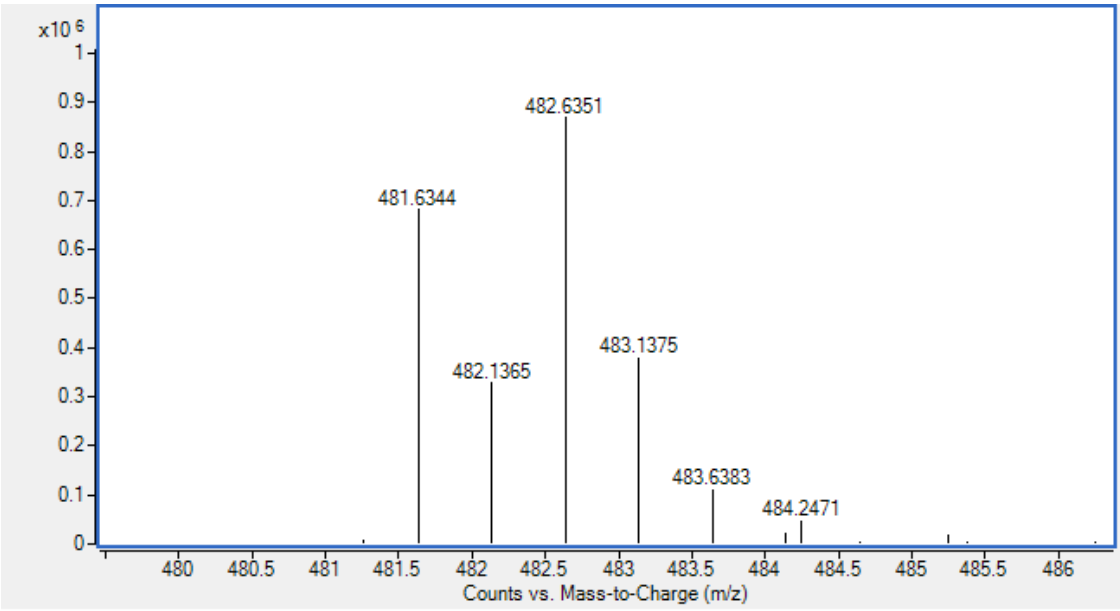

Figure 5.10 High resolution mass spectrum of **EuL4**.

Synthesis of EuL5

The synthesis of chromophore **3C** was mentioned in the synthesis in Chapter 3. **5P** was prepared from nucleophillic substitution between bromine derivative **3C** and

DO3AE in the presence of potassium carbonate. The isolated yield of **5P** was 39%. Then, the acid deprotection of Boc group could be achieved in the presence of trifluoroacetic acid (TFA) and CH_2Cl_2 (v/v=1:1). Yield was 37%. In this case, ethyl ester protecting group of cyclen was stable in acidic deprotection.

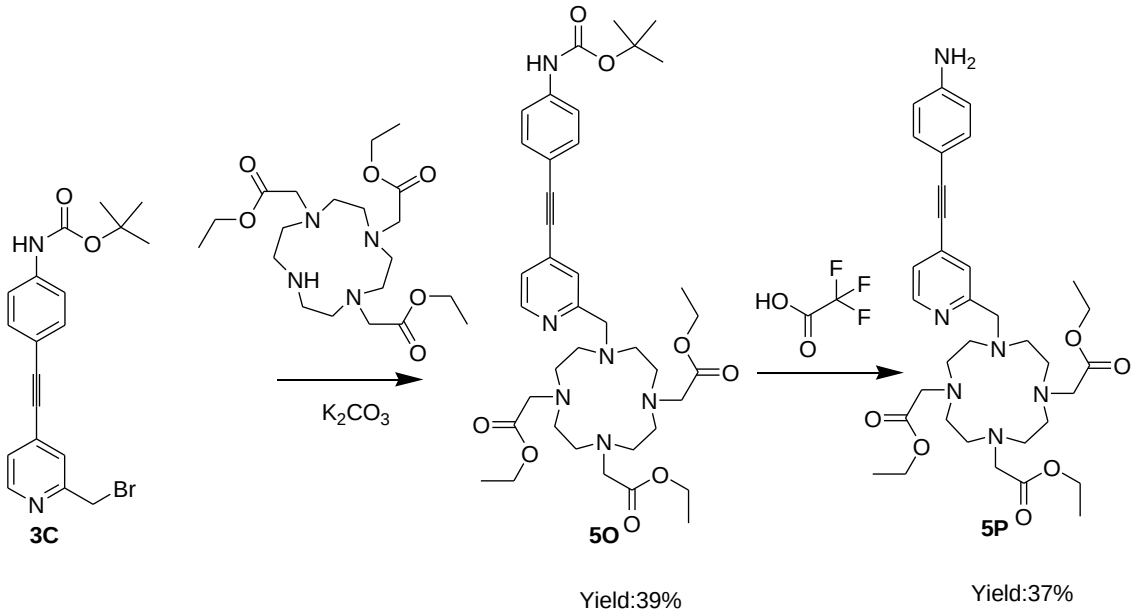

Scheme 3.3 Synthetic Route to **5P**.

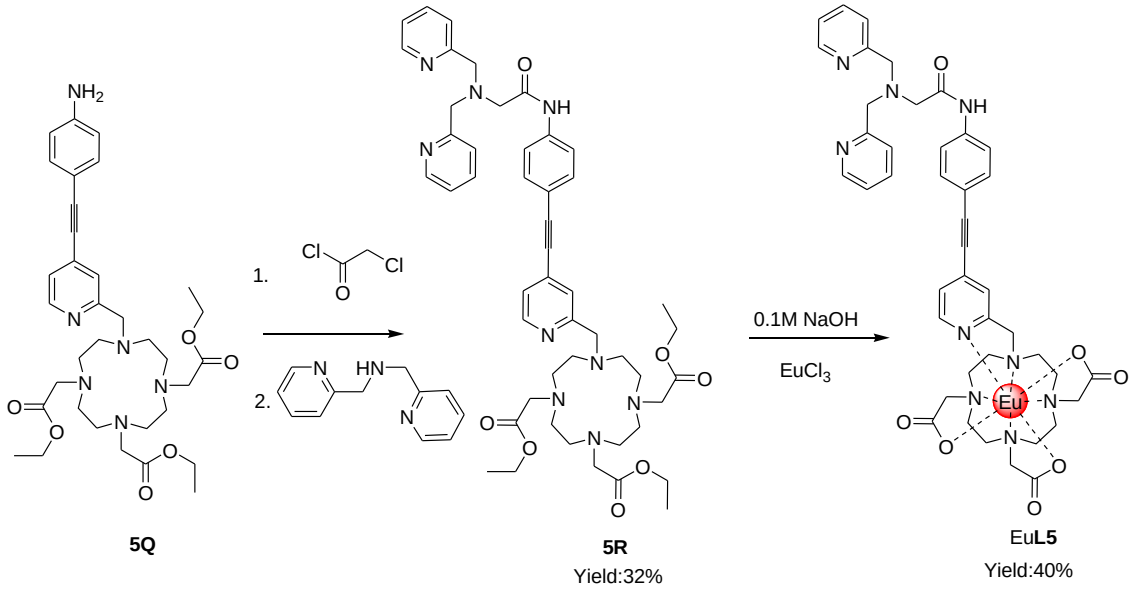

Scheme 3.4 Synthetic Route to **EuL5**.

5R was prepared by reaction between 2-chloroacetyl chloride and **5Q** in the presence of triethylamine. 1 eqv of 2-chloroacetyl chloride was added in order to

eliminate any remaining unreacted 2-chloroacetyl chloride. After confirming the completion of reaction, 1 eqv of dipicolylamine was added to the reaction mixture and stirred overnight. The crude product was purified several times through column chromatography and the yield was 40%. Deprotection of tris-ethylester protection group was carried out by mixing with 0.1M NaOH. Then, the pH of solution was maintained at pH 7 and equimolar $EuCl_3.6H_20$ was added into the aqueous reaction mixture. The reaction mixture was refluxed overnight and the desired products could be obtained by recrystallization in a mixture of the MeOH and diethyl ether. **EuL5Zn** was prepared by mixing **EuL5** and 1 eqv of $ZnCl_2$ in room temperature. The high-resolution mass spectra (ESI+) showed peaks corresponding to the protonated Eu(III) complexes **EuL5** and double protonated Eu(III)-Zn(II) complexes **EuL5Zn** with characteristic Eu(III) isotopic pattern entities which confirmed the formation of the desired Eu(III) complexes.(**Figures 5.11** & **5.12**)

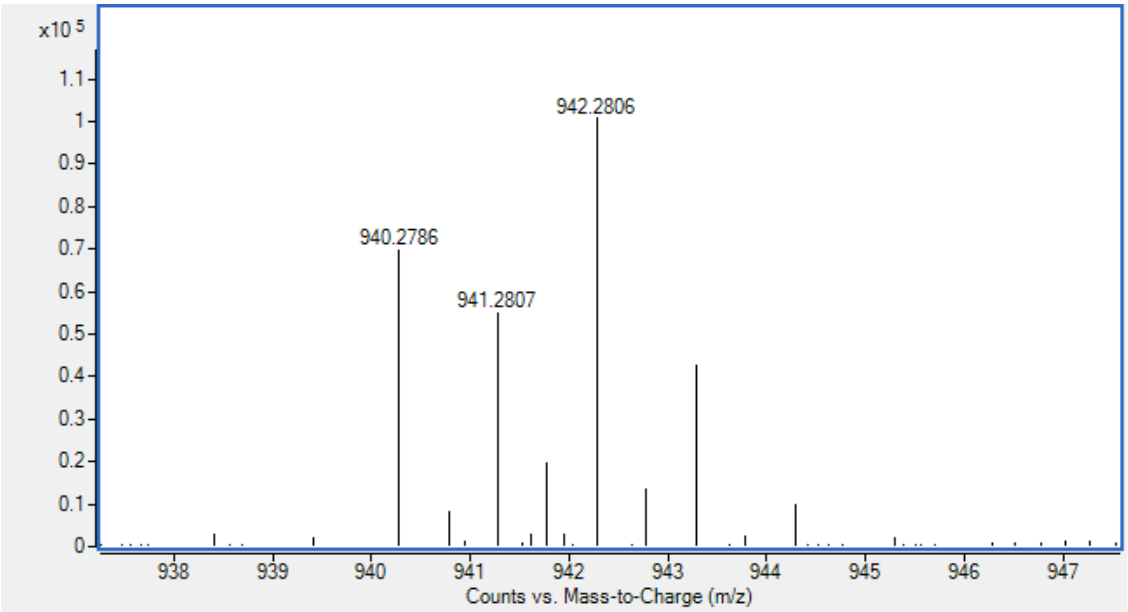

Figure 5.11 High resolution mass spectrum of **EuL5**.

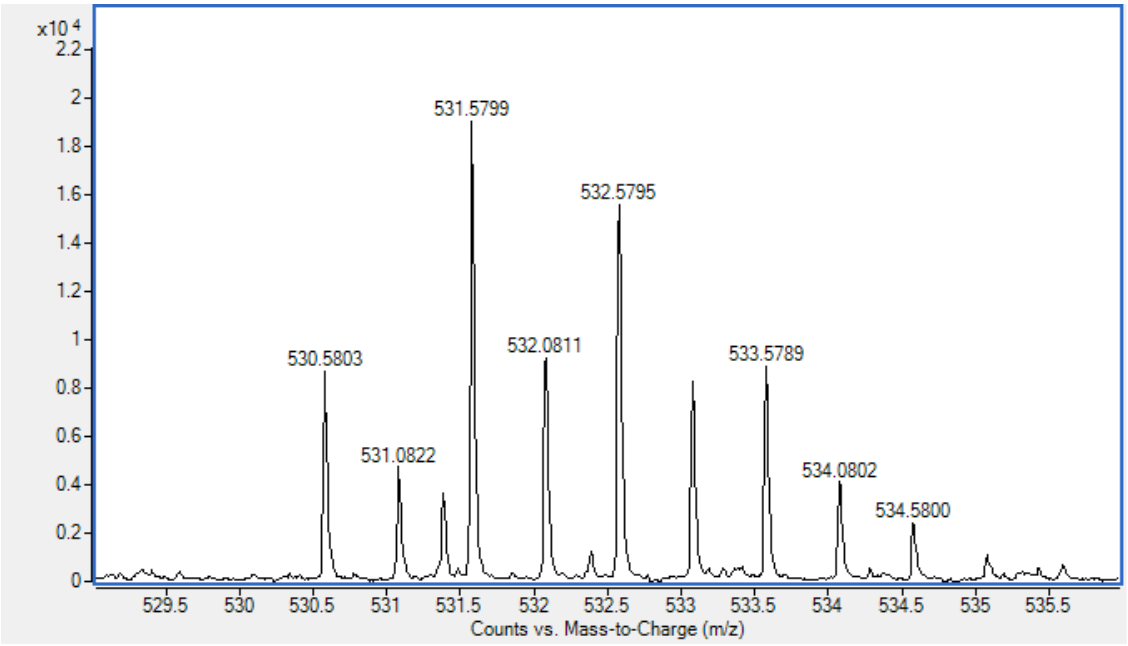

Figure 5.12 High resolution mass spectrum of **EuL5Zn**.

5.3b Photophysical study

UV-vis and excitation spectra

The photophysical properties of **EuL3**, **EuL4** and **EuL5** were studied. Their UV-vis and excitation spectra were shown in **Figures 5.13**, **5.14** and **5.15**. The absorption peaks of **EuL3**, **EuL4** and **EuL5** were located at 309nm, 307nm and 323nm respectively which were corresponded to the π to π^* transitions associated to the aromatic chromophore moieties. The molar extinction coefficients of **EuL3**, **EuL4** and **EuL5** were calculated as 9299 M^{-1}, 13473 M^{-1} and 13161 M^{-1} respectively. The UV-vis absorption spectra were similar to the corresponding excitation spectra and indicated that there was an energy transfer occurring from the chromophore moieties to the Eu(III) ion centre.

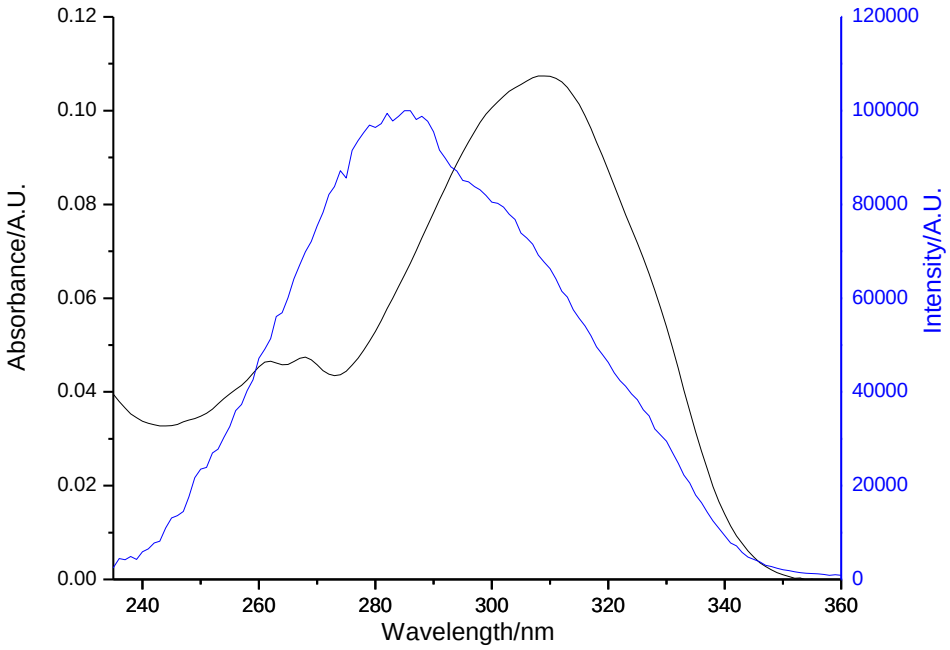

Figure 5.13 UV/Vis absorption spectrum (black), excitation spectra of **EuL3** (blue, λ_{em} =616 nm) (0.01M HEPES, pH 7.4).

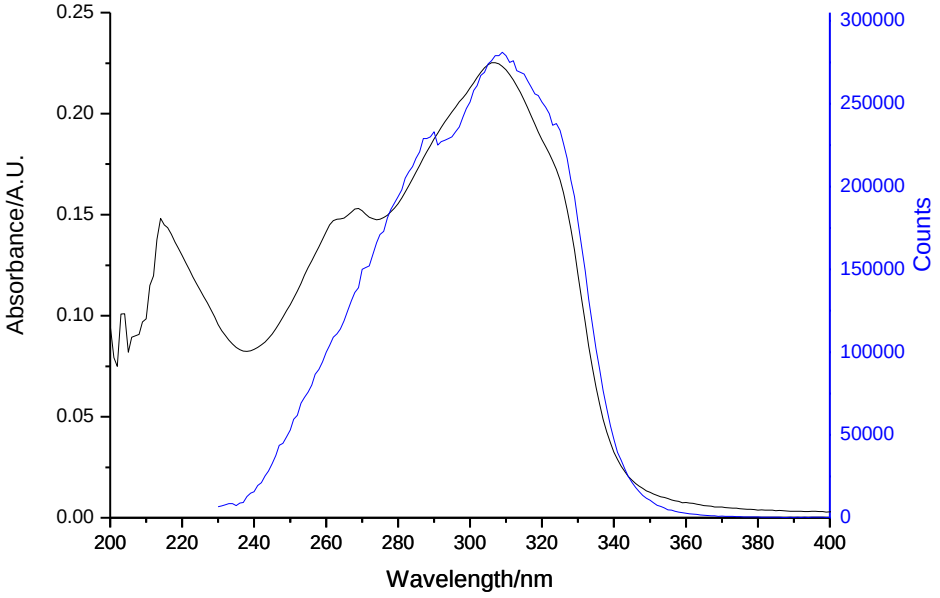

Figure 5.14 UV/Vis absorption spectrum (Black), excitation spectra of **EuL4** (blue, λ_{em} =616 nm) (0.01M HEPES, pH 7.4).

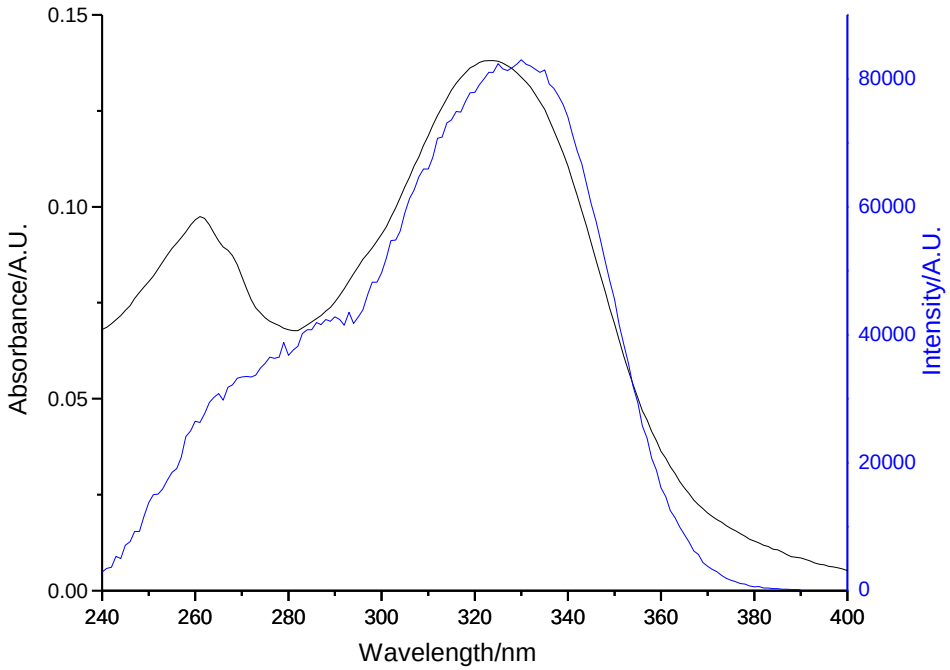

Figure 5.15 UV/Vis absorption spectrum (Black), excitation spectrum of **EuL5** (blue, λ_{em} =616 nm) (0.01M HEPES, pH 7.4).

Titration Emission Spectra and Job's plot

Upon the addition of Zn(II) ion (0 to 2 eqv) to the aqueous solution of **EuL3** or **EuL4**, there was gradual enhancement of $^5D_0 \rightarrow {}^7F_J$ transitions (J = 0–4 at 578, 590, 612, 650 and 695 nm respectively) and those $^5D_0 \rightarrow {}^7F_J$ transitions was characteristic of the emission spectra of Eu (III) ion while **EuL5** demonstrated luminescent quenching. There was one sharp peak at the $^5D_0 \rightarrow {}^7F_0$ transition centred at 580 nm, which suggested that there was only a single species present in the aqueous solution. (**Figure 5.16**, **5.17 and 5.18**)

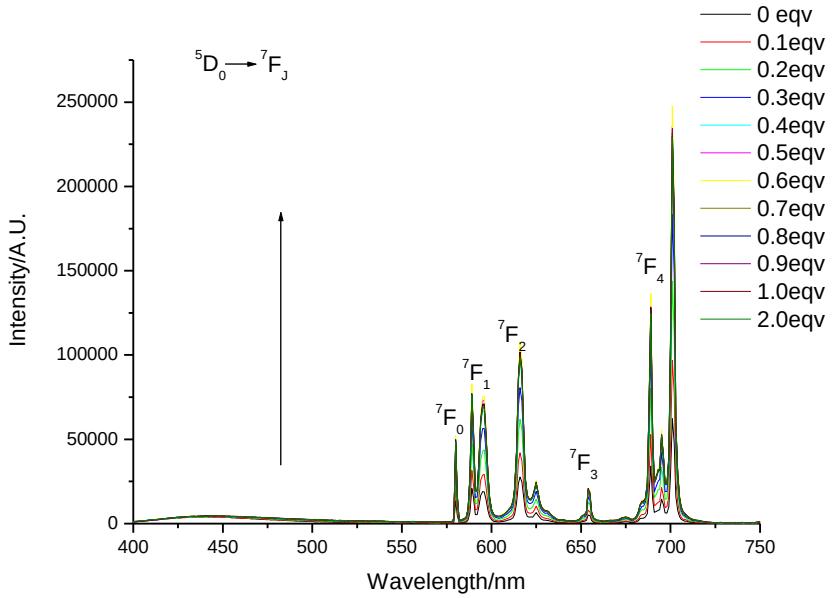

Figure 5.16 Emission spectra of 10 µM aqueous solution upon addition of aliquots of various equiv of Zn(II) ion with respect to **EuL3** (0.01 M HEPES, pH=7.4, λ_{ex}=350 nm).

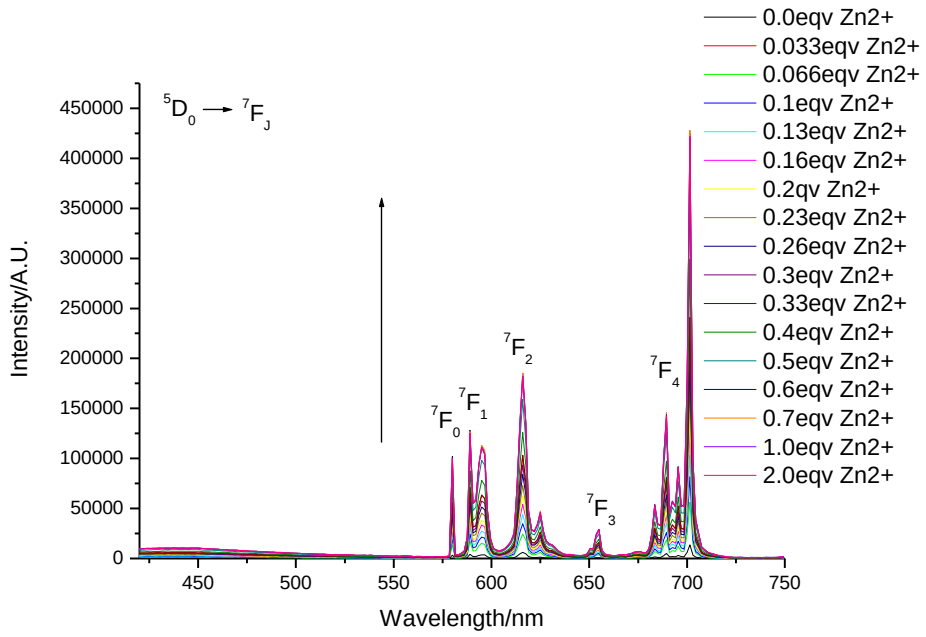

Figure 5.17 Emission spectra of 10 µM aqueous solution upon addition of aliquots of various equiv of Zn(II) ion with respect to **EuL4** (0.01 M HEPES, pH=7.4, λ_{ex}=350 nm).

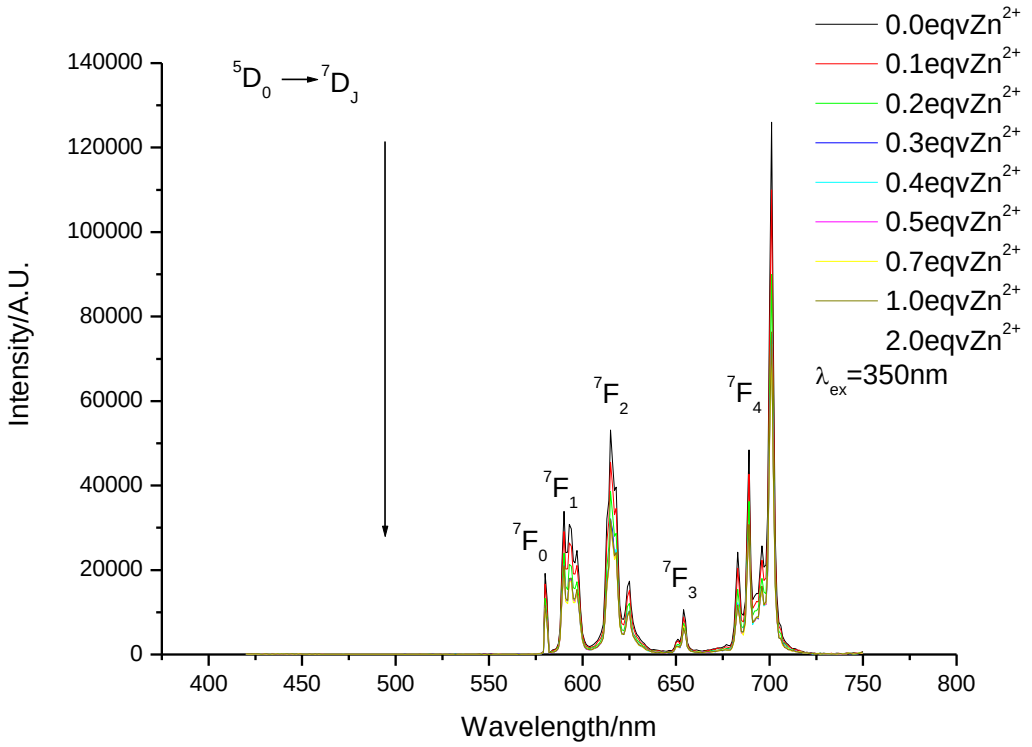

Figure 5.18 Emission spectra of 10 μM aqueous solution upon addition of aliquots of various equiv of Zn(II) ion with respect to **EuL5** (0.01 M HEPES, pH=7.4, λ_{ex}=350 nm).

Moreover, hypersensitive splitting of electric dipole transition $^5D_0 \rightarrow {}^7F_2$ (I_{ED}) did not change significantly, indicating the coordination environment of Eu(III) was not influenced during titration. Asymmetry ratio of the electric dipole transition $^5D_0 \rightarrow {}^7F_2$ (I_{ED}) and magnetic dipole transition $^5D_0 \rightarrow {}^7F_1$ (I_{MD}) gave information of the coordination environment of the Eu (III) ion. The I_{ED} /I_{MD} ratio of did not changed significantly before and after addition of Zn(II) ion and their values were summarized in **Table 5.2**. Therefore, the chemical environment of Eu (III) ions was not influenced significantly. The binding stoichiometry was determined by Job's plot. In **Figures 5.19**, **5.20** and **5.21**, the maximum point was located at 0.5 at x-axis of Zn(II) ion/mixture of Zn(II) ion and Eu(III) complexes, indicating that the optimal binding ratio between Eu(III) complexes and Zn(II) ion was 1:1.

	Asymmetric raito without Zn(II) ion	Asymmetric raito with Zn(II) ion
EuL3	1.54	1.56
EuL4	1.32	1.34
EuL5	1.47	1.49

Table 5.2 Summary of Asymmetric raito of **EuL3**, **EuL4** and **EuL5** before and after addition of Zn(II) ion.

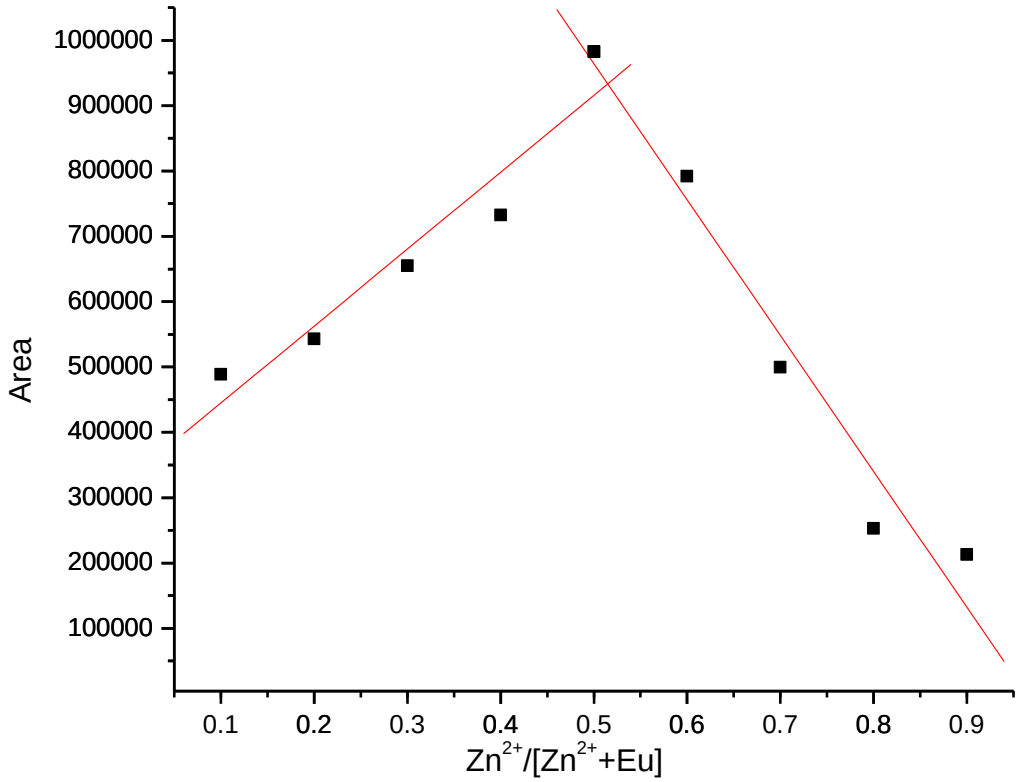

Figure 5.19 Job's plot of **EuL3** and Zn(II) ion.

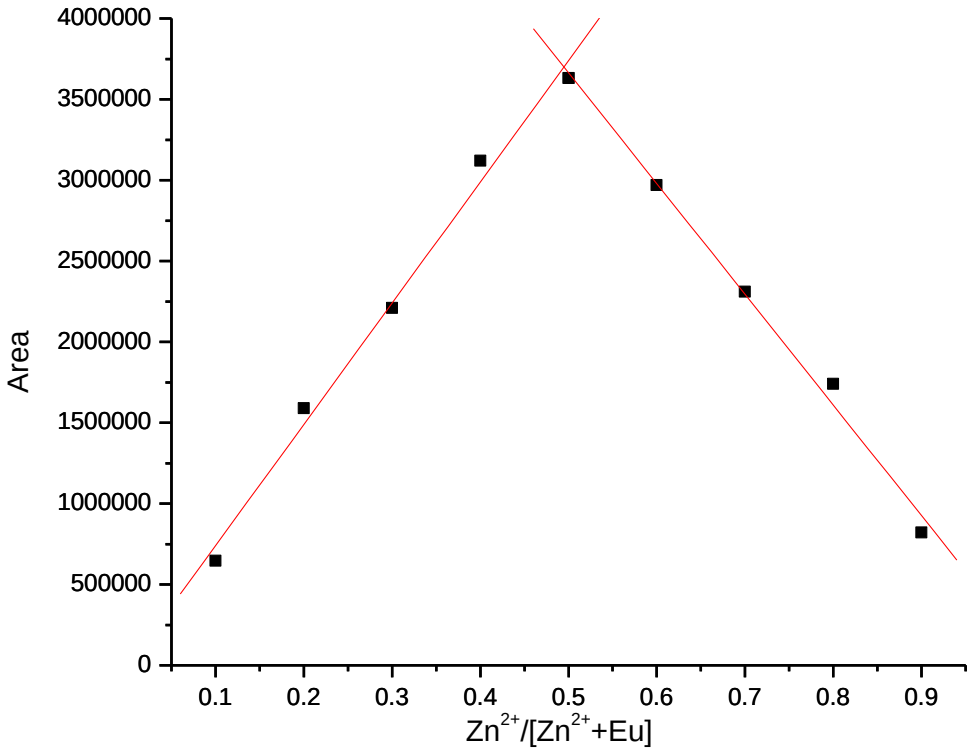

Figure 5.20 Job's plot of **EuL4** and Zn(II) ion.

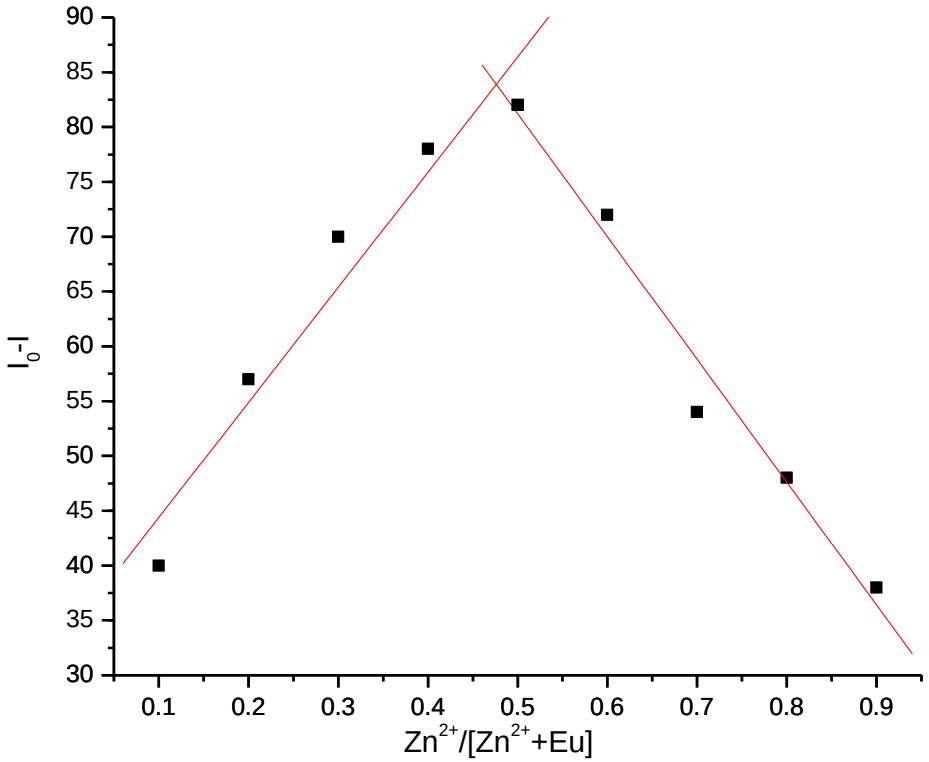

Figure 5.21 Job's plot of **EuL5** and Zn(II) ion.

Quantum yields

The quantum yields were calculated by the comparative method. By maintaining the same excitation wavelength and slit bandwidths, the relative quantum yields before and after addition of Zn(II) ion were determined relative to a quinine sulfate of a known quantum yield (Φ = 0.577) in 0.1 M sulfuric acid. The relative quantum yields of **EuL3** and **EuL4** before additon of Zn(II) ion were smaller than those after addition of Zn(II) ion and vice versa for **EuL5**. Their quantum yields were summarized in **Table 5.3**. The quantum yield of **EuL5** without Zn(II) ion was calculated and it was the highest among the three sensors under investigation since its chromophore contained pyridine which was used for direct coordination towards Eu(III) ion for better energy transfer from chromophore to the Eu(III) ion centre.

	Quantum yield (no Zn(II) ion)	Quantum yield (Add Zn(II) ion)
EuL3	0.27±0.03 %	1.08±0.06 %
EuL4	1.2±0.08 %	5.4±0.12 %
EuL5	4.69±0.05 %	3.42±0.53 %

Table 5.3 Summary of quantum yields of of **EuL3**, **EuL4** and **EuL5** before and after addition of Zn(II) ion.

Lifetime and q value

The luminescent response could be influenced by the presence of O-H (such as water molecules) oscillators directly bound to the Eu(III) ion since O-H oscillators would provide the radiationless decay via energy transfer from electronic to vibrational levels. The measurement of the hydration states was done by the measuring the luminescence lifetimes in H_2O and D_2O upon emission at 616 nm.

Generally, the lifetime without Zn(II) ion in D_2O was longer than that in H_2O. (**Figures 5.22-5.27**) The lifetimes measured in HEPES were similar to the values in

H_2O. Based on lifetimes in D_2O and H_2O, the q value was equal to one in the case of complex alone and other case the complex with Zn(II) ion, indicating that there was one bound water molecule coordinating directly with Eu (III) ion and that the geometric coordination/complex was stable during the Zn(II) ion titrations with no anion or solvent exchange. The lifetimes were summarized in **Table 5.4**.

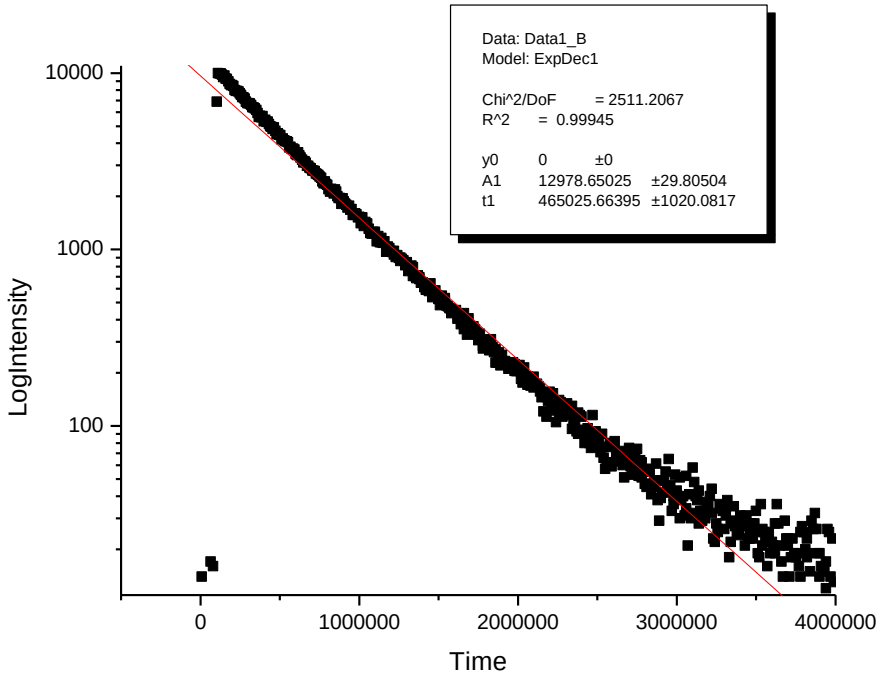

Figure 5.22 Decay curve of luminescence lifetime measurement of **EuL3** in H_2O.

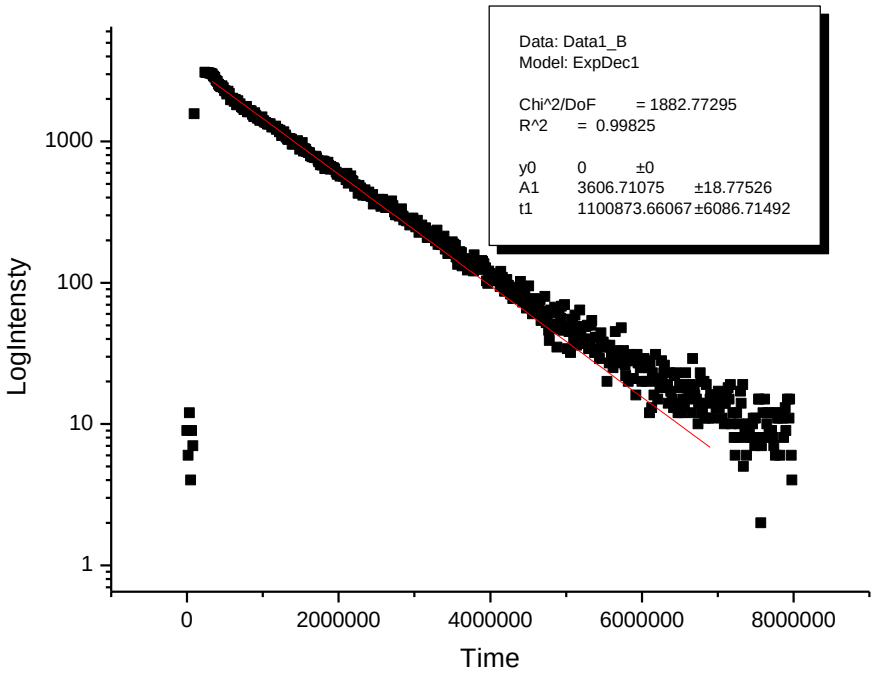

Figure 5.23 Decay curve of luminescence lifetime measurement of **EuL3** in D_2O.

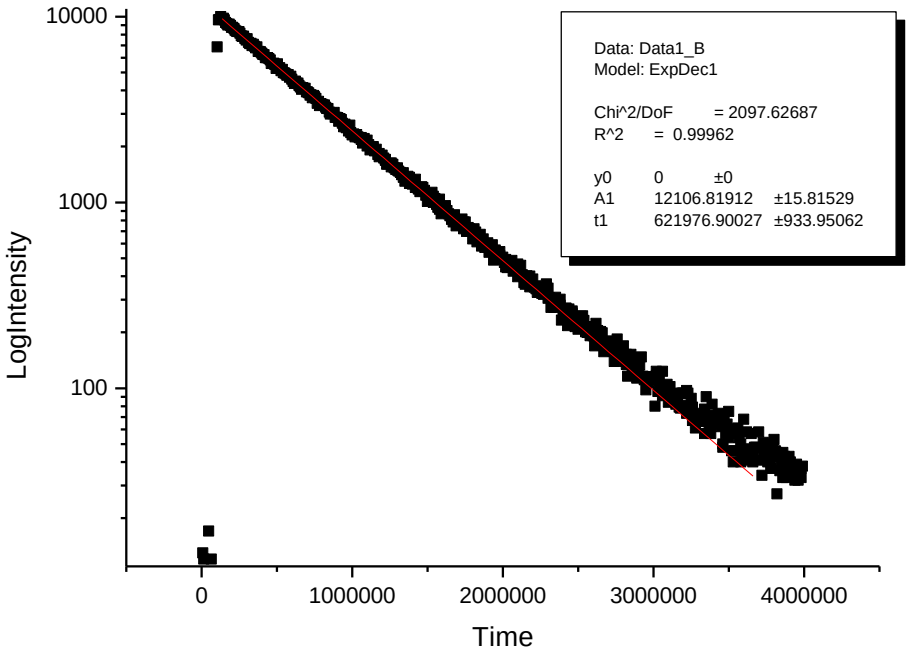

Figure 5.24 Decay curve of luminescence lifetime measurement of **EuL4** in H_2O.

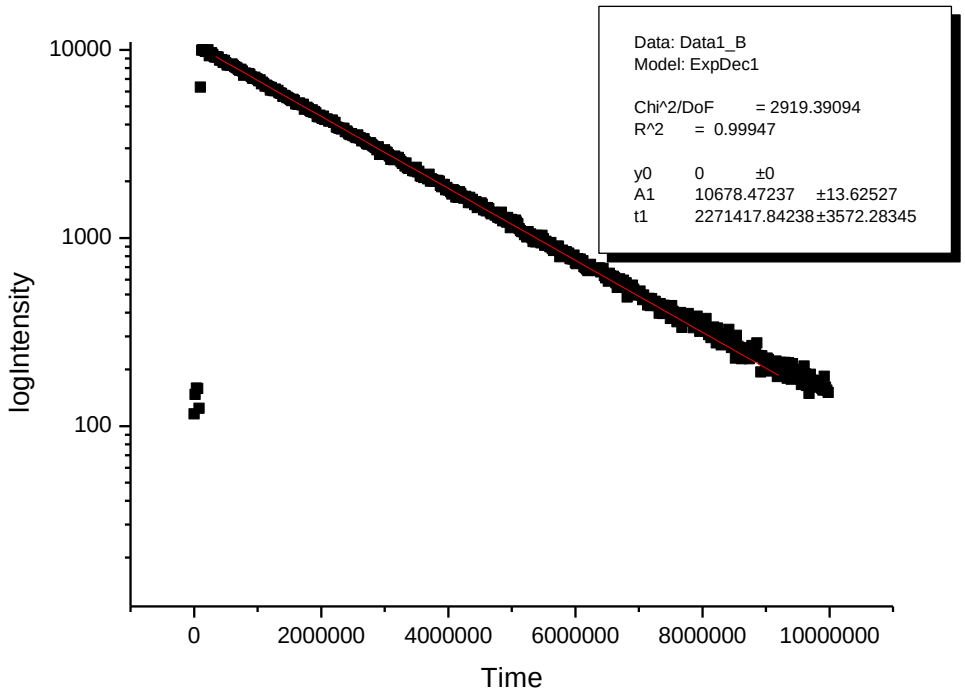

Figure 5.25 Decay curve of luminescence lifetime measurement of **EuL4** in D_2O.

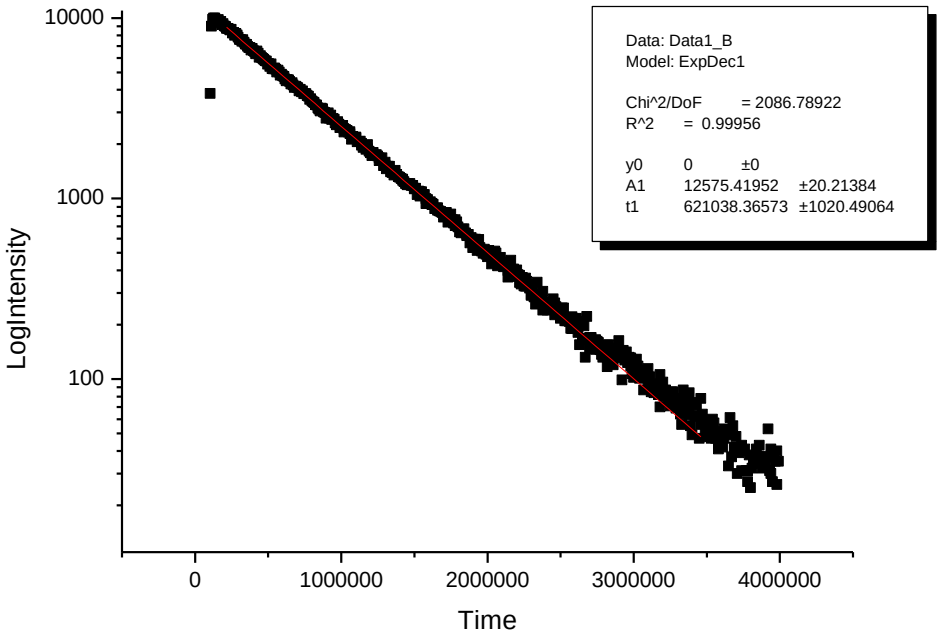

Figure 5.26 Decay curve of luminescence lifetime measurement of **EuL5** in H_2O.

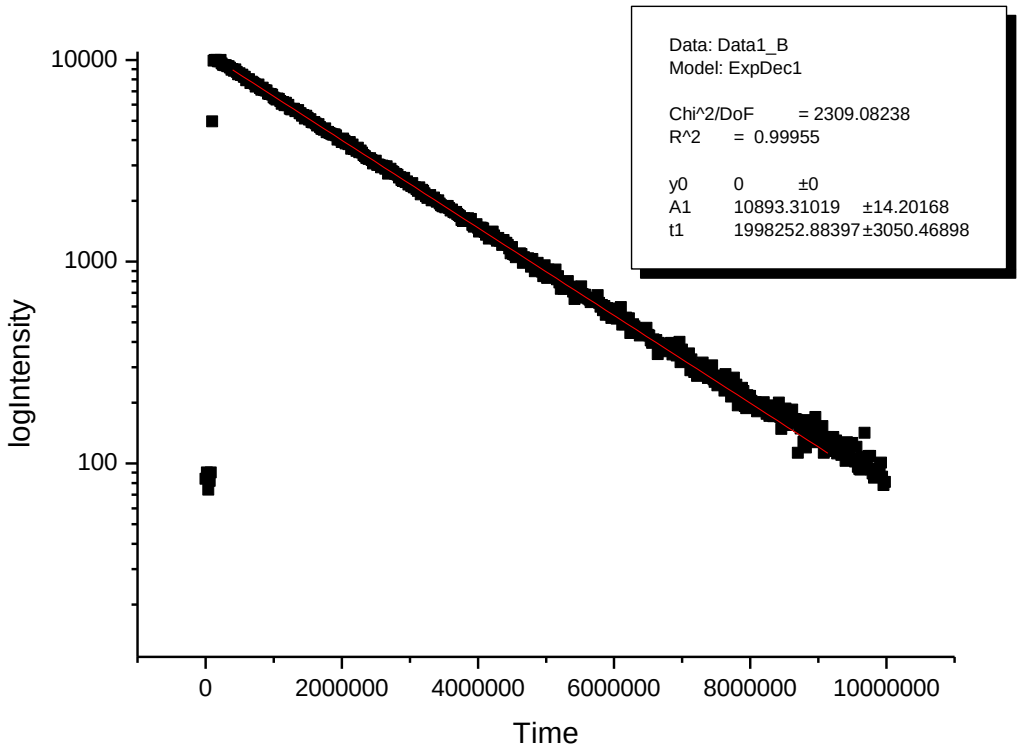

Figure 5.27 Decay curve of luminescence lifetime measurement of **EuL5** in D_2O.

	Lifetime in D_2O (ms)	Lifetime in H_2O (ms)
EuL3	1.5	0.47
EuL4	2.2	0.62
EuL5	2.0	0.62

Table 5.3 Summary of lifetimes of **EuL3**, **EuL4** and **EuL5** in D_2O and H_2O.

Setectivity Test

The luminescent responses of **EuL3 EuL4** and **EuL5** towards various cations were studied in 10 mM HEPES buffer (pH 7.4). (**Figures 5.28-5.30**) Generally, their luminescent responses were not significantly influenced upon addition of some common alkali and alkaline earth cations such as 0.1M K(I) ion, 0.1M Na(I) ion, 0.1mM Mg(II) ion, 0.1mM Ca(II) ion ion and 1 eqv of Ba(II) ion. Moreover, they did not respond to Al(III) ion, Mn(II) ion, Pb(II) ion, Pd(II) ion and Cu(I) ion. **EuL3** and **EuL4** displayed slight luminescence enhancement upon addition of Cd(II) ion and Hg(II) ion but the

extent of enhancement was the largest upon the addition of Zn(II) ion. Unlike **EuL3** and **EuL4**, **EuL5** exhibited negligible luminescence change upon addition of Cd(II) ion and Hg(II). However, when Zn(II) ion was added to the mixture solution of complex and other cations, there was generally luminescent enhancement (**EuL3** and **EuL4**) and quenching (**EuL5**).

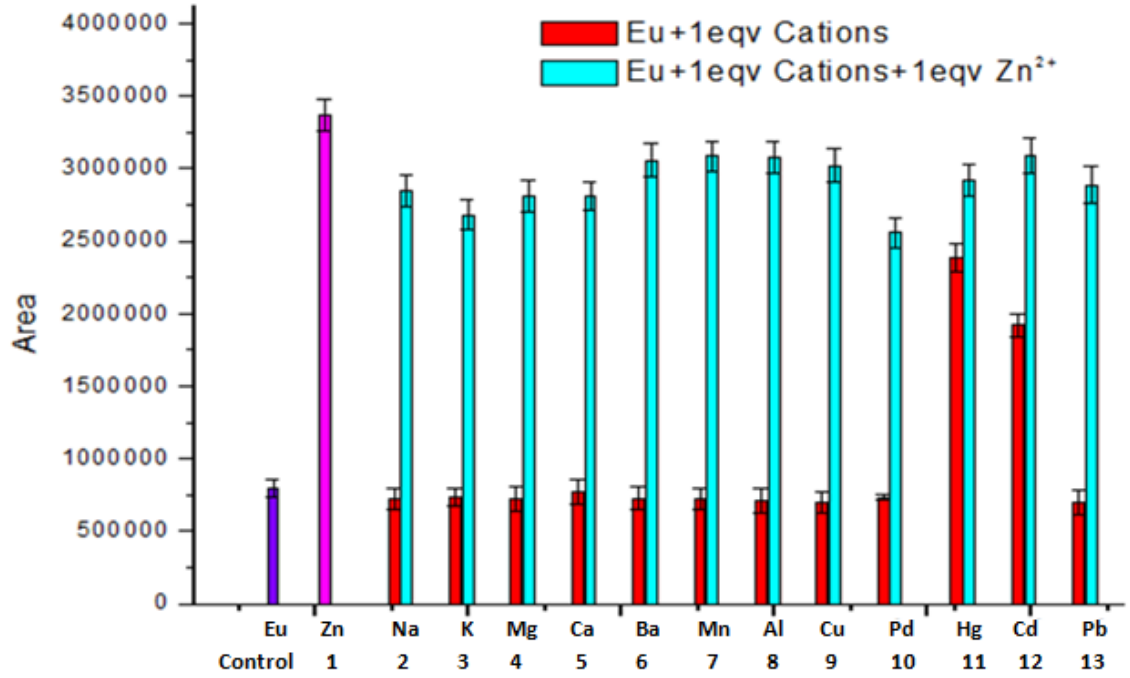

Figure 5.28 Changes in luminescence intensity of [**EuL3**] (10 μM) in 10 mM HEPES (excitation: 350 nm). Control : **EuL3 only**, 1: **EuL3**+1eqv Zn(II) ion , 2: 0.1M K(I)ion, 3: 0.1M Na(I) ion, 4: 0.1mM Mg(II) ion,5: 0.1mM Ca(II) ion,6: 1eqv Ba(II) ion,7: 1eqv Mn(II) ion,8. 1eqv Al(III) ion, 9. 1eqv Cu(I) ion, 10. 1eqv Pd(II) ion, 11: 1eqv Hg(II) ion, 12: 1eqv Cd(II) ion, 13: 1eqv Pb(II) ion.

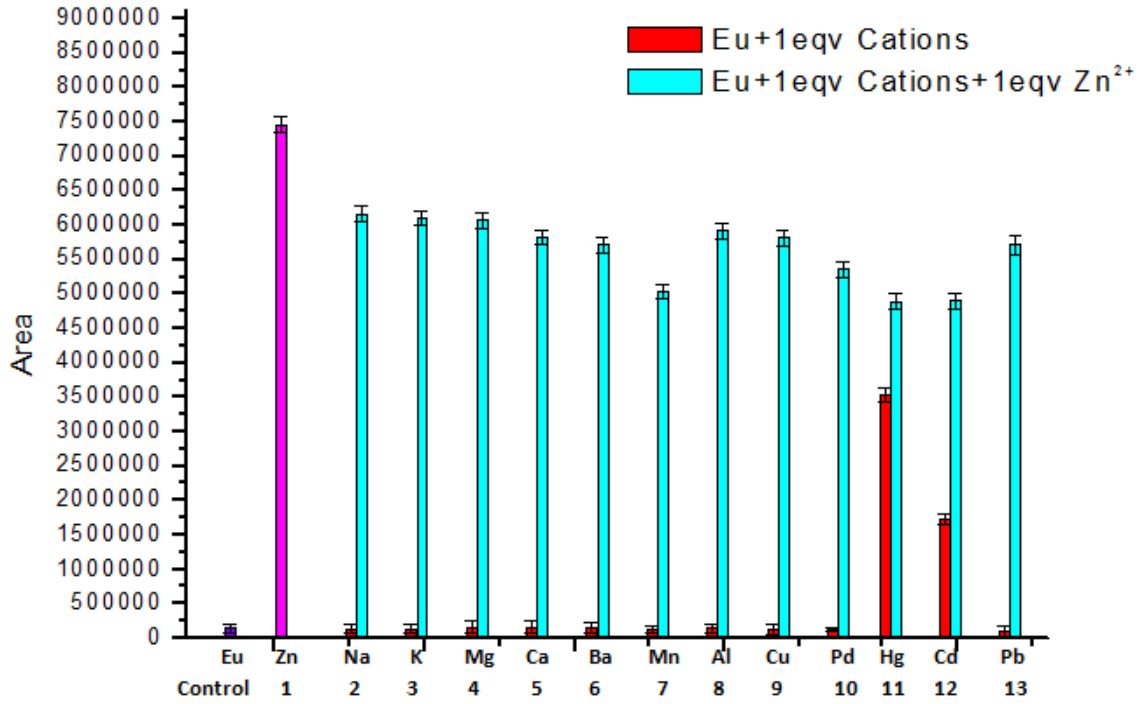

Figure 5.29 Changes in luminescence intensity of [**EuL4**] (10 μM) in 10 mM HEPES (excitation: 350 nm). Control : **EuL4 only**, 1: **EuL4**+1eqv Zn(II) ion , 2: 0.1M K(I)ion, 3: 0.1M Na(I) ion, 4: 0.1mM Mg(II) ion,5: 0.1mM Ca(II) ion,6: 1eqv Ba(II) ion,7: 1eqv Mn (II) ion,8. 1eqv Al(III) ion, 9. 1eqv Cu(I) ion, 10. 1eqv Pd(II) ion, 11: 1eqv Hg(II) ion, 12: 1eqv Cd(II) ion, 13: 1eqv Pb(II) ion.

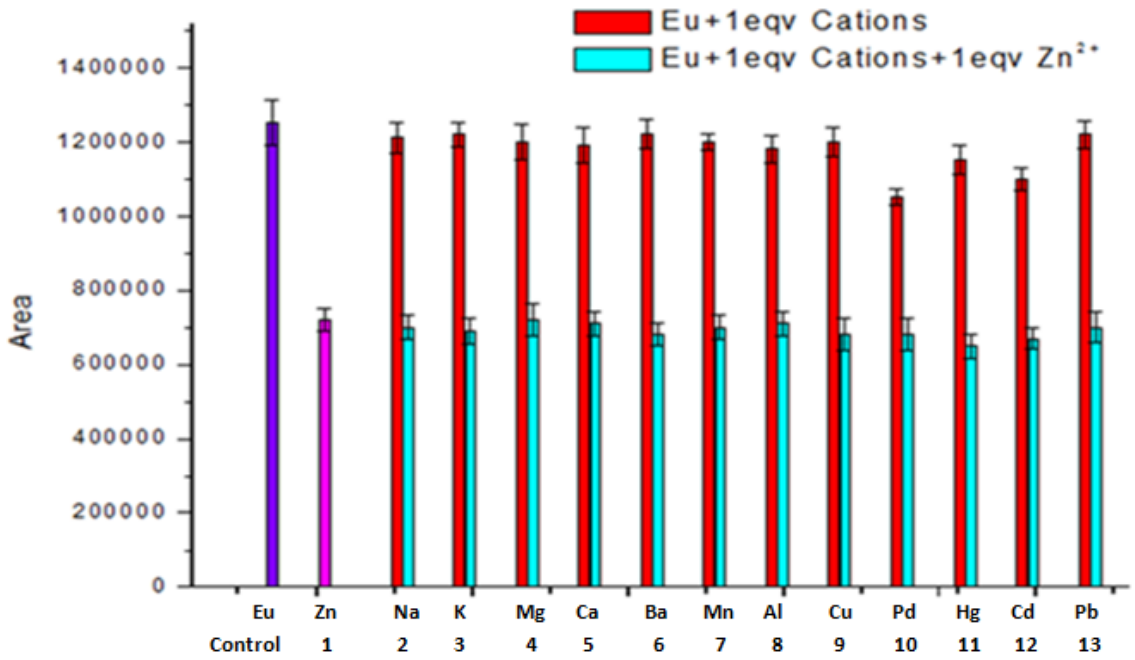

Figure 5.30 Changes in luminescence intensity of [**EuL5**] (10 μM) in 10 mM HEPES (excitation: 350 nm). Control : **EuL5 only**, 1: **EuL5**+1eqv Zn(II) ion , 2: 0.1M K(I)ion, 3: 0.1M Na (I) ion, 4: 0.1mM Mg(II) ion, 5: 0.1mM Ca(II) ion, 6: 1eqv Ba(II) ion,7: 1eqv Mn(II) ion, 8. 1eqv Al(III) ion, 9. 1eqv Cu(I) ion, 10. 1eqv Pd(II) ion, 11: 1eqv Hg(II) ion, 12: 1eqv Cd(II) ion, 13: 1eqv Pd(II) ion.

Binding Constants towards Cations

The binding constant is quantitative measurements of binding events between sensor and cations. Based on results shown in **Table 5.4**, sensors had the largest binding constants with Zn(II) ion among those of Hg(II) ion and Cd(II) ion and therefore sensors showed good selectivity towards Zn(II) ion. Their binding constants towards Hg(II) ion and Cd(II) ion were summarized in **Table 5.4**.

Binding Constants (M^{-1})	Zn(II) ion	Cd(II) ion	Hg(II) ion
EuL3	51954.68±7834	42259.84±6334	41196.06±2367
EuL4	636031.11±5936	44434.82±4353	52951.86±3161
EuL5	65906.22±3236	/	/

Table 5.3 Summary of binding constants of **EuL3**, **EuL4** and **EuL5**.

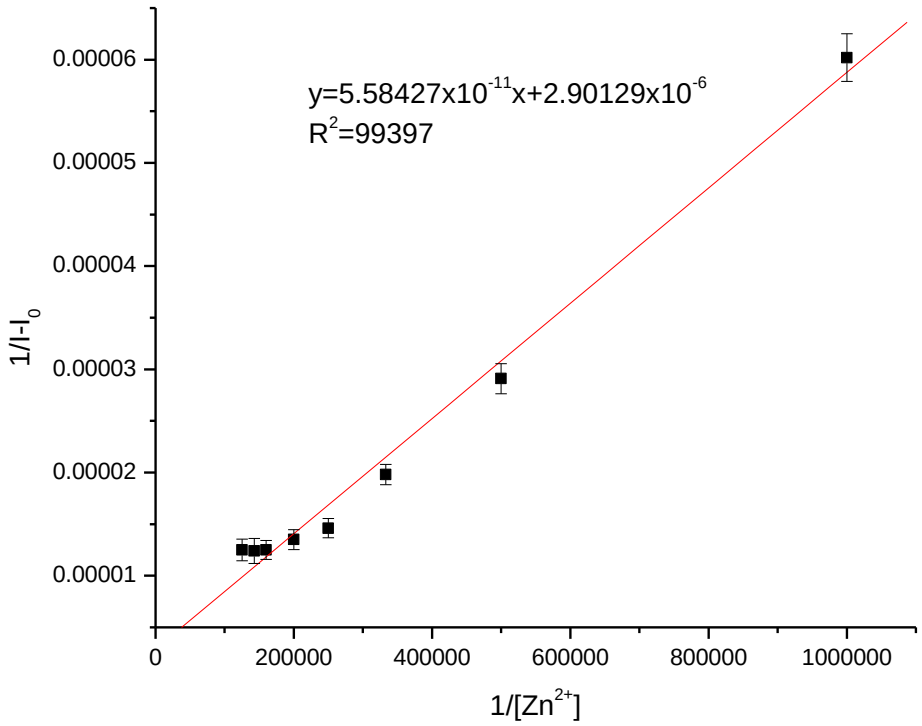

Figure 5.31 Fitting of fluorescence Zn(II) ion titration curve of **EuL3**.

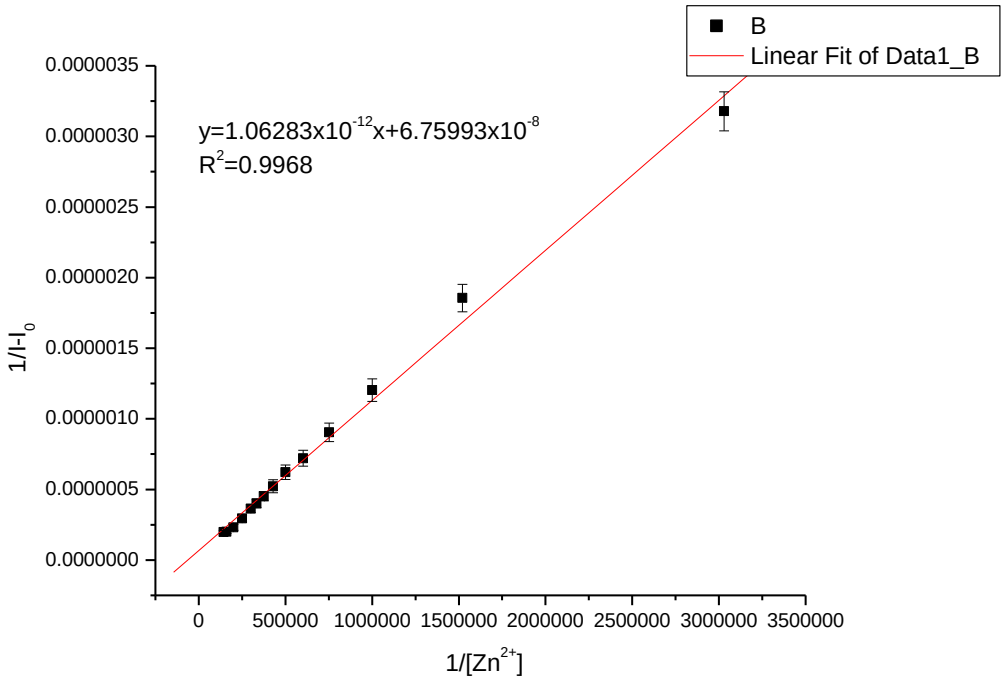

Figure 5.32 Fitting of fluorescence Zn(II) ion titration curve of **EuL4**.

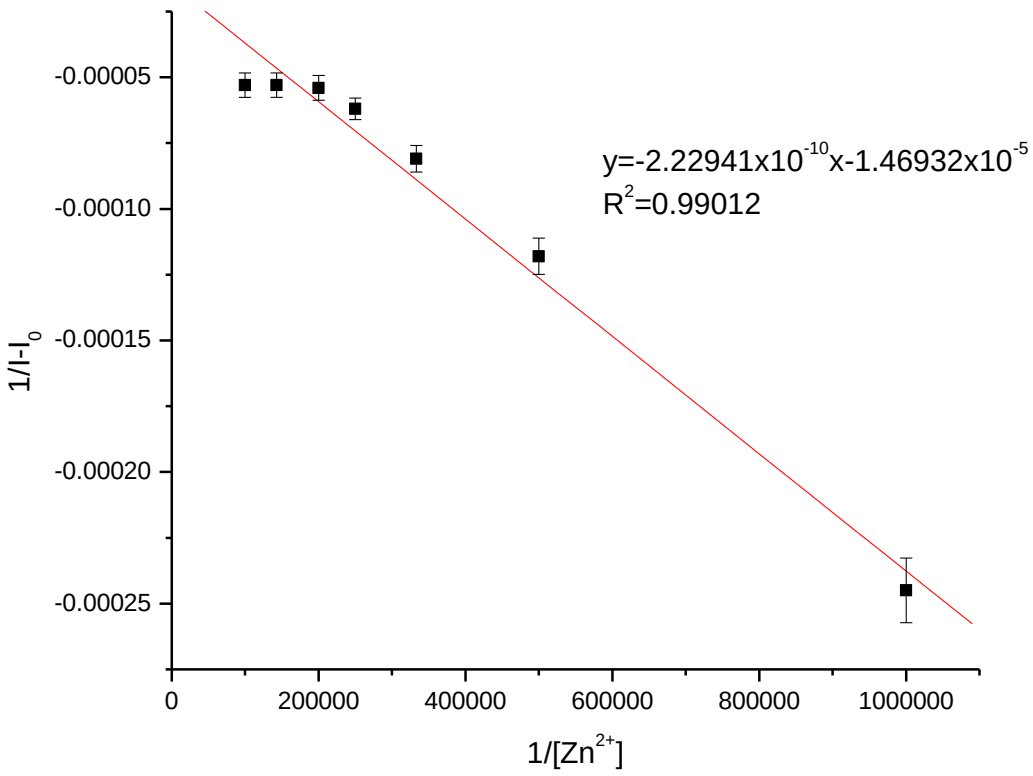

Figure 5.33 Fitting of fluorescence Zn(II) ion titration curve of **EuL5**.

Sensing of ATP

As discussed before, ATP can be recognized by the use of a zinc complex bearing vacant coordination sites for ATP. Complex of zinc and dipicolylamine is one of the most commonly receptors for detection of ATP.[21]-[23] Since dipicolylamine is a tridentate ligand with three nitrogen donors to chelate with Zn(II) ion and leaves coordination sites free for ATP binding. Zinc–dipicolylamine receptors usually show a good selectivity towards phosphate oxoanions over other anions in aqueous solution.

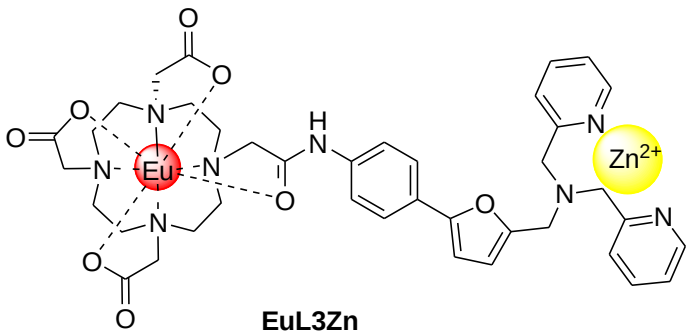

EuL3Zn

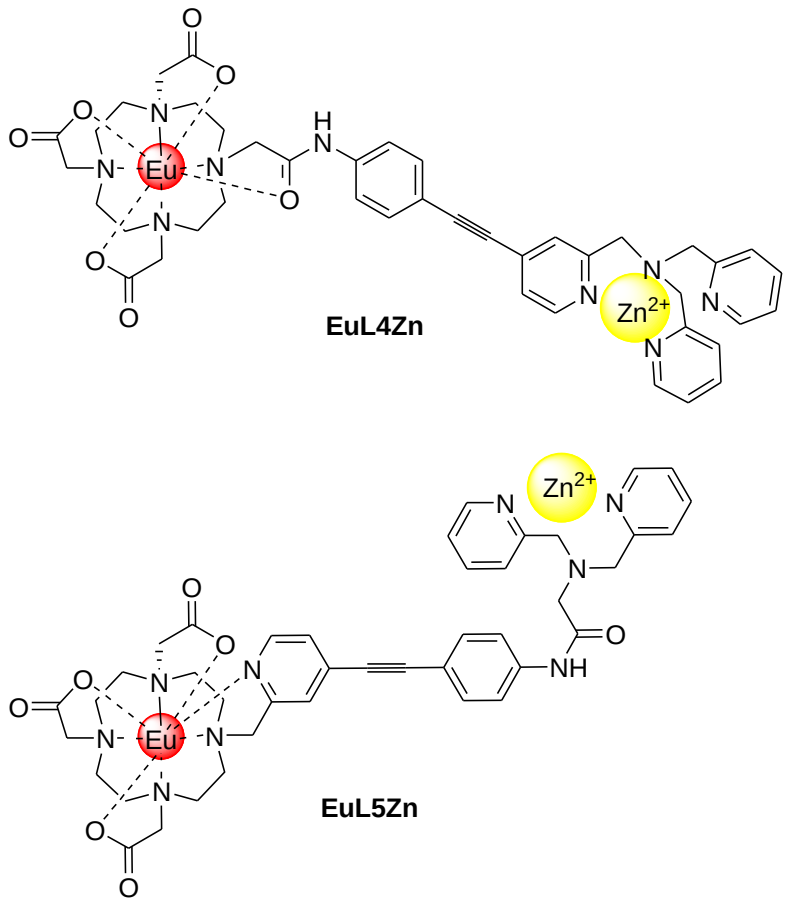

Figure 5.35 Structures of **EuL3Zn**, **EuL4Zn** and **EuL5Zn**.

Titration emission spectra with ATP and Job's plot

To test the luminescent responsef **EuL3Zn**, **EuL4Zn** and **EuL5Zn** towards ATP, the titrations with ATP were performed. Upon addition of ATP (0 to 5 eqv) to the aqueous solutions of **EuL3Zn**, **EuL4Zn** and **EuL5Zn** individually, only **EuL5Zn** demonstrated a significant luminescent enhancement of the narrow structured emission patterns $^5D_0 \rightarrow {}^7F_J$ (J=0-4) transitions, (**Figure 5.38**) while **EuL3Zn** showed only slight quenching (**Figure 5.36**) and **EuL4Zn** displayed no luminescent changes. (**Figure 5.37**)

During titration, there was one sharp peak at the $^5D_0 \rightarrow {}^7F_0$ transition centering at 580 nm, suggesting that there was only a single species in the aqueous solution and the coordination environment of Eu(III) ion was not influenced by the titration of ATP. For instance, the asymmetric I_{ED} /I_{MD} ratio of **EuL5Zn** before and after addition of ATP was calculated as 1.49 and 1.50 respectively and hypersensitive splitting of electric dipole transition $^5D_0 \rightarrow {}^7F_2$ (I_{ED}) remained unchanged. The binding stoichiometry

between ATP and **EuL5Zn** was determined by Job's plot. In **Figure 5.39**, the maximum point was found at 0.5 of ATP ion/mixture of ATP ion and complex, suggesting that a binding ratio of 1:1 between **EuL5Zn** and ATP ion was optimal.

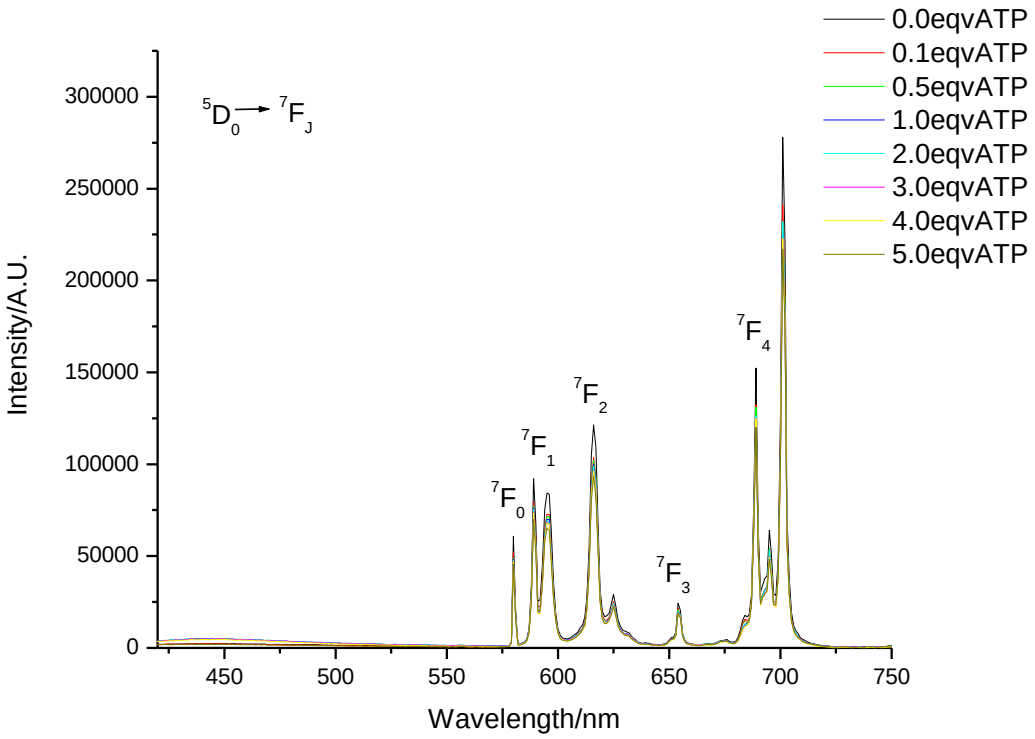

Figure 5.36 Emission spectra of 10 μM aqueous solution upon addition of aliquots of various equiv of ATP with respect to **EuL3Zn** (0.01 M HEPES, pH=7.4, λ_{ex}=350 nm).

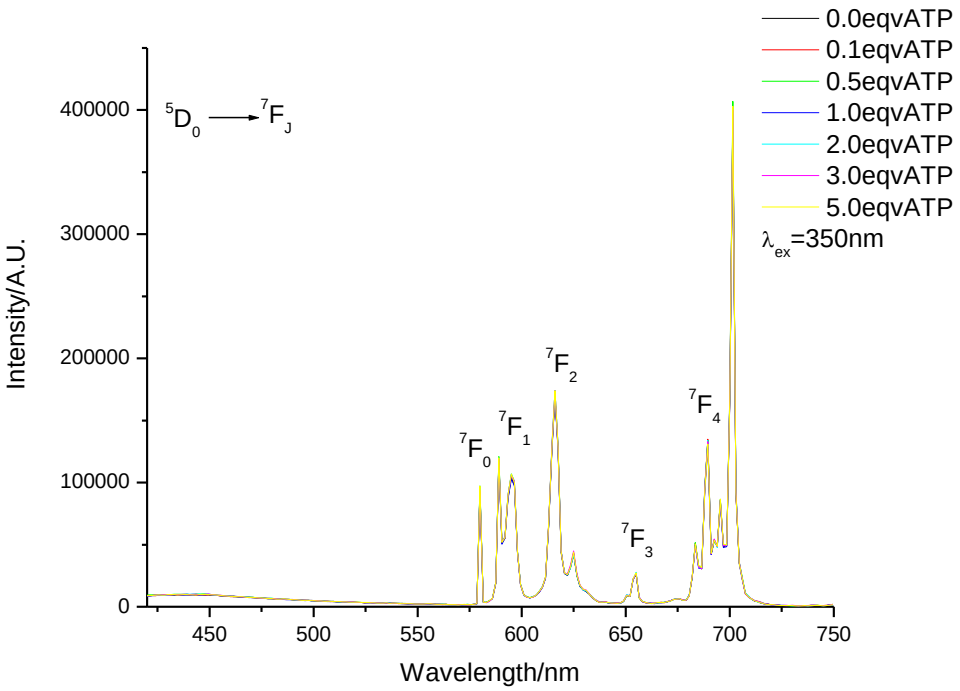

Figure 5.37 Emission spectra of 10 µM aqueous solution upon addition of aliquots of various equiv of ATP with respect to **EuL4Zn** (0.01 M HEPES, pH=7.4, λ_{ex}=350 nm).

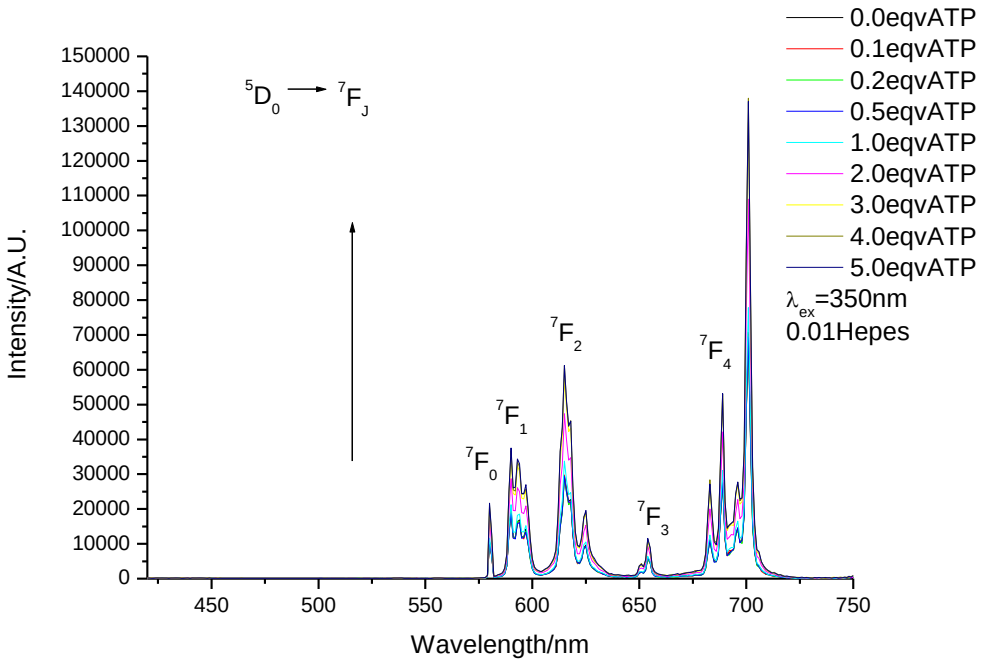

Figure 5.38 Emission spectra of 10 µM aqueous solution upon addition of aliquots of various equiv of ATP with respect to **EuL5Zn** (0.01 M HEPES, pH=7.4, λ_{ex}=350 nm).

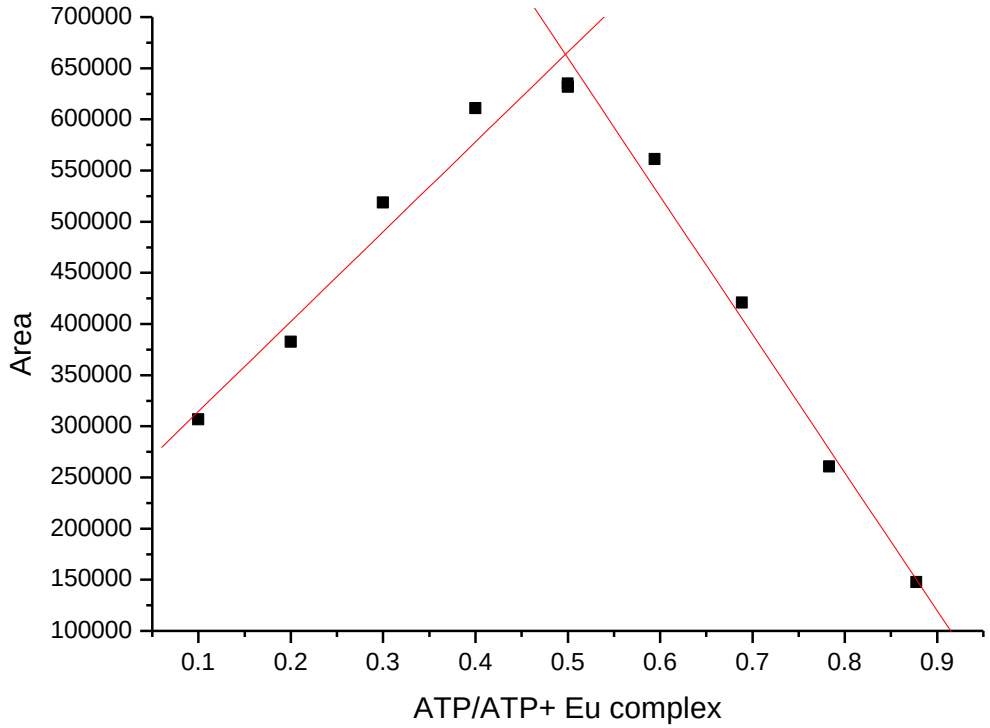

Figure 5.39 Job's plot of **EuL5Zn** and ATP.

UV-vis and excitation spectra of EuL5Zn

As **EuL5Zn** showed good response towards ATP, its photophyscial properties and corresponding selectivity towards other anions were studied. UV-vis and excitation spectra of **EuL5Zn** were dipicted in **Figure 5.40**. The absorption peak maximum was located at 323nm, which was π to π^* transitions associated to the aromatic chromophore moieties. The molar extinction coefficients of **EuL5Zn** were calculated as 13881 M^{-1}. The absorption spectra were similar to the corresponding excitation spectra, indicating that energy transfer occurred from the chromophore moieties to the Eu(III) ion centre.

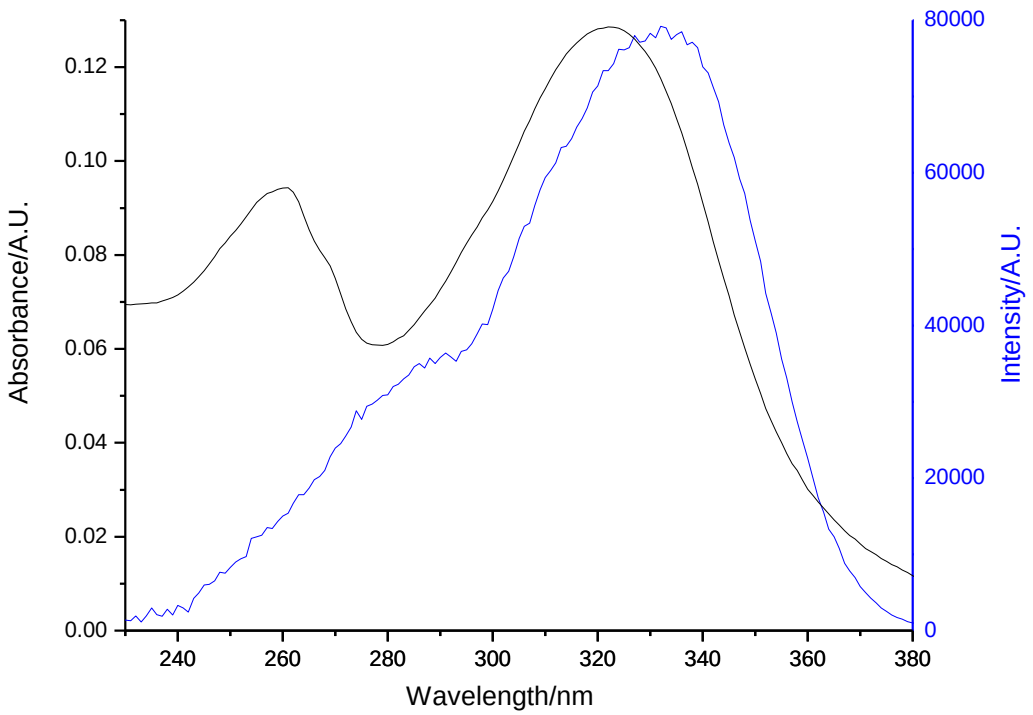

Figure 5.40 UV/Vis absorption spectra (Black), excitation spectra of **EuL5Zn** (blue, λ_{em} =616 nm) (0.01M HEPES, pH 7.4).

Quantum yield, lifetime and q value of EuL5Zn

The quantum yield of **EuL5Zn** was measured by the comparative method. By keeping the excitation wavelength and slit bandwidths constant, the relative quantum yields of **EuL5Zn** before and after addition of ATP ion were determined relative to a quinine sulfate of a known quantum yield (Φ = 0.577) in 0.1 M sulfuric acid. The relative quantum yields were 3.42±0.53 % (No ATP) and 5.23±0.12 % (with ATP).

The luminescence intensity can be influenced by O-H oscillators directly bound to the Eu(III) ion because energy would be lost in the radiationless decay via energy transfer from electronic to vibrational levels. The hydration states were analysed by the measuring the luminescence lifetimes in H_2O and D_2O upon emission at 616 nm.

The lifetime of **EuL5Zn** with ATP in D_2O was 2.0 ms, which was longer than that in H_2O (0.62ms). The lifetimes measured in HEPES were similar to those of H_2O. Based on the lifetimes in D_2O and H_2O, the q value was calculated as one, indicating

that there was a water molecule coordinating directly with Eu(III) ion. Since the hydration state remained unchanged, the geometric coordination/complex was stable during the ATP titrations with no anion or solvent exchange.

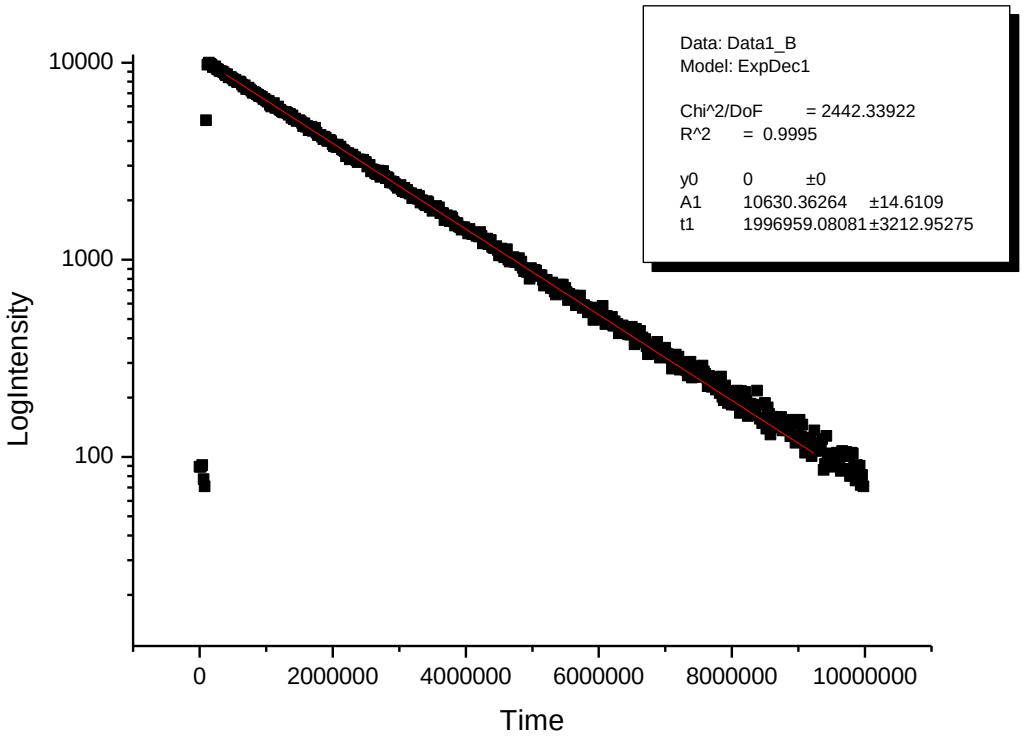

Figure 5.41 Decay curve of luminescence lifetime measurement of **EuL5Zn** in D_2O.

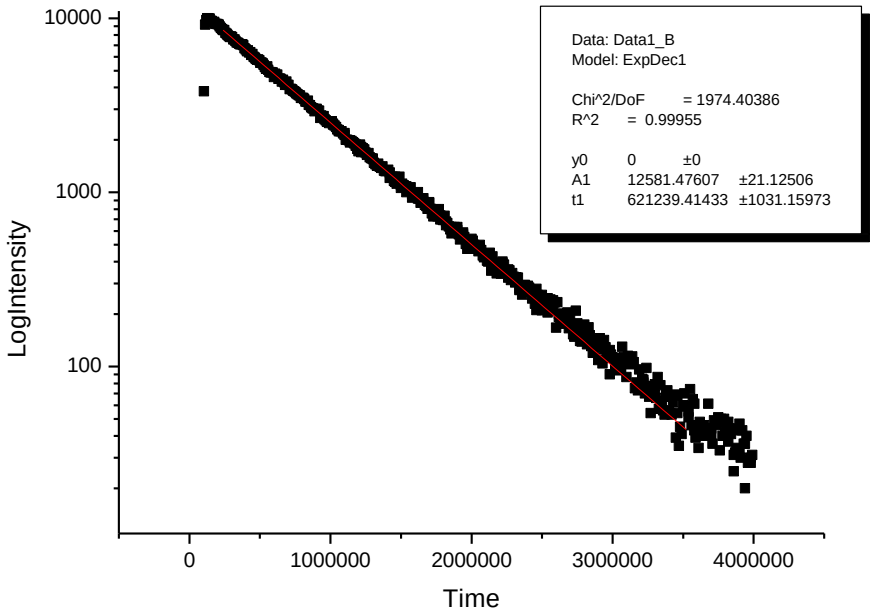

Figure 5.42 Decay curve of luminescence lifetime measurement of **EuL5Zn** in H_2O.

Selective test of EuL5Zn

The selectivity test of **EuL5Zn** towards common anions was done in 10 mM HEPES buffer (pH 7.4). Upon the addition of various anions, including AMP, pyrophosphate, sodium phosphate dibasic, sodium citrate, sodium ascorbate, potassium acetate, potasium iodide, potassium bromide and sodium hydrogen carbonate, luminescent response did not change significantly (**Figure 5.43**). It was worth noting that **EuL5Zn** can distinguish ATP from ADP, AMP and pyrophosphate which were common targets for recognition of DPA-Zn receptor. The addition of ADP could cause only small enhancement of luminescent response of **EuL5Zn**, but the extent was smaller than that of ATP.

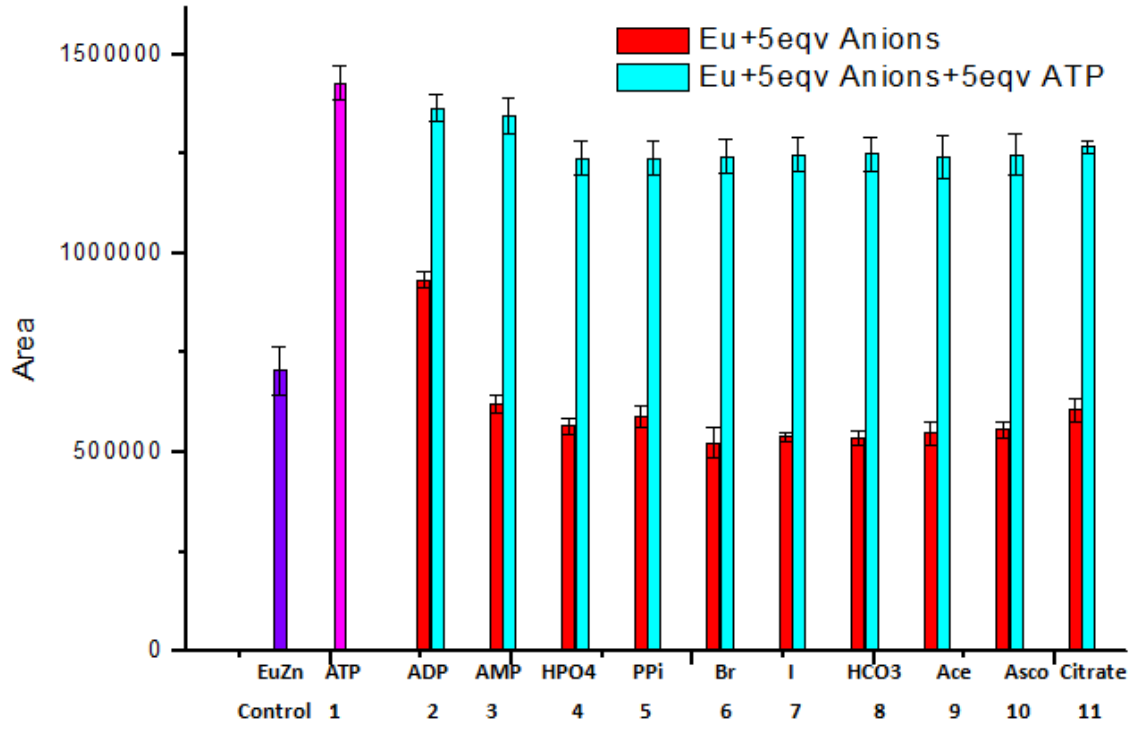

Figure 5.43 Changes in luminescence intensity of [**EuL5Zn**] (10 μM) in 10 mM HEPES (excitation: 350 nm). Control: Eu**L5**Zn, 1: adenosine triphosphate (ATP), 2: adenosine diphosphate (ADP), 3: adenosine monophosphate (AMP), 4: sodium phosphate dibasic, 5: pyrophosphate, citrate, 6: potassium bromide, 7: potasium iodide, 8: sodium hydrogen carbonate, 9: potassium acetate,10: sodium ascorbate. Cyan bar: additon of ATP to solution of **EuL5Zn** and anions.

To test the selectivity of **EuL5Zn** towards metal cations, the luminescent response of **EuL5Zn** was also measured in 10 mM HEPES buffer upon addition of various metal cations. Generally, the luminescent response of **EuL5Zn** did not significantly influence upon the addition of common alkali and alkaline earth cations such as 0.1M K(I) ion, 0.1M Na(I) ion, 0.1mM Mg(II) ion, 0.1mM Ca(II) ion ion and 1 eqv of Ba(II) ion or upon the addition of some transition metal cations such as Mn(II) ion, Al(III) ion, Cu(I) ion, Cd(II) ion, Hg(II) ion and Pd(II).

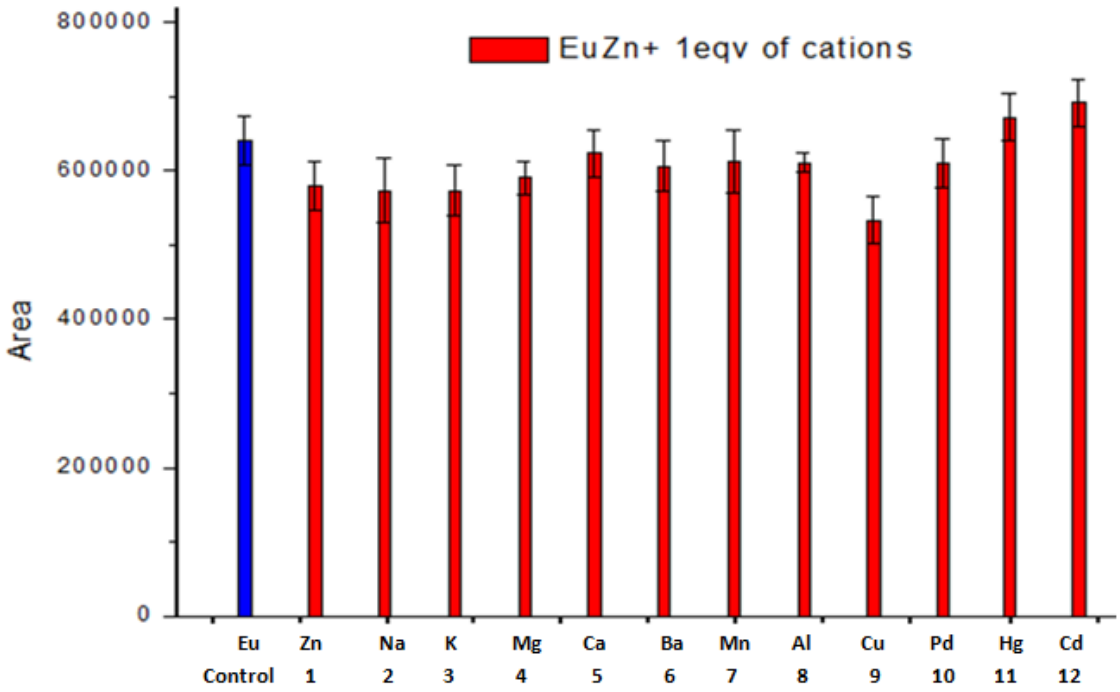

Figure 5.44 Changes in luminescence intensity of [**EuL5Zn**] (10 μM) in 10 mM HEPES (excitation: 330 nm). Control : **EuL5Zn only**, 1: **EuL5Zn**, 2: 0.1M Na(I)ion, 3: 0.1M K(I) ion, 4: 0.1mM Mg(II) ion,5: 0.1mM Ca(II) ion,6: 1eqv Ba(II) ion,7: 1eqv Mn (II) ion,8. 1eqv Al(III) ion, 9. 1eqv Cu(I) ion, 10. 1eqv Pd(II) ion, 11: 1eqv Hg(II) ion, 12: 1eqv Cd(II) ion.

Titration emission spectra and bindng constants of EuL5Zn with ADP and AMP

The titration graphs of **EuL5Zn** with **ADP** or **AMP** were shown in **Figure 5.45** and **5.46**. Excitation at 350 nm gave good sensitization of Eu(III) luminescence with little residual fluorescence. Hypersensitive splitting of transition $^5D_0 \rightarrow {}^7F_2$ and asymmetric ratio before and after addition of ADP or AMP remained the same, indicating that ADP or AMP could not influence the Eu(III) ion coordination environment. Binding constants towards ATP and ADP were calculated as 77869.73M^{-1} and 12776.22M^{-1}. Owing to the larger binding constants and most significant enhancement of luminescence upon addition of ATP among other anions, **EuL5Zn** was expected to be a highly selective ATP sensor.

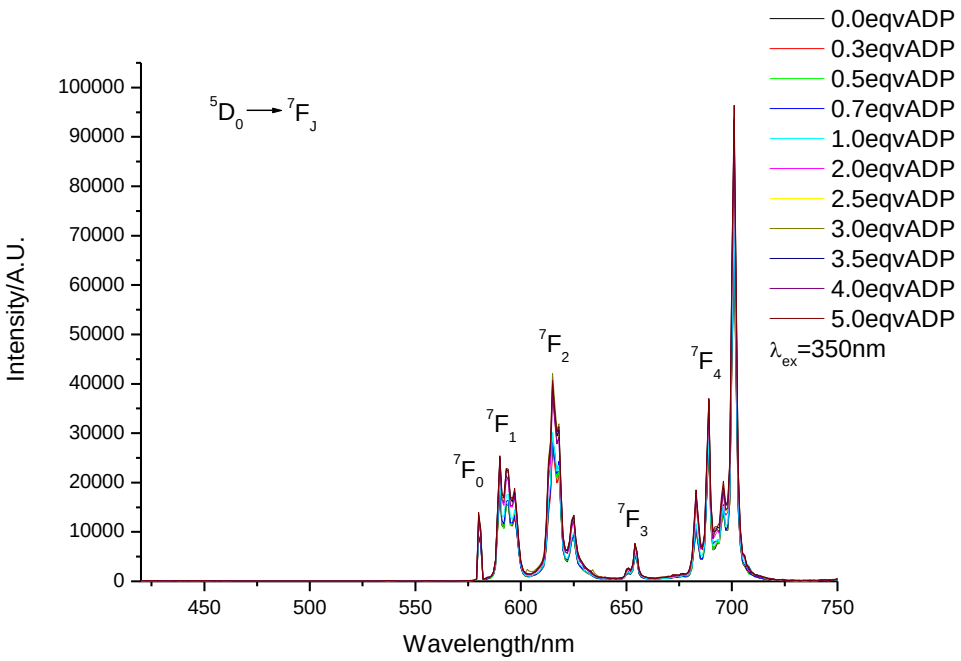

Figure 5.45 Emission spectra of 10 µM aqueous solution upon addition of aliquots of various equiv of ADP with respect to **EuL5Zn** (0.01 M HEPES, pH=7.4, λ_{ex}=350 nm).

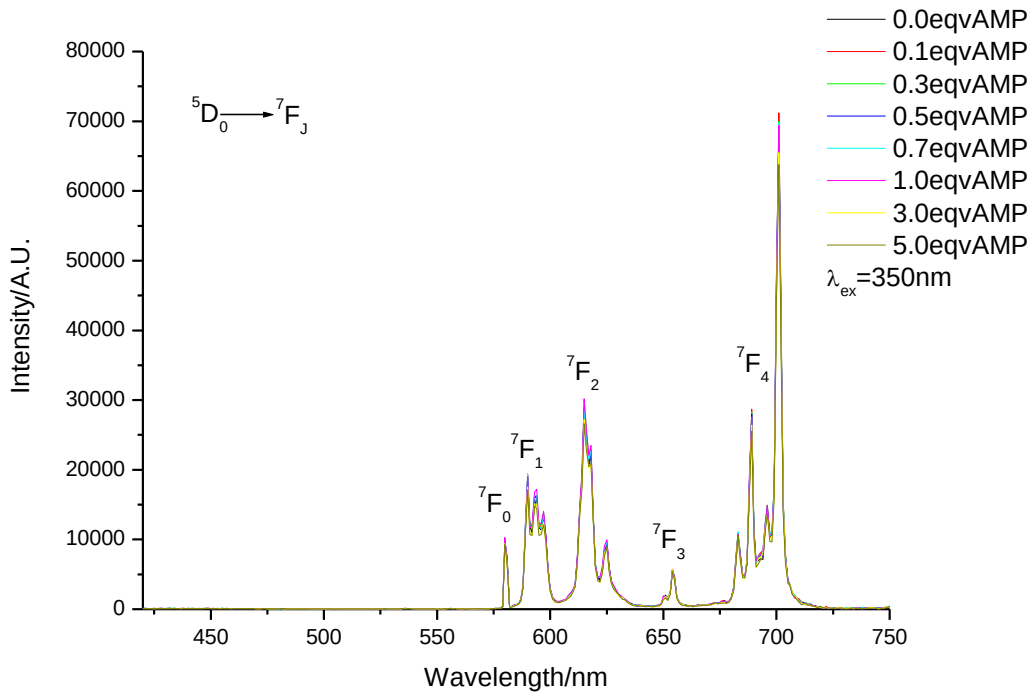

Figure 5.46 Emission spectra of 10 µM aqueous solution upon addition of aliquots of various equiv of AMP with respect to **EuL5Zn** (0.01 M HEPES, pH=7.4, λ_{ex}=350 nm).

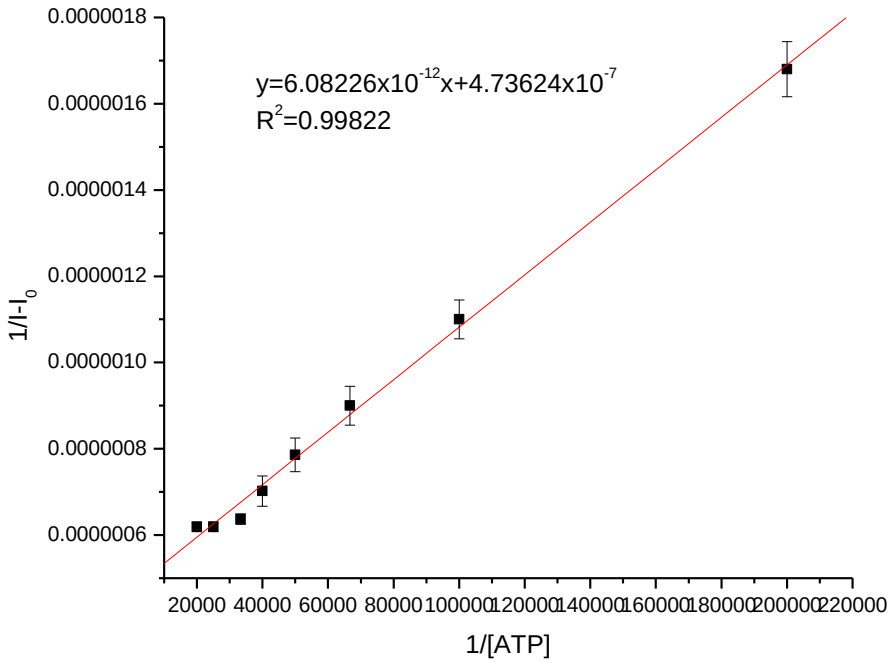

Figure 5.47 Fitting of fluorescence ATP titration curve of **EuL5Zn**.

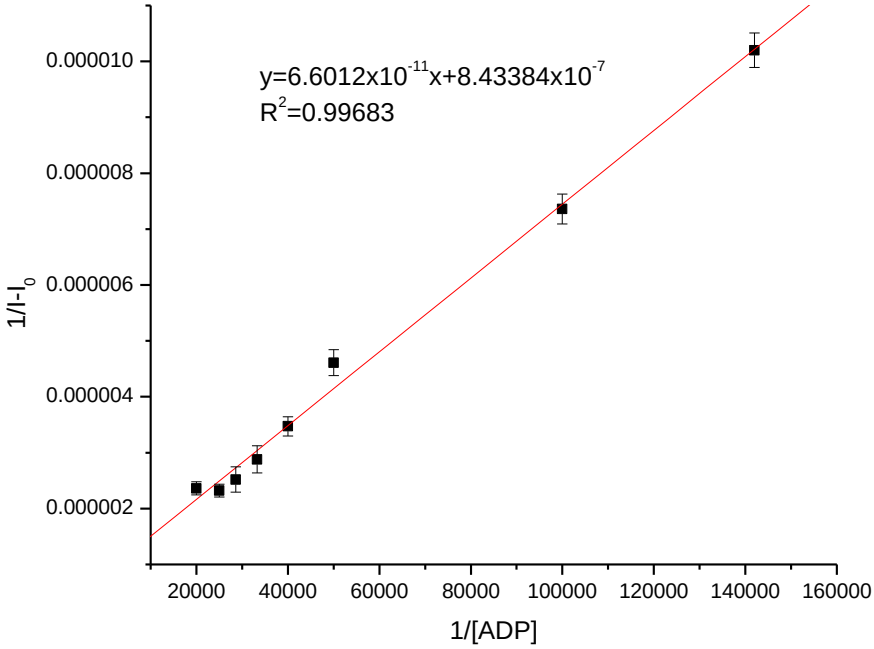

Figure 5.48 Fitting of fluorescence ADP titration curve of **EuL5Zn**.

5.5 Conclusions

A novel series of optical Zn(II) ion probes have been synthesised. Incorporated with a dipicolylamine receptor, **EuL3**, **EuL4** and **EuL5** had selective recognition of Zn(II) ion over other metal cations with the largest binding constants towards Zn(II) ion.

Photophysical solution studies have been done. The absorption peaks of **EuL3**, **EuL4** and **EuL5** were located at 309nm, 307nm and 323nm with molar extinction coefficients 9299 M^{-1}, 13473 M^{-1} and 13161 M^{-1} respectively. Upon titration with Zn(II) ion, **EuL3** and **EuL4** demonstrated luminescent enahancement on chelation of Zn(II) ion while **EuL5** showed quenching. The binding ratio between probes and Zn(II) ion was 1:1 and their q values were one. Their quantum yields were determined and **EuL5** without Zn(II) ion had the highest since its chromophore contained pyridine which was used for direct coordination towards Eu(III) ion for better energy transfer from the chromophore to the Eu(III) ion centre.

Upon chelation with Zn(II) ion, **EuL5Zn** displayed good selectivity towards ATP over other anions in aqueous solution. It demonstrated luminescent enahancement on chelation of ATP and its quantum yields increased from 3.42±0.53 % to 5.23±0.12 %. It is worth noting that it could distinguish ATP from ADP and AMP. Due to the larger binding constants and most significant enhancement of luminescence upon addition of ATP among other anions, **EuL5Zn** was developed to be a potential selective ATP sensor.

5.6 References

[1] P.Jiang and Z. Guo, *Coord. Chem. Rev*., 2004, **248**, 205 –229.

[2] N. C. Lim, H. C. Freake and C. Bruckner, *Chem. Eur. J*., 2005, **11**, 38–49.

[3] K. P. Carter, A. M. Young and A. E. Palmer, *Chem. Rev*., 2014, **114**, 4564–601.

[4] A. I. Bush and R. E. Tanzi, *Proc. Natl. Acad. Sci. U. S. A*., 2002, **99**, 7317-7319.

[5] A. I. Bush, R. D. Moir, K. M. Rosenkranz and R. E. Tanzi, *Science*., 1995, **268**, 1921-1923.

[6] M. P. Cuajungco and K. Y.Faget, *Brain Res. Rev*., 2003, **41**, 44-56.

[7] L. Rossi, S. Migliaccio, A. Corsi, M. Marzia, P. Bianco, A. Teti, L. Gambelli, S. Cianfarani, F. Paoletti and F. Branca, *J. Nutr*., 2001, **131**, 1142-1146.

[8] A. D. McNall, T. D. Etherton and G. J. Fosmire, *J. Nutr*., 1995, **125**, 874-879.

[9] R. Buzina, M. Jusic, J. Sapunar and N. Milanovic, *Am. J. Clin. Nutr*. 1980, **33**, 2262-2267.

[10] J.R. Duncan and L.S. Hurley, *Exp. Biol. Med*., 1978, **159**, 39–43.

[11] T.J.McCarthy, J.J. Zeelie and D.J. Krause, *J Clin Pharm Ther*., 1992, **17**, 51-54.

[12] H. M. N. H. Irving and R. J. O. Williams, J. Chem. Soc, 1953, 3192–3210.

[13] K. L. Haas and K. J. Franz, Chem. Rev., 2009, **109**, 4921–4960.

[14] J. R. Lin, C. J. Chu, P. Venkatesan and S. P. Wu, *Sensors and Actuators B: Chemical*., 2015, **207**, 563-570.

[15] X. Tian, X. Guo, F. Yu and L. Jia, *Sensors and Actuators B: Chemical*., 2016, **232**,181-187.

[16] C. Patraa, A. K. Bhanjaa, C. Sena, D. Ojhab, D. Chattopadhyay, A. Mahapatraa and C. Sinha, *Sensors and Actuators B: Chemical*., 2016, **228**, 287-294.

[17] P. Ritter, *Biochemistry, a foundation*, Creation Research Society Quarterly, 1999.

[18] E. Kimura, *Tetrahedron*, 1992, **48**, 6175–6217.

[19] E. Kimura, T. Shiota, T. Koike, M. Shim and M. Kodama, *J. Am. Chem. Soc*., 1990, **112**, 5805–5811.

[20] E. Kimura, S. Aoki, T. Koike and M. Shiro, *J. Am. Chem. Soc*., 1997, **119**, 3068–3076.

[21] A. Ojida, I. Takashima, T. Kohira, H. Nonaka and I. Hamachi, *J. Am. Chem. Soc*., 2008, **130**, 12095–12101.

[22] Y. Kurishita, T. Kohira, A. Ojida and I. Hamachi, *J. Am. Chem. Soc*., 2010, **132**, 13290–13299.

[23] A. Ojida, H. Nonaka, Y. Miyahara, S. Tamaru, K. Sada and I. Hamachi, *Angew. Chem., Int. Ed*., 2006, **45**, 5518–5521.

[24] D. Amilan Jose, Sandhya Mishra, Amrita Ghosh, Anupama Shrivastav, Sanjiv K. Mishra and Amitava Das, *Org. Lett*.,2007, **9**,1979-1982.

5.7 Appedix

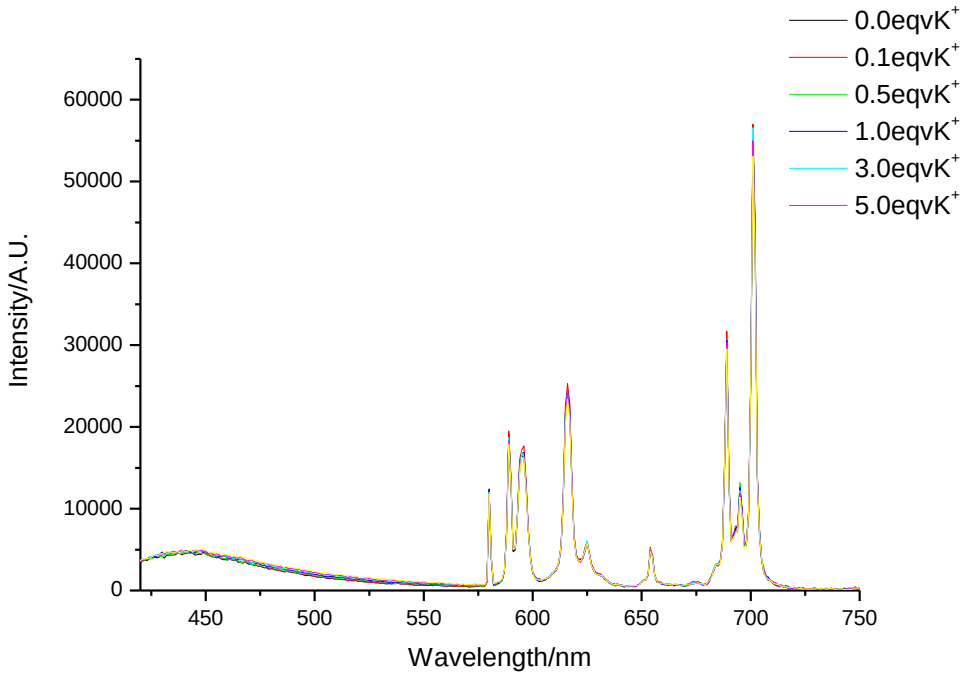

Figure 5.51 Emission spectra of 10 μM aqueous solution upon addition of aliquots of various equiv of K(I) ion with respect to **EuL3** (0.01 M HEPES, pH=7.4, λ_{ex}=350 nm).

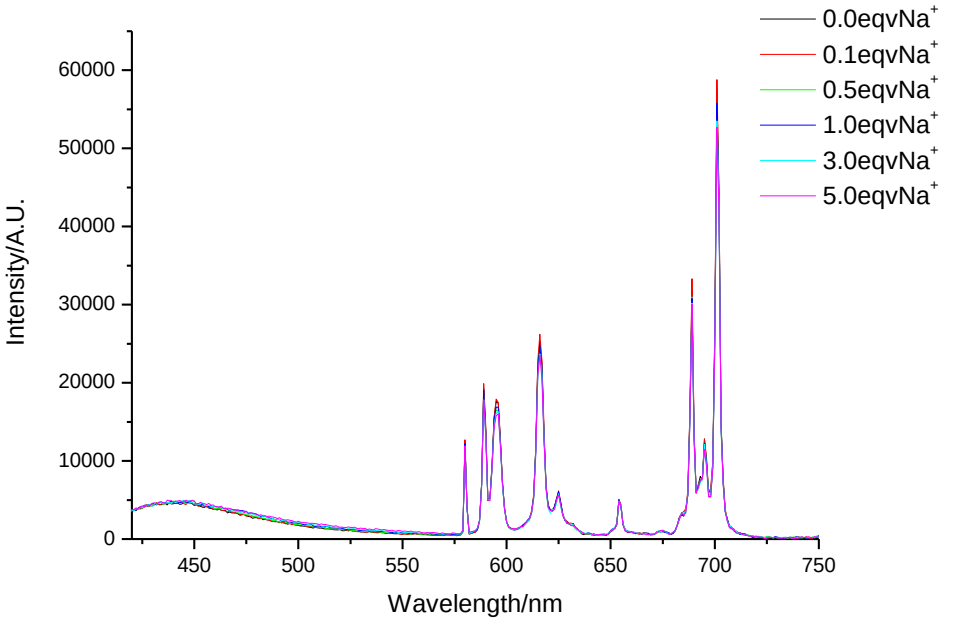

Figure 5.52 Emission spectra of 10 μM aqueous solution upon addition of aliquots of various equiv of Na(I) ion with respect to **EuL3** (0.01 M HEPES, pH=7.4, λ_{ex}=350 nm).

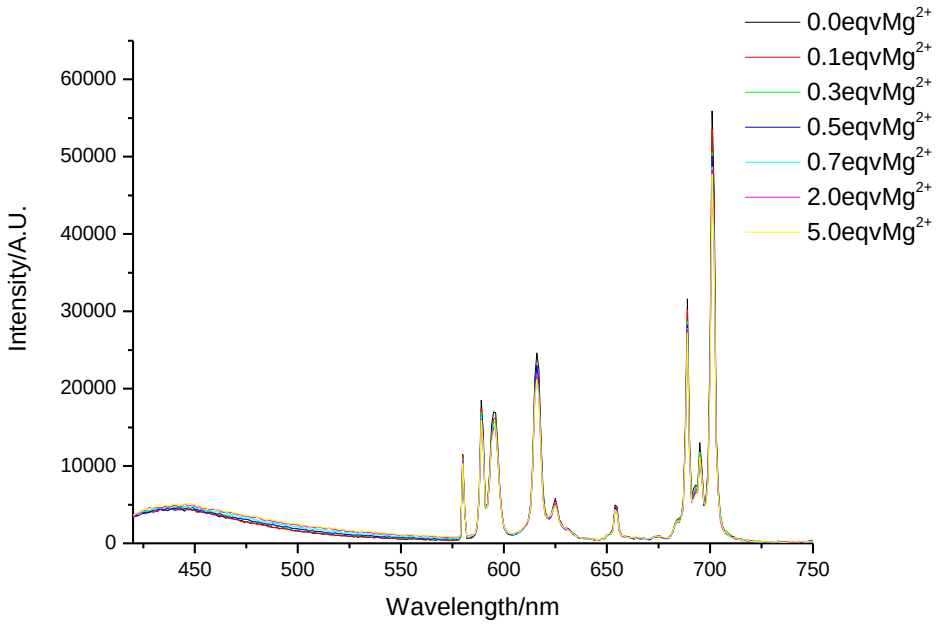

Figure 5.53 Emission spectra of 10 µM aqueous solution upon addition of aliquots of various equiv of Mg(II) ion with respect to **EuL3** (0.01 M HEPES, pH=7.4, λ_{ex}=350 nm).

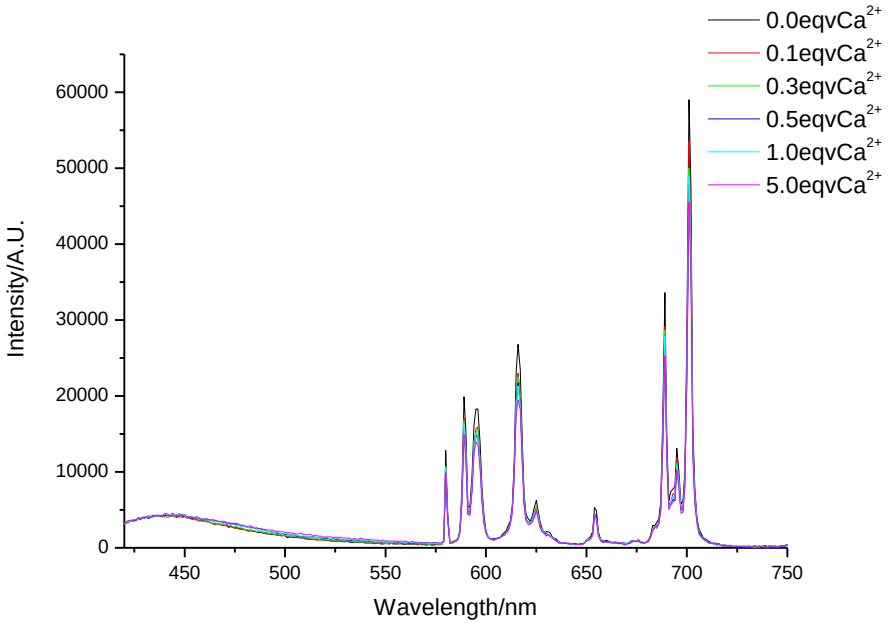

Figure 5.54 Emission spectra of 10 µM aqueous solution upon addition of aliquots of various equiv of Ca(II) ion with respect to **EuL3** (0.01 M HEPES, pH=7.4, λ_{ex}=350 nm).

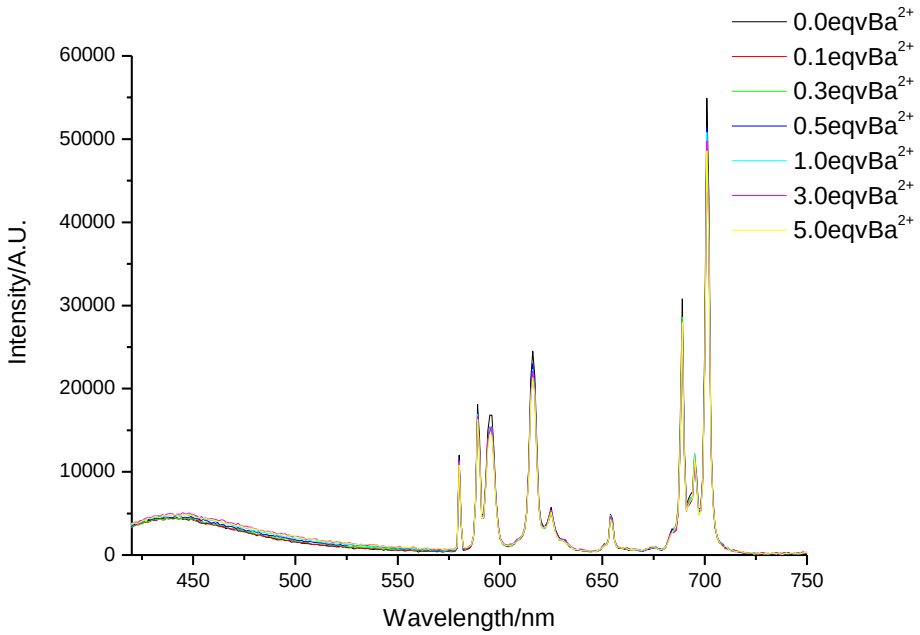

Figure 5.55 Emission spectra of 10 µM aqueous solution upon addition of aliquots of various equiv of Ba(II) ion with respect to **EuL3** (0.01 M HEPES, pH=7.4, λ_{ex}=350 nm).

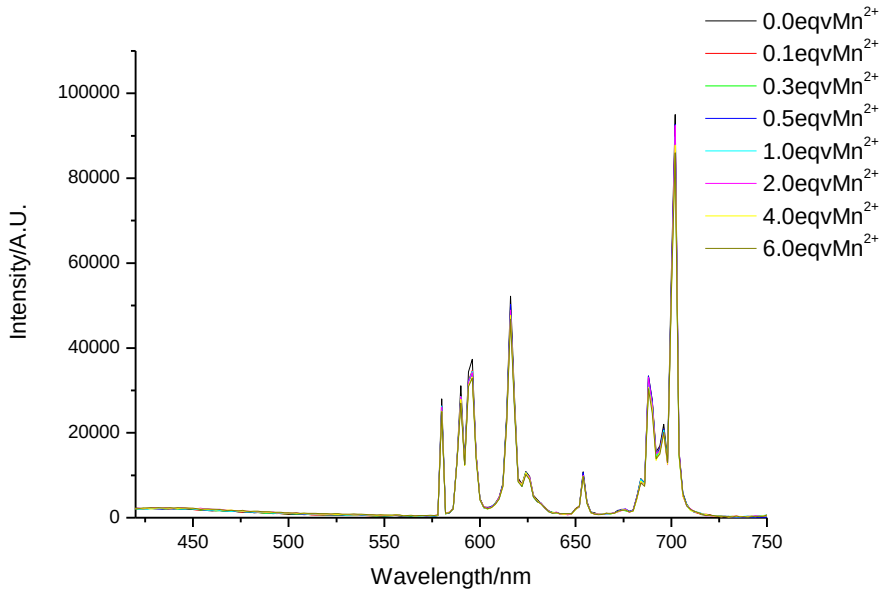

Figure 5.56 Emission spectra of 10 µM aqueous solution upon addition of aliquots of various equiv of Mn(II) ion with respect to **EuL3** (0.01 M HEPES, pH=7.4, λ_{ex}=350 nm).

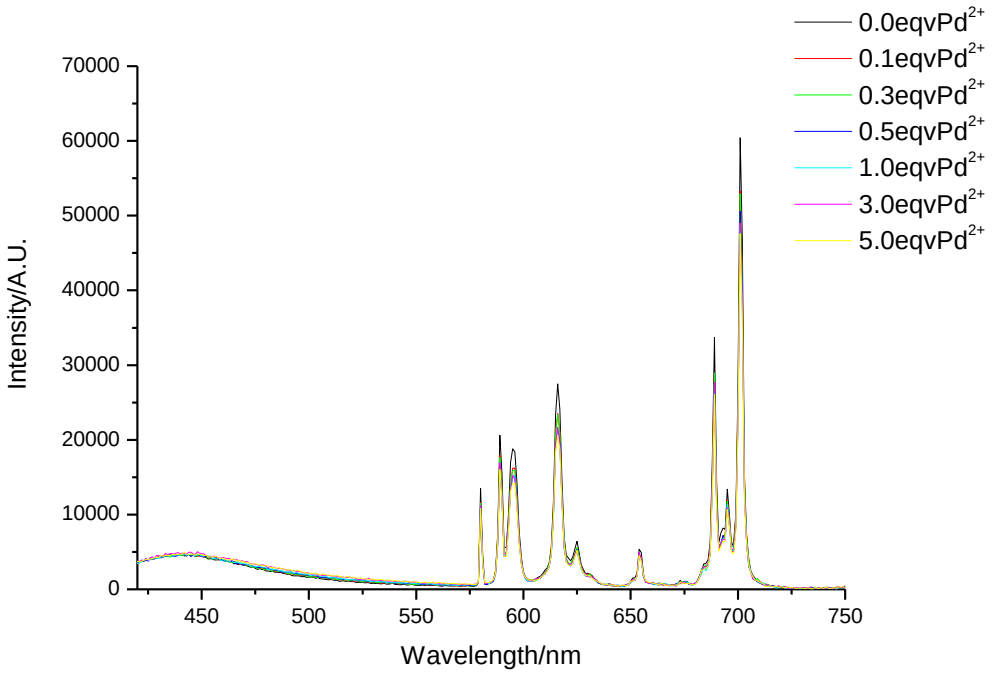

Figure 5.57 Emission spectra of 10 μM aqueous solution upon addition of aliquots of various equiv of Pd(II) ion with respect to **EuL3** (0.01 M HEPES, pH=7.4, λ_{ex}=350 nm).

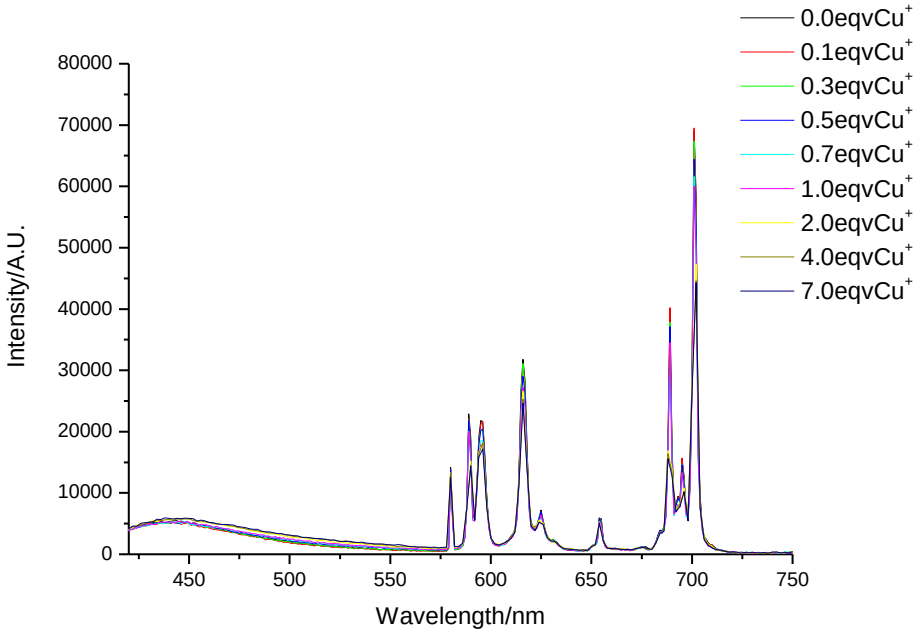

Figure 5.58 Emission spectra of 10 μM aqueous solution upon addition of aliquots of various equiv of Cu(I) ion with respect to **EuL3** (0.01 M HEPES, pH=7.4, λ_{ex}=350 nm).

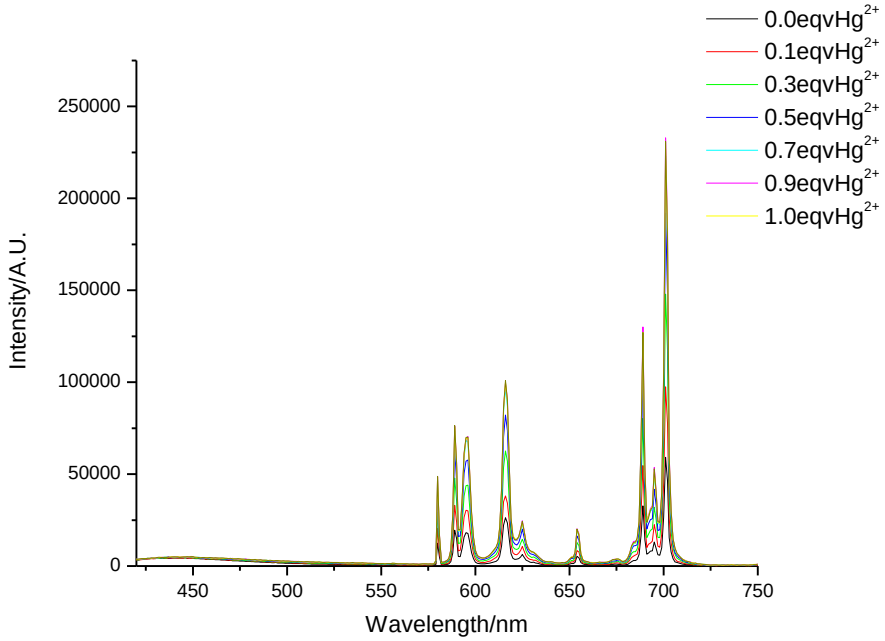

Figure 5.59 Emission spectra of 10 µM aqueous solution upon addition of aliquots of various equiv of Hg(II) ion with respect to **EuL3** (0.01 M HEPES, pH=7.4, λ_{ex}=350 nm).

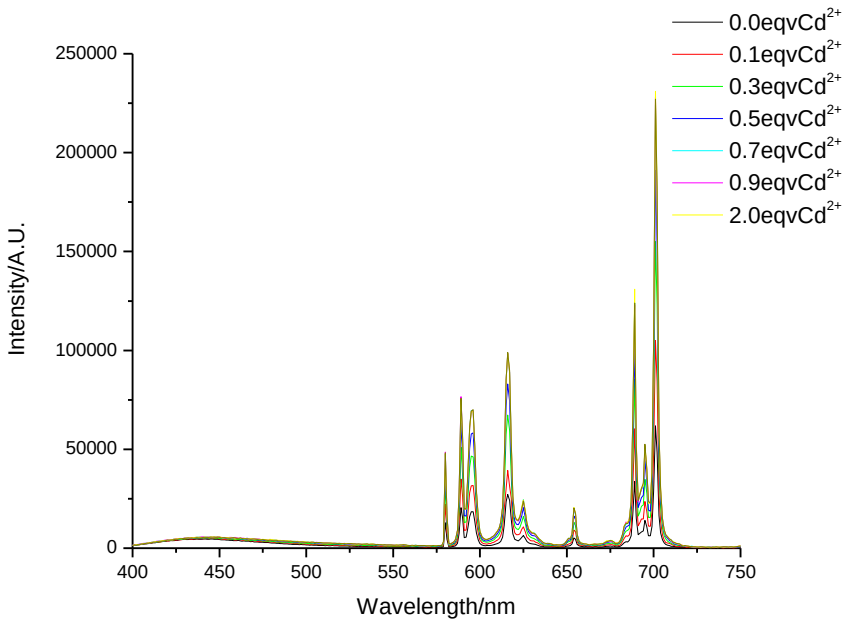

Figure 5.60 Emission spectra of 10 µM aqueous solution upon addition of aliquots of various equiv of Cd(II) ion with respect to **EuL3** (0.01 M HEPES, pH=7.4, λ_{ex}=350 nm).

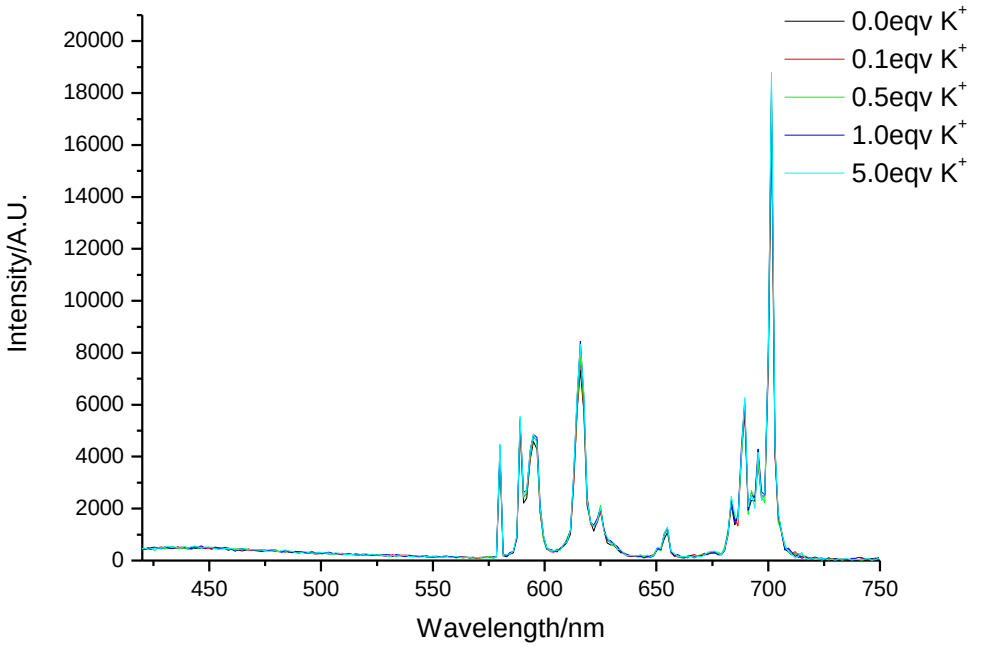

Figure 5.61 Emission spectra of 10 μM aqueous solution upon addition of aliquots of various equiv of K(I) ion with respect to **EuL4** (0.01 M HEPES, pH=7.4, λ_{ex}=350 nm).

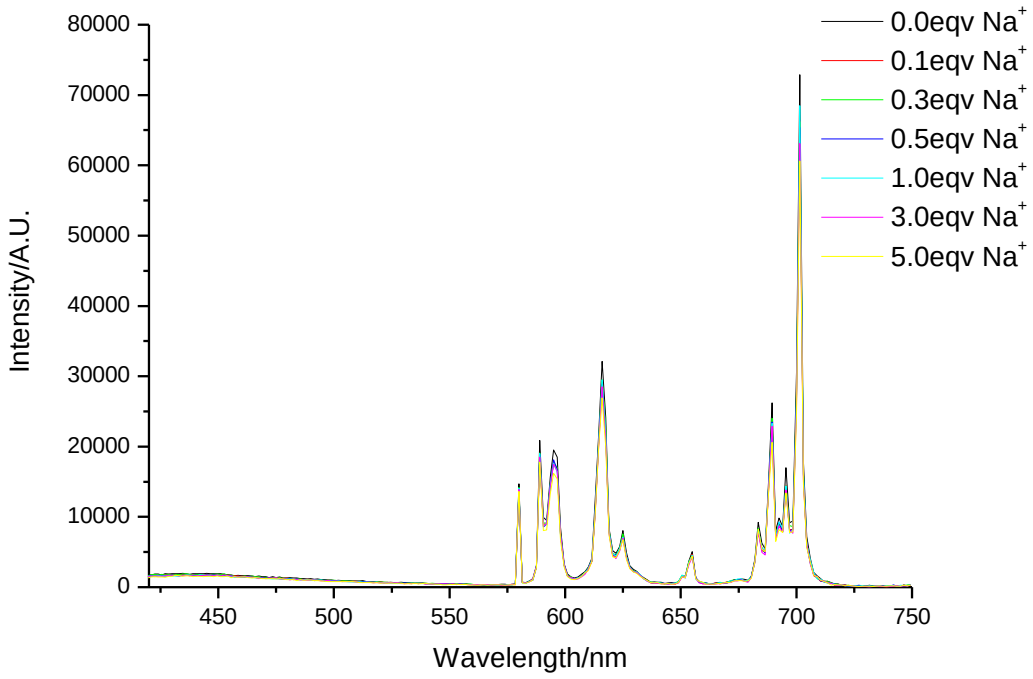

Figure 5.62 Emission spectra of 10 μM aqueous solution upon addition of aliquots of various equiv of Na(I) ion with respect to **EuL4** (0.01 M HEPES, pH=7.4, λ_{ex}=350 nm).

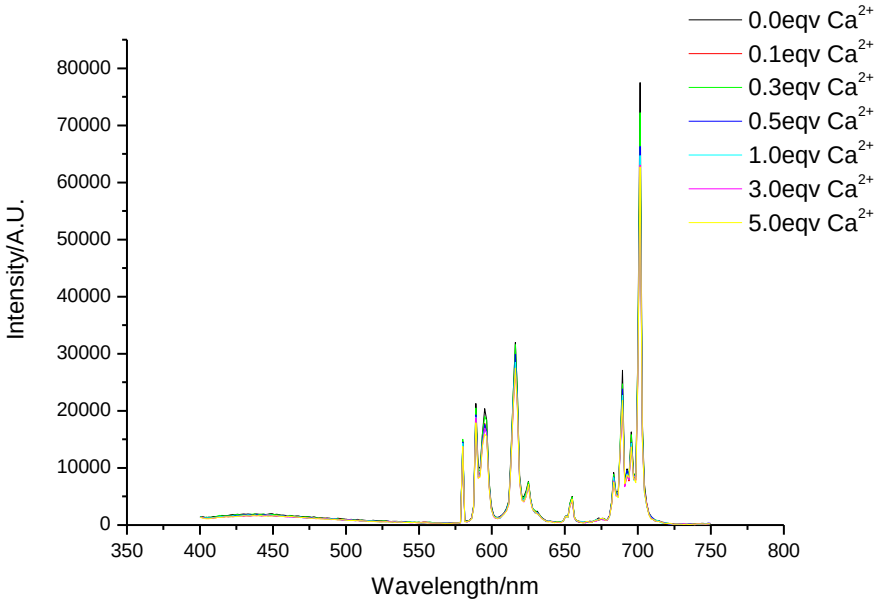

Figure 5.63 Emission spectra of 10 μM aqueous solution upon addition of aliquots of various equiv of Ca(II) ion with respect to **EuL4** (0.01 M HEPES, pH=7.4, λ_{ex}=350 nm).

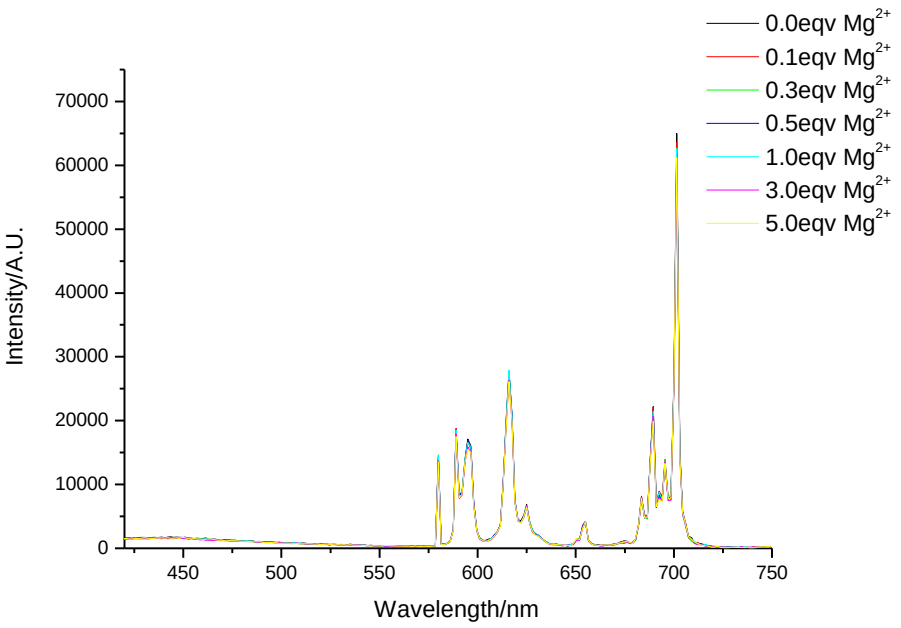

Figure 5.64 Emission spectra of 10 μM aqueous solution upon addition of aliquots of various equiv of Mg(II) ion with respect to **EuL4** (0.01 M HEPES, pH=7.4, λ_{ex}=350 nm).

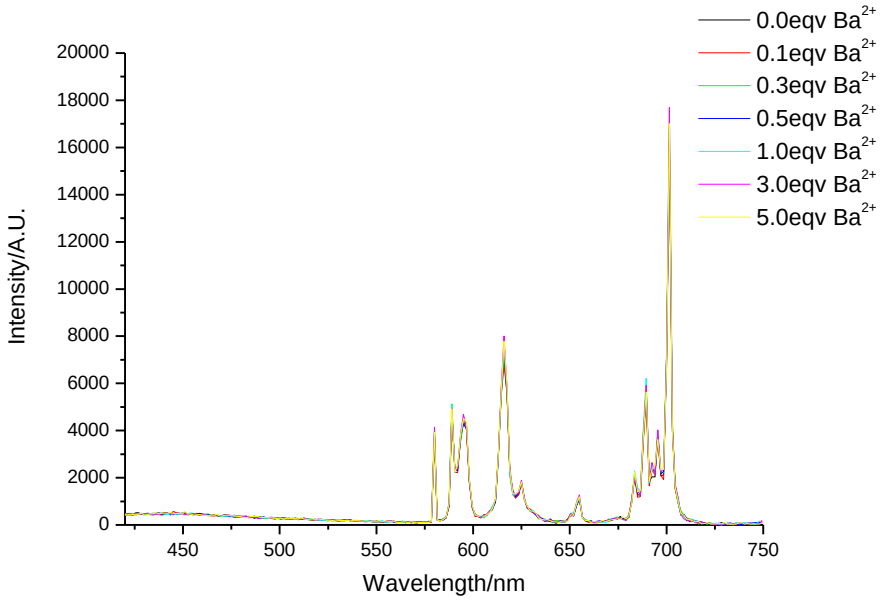

Figure 5.65 Emission spectra of 10 µM aqueous solution upon addition of aliquots of various equiv of Ba(II) ion with respect to **EuL4** (0.01 M HEPES, pH=7.4, λ_{ex}=350 nm).

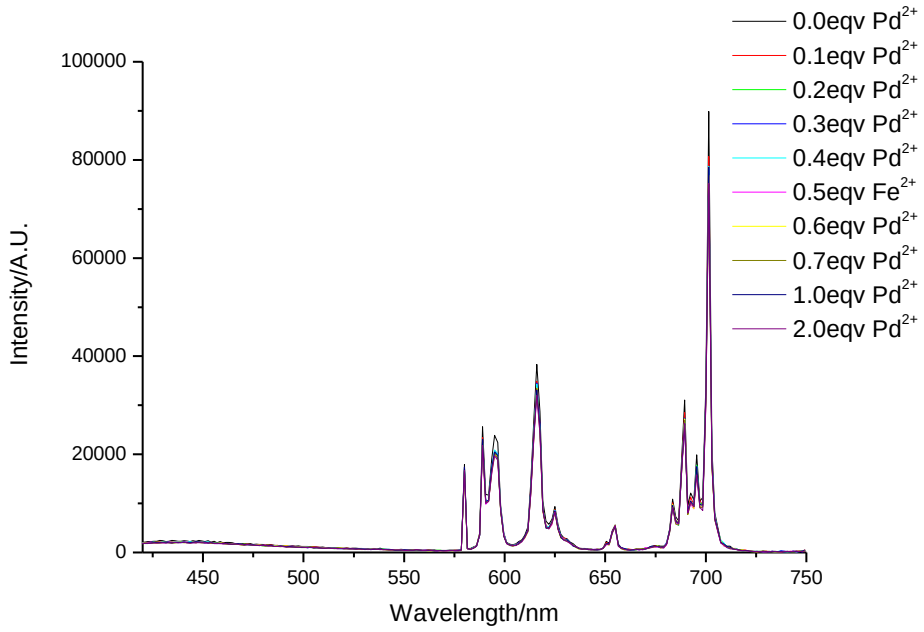

Figure 5.66 Emission spectra of 10 µM aqueous solution upon addition of aliquots of various equiv of Pd(II) ion with respect to **EuL4** (0.01 M HEPES, pH=7.4, λ_{ex}=350 nm).

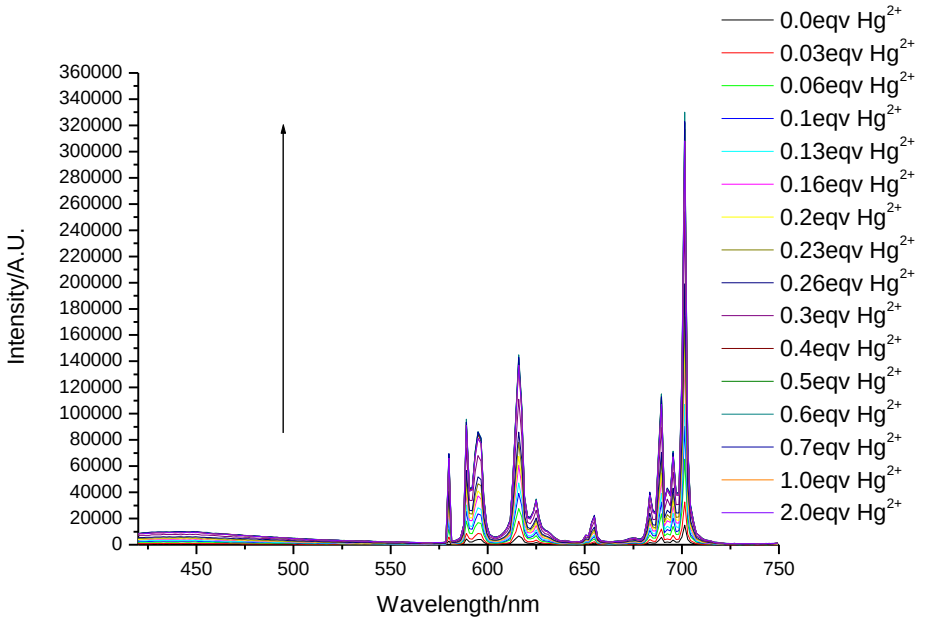

Figure 5.67 Emission spectra of 10 µM aqueous solution upon addition of aliquots of various equiv of Hg(II) ion with respect to **EuL4** (0.01 M HEPES, pH=7.4, λ_{ex}=350 nm).

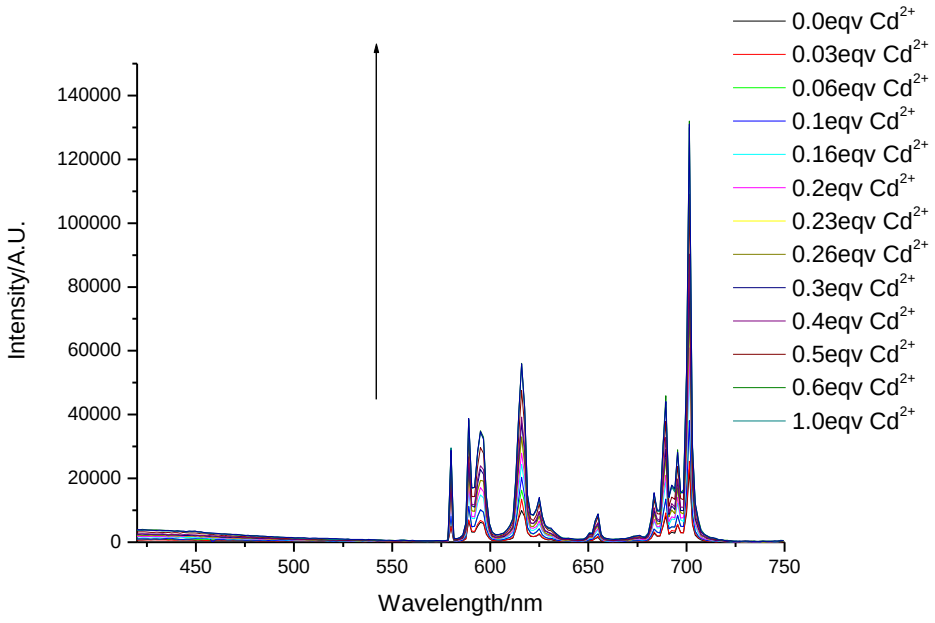

Figure 5.68 Emission spectra of 10 µM aqueous solution upon addition of aliquots of various equiv of Cd(II) ion with respect to **EuL4** (0.01 M HEPES, pH=7.4, λ_{ex}=350 nm).

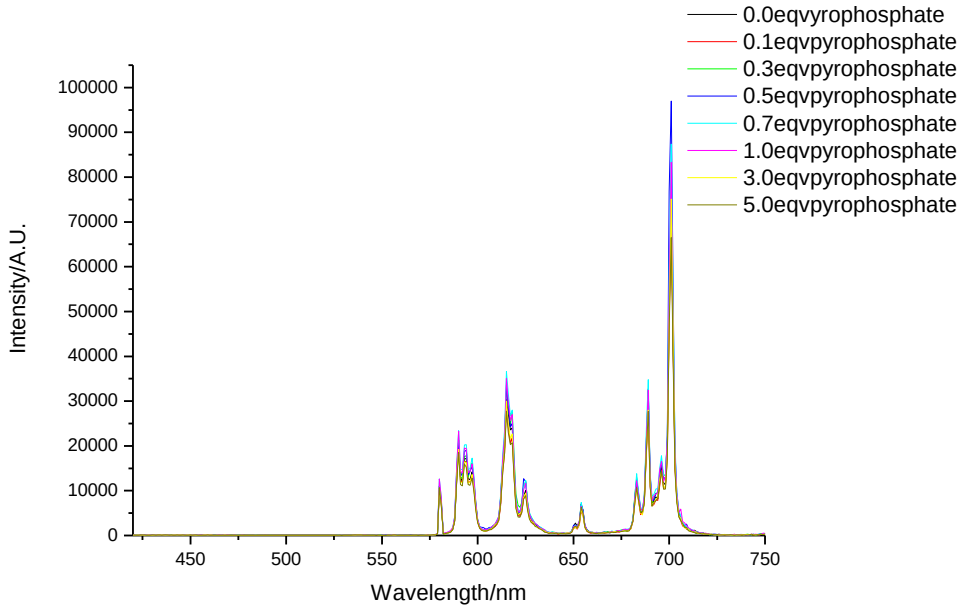

Figure 5.69 Emission spectra of 10 μM aqueous solution upon addition of aliquots of various equiv of pyrophosphate ion with respect to **EuL5Zn** (0.01 M HEPES, pH=7.4, λ_{ex}=350 nm).

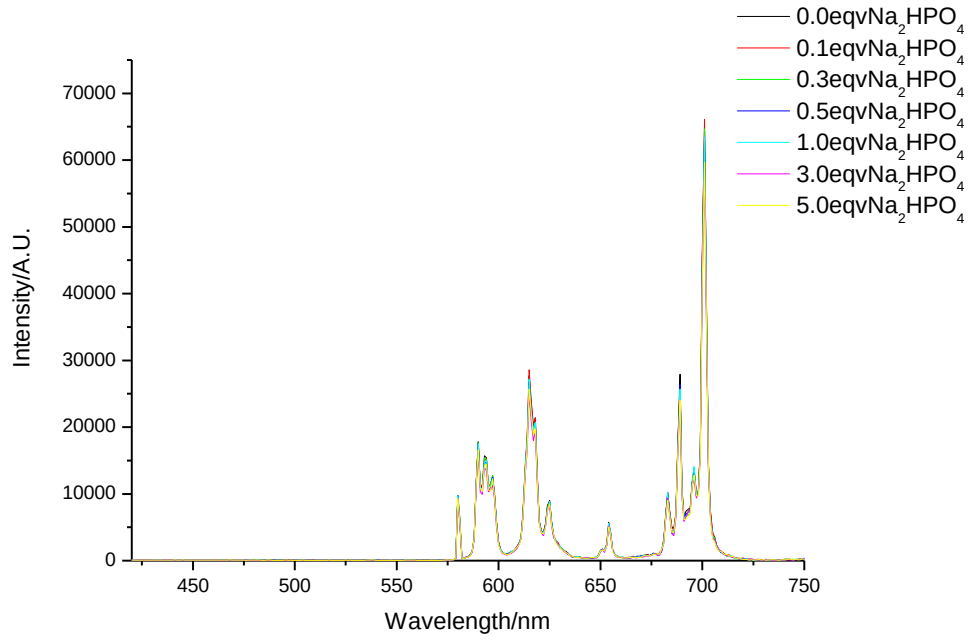

Figure 5.70 Emission spectra of 10 μM aqueous solution upon addition of aliquots of various equiv of Na_2HPO_4 ion with respect to **EuL5Zn** (0.01 M HEPES, pH=7.4, λ_{ex}=350 nm).

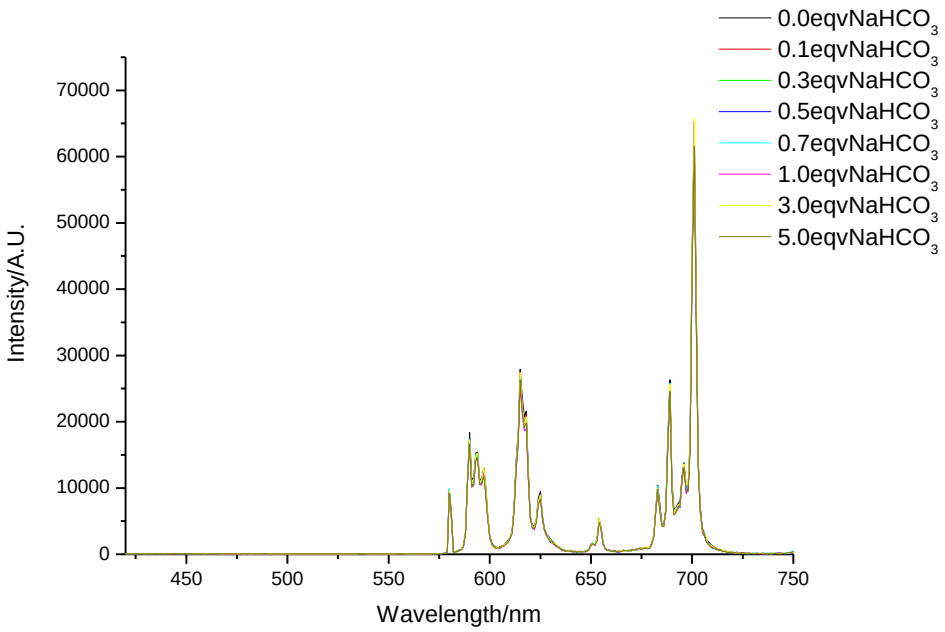

Figure 5.71 Emission spectra of 10 µM aqueous solution upon addition of aliquots of various equiv of $NaHCO_3$ ion with respect to **EuL5Zn** (0.01 M HEPES, pH=7.4, λ_{ex}=350 nm).

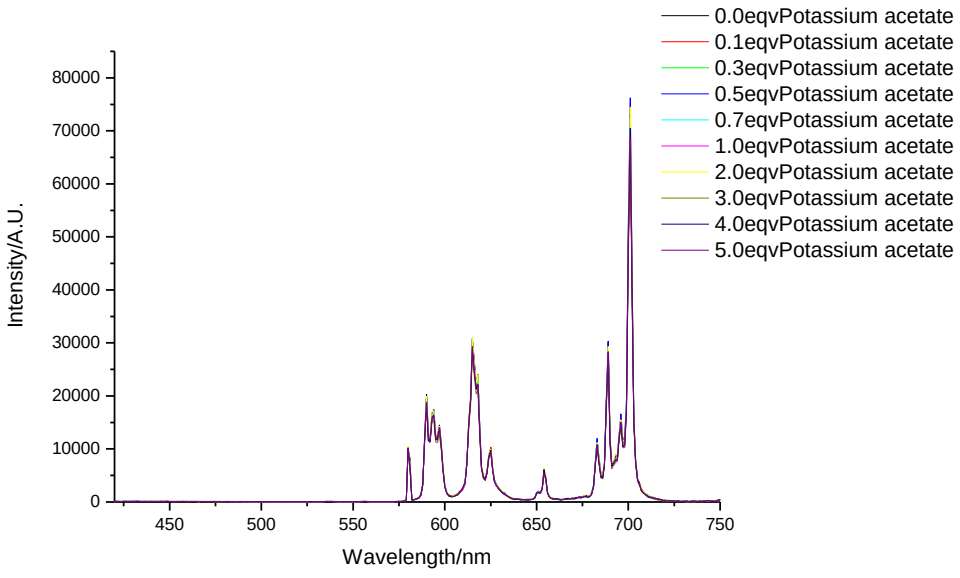

Figure 5.72 Emission spectra of 10 µM aqueous solution upon addition of aliquots of various equiv of potassium acetate with respect to **EuL5Zn** (0.01 M HEPES, pH=7.4, λ_{ex}=350 nm).

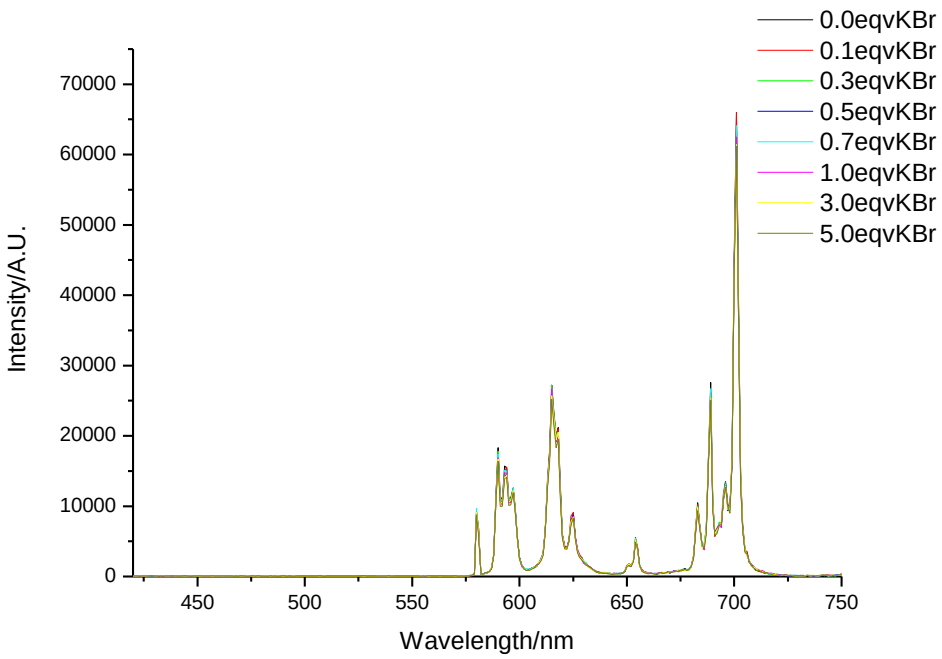

Figure 5.73 Emission spectra of 10 μM aqueous solution upon addition of aliquots of various equiv of KBr with respect to **EuL5Zn** (0.01 M HEPES, pH=7.4, λ_{ex}=350 nm).

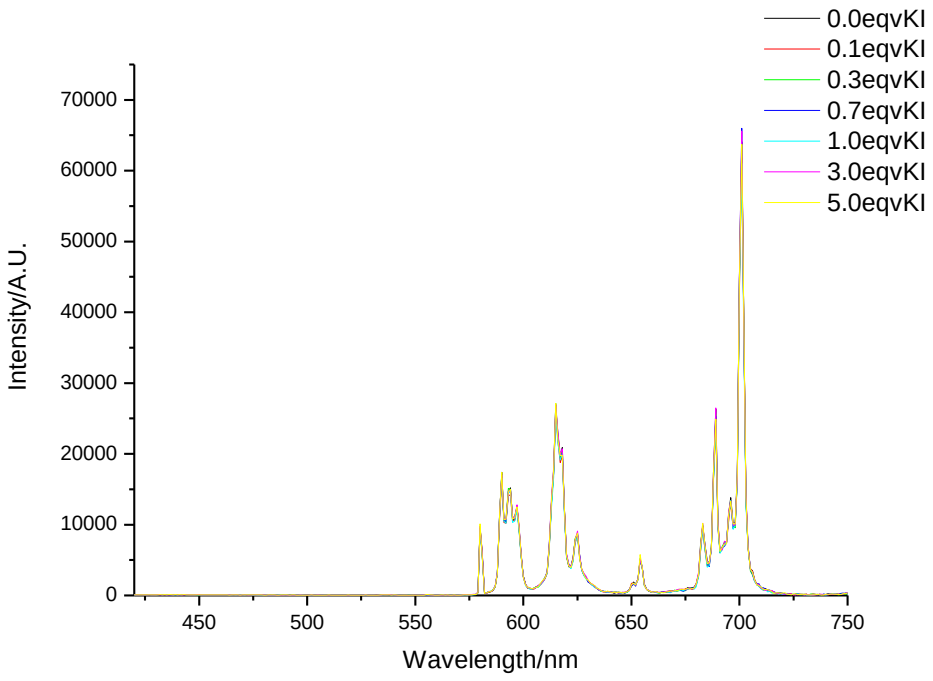

Figure 5.74 Emission spectra of 10 μM aqueous solution upon addition of aliquots of various equiv of KI with respect to **EuL5Zn** (0.01 M HEPES, pH=7.4, λ_{ex}=350 nm).

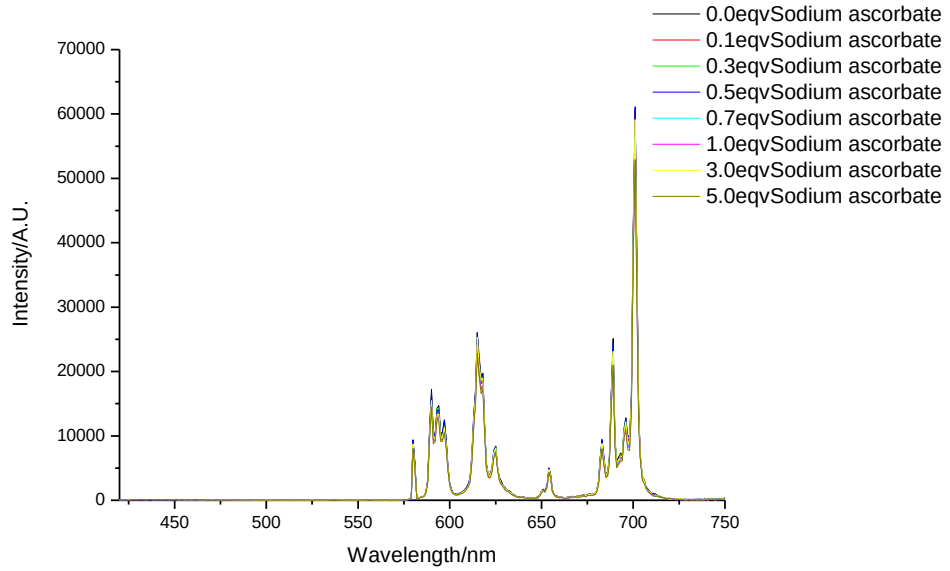

Figure 5.75 Emission spectra of 10 μM aqueous solution upon addition of aliquots of various equiv of sodium ascorbate with respect to **EuL5Zn** (0.01 M HEPES, pH=7.4, λ_{ex}=350 nm).

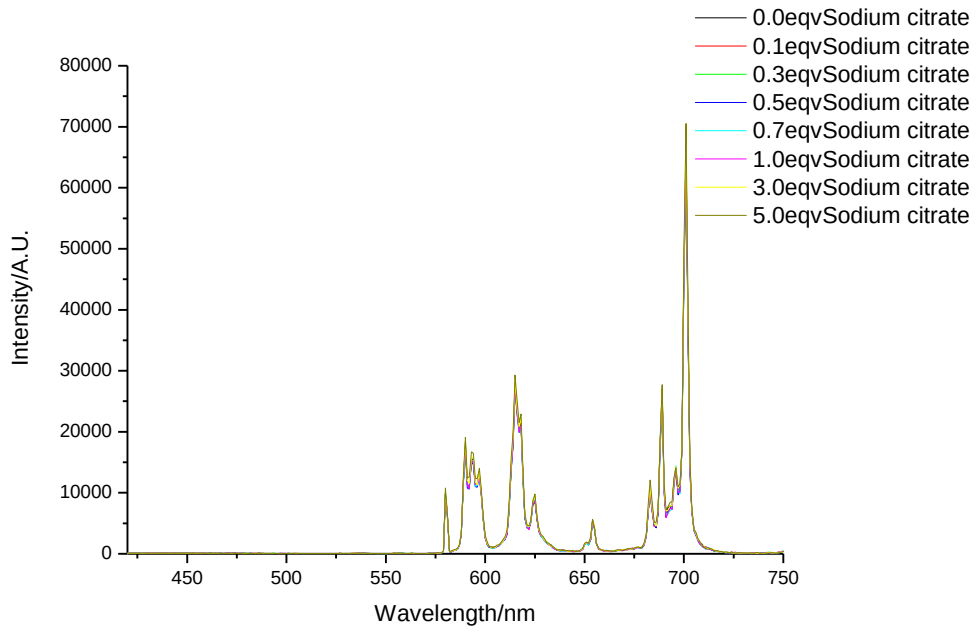

Figure 5.76 Emission spectra of 10 μM aqueous solution upon addition of aliquots of various equiv of sodium citrate with respect to **EuL5Zn** (0.01 M HEPES, pH=7.4, λ_{ex}=350 nm).

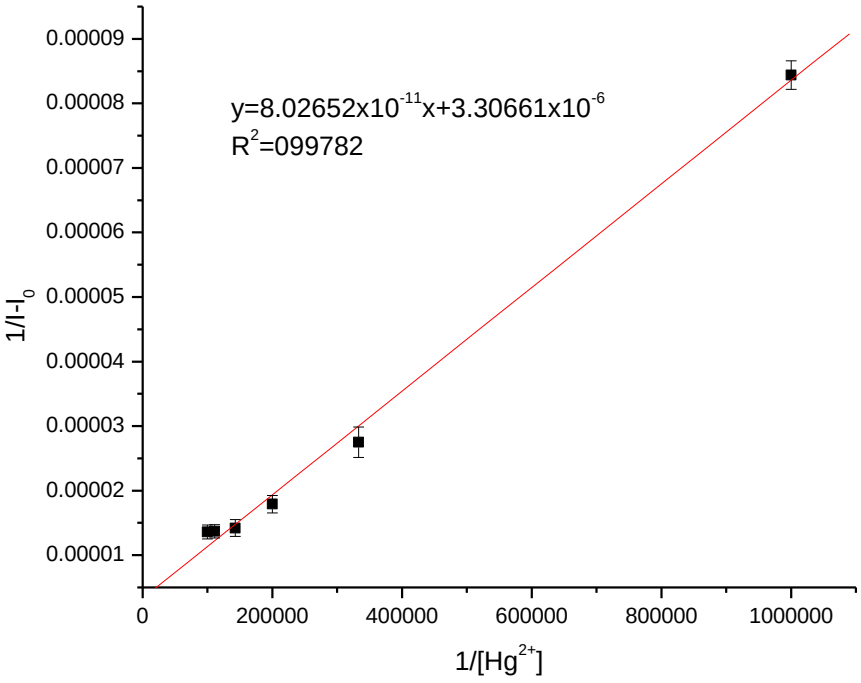

Figure 5.77 Fitting of fluorescence Hg(II) ion titration curve of **EuL3**.

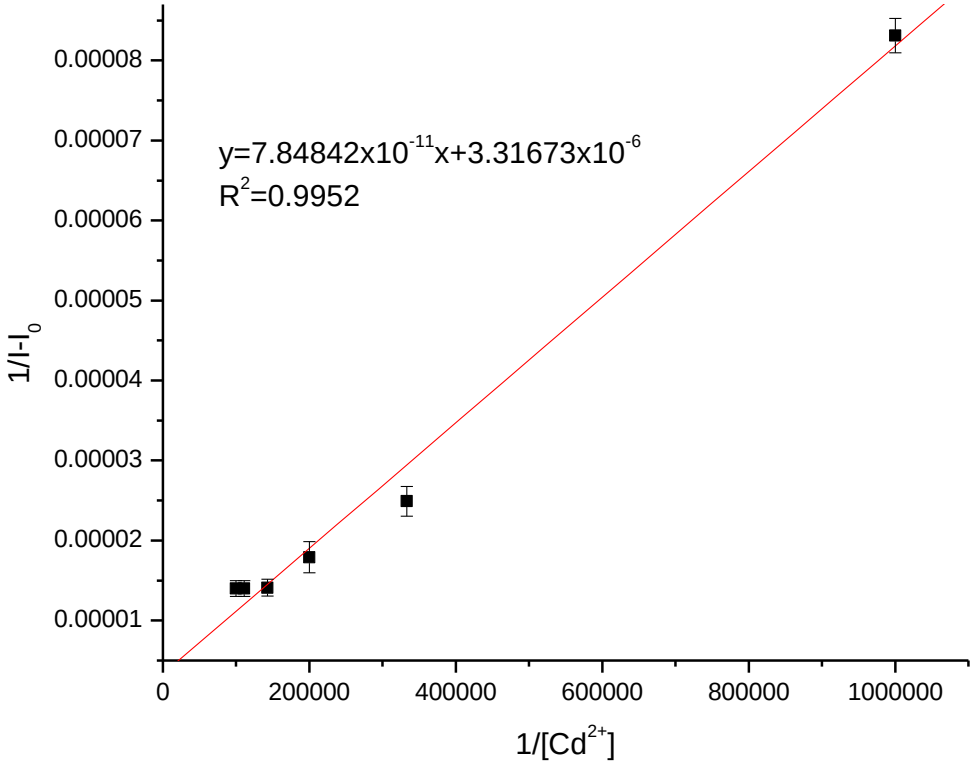

Figure 5.78 Fitting of fluorescence Cd(II) ion titration curve of **EuL3**.

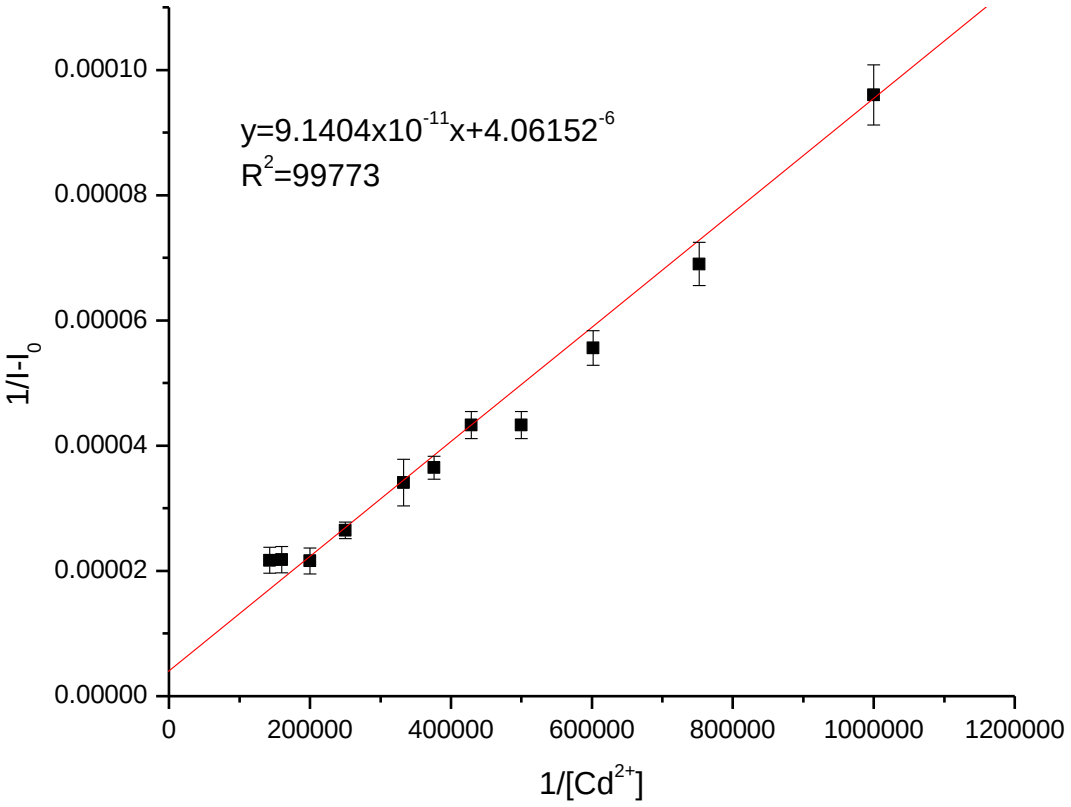

Figure 5.79 Fitting of fluorescence Cd(II) ion titration curve of **EuL4**.

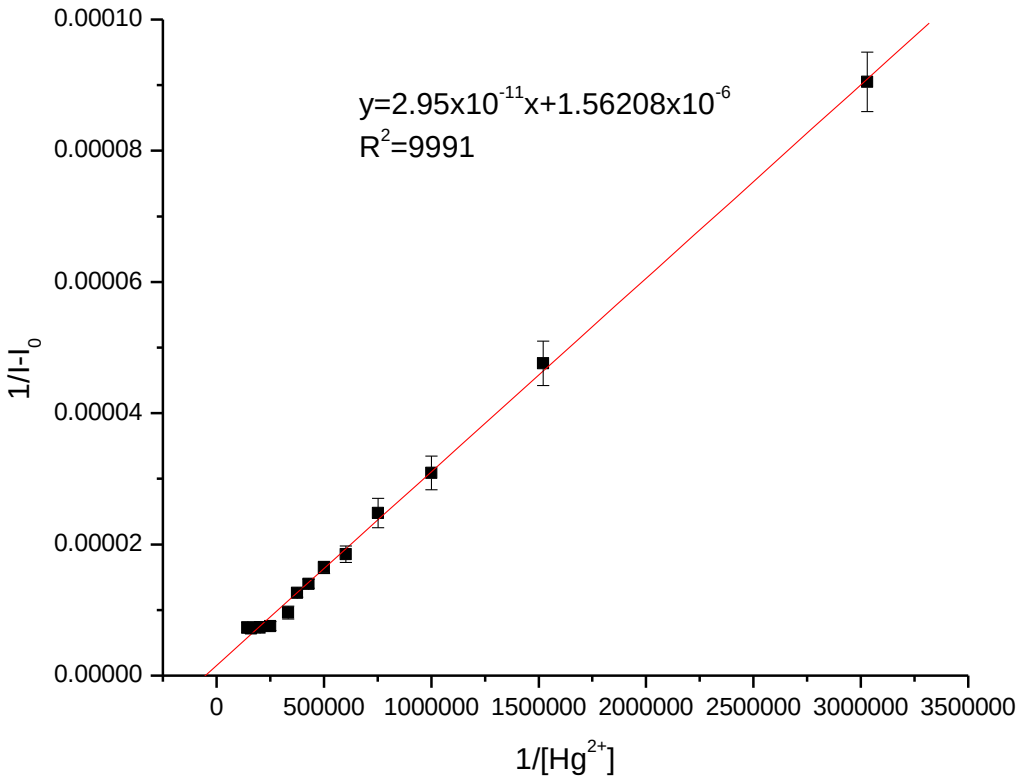

Figure 5.81 Fitting of fluorescence Hg(II) ion titration curve of **EuL4**.

CHAPTER 6

Development of lanthanide complexes for detection of Cu(I) ion

6.1 Introduction

Copper is the third most abundant trace element after zinc and iron in the human body[1][2] with ≈80–100 mg storage.[3] Cuprous Cu(I) and cupric Cu(II) are two major oxidation states of copper in biological systems [1] and their oxidation states are always dependent on the nature of environment. For example, cuprous Cu(I)is more prevalent in the reducing intracellular environment while cupric Cu(II) is more common in the oxidizing intracellular environment.

Like zinc, copper is often chelated by proteins are stored in labile pool. [4] For instance, the trafficking of cellular copper to enzymes is mediated by copper chaperone proteins.[5][6] Proper trafficking is important since abnormality in copper trafficking and perturbation of copper balance as a result of diet or disease status can lead to serious diseases such as Wilson's disease[7] , Menkes syndrome [8] and Alzheimer's disease.[9][10] **Table 6.1** lists some neurological diseases in whose pathogenesis is copper directly or indirectly implicated.[11] Excess copper is toxic and its redox cycling between Cu(I) and Cu(II) ion can catalyse the production of hydroxyl radicals, leading to subsequent oxidative damages to DNA, proteins and other biomolecules.[12][13] It is also able to displace other essential metals (e.g. zinc) in proteins. Therefore, maintaining a good balance of copper homeostasis is crucial within an organism.

Copper plays a crucial role in physiological processes.[14] For instance, its redox activity makes it an essential cofactor in many enzymes such as cytochrome c oxidase (CcO), Cu/Zn superoxide dismutase (SOD1), ceruloplasmin (Cp), and dopamine β monooxygenase (DβM) and allows these enzymes to function properly.[15]-[17] For example, copper regulates the expression of the functional activity of SOD1 and a low level of copper will decrease the activity of SOD1.[18] Moreover, copper is related to the building up of immune response to infection during the inflammatory process.

Copper-binder Cp is an acute-phase reactive protein to stress and trauma; it is elevated in response to inflammation, infection and chronic diseases. Copper is also needed for the functioning and maturation of T cells.

Disease	Characteristics	Neuronal effects
Alzheimer's disease (AD)	● Familial AD caused by a mutations in amyloid precursor protein ● Adult-onset dementia	● Amyloid protein accumulation ● Self-aggregating plaques
Huntington's disease	● Autosomal dominant trait ● Teenage- or adult-onset ● Severe movement disorder	● Polyglutamine triplet repeat expansion ● Pro-oxidative activities
Menkes disease	● X-linked recessive gene ● Poor copper absorption and distribution ● Connective tissue problems	● Dysmyelination ● Intracranial vessels abnormalities ● Delayed myelination
Parkinson's disease	● Primary movement disorder ● Akinesia/ Bradykinesia	● Death of dopaminergic neurons ● Accumulation of intracellular inclusions
Prion diseases	● Transmissable neurodegenerative disease ● Spongiform encephalopathy	● Possible inappropriate metallation of prion protein with Mn instead of Cu

Table 6.1 Summary of some neurological diseases that involve copper metabolism.[11]

There are various classical methods for detection of copper such as inductively coupled plasma mass spectrometry,[19]-[22] positron emission tomography, [23] radiolabelling, [24] and synchrotron X-ray fluorescence microprobe[25][26], but these

techniques require special instruments or reagent (e.g. radiolabelling copper). Other traditional methods for measuring copper such as mass spectroscopy,[27] electron spin resonance,[28] and atomic absorption spectroscopy [29][30] are only suitable for measuring bulk samples and samples will end up being destroyed. Moreover, those techniques have some drawbacks such as sophisticated instrumentation, a complex procedure and expensive instrumentation. In contrast, optical detection is one of powerful methods for detecting copper since it is non-invasive, simple, sensitive, selective, convenient and low-cost.

To design a suitable optical chemical sensor for detecting Cu(I), it is important to understand some properties of Cu(I) and hence its coordination preference. Some factors such as donor atoms of ligands can be taken in consideration. Cu(I) is classified as a soft acid and its coordination chemistry is dominated by a soft donating ligands such as sulfur containing species. Unlike Cu(I), Cu(II) is considered as a borderline hard acid which has higher preference for interaction with oxygen- and nitrogen-donating ligands, followed by chloride and sulfur-containing species. Furthermore, as a d^9 system, Cu(II) has high preference for a four coordinate square planar geometry or six coordinate octahedral, both of which supply substantial ligand field stabilization energies. In contrast, Cu(I) has a fully filled d shell and therefore electronic stabilization effects are therefore absent. Its preferred coordination geometry is a tetrahedral geometry. Therefore, the design of selective receptor for recognition of Cu(I) can be based on the above information.

There are some studies of polythioether ligands in literature.[31]-[33] For instance, polythioether ligands with four to five sulfur donor atoms displayed strong affinities for Cu(I) and stability constants ranging from logK=10 to 15.[32][33] **Figure 6.1** shows the binding affinities and redox potentials of some Cu(I) receptors. **C** and **E** demonstrated a significant difference in both stability constant for the Cu(II) complex and redox

potential while the stability constant for the Cu(I) complex had very small changes, suggesting that **C** could distinguish Cu(I) ion from Cu(II) ion since it could form more stable complex with Cu(I) ion than that with Cu(II) ion and higher redox potential tended to favor Cu(I) ion. Moreover, opening chained **A** had smaller stability constant for the Cu(II) complex than closed ring **C**. The higher redox potential of **A** also favored the chelation of Cu(I) ion. Based on the above information, the sulfur-rich open ring woul provide the coordination environment to stabilize Cu(I) to form stable complex.

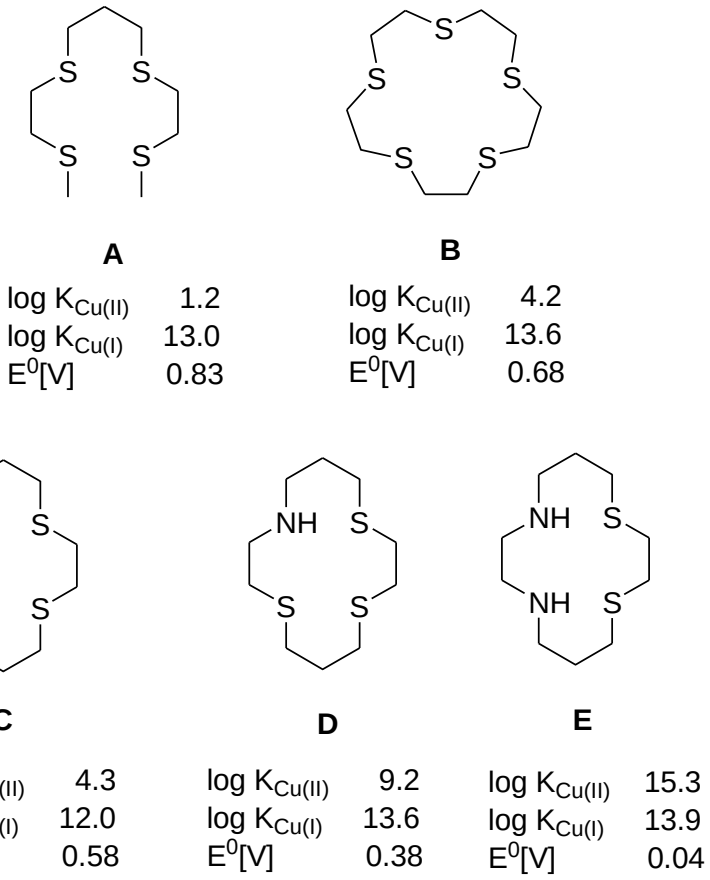

Figure 6.1 Summary of binding affinities and redox potentials of Cu(I) receptors. [34][35]

6.2 Design of probes

The structures of Cu(I) ion sensors of **EuL6**, **EuL7**, **EuL8**, **EuL9** and **EuL10** are shown in **Figure 6.2**. Generally, they consist of three main parts. The first is a thioether-rich receptor for chelation of Cu(I) ion. As discussed in Introduction, the sulphur-rich receptor has shown good selectivity towards Cu(I) ion. The second is an Eu chelator, which is macrocycle, and which provides a nine-coordination environment for Eu(II) ion and therefore there is no water molecule in the first inner coordination environment in theory. There is one ethoxyacetic acid as a side arm in the Eu chelator and the overall complex will be more hydrophilic and hence more water soluble. The third is the chromophore which is not conjugated with any receptor. Since Cu(I) is a transition metal and leads to quenching of the excited state through spin-orbital coupling, it is to electronically decouple the receptor from the chromophore itself.

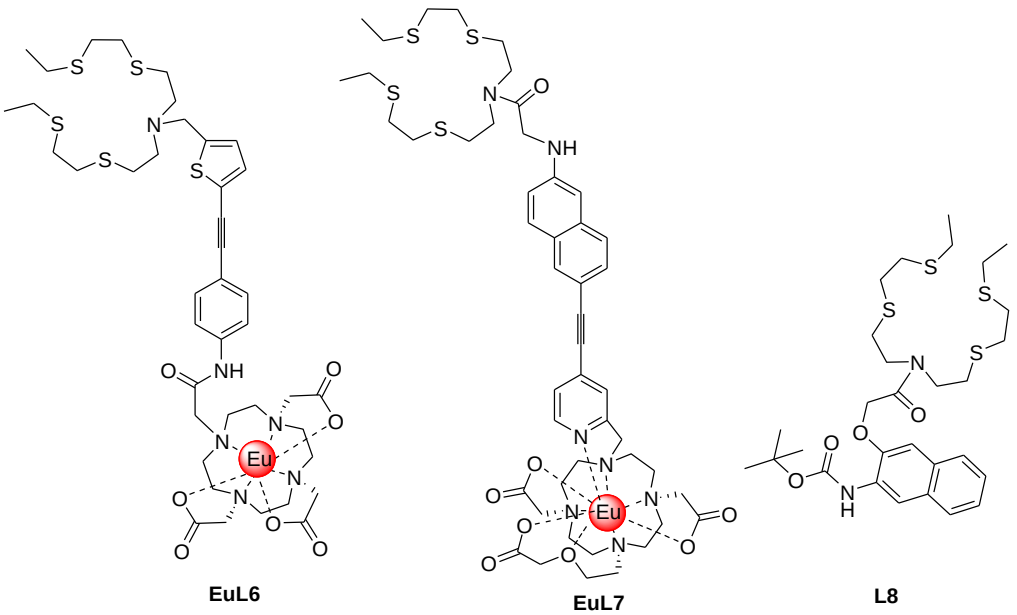

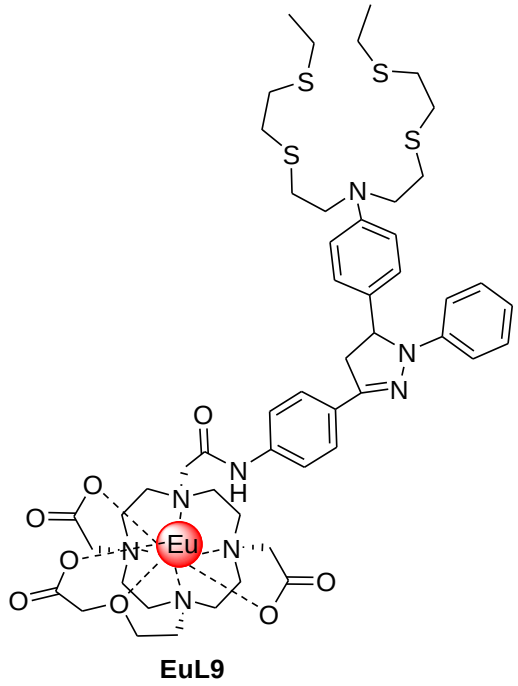

EuL9

Figure 6.2 Structures of **EuL6**, **EuL7**, **L8** and **EuL9**.

6.3 Results and discussion

6.3.1 Synthesis of probes

Synthesis of EuL6

The synthetic pathways of **EuL6** are comprised of eleven steps which are showed in the scheme below. The eleven steps synthesis can be divided into a few main parts: 1) the synthesis of a chromophore and a thiol receptor, 2) incorporation of **4G** into the thiol receptor, 3) incorporation of **DO3AT** and 4) basic deprotection and Eu(III) ion complexation.

Its synthesis started with the synthesis of the thiol receptor **6B**. 2-(ethylthio)ethanethiol reacted with thiourea under reflux, followed by basic hydrolysis with sodium hydroxide t afford **6A** (yield 64%). Other reactions had also been tried before, including reaction between ethane-1,2-dithiol and iodoethane, but the yield was not good. **6B** was prepared by reaction between **6A** and bis(2-chloroethyl)amine and the yield was 52%.

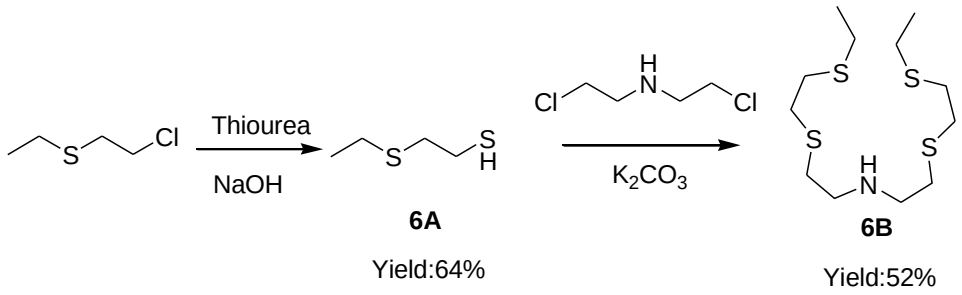

Scheme 6.1 Synthetic Routes to **6B**.

Bromination of thiophene-2-carbaldehyde led to **6C** with a yield of 87%. In this reaction, sodium biocarbonate was used since it was a mild base and aldehyde was stable. Then, **6C** had a reduction with sodium borohydride to form **6D** with a yield of 80%.

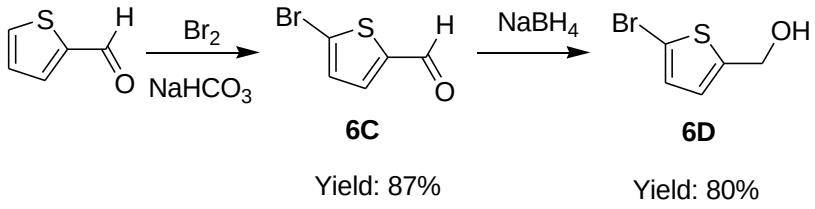

Scheme 6.2 Synthetic Routes to **6D**.

6E was prepared by Sonogashira coupling between ethynyltrimethylsilane and (4-bromopyridin-2-yl)methanol in the presence of a trace amount of catalysis $PdCl_2(PPh_3)_2$ to give the product in 53 % yield. **6E** had a mild appel reaction in which triphenylphosphine (PPh_3) and tetrabromomethanes (CBr_4) were reagents to convert with alcohols into the corresponding alkyl bromine. **6E** and PPh_3 were first mixed together and CBr_4 was added to the reaction mixture and stirred for three hours at room temperature. The yield was 58%. Then, **6F** had nucleophilic substitution with **6B** to have **6G** with a yield of 49%

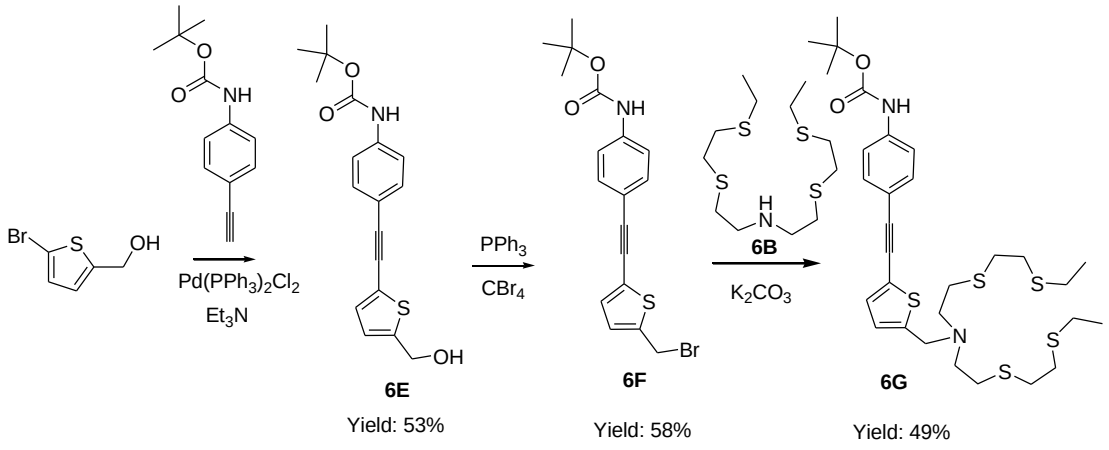

Scheme 6.3. Synthetic Route to **6G**.

6G had acidic deprotection with 0.1M hydrochloric acid to have **6H** with yield 46%. **6H** had reaction with chloroacetyl choride, followed by nucleophilic substitution with **DO3AT** to give **6J**. The yield was 30% Deprotection of tert-butylester was done by mixing with trifluoroacetic acid. Then, the pH of the solution was maintained at pH 7 and equimolar $EuCl_3.6H_2O$ was added into the aqueous reaction mixture. The reaction mixture was refluxed overnight and the desired products could be obtained by recrystallization in a mixture of ethanol and diethyl ether or chloroform. The high-resolution mass spectra (ESI+) showed peaks corresponding to the double charged Eu(III) complexes **EuL6** and 2 sodium ions with characteristic Eu(III) isotopic pattern entities which confirmed the formation of the desired Eu(III) complexes.(**Figure 6.3**).

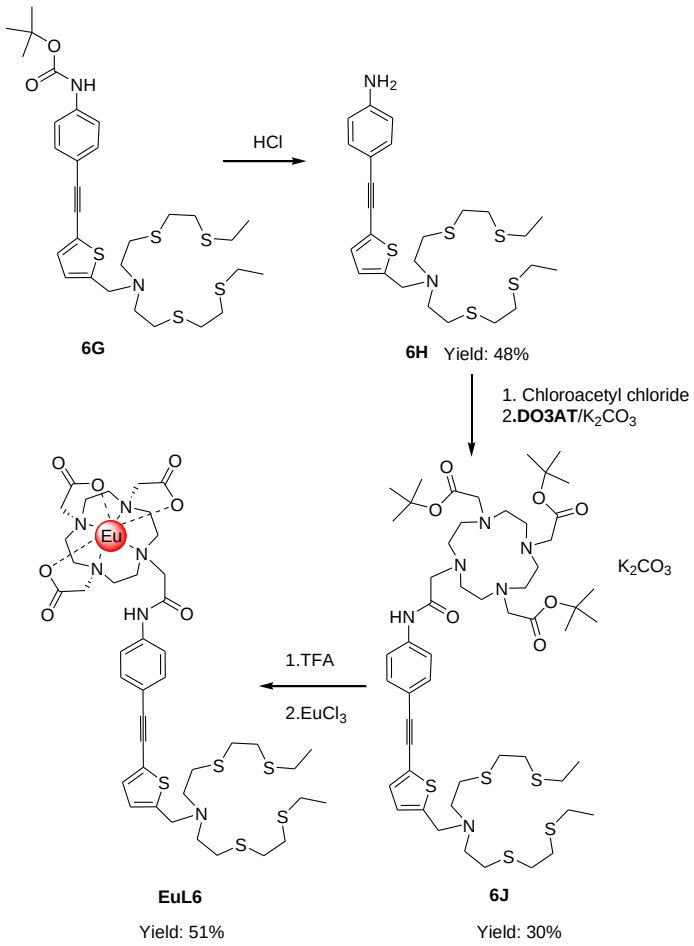

Scheme 6.4 Synthetic Route to **EuL6**.

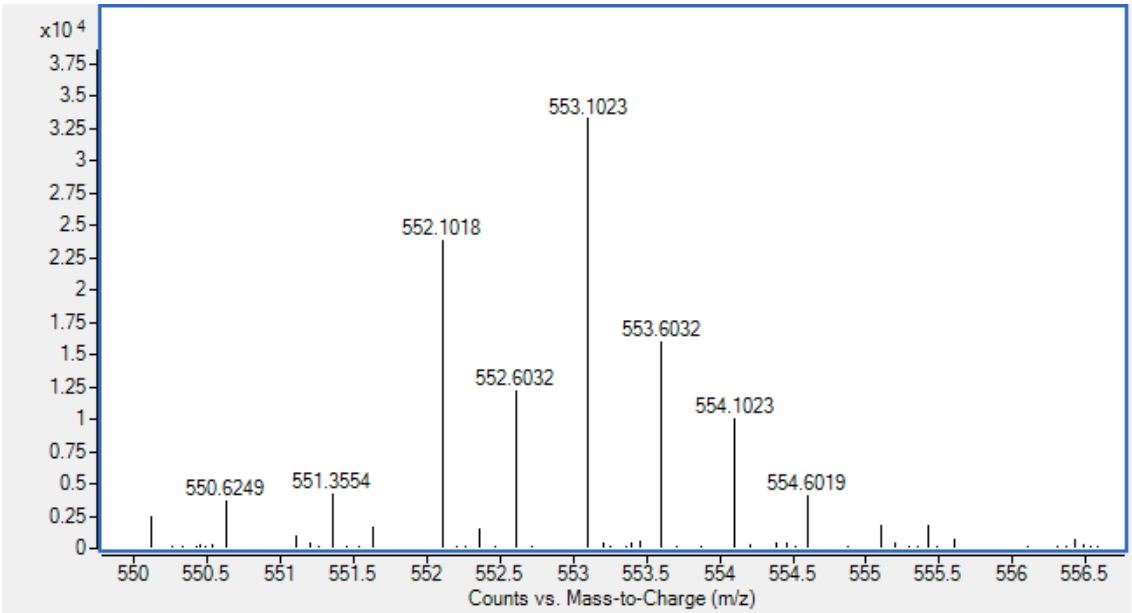

Figure 6.3 High resolution mass spectrum of **EuL6**.

Synthesis of EuL7

There were nine steps in the synthesis of **EuL7**. The first step was the reaction of

1.1 eqv of $(Boc)_2$ with 6-bromonaphthalen-2-amine to give protected **6K** in 53% yield. This protection would lower the polarity of **6K** for easy purification and prevent the reaction of amine in the following reaction. **6L** was prepared through the Sonogashira coupling between compound **6K** and ethynyltrimethylsilane in the presence of a catalytic amount of $PdCl_2(PPh_3)_2$ in 66% yield. Then, the TBAF was the deprotecting reagent for Si protection group and the reaction was stirred for three hours. Then, work up was solvent extraction with water to get rid of any excess TBAF and purified crude product through column chromatography to get the desired product with a yield of 46%.

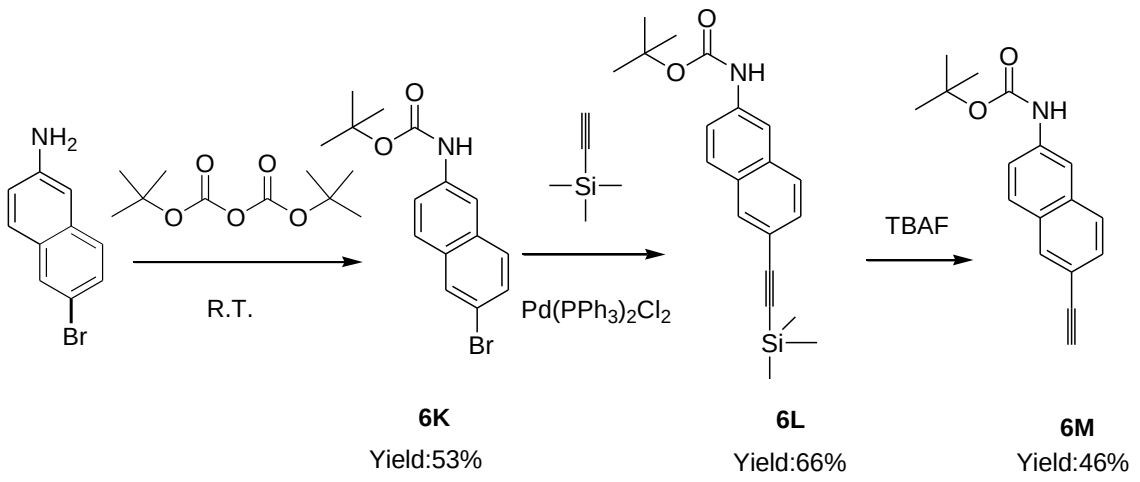

Scheme 6.5 Synthetic Route to **6M**.

6N was prepared through the Sonogashira coupling between **6M** and (4-bromopyridin-2-yl)methanol in the presence of a catalytic amount of $PdCl_2(PPh_3)_2$ under N_2. The solvents should be degassed and dried before use. During the reaction, a yellow solid was formed which was the salt of triethylamine. The crude product was purified through column chromatography. The yield was 46%. In the next step, few methods had been applied. Initially, PBr_3 or PBr_5 was used. However, a lower yield was obtained due to the higher reactivity of PBr_3 and hence more side products were formed. The other method made use of MsCl to convert alcohol group into more labile OMs and **6O** with a yield of 55% was afforded. **6O** was then reacted with **DO3A-ME** in the presence of potassium carbonate to have **6P** with a yield of 45%.

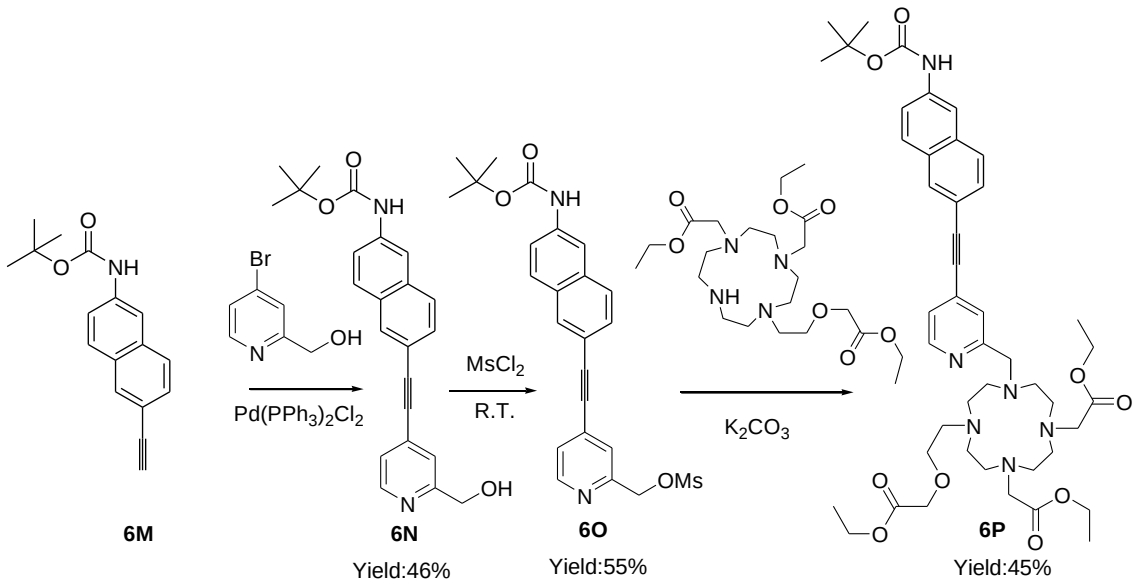

Scheme 6.5 Synthetic Route to **6P**.

6P had acidic deprotection in presence of trifluoroacetic acid (TFA) and CH_2Cl_2 (v/v=1:1) with the yield 80%. The reaction was stirred for three hours. Purification was done through recrystallization. Then, **6Q** was first reacted with chloroacetyl chloride in the presence of TEA. Without any further purification, it reacted with **6B** and gave final a yield of 54%. Deprotection of tris-ethylester was done by mixing with 0.1M NaOH. Then, the pH of the solution was maintained at pH 7 and the equimolar $EuCl_3.6H_2O$ was added into the aqueous reaction mixture. The reaction mixture was refluxed overnight and the desired product could be obtained by recrystallization it in a mixture of the MeOH and diethyl ether or chloroform. The high-resolution mass spectra (ESI+) showed peaks corresponding to the double protonated Eu(III) complexes **EuL7** with characteristic Eu(III) isotopic pattern entities, which confirmed the formation of the desired Eu(III) complexes.(**Figure 6.4**)

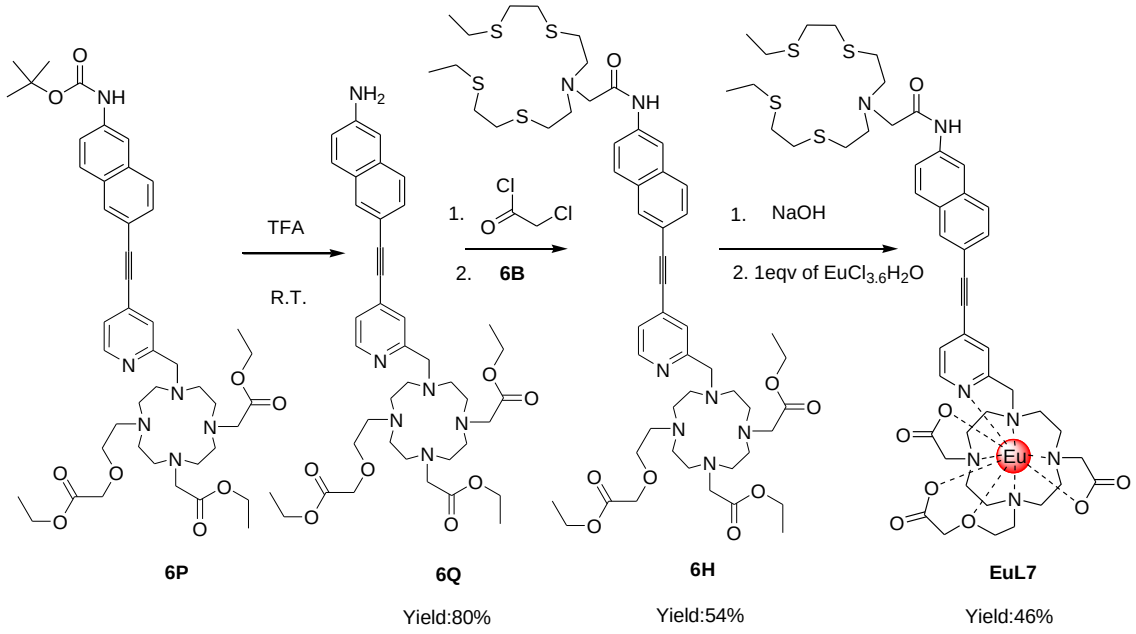

Scheme 6.6. Synthetic Route to **EuL7**.

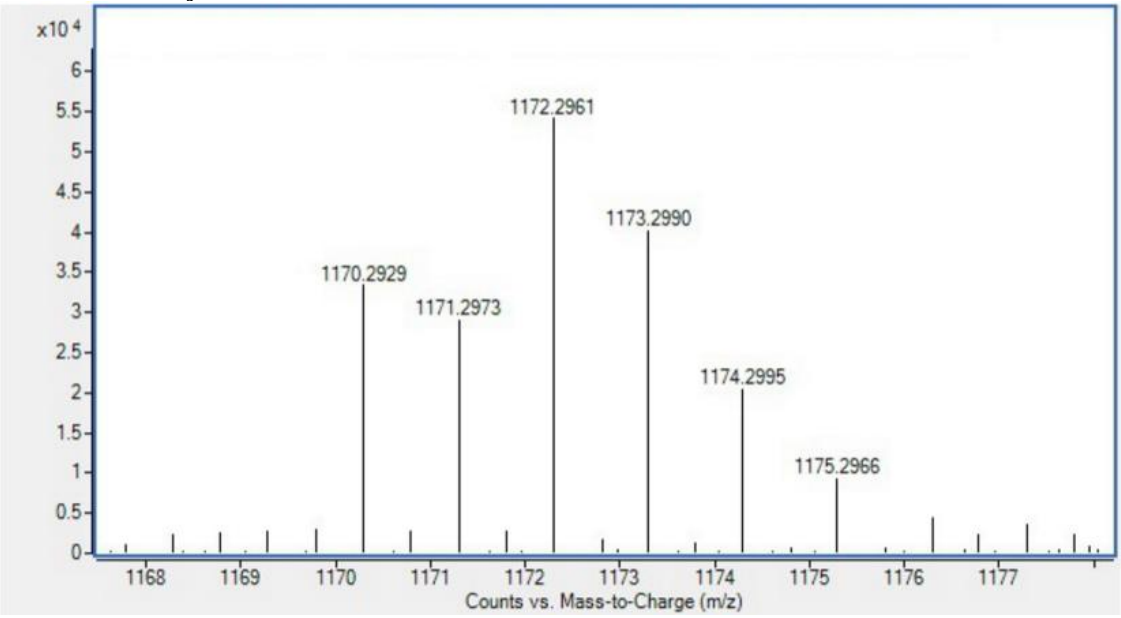

Figure 6.4. High resolution mass spectrum of **EuL7**.

Synthesis of L8

The synthesis of **L8** was started with reaction between 3-aminonaphthalen-2-ol and 1.1 eqv of $(Boc)_2$ to afford **6I** in 58% yield. **6B** reacted with chloroacetyl chloride and the resultant mixture was stirred at room temperature overnight. **6J** was isolated in a yield of 62%. Then, **6I** and **6J** were mixed with K_2CO_3 and NaI under reflux and **L8** was purified and isolated with a yield of 56%.

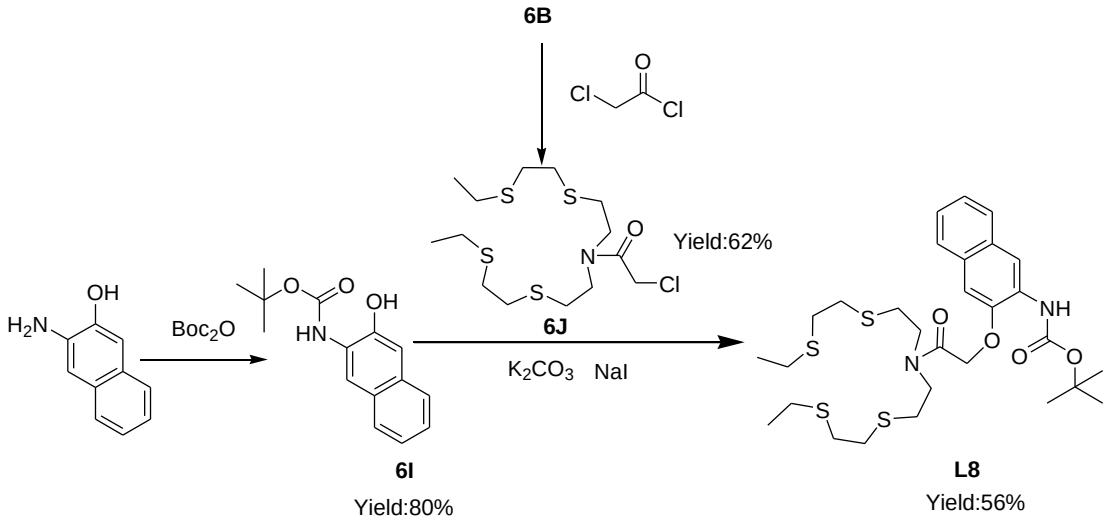

Scheme 6.7 Synthetic Route to **L8**.

Synthesis of EuL9

Vilsmeier-Haack reaction was used for the reaction between **1** and excess $POCl_3$ which was first mixed with dry dimethylformamide (DMF) to generate the reactive species N-(chloromethylene)-N-methylmethanaminium in which **6R** would be added dropwise to the reaction mixture and then stirred at 90 ^{0}C. After the reaction competed, the reaction mixture would be neutralized and filtered to give the yellow solid which was then recrystalized in absolute ethanol to afford white solid with yield 70%. **6R** had nucleophilic substitution reaction with excess 2-(ethylthio)ethanethiol and sodium ethoxide under reflux. The crude product was purified through column chromatography to have a yield of 46%.

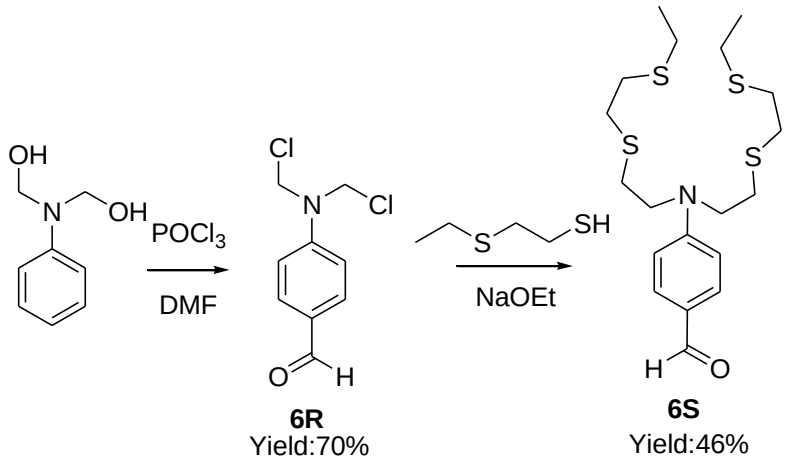

Scheme 6.8 Synthetic Route to **6S**.

1-(4-aminophenyl)ethanone was first protected by Boc group to afford **6T** in a yield of 71%. The next step involved aldol condensation between **6T** and **6S**. Aldol condensation usually involves the use of base or acid under reflux. Several acids or bases were used, including acetic acid, HCl and K_2CO_3. Finally, it was found NaOH can have better yield and the crude was purified through column chromatography with yield: 52%. Aldol condensation between **6U** and 1-phenylhydrazine was done in concentrated sulfuric acid in room temperature to make **6V** and the crude was purified through column chromatography in 49% yield.

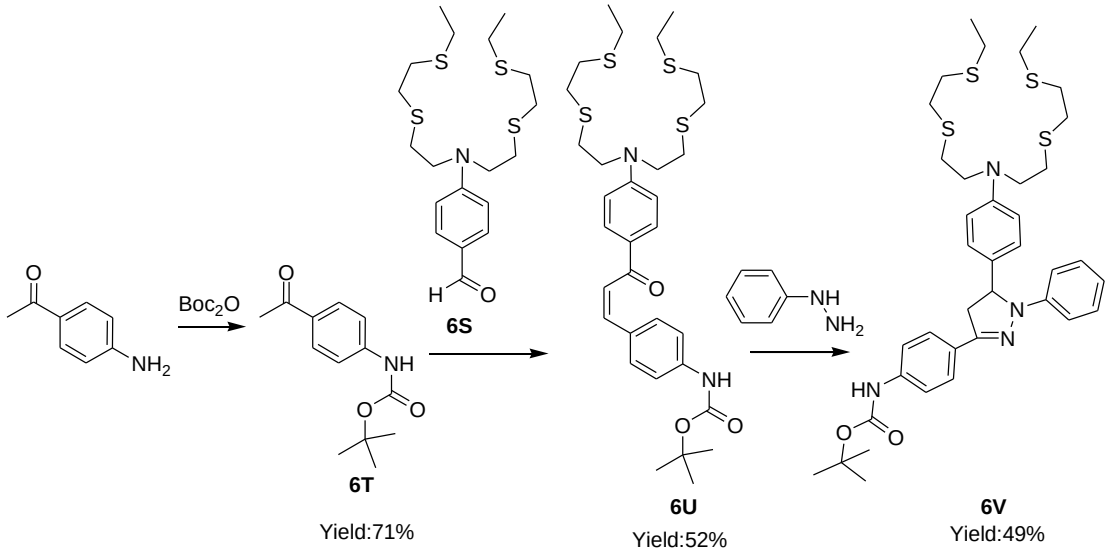

Scheme 6.9 Synthetic Route to **6V**.

6W was prepared in acidic deprotection in the presence of hydrochloric acid in a yield of 71%. The reaction was stirred for three hours. Purification was done through recrystallization. Then, **6X** was reacted with chloroacetyl chloride in the presence of TEA. Without any further purification, it reacted with **DO3A-ME** in a final yield of 39%. Deprotection of tris-ethylester was done by mixing with 0.1M NaOH. Then, the pH of the solution was maintained at pH 7 and the equimolar $EuCl_3.6H_2O$ was added into the aqueous reaction mixture. The reaction mixture was refluxed overnight and the desired product could be obtained by recrystallization in a mixture of the MeOH and diethyl ether or chloroform. The high-resolution mass spectra (ESI+) showed peaks

corresponding to the double protonated Eu(III) complexes **EuL9** with two sodium ions with characteristic Eu(III) isotopic pattern entities, which confirmed the formation of the desired Eu(III) complex.(**Figure 6.5**)

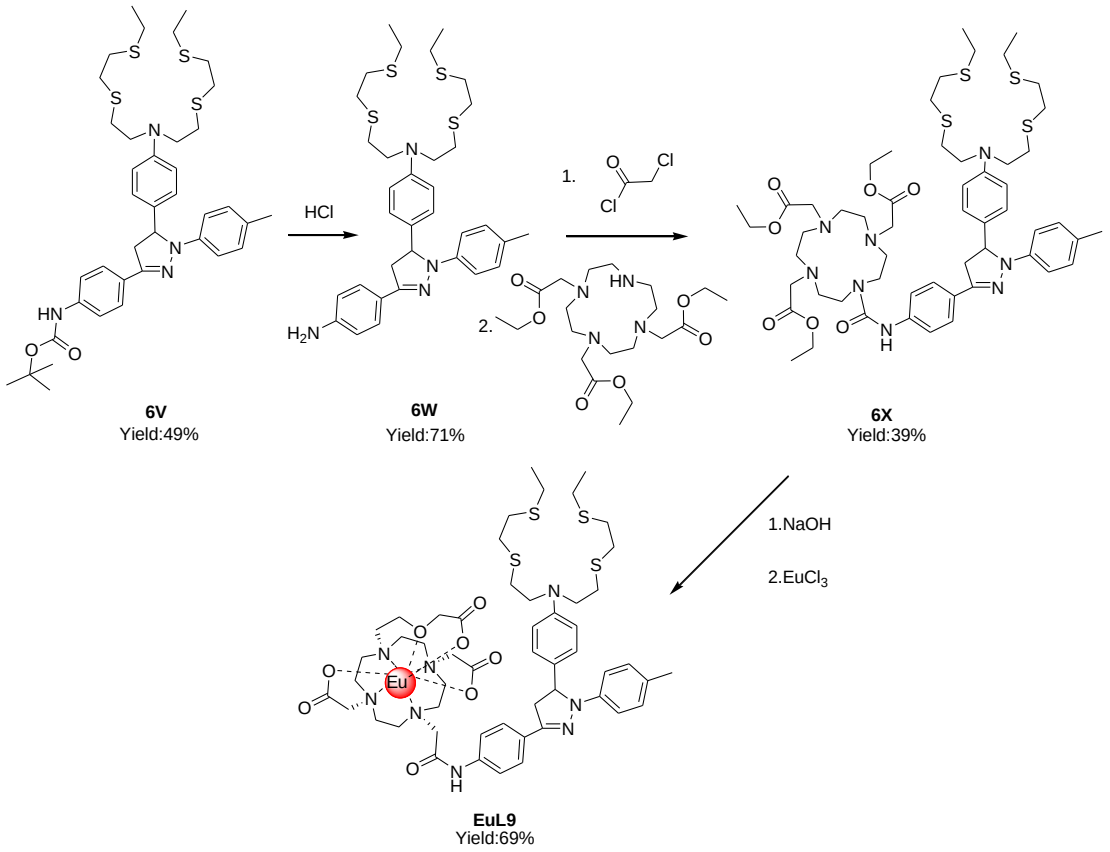

Scheme 6.9 Synthetic Route to **EuL9**.

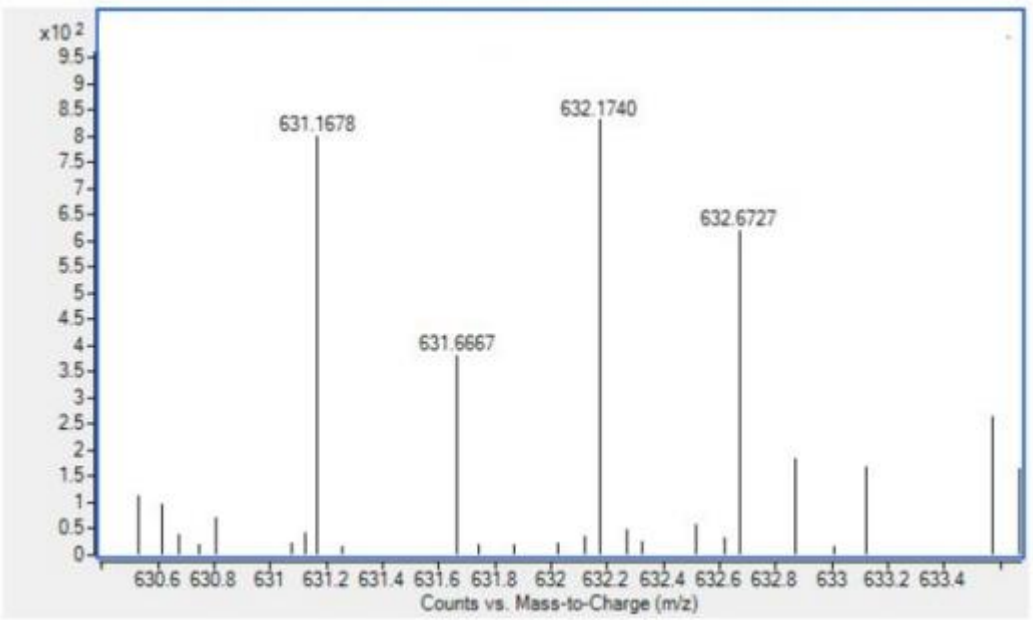

Figure 6.5 High resolution mass spectrum of **EuL9**.

6.3.2 Photophysical study

UV-vis, titration emission spectra, quantum yield and Job's plot of EuL6

The photophysical properties of **EuL6** were studied. Its absorption spectrum without Cu(I) was measured and its absorption peak was located at 321 nm, which was corresponded to π to π* a transition of the aromatic moieties. Its molar extinction coefficient was $19259M^{-1}$.

Upon excitation at 350nm and addition of Cu(I), **EuL6** (10 μM) showed slightly enhanced emission intensity of four narrow structured emission characteristic patterns of the $^5D_0 \rightarrow ^7F_J$ transitions characteristic of the Eu(III) ions with enhanced quantum yield from 0.86±0.03% to 1.2±0.04%. Hypersensitive splitting of transition $^5D_0 \rightarrow ^7F_2$ remained similar and the asymmetric ratios before and after addition of Cu(I) ion were similar (1.25 without Cu(I) ion) and (1.27 with Cu(I) ion), indicating that Cu(I) ion did not interrupt the environment of **EuL6** during titration. There was one sharp component located at 580.0 nm corresponding to the $^5D_0 \rightarrow ^7F_0$ transition of Eu (III) complexes, which was indicative of a single species in solution. Job's plot was showed in **Figure 6.8** and there was a peak at 0.5 of Cu(II) ion/Cu(II) ion and complex, suggesting that the optimal binding ratio between **EuL6** and Cu(I) was 1:1.

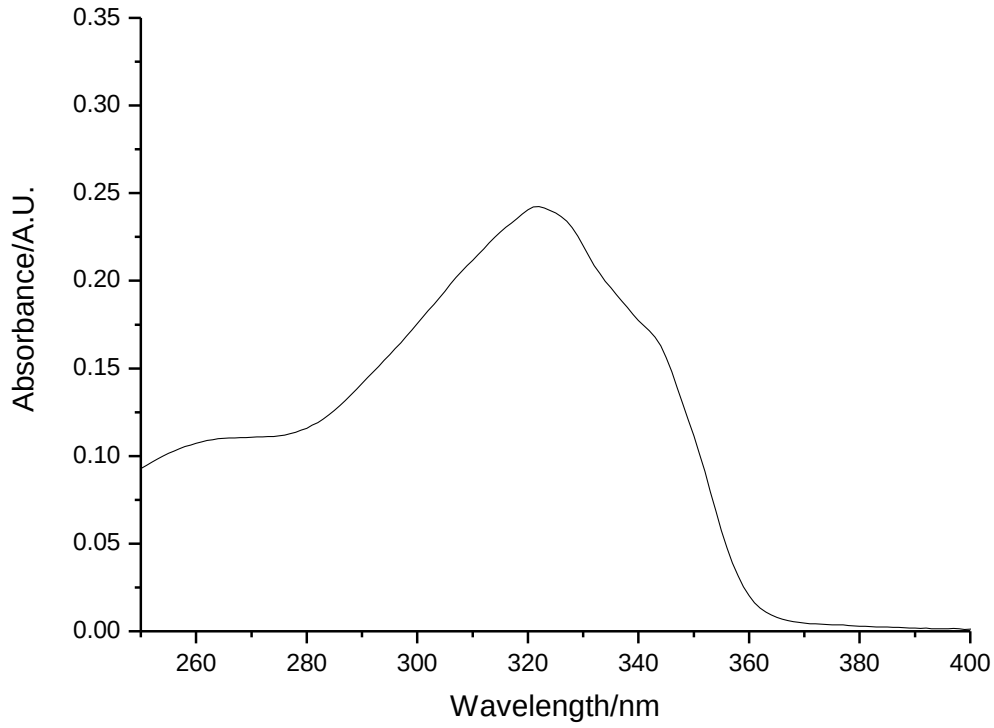

Figure 6.6 UV/Vis absorption spectrum of **EuL6** (0.01M HEPES, pH7.4)

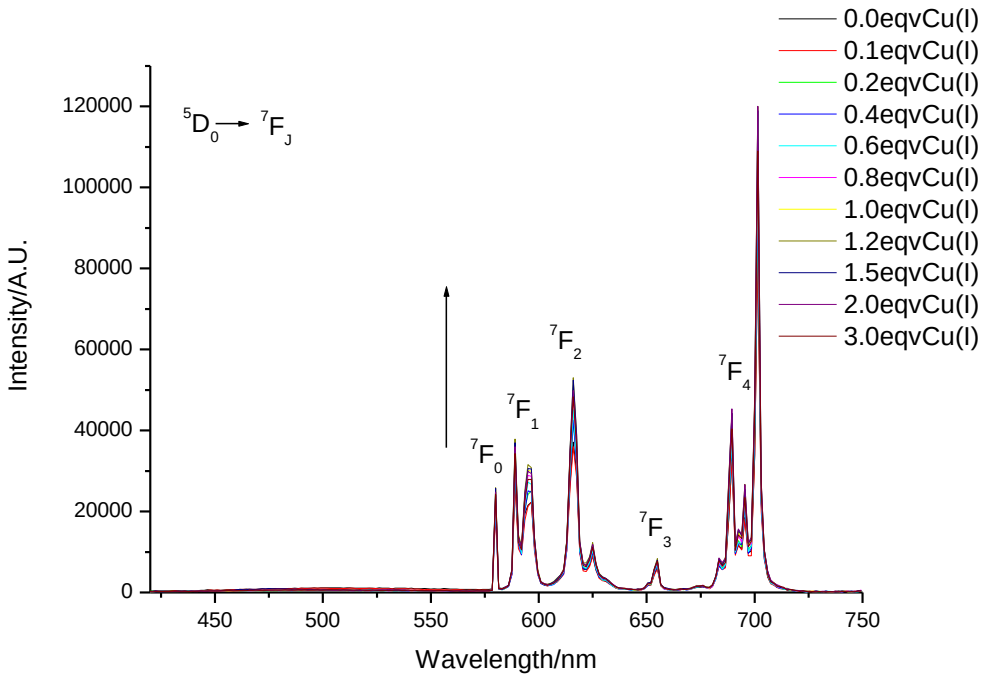

Figure 6.7 Emission spectrum of 10 µM aqueous solution upon addition of aliquots of various equiv of Cu(I) ions with respect to **EuL6** (0.01M HEPES, pH=7.4, λ_{ex}=350nm).

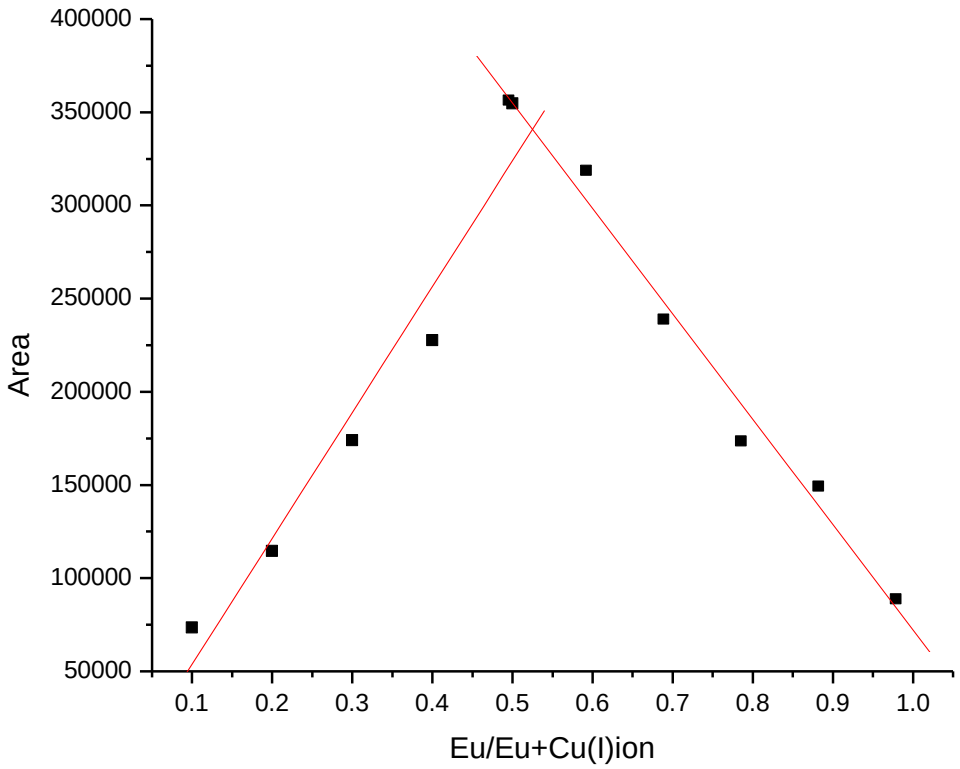

Figure 6.8 Job's plot of **EuL6**.

Lifetime and q value

The luminescent intensity could be influenced by the presence of O-H (such as water molecules) oscillators directly bound to the Eu(III) ion since O-H oscillators would provide the radiationless decay via energy transfer from electronic to vibrational levels. The measurement of the hydration states was done by the measuring the luminescence lifetimes in H_2O and D_2O upon emission at 616 nm.

The decay curve of **EuL6** was measured HEPES, water and D_2O, in the absence and presence of Cu(I). The lifetimes in HEPES and water without Cu(I) were similar (0.48ms and 0.44ms) and were shorter than lifetime in the presence of Cu(I) the lifetime time (0.516ms). The q value of the Eu(III) complex was one and it was unchanged after addition of one eqv of Cu(I) ion, which indicated the complex was stable.

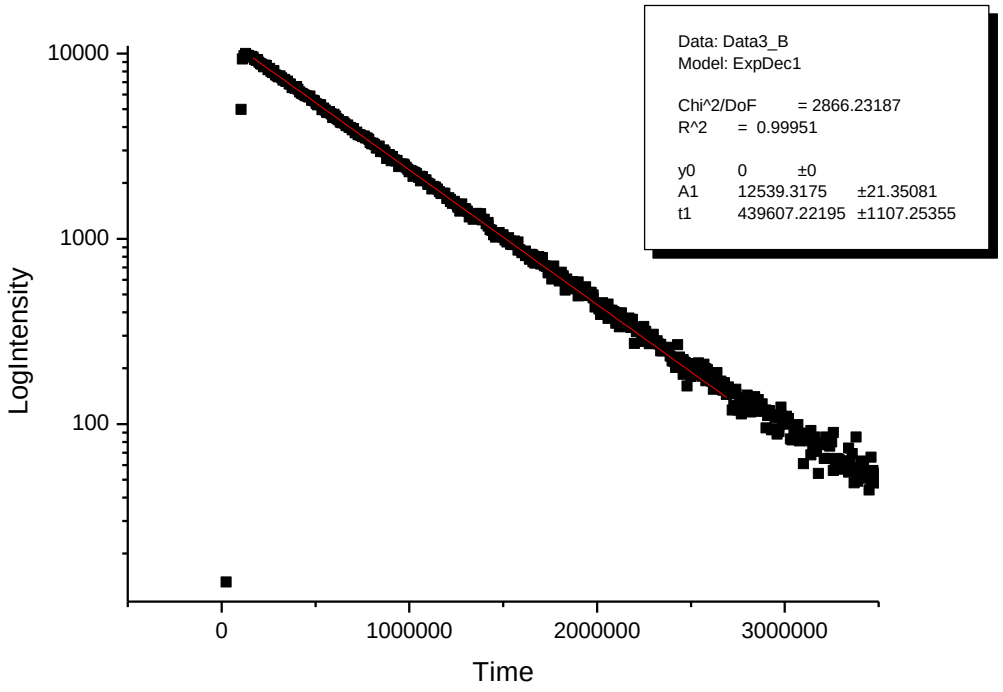

Figure 6.9 Decay curve of luminescence lifetime measurement of **EuL6** in H_2O.

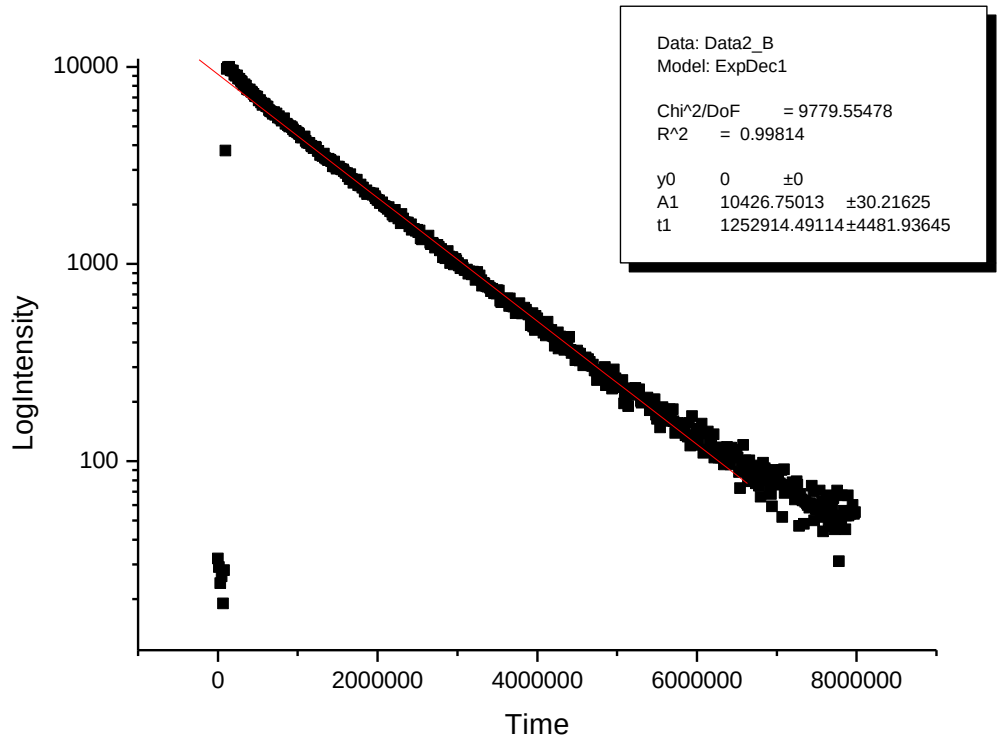

Figure 6.10 Decay curve of luminescence lifetime measurement of **EuL6** in D_2O.

Selectivity test of EuL6

The luminescent responses of **EuL6** towards various cations were investigated in 10 mM HEPES buffer (pH 7.4). Generally, luminescent responses were not influenced significantly upon addition of some common alkali and alkaline earth cations such as 0.1M K(I) ion, 0.1M Na(I) ion, 0.1mM Mg(II) ion, 0.1mM Ca(II) ion ion and 1 eqv of Ba(II) ion. Addition of some transition metals such as Mn(II) ion, Fe(II) ion, Zn(II), Cd(II) ion and Cu(II) ion displayed no significant changes in luminescence. However, when Cu(I) ion was added to the mixture solution of the complex and other cations, there was generally little luminescent enhancement.

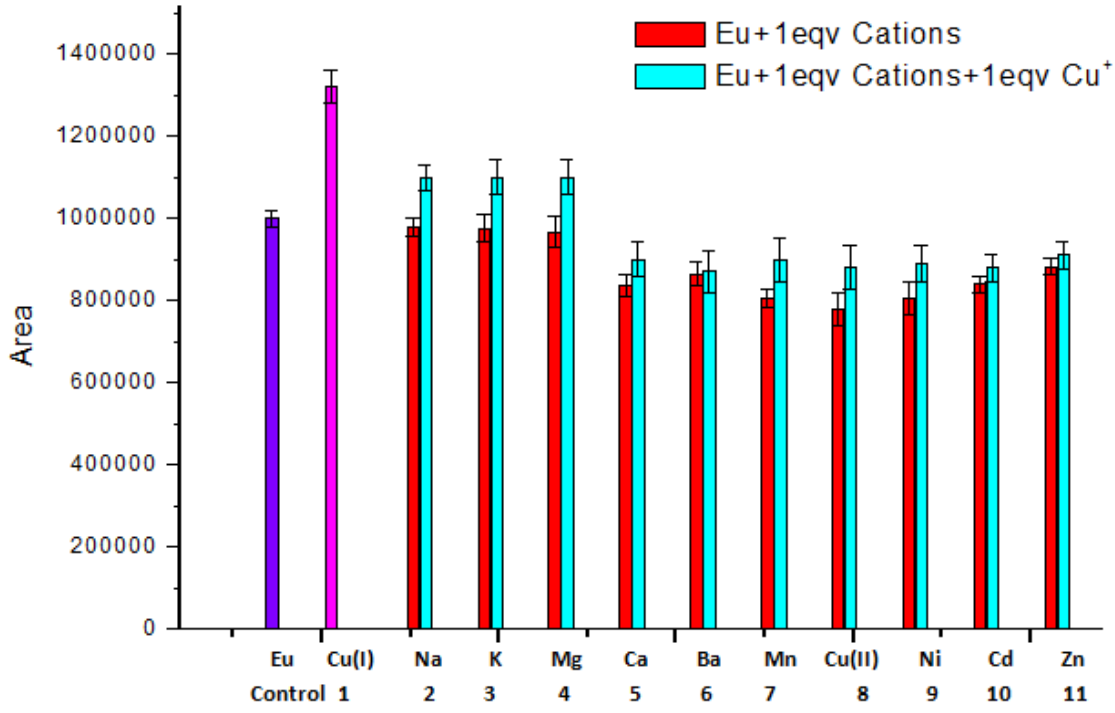

Figure 6.11 Changes in the luminescence intensity of [**EuL6**] (10 μM) in 10 mM HEPES with/without Cu(I) ion (excitation: 350 nm). Control 1: **EuL6 only**, 1: **EuL6**+1eqv Cu(I) ion only, 2: 1eqv Na(I) ion, 3: 1eqv M K(I) ion,4: 1eqv Ca(II) ion, 5: 1eqv Mg(II) ion, 6: 1eqv Ba(II) ion,7. 1eqv Mn(II) ion, 8. 1eqv Cu(II) ion, 9. 1eqv Ni(II) ion, 10. 1eqv Cd(II) ion, 11: 1eqv Zn (II) ion.

UV-vis and titration emission spectra of EuL7

The UV-vis spectrum of **EuL7** were shown in **Figure 6.12** and the maximum absorption band was centred at 338 nm, which corresponded to the π to π* transitions of the aromatic moieties. Upon excitation at 350 nm, **EuL7** displayed narrow structured emission patterns of the $^5D_0 \rightarrow ^7F_J$ (J=0-4) transitions that were characteristic of the Eu(III) ions, but there were no obvious changes upon addition of Cu(I) ion. (**Figure 6.13**)

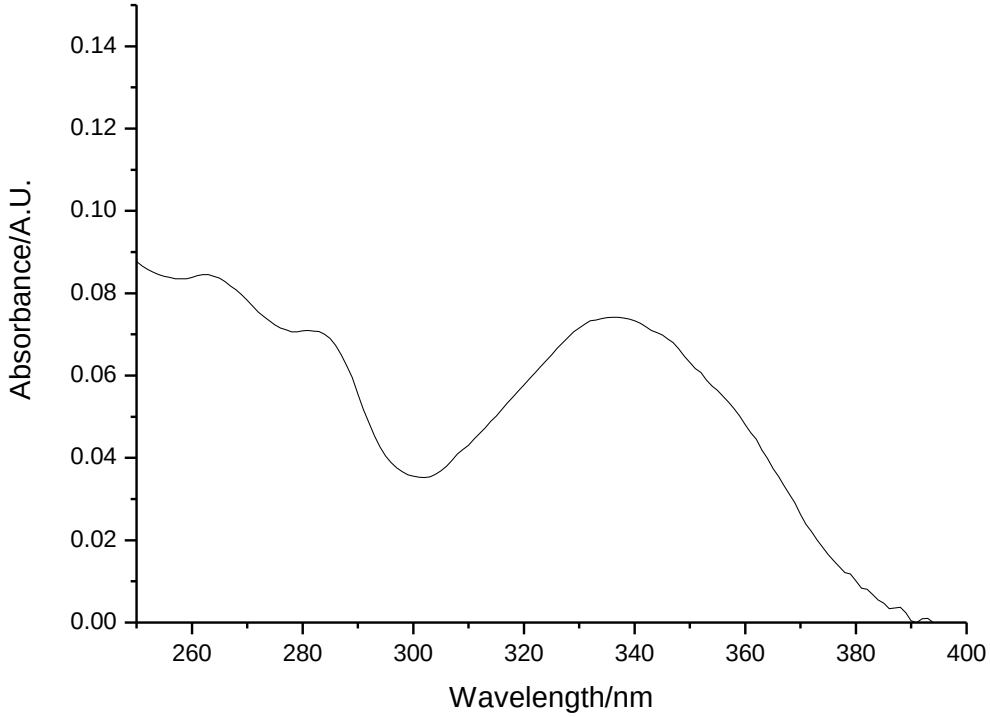

Figure 6.12 UV/Vis absorption spectrum of **EuL7** (0.01M HEPES, pH 7.4).

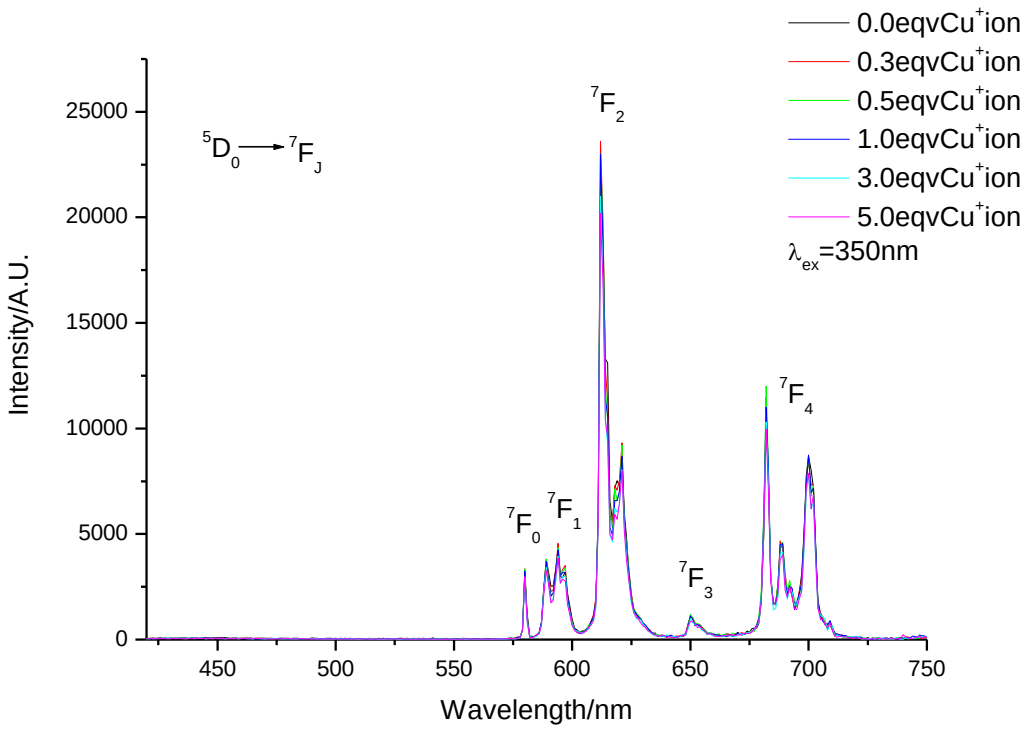

Figure 6.13 Emission spectra of 10 μM aqueous solution upon addition of aliquots of various equiv of Cu(I) ions with respect to **EuL7** (0.01M HEPES, pH=7.4, λ_{ex}=350nm).

Selectivity test of EuL7 towards Hg(II) ion

Since there were no significant responses towards Cu(I) ion, the selectivity test towards other cations was performed in 10 mM HEPES buffer (pH 7.4).(**Figure 6.14**) Generally, luminescent response was greatly influenced by addition of Hg(II) ion. **EuL7** did not respond to the addition of other common alkali and alkaline earth cations such as 0.1M K(I) ion, 0.1M Na(I) ion, 0.1mM Mg(II) ion, 0.1mM Ca(II) ion and 1 eqv of Ba(II) ion and transition metals such as Mn(II) ion, Fe(II) ion, Zn(II), Cd(II) ion, Co(II)ion, Ni(II) ion, Cu(I) ion and Cu(II) ion. Nevertheless, when Hg(II) ion was added to the solution mixture of the complex and other cations, there was generally luminescent enhancement to a certain extent that was comparable to the case of complex and Hg(II) ion, which indicated that **EuL7** selectively responded to Hg(II) ion in the presence of other cations.

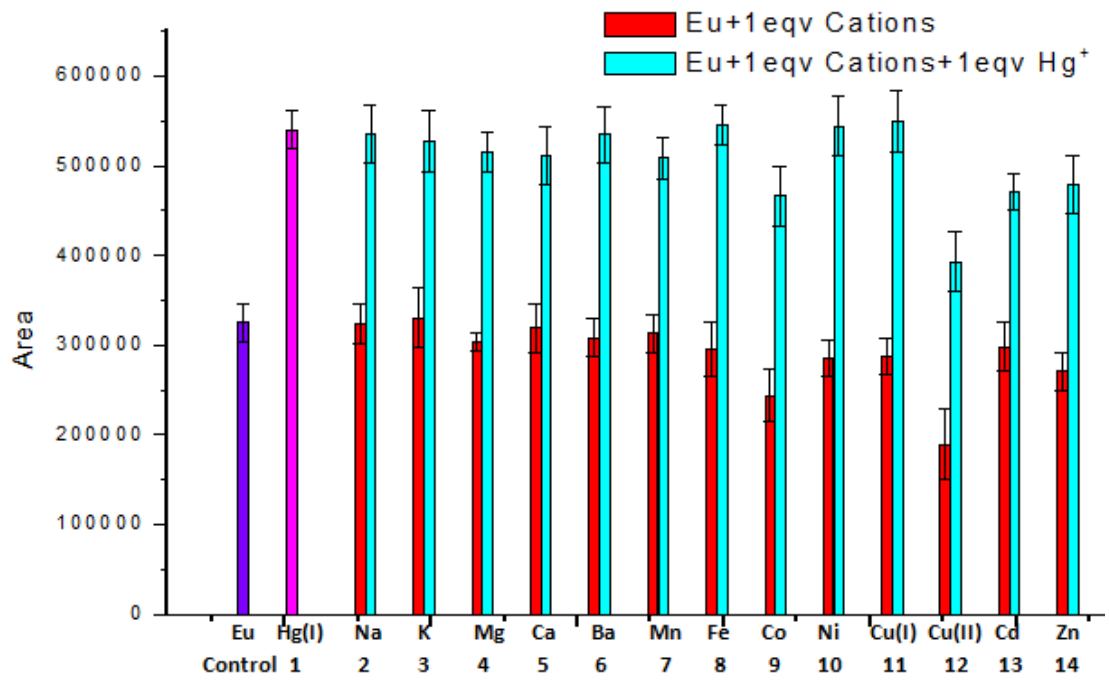

Figure 6.14 Changes in luminescence intensity of [**EuL7**] (10 µM) in 10 mM HEPES with/without Hg(II) ion (excitation: 350 nm). Control 1: **EuL7 only**, 1: **EuL7**+1eqv Hg(II)ion only, 2: 0.1M Na(I) ion, 3: 0.1M K(I) ion, 4: 0.1mM Ca(II) ion, 5: 0.1mM Mg(II) ion,6: 1eqv Ba(II) ion,7. 1eqv Mn(II) ion, 8. 1eqv Fe(II) ion, 9. 1eqv Co(II) ion, 10. 1eqv Ni(II) ion, 11: 1eqv Cu(I) ion, 12: 1eqv Cu(II) ion, 13: 1eqv Cd(II) ion, 14: 1eqv Zn(II) ion, 15 (red bar): (Cyan bar): mixture of cations from 2 to 14 +1eqv Hg(II)ion

Quantum yield of EuL7, lifetime and q value with Hg(II) ion

Upon excitation at 350 nm and on the addition of Hg(II) ion (0-2 eqv Hg (II) ion), there was an luminescent enhancement of narrow structured emission patterns of $^5D_0 \rightarrow ^7F_J$ (J=0-4) transitions characteristic of Eu(III) ions. (**Figure 6.15**) The quantum yields before and after addition of Hg(II) ion were 4.08±0.03% and 8.82±0.02% respectively. During the titration with Hg(II) ion, there was one sharp component centred at 580 nm, which corresponded to the $^5D_0 \rightarrow ^7F_0$ transition of Eu(III) complexes. Asymmetric ratios before and after addition of Hg(II) ion were similar (3.72 without Hg(II) ion and 3.77 with Hg(II) ion), indicating there was only one single species and **EuL7** was in solution. The binding stoichiometry was determined by Job's plot. In

Figure 6.16, the maximum point was located at 0.5 of Hg(II) ion/mixture of Hg(II) ion and **EuL7**, suggesting that the optimal binding ratio between Eu(III) complexes and Hg(II) ion was 1:1.

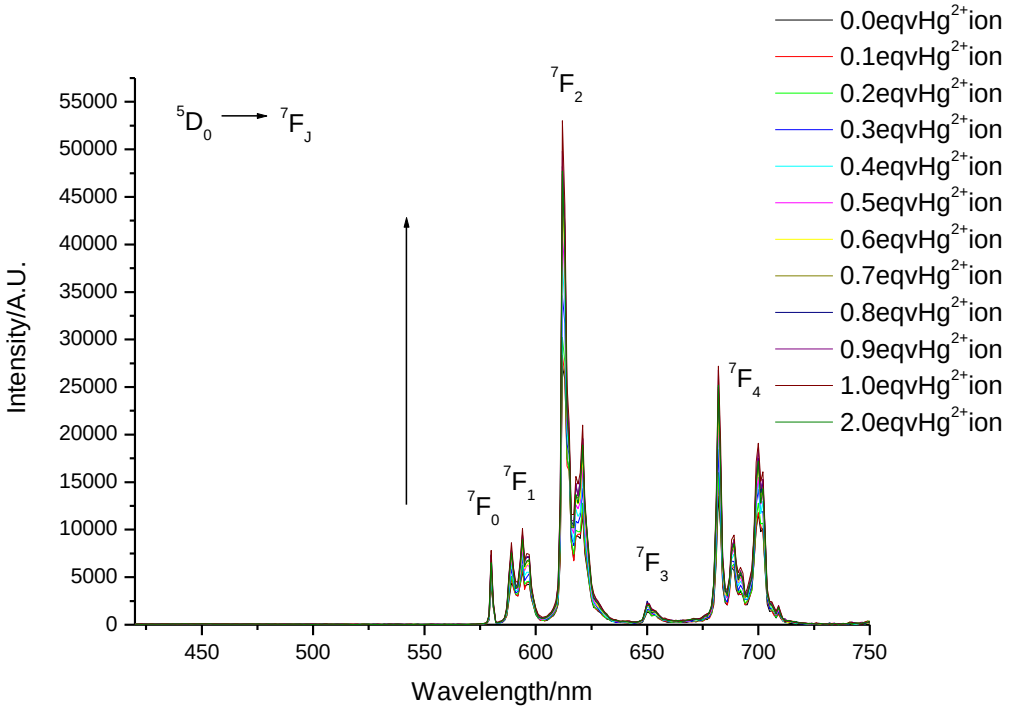

Figure 6.15 Emission spectrum of 10 μM aqueous solution upon addition of aliquots of various equiv of Hg(II) ions with respect to **EuL7** (0.01M HEPES, pH=7.4, λ_{ex}=350nm).

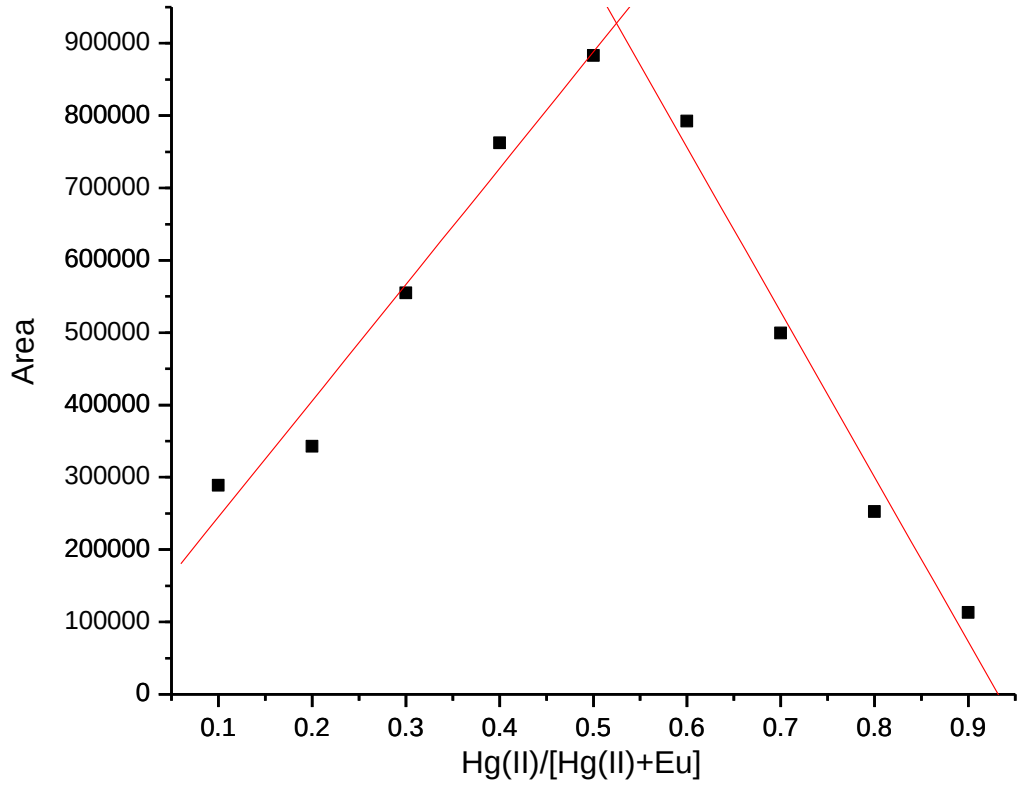

Figure 6.16 Job's plot of **EuL7** and Hg(II) ion.

Liftetime and q value

The hydration states were analyzed by the measurement of luminescence lifetimes in H_2O and D_2O upon emission at 616 nm. Their lifetime without Hg(II) ion in H_2O (0.55ms) was longer than that in D_2O (0.71ms). (**Figures 6.17** & **6.18**) The lifetimes measured in HEPES were similar to the lifetimes in H_2O. Based on their lifetimes in D_2O and H_2O, the hydration state was calculated as zero in the presence and absence of Hg(II) ion, indicating that there was no bound water molecule coordinating directly with Eu (III) ion and that **EuL7** was stable during the Hg(II) ion titrations with no solvent or cation exchange.

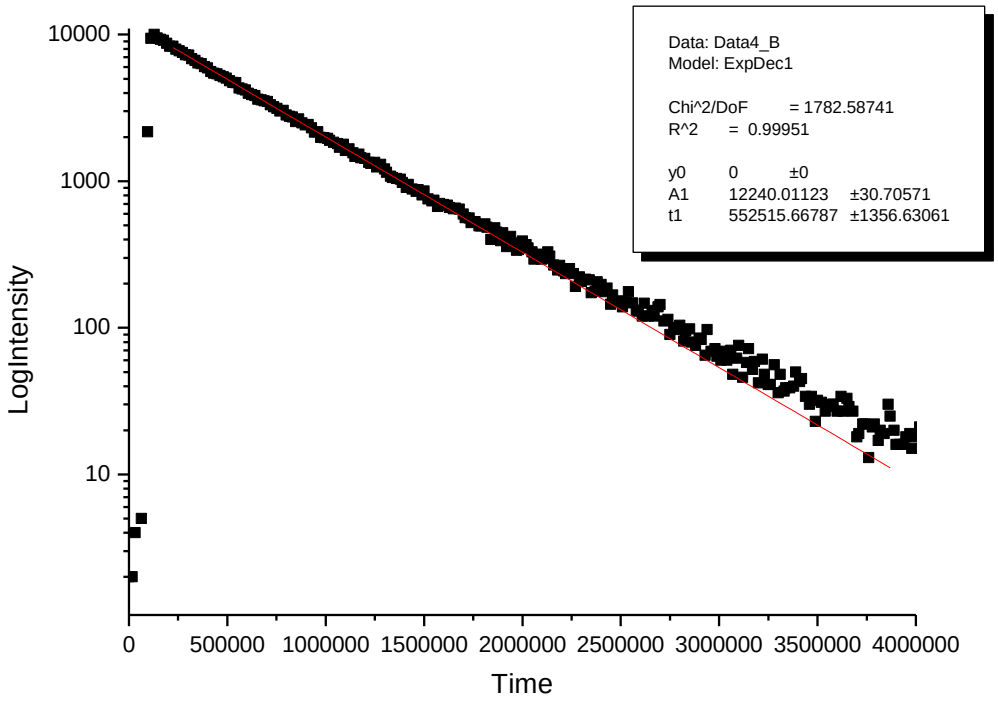

Figure 6.17 Decay curve of luminescence lifetime measurement of **EuL7** in H_2O.

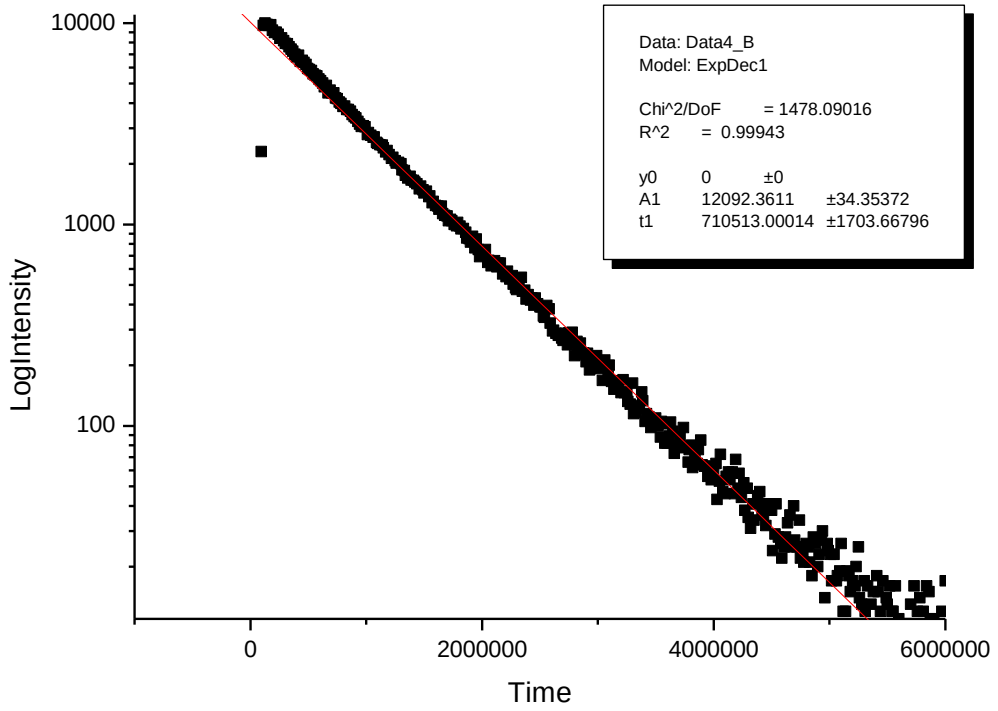

Figure 6.18 Decay curve of luminescence lifetime measurement of **EuL7** in D_2O.

Binding Constants towards Hg(II) ion

The binding constant for Hg(II) ion was calculated as 50800±5223M^{-1}.

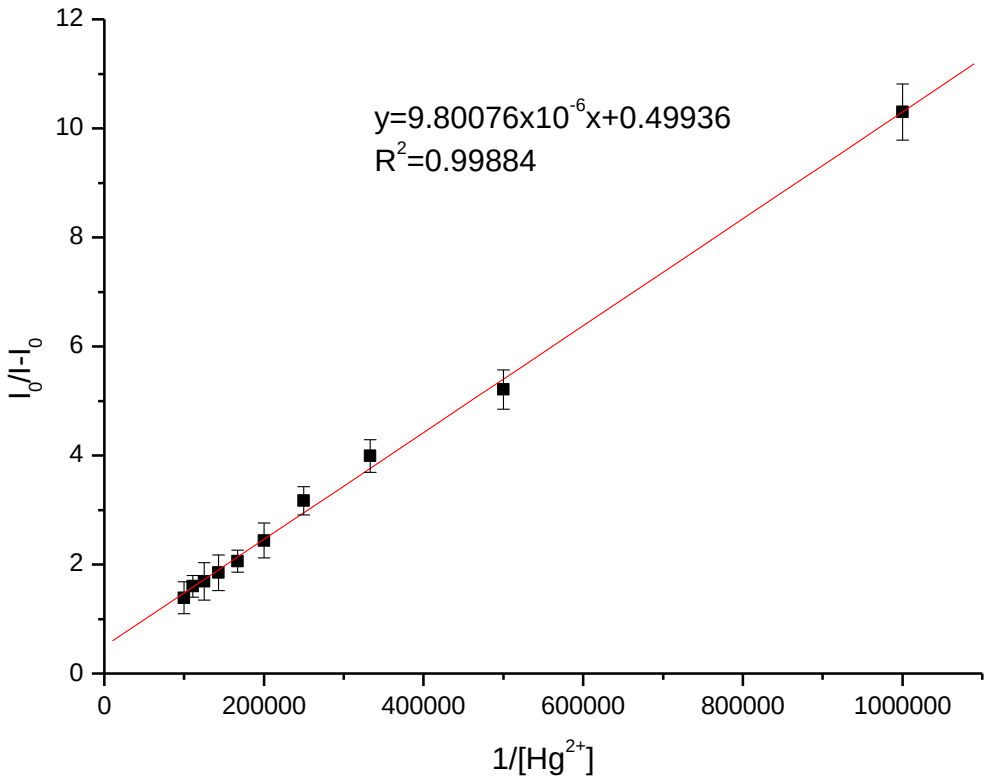

Figure 6.19 Fitting of luminescent intensity of Hg(II) ion titration curve of **EuL7**.

Selectivity test of L8 towards cations

L8 was an intermediate for testing the selectivity towards Cu(I) ion. If **L8** showed a good selectivity towards Cu(I) ion, its synthesis would continue to make its corresponding Eu(III) complex. Therefore, its selectivity test was first done in 10 mM mixture of ACN:0.01M HEPES. Based on the results of the selectivity test, **L8** did not have any responses towards Cu(I) ion or other cations.Therefore, **L8** was failed to be a Cu(I) sensor.

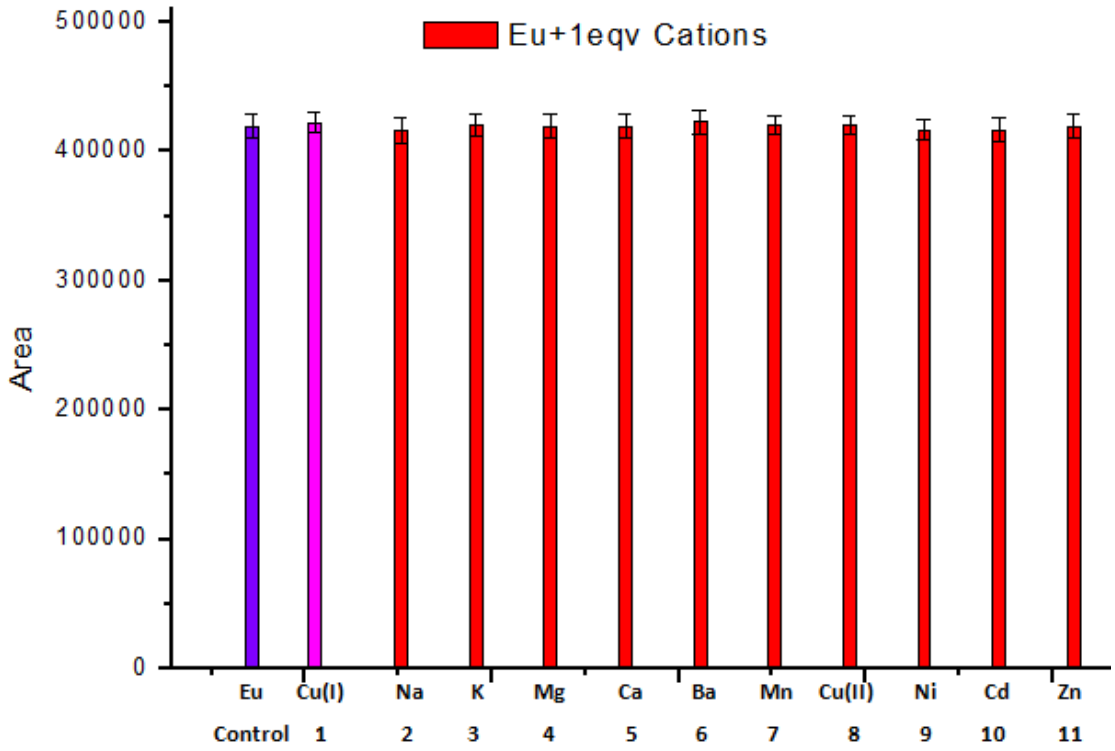

Figure 6.20 Changes in luminescence intensity of [**L8**] (10 μM) in the mixture of ACN:0.01M HEPES with/without Cu(I) ion (excitation: 350 nm). Control 1: **EuL8 only**, 1: **EuL8**+1eqv Cu(I) ion only, 2: 1eqv Na(I) ion , 3: 1eqv K(I) ion,4: 1eqv Ca(II) ion, 5: 1eqv Mg(II) ion,6: 1eqv Ba(II) ion,7. 1eqv Mn(II) ion, 8. 1eqv Cu(II) ion, 9. 1eqv Ni(II) ion, 10. 1eqv Cd(II) ion, 11: 1eqv Zn(II) ion.

Selectivity test of 6V intermediate towards cations

6V is the intermediate of **EuL9** and could be used to examine in selectivity towards Cu(I) ion. If it demonstrated good selectivity towards Cu(I) ion, its synthesis of Eu(III) complex would continue. Its luminescent response towards various Cu(I) ion was first measured in mixture of ACN:0.01M HEPES. As shown in **Figure 6.21**, **6V** did not respond towards common alkali and alkaline earth cations such as 0.1M K(I) ion, 0.1M Na(I) ion, 0.1mM Mg(II) ion, 0.1mM Ca(II) ion ion and 1 eqv of Ba(II) ion and transition metals such as Mn(II) ion, Fe(II) ion, Zn(II), Cd(II) ion, Co(II)ion, Ni(II) ion, Cu(I) ion and Cu(II) ion. When Cu(I) ion was added towards the solution mixture of the complex and other cations, there was generally slight luminescent enhancement.

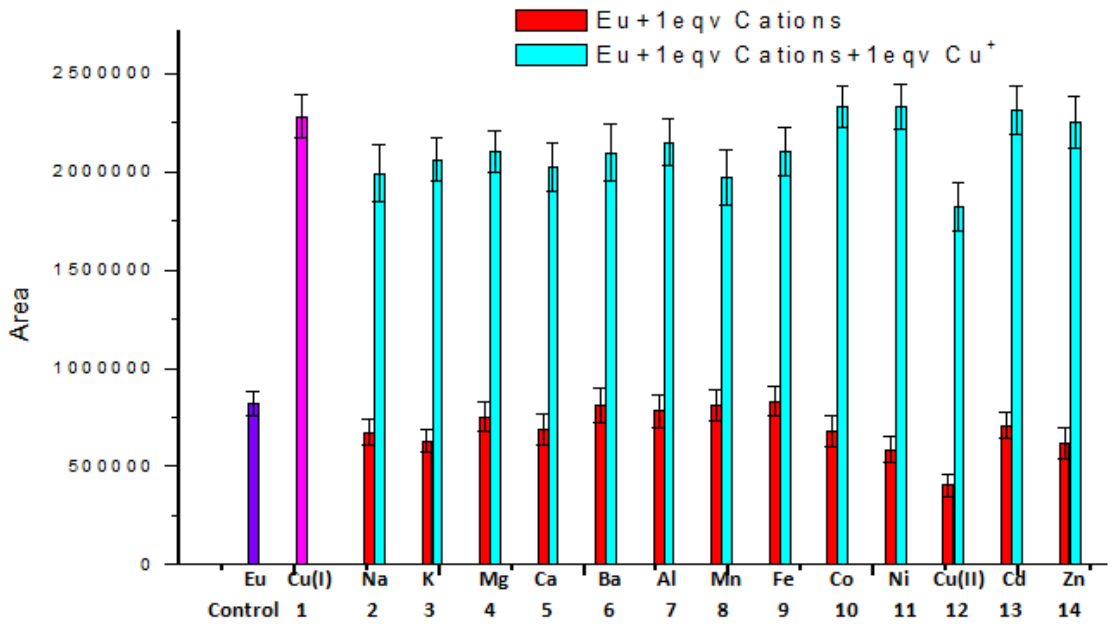

Figure 6.21 Changes in luminescence intensity of [**6V**] (10 μM) in a mixture of ACN:0.01M HEPES with/without Cu(I) ion (excitation: 350 nm). Control 1: **6V only**, 1: **6V** +1eqv Cu(I) ion only, 2: 0.1M Na(I) ion, 3: 0.1M K(I) ion,4: 0.1mM Mg(II) ion, 5: 0.1mM Ca(II) ion,6: 1eqv Ba(II) ion, 7: 1eqv Al(III) ion, 8. 1eqv Mn(II) ion, 9. 1eqv Fe(II) ion, 10. 1eqv Co(II) ion, 11. 1eqv Ni(II) ion, 12: 1eqv Cu(II) ion, 13: 1eqv Cd(II) ion, 14: 1eqv CZ (II) ion. (Cyan bar): mixture of cations from 2 to 14 +1eqv Hg(II)ion

UV-vis and titration emission of EuL9

The UV-vis and emission spectra were measured and shown in **Figure 6.22**. The absorption peak was located at 380nm, which corresponded to the π to π* transitions associated to the aromatic chromophore moieties. However, there was only ligand emission peak but no characteristic peaks of Eu (III) ion. On the titration of Cu(I) ion, the emission spectrum was similar to that without Cu(I) ion. This result might not match with the result of the selectivity test of **6V**. Chromophore, which was not suitable for sensitization of Eu(III) ion, might be reason to have only ligand fluorescence. Other cations had been titration with **EuL9**, but similar results were found.

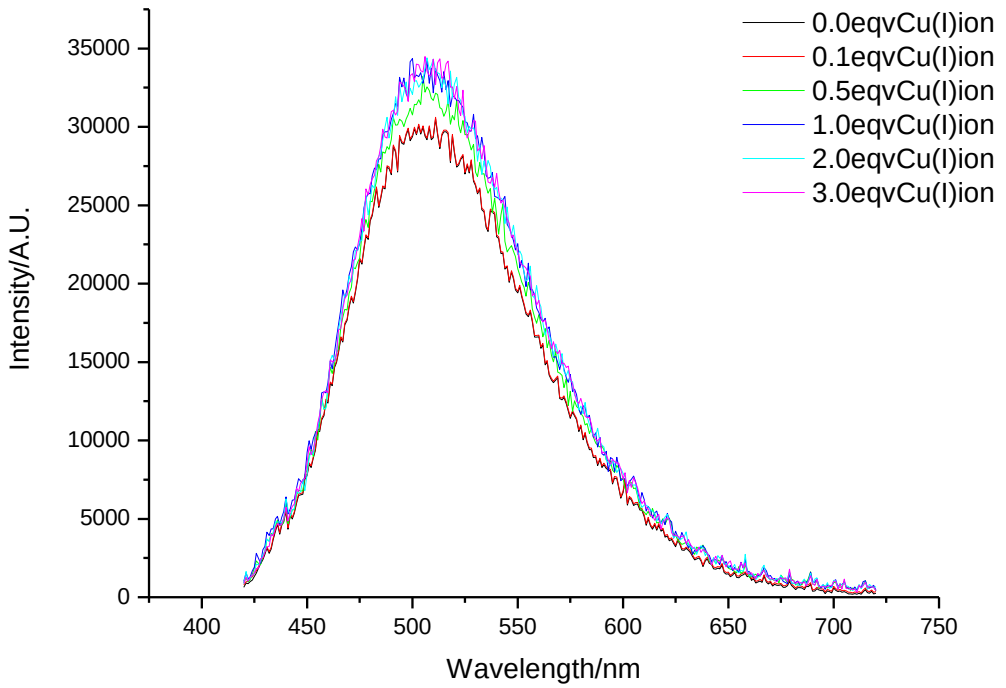

Figure 6.22 Emission spectra of 10 μM aqueous solution upon addition of aliquots of various equiv of Cu(I) ion with respect to **EuL9** (HEPES, pH=7.4, λ_{ex}=350nm)

6.4 Conclusion

Three Eu(III) complexes, **EuL6**, **EuL7** and **EuL9**, as well as **L8** intermediate were successfully synthesized and they demonstrated differences in their selectivity towards Cu(I) ion. **EuL6** showed a turn-on response when treated with Cu(I) ion, but its poor turn on ratio made it unsuitable to be a Cu(I) ion sensor. **EuL7** only responded to Hg(II) ion and its quantum yields before and after addition of Hg(II) ion were 4.08±0.03%and 8.82±0.02% respectively and its binding constants towards Hg(II) ion was calculated as 50800±5223M^{-1}. **L8** did not respond to Cu(I) ion or other common cations and therefore its synthesis was stopped. The intermediate **6V** of **EuL9** showed a good selectivity towards Cu(I) ion, but **EuL9** was nonemissive and did not respond to Cu(I) ion due to poor sensitization of Eu(III) ion, resulting in ligand fluorescence.

6.5 Future work

The copper sensors developed in this chapter require some improvement. **EuL9** is nonemissive, but its intermediate demonstrated good selectivity to Cu(I) ion. Therefore the structural modification will still focus on the pyrazolines conjugated with thiol receptor. Generally, the electronic transition within pyrazolines is an intramolecular charge transfer from the aromatic ring attached to N1 to the N2-C3-aryl π-system. The transition energy is strongly affected by the nature of the groups in the 1- and 3-position of the pyrazoline ring. Therefore, the UV absorption maximum peak will be blue shifted if electron withdrawing ability of R_1 increases. Therefore, some structures of Cu(I) ion sensor are proposed below.

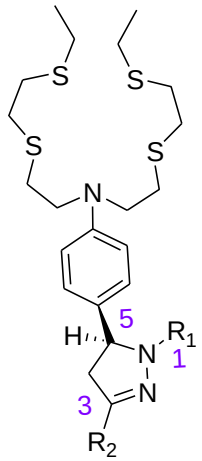

Figure 6.23 Structure of pyrazolines conjugated with thiol receptor.

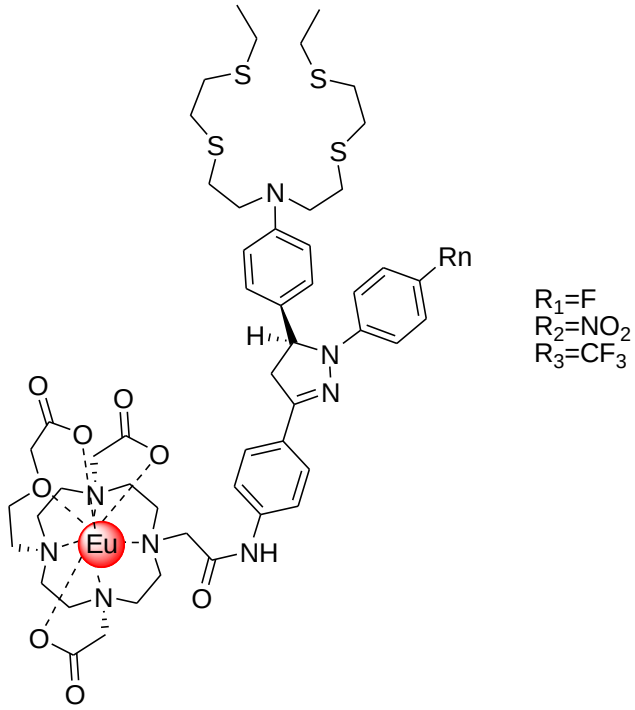

Figure 6.24 Proposed structure of Cu(I) ion sensor.

References

[1] E. L. Que, D. W. Domaille and C. J. Chang, *Chem. Rev.*, 2008, **108**, 1517–1549.

[2] E. Gaggelli, H. Kozlowski, D. Valensin, and G. Valensin, *Chem. Rev*., 2006, **106**, 1995–2044.

[3] A. Hordyjewska and Ł. Popiołek, J. Kocot, *Biometals*., 2014, **27**, 611–621.

[4] M. L. Schlief and J. D. Gitlin, *Mol. Neurobiol*., 2006, 33, 81-90.

[5] A. Dancis, D. S. Yuan, D. Haile, C. Askwith, D. Eide, C. Moehle, J. Kaplan and R. D.Klausner, *Cell*., 1994, **76**, 193-410.

[6] A. Dancis, D. Haile, D. S. Yuan and R. D. Klausner, *J. Biol. Chem*., 1994, **269**, 25660-25667.

[7] J. F. B Mercer, *Trends Mol. Med*., 2001, **7**, 64-69.

[8] M. D. Harrison and C. T. Dameron, *J. Biochem. Mol. Toxicol*., 1999, **13**, 93-106.

[9] D. Strausak, J. F. B. Mercer, H. Dieter, W. Stremmel and G. Multhap, *Brain Res. Bull*., 2001, **55**, 175-185.

[10] D. J. Waggoner, T. B. Bartnikas and J. D. Gitlin , *Neurobiol. Dis*. 1999, **6**, 221-230.

[11] V. Desai and S. G. Kaler, *Am. J. Clin. Nutr*., 2008, **88**, 855S– 858S.

[12] L. S. Field, E. Luk and V. C. Culotta, *J. Bioenerg. Biomembr.*, 2002, **34**, 373- 379.

[13] D. L. Huffman and T. V. O'Halloran, *Annu. Rev. Biochem*., 2001, **70**, 677-701.

[14] E. D. Harris, *Nutr. Res*., 2001, **59**, 281-285.

[15] G.G. Zucconi, S. Cipriani, R. Scattoni, I. Balgkouranidou, D.P. Hawkins and K.V. Ragnarsdottir, *Neuropathol. Appl. Neurobiol*., 2007, **33**, 212–25.

[16] A.C. Rinaldi, *Biometals*., 2000,**13**, 9–13.

[17] S.G. Kaler, *Pediatr. Dev. Pathol*., 1998, **11**, 85–98.

[18] E.D. Harris, *J. Nutr*., 1992, **122**, 636-640.

[19] P. Silva, J. Dorea and G. Boaventura, *Bio. Trace. Elem. Res*., 1997, **59**, 1-3.

[20] L. Chew, D. Bradley, A. Mohd and M. Jamil, *Appl. Radiat. Isot.* 2000, **53**, 633-635.

[21] L. T. Chew, D. A. Bradley, A. Y. Mohd and M. M. Jamil, *Appl. Radiat. Isot*., 2000, **53**, 633-638.

[22] P. R. Silva, J. G. Dorea and G. R.. Boaventura, *Biol. Trace Elem. Res*., 1997, **59**, 57-62.

[23] S. Smith, *J. Inorg. Biochem*., 2004, **98**, 1874-1901.

[24] J. Camakaris, M. Petris, L. Bailey, P. Shen, P. Lockhart, T. Glover, C. Barcroft, J. Patton and J. Mercer, *Hum. Mol. Genet*., 1995, **4**, 2117-2123.

[25] B. Twining, S. Baines, N. Fisher, J. Maser, S. Vogt, C. Jacobsen, A. Tovar-Sanchez and S. Sanudo-Wilhelmy, *Anal. Chem*., 2003, **75**, 3806-3816.

[26] B. Twining, S .Baines, N. Fisher and C. Jacobsen, J. Maser, *J. Phys. IV*.,2003, **104**, 435-438.

[27] T.-J. Hwang and S.-J. Jiang, *J. Anal. At. Spectrom*., 1996, **11**, 353-357.

[28] K. Minakata, O. Suzuki and F. Horio, *Clin. Chem*., 2001, **47**, 1863-1865.

[29] M. A. Evenson, *Methods Enzymol*., 1988, **158**, 351-357.

[30] J. H. Freedman and J. Peisach, *Anal. Biochem*., 1984, **141**, 301-310.

[31] T. Cooper, M. Mayer, K. Leung, L. Ochrymowycz and D. Rorabacher, *Inorg. Chem*., 1992, **31**, 3796-3804.

[32] L. Sokol, L. Ochrymowycz and D. Rorabacher, *Inorg. Chem*., 1981, **20**, 3189-3195.

[33] E. Ambundo, M. Deydier, A. Grall, N. Aguera-Vega, L. Dressel, T. Cooper, M. Heeg, L. Ochrymowycz and D. Rorabacher, *Inorg. Chem*., 1999, **38**, 4233-4242.

[34] M. M. Bernardo, M. J. Heeg, R. R. Schroeder, L. A. Ochrymowycz and D. B. Rorabacher, *Inorg. Chem*., 1992, **31**, 191-198.

[35] B. C. Dunn, P. Wijetunge, J. R. Vyvyan, T. A. Howard, A. J. Grall, L. A. Ochrymowycz and D. B. Rorabacher, *Inorg. Chem*., 1997, **36**, 4484-4489.

6.7 Appedix

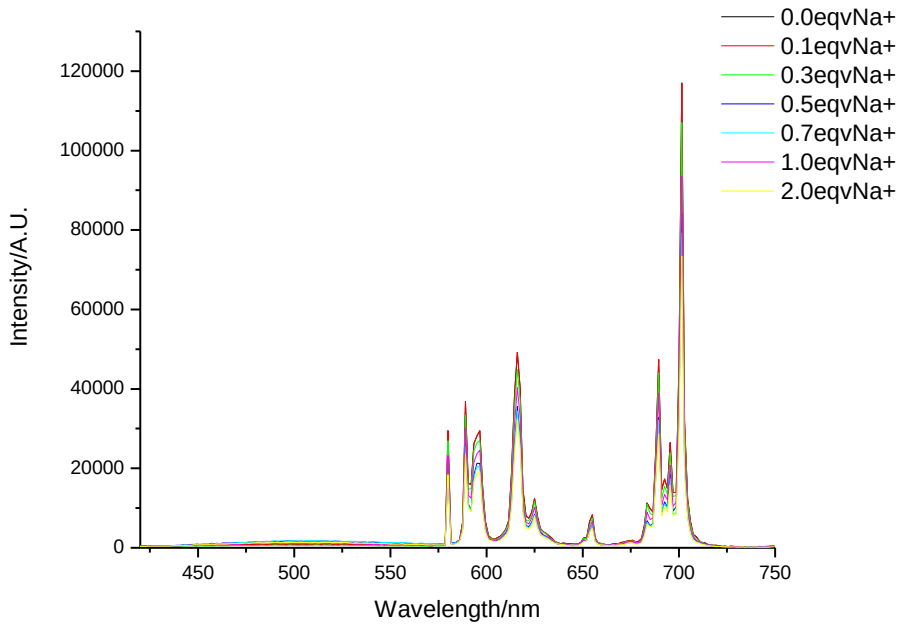

Figure 6.25 Emission spectra of 10 μM aqueous solution upon addition of aliquots of various equiv of Na(I) ions with respect to **EuL6** (0.01M HEPES, pH=7.4, λ_{ex}=350nm).

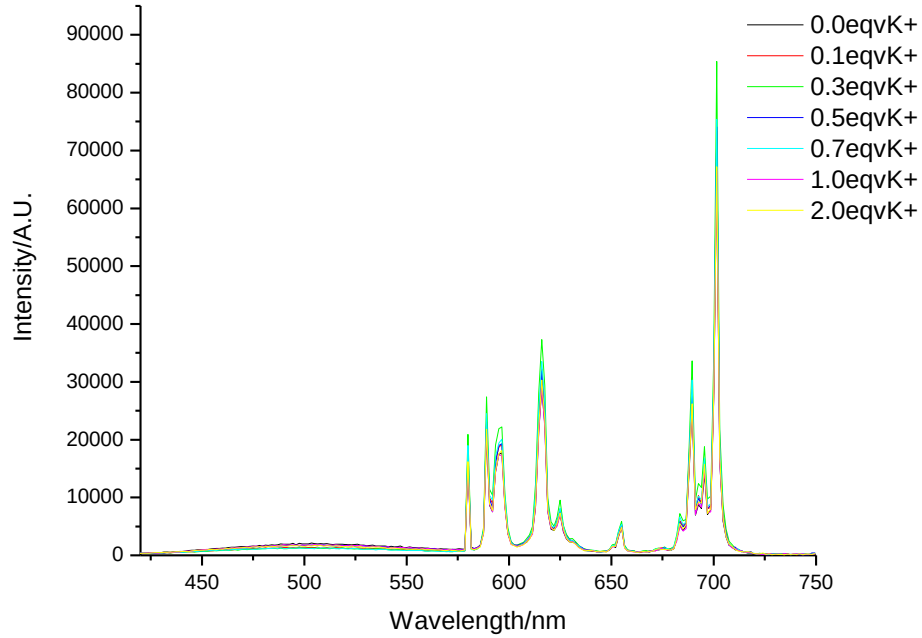

Figure 6.26 Emission spectra of 10 μM aqueous solution upon addition of aliquots of various equiv of K(I) ions with respect to **EuL6** (0.01M HEPES, pH=7.4, λ_{ex}=350nm).

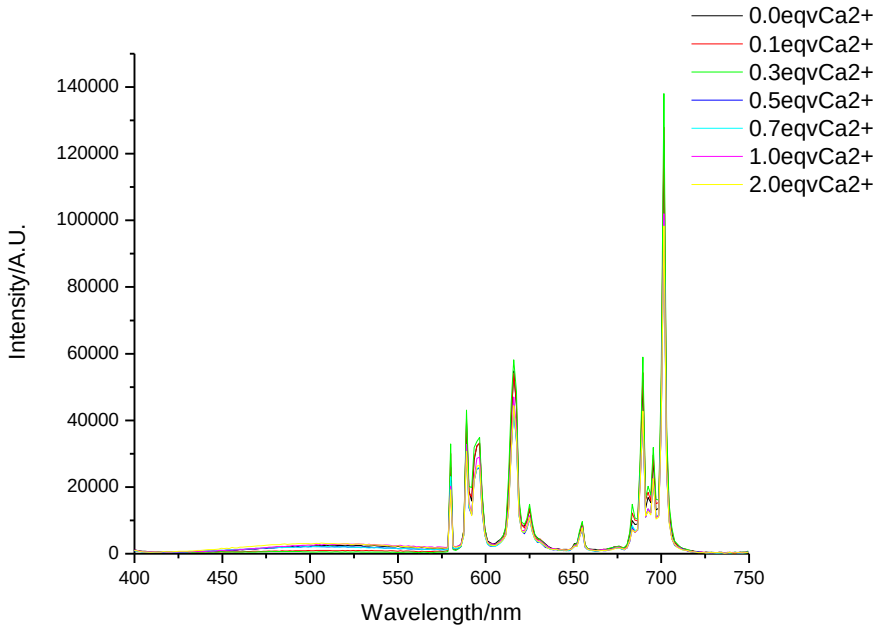

Figure 6.27 Emission spectra of 10 µM aqueous solution upon addition of aliquots of various equiv of Ca(II) ions with respect to **EuL6** (0.01M HEPES, pH=7.4, λ_{ex}=350nm).

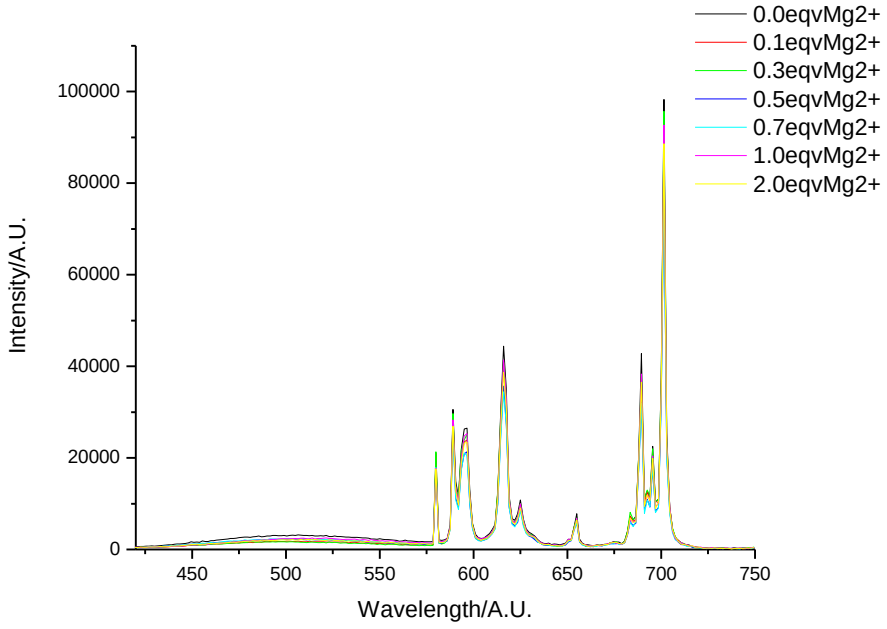

Figure 6.28 Emission spectra of 10 µM aqueous solution upon addition of aliquots of various equiv of Mg(II) ions with respect to **EuL6** (0.01M HEPES, pH=7.4, λ_{ex}=350nm).

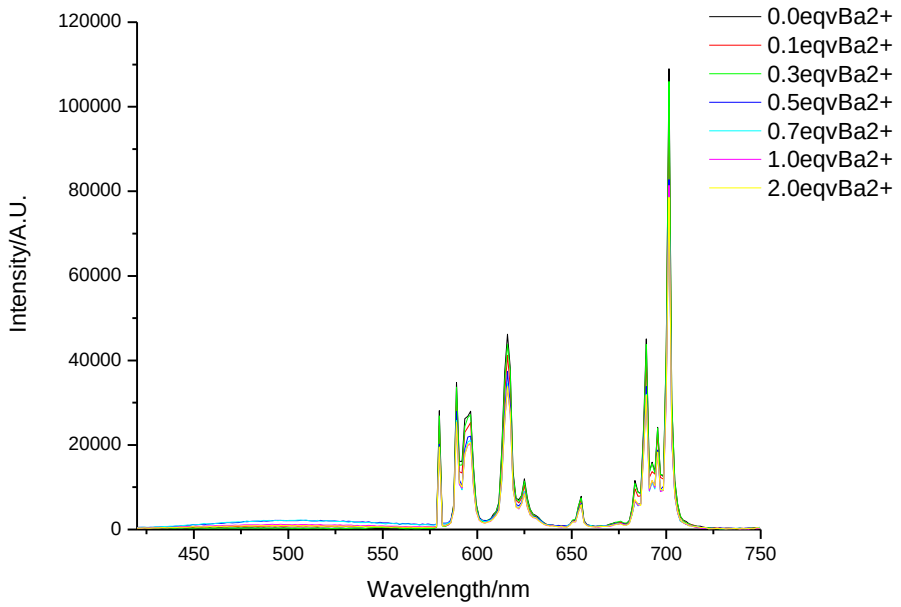

Figure 6.29 Emission spectra of 10 µM aqueous solution upon addition of aliquots of various equiv of Ba(II) ions with respect to **EuL6** (0.01M HEPES, pH=7.4, λ_{ex}=350nm).

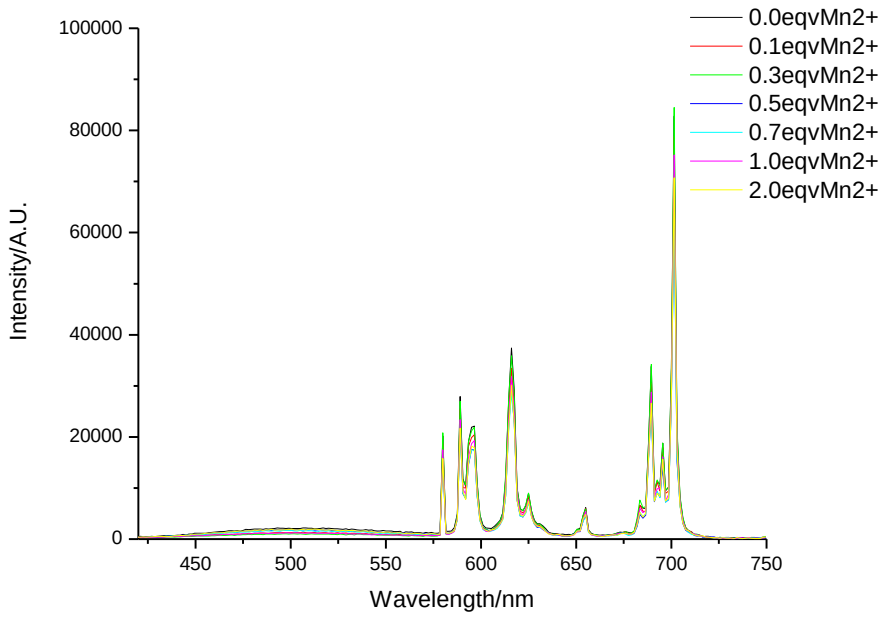

Figure 6.30 Emission spectra of 10 µM aqueous solution upon addition of aliquots of various equiv of Mn(II) ions with respect to **EuL6** (0.01M HEPES, pH=7.4, λ_{ex}=350nm).

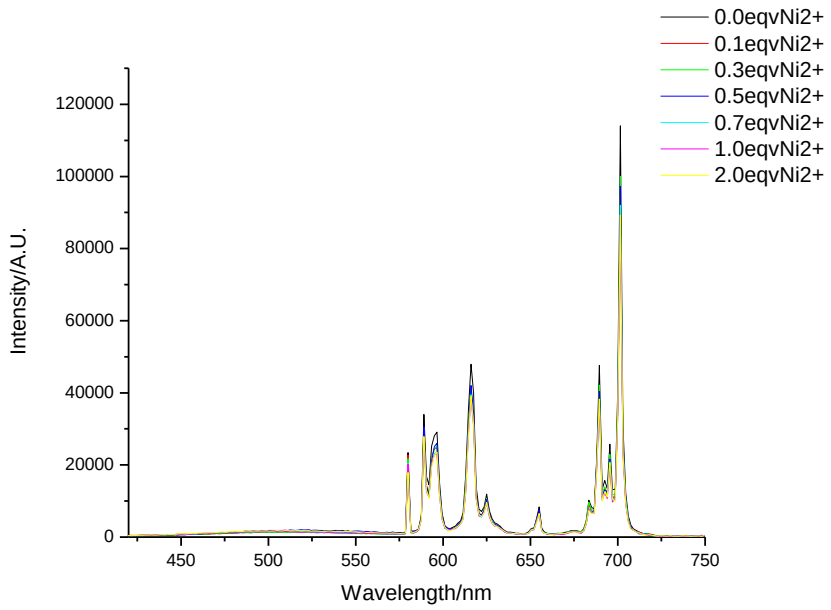

Figure 6.31 Emission spectra of 10 µM aqueous solution upon addition of aliquots of various equiv of Ni(II) ions with respect to **EuL6** (0.01M HEPES, pH=7.4, λ_{ex}=350nm).

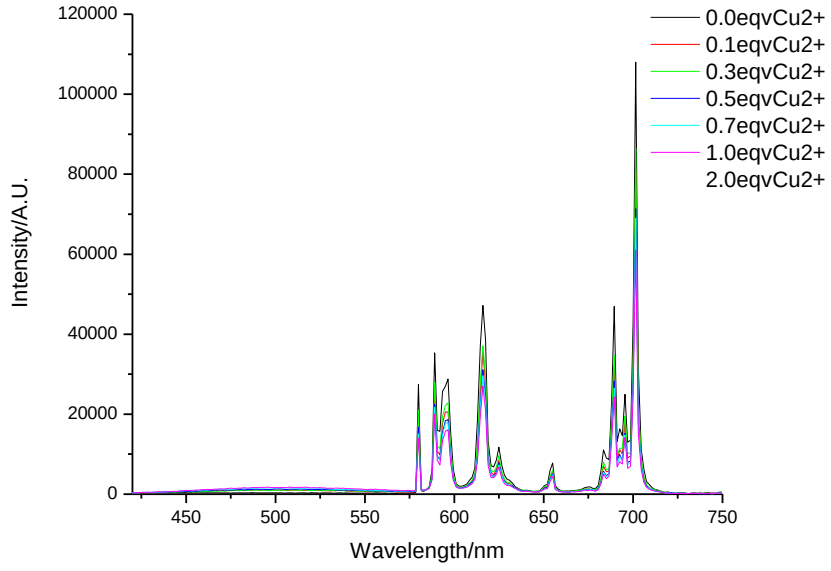

Figure 6.32 Emission spectra of 10 µM aqueous solution upon addition of aliquots of various equiv of Cu(II) ions with respect to **EuL6** (0.01M HEPES, pH=7.4, λ_{ex}=350nm).

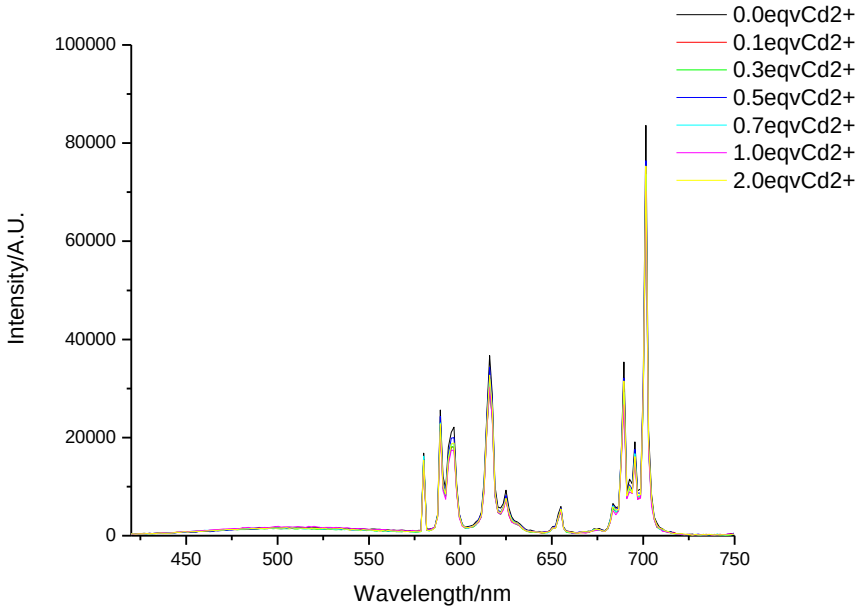

Figure 6.33 Emission spectra of 10 μM aqueous solution upon addition of aliquots of various equiv of Cd(II) ions with respect to **EuL6** (0.01M HEPES, pH=7.4, λ_{ex}=350nm).

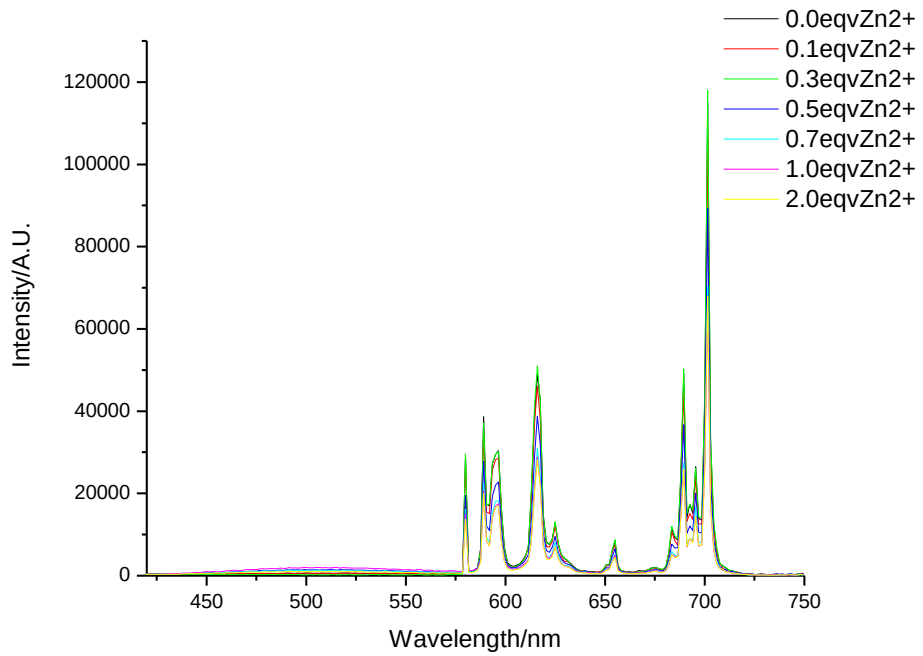

Figure 6.34 Emission spectra of 10 μM aqueous solution upon addition of aliquots of various equiv of Zn(II) ions with respect to **EuL6** (0.01M HEPES, pH=7.4, λ_{ex}=350nm).

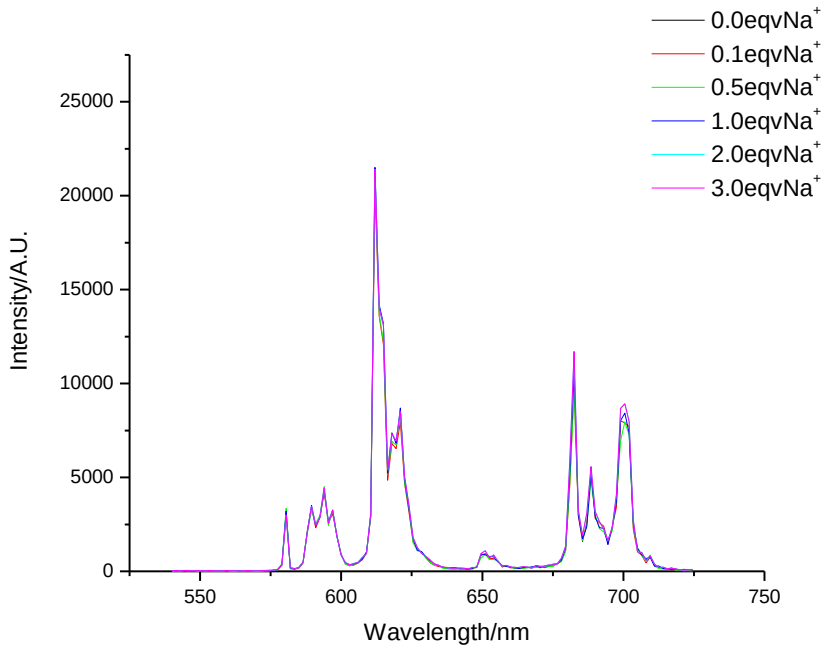

Figure 6.35 Emission spectra of 10 µM aqueous solution upon addition of aliquots of various equiv of Na(I) ions with respect to **EuL7** (0.01M HEPES, pH=7.4, λ_{ex}=350nm).

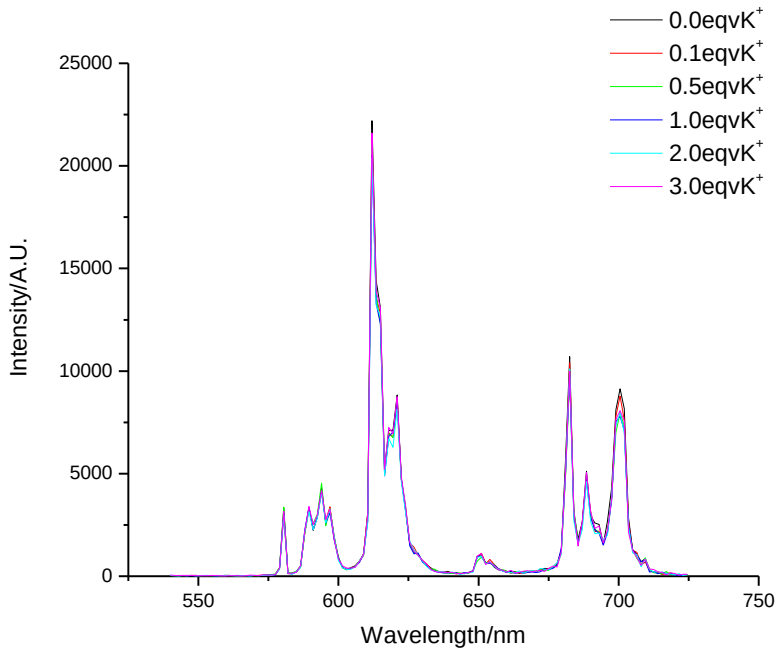

Figure 6.36 Emission spectra of 10 µM aqueous solution upon addition of aliquots of various equiv of K(I) ions with respect to **EuL7** (0.01M HEPES, pH=7.4, λ_{ex}=350nm).

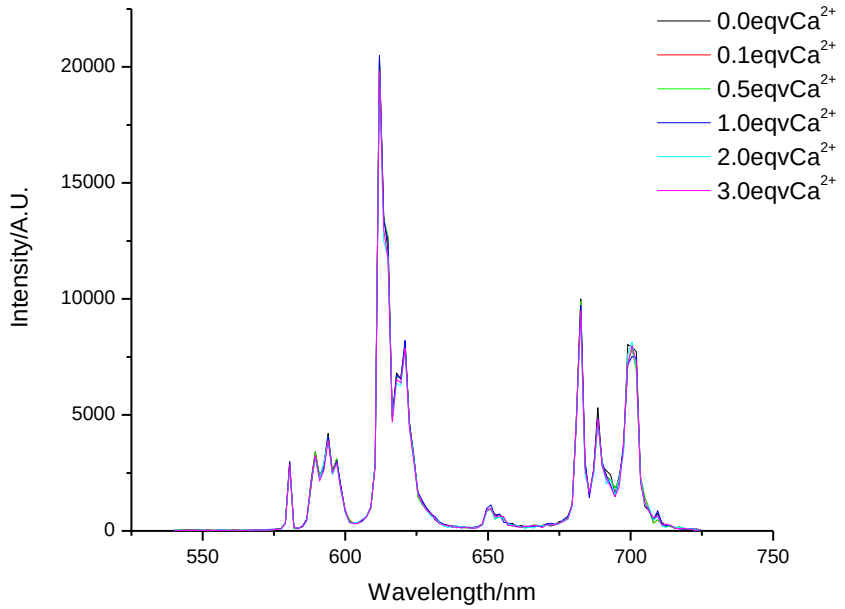

Figure 6.37 Emission spectra of 10 µM aqueous solution upon addition of aliquots of various equiv of Ca(II) ions with respect to **EuL7** (0.01M HEPES, pH=7.4, λ_{ex}=350nm).

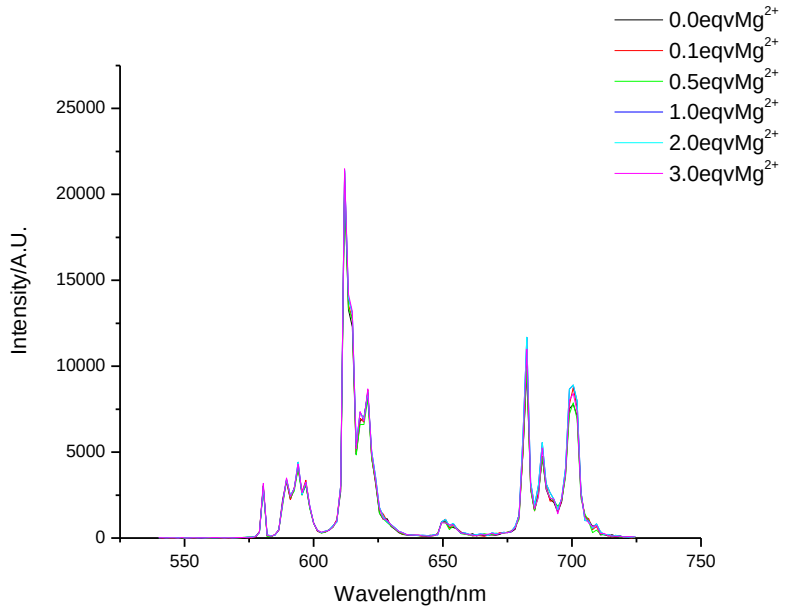

Figure 6.38 Emission spectra of 10 µM aqueous solution upon addition of aliquots of various equiv of Mg(II) ions with respect to **EuL7** (0.01M HEPES, pH=7.4, λ_{ex}=350nm).

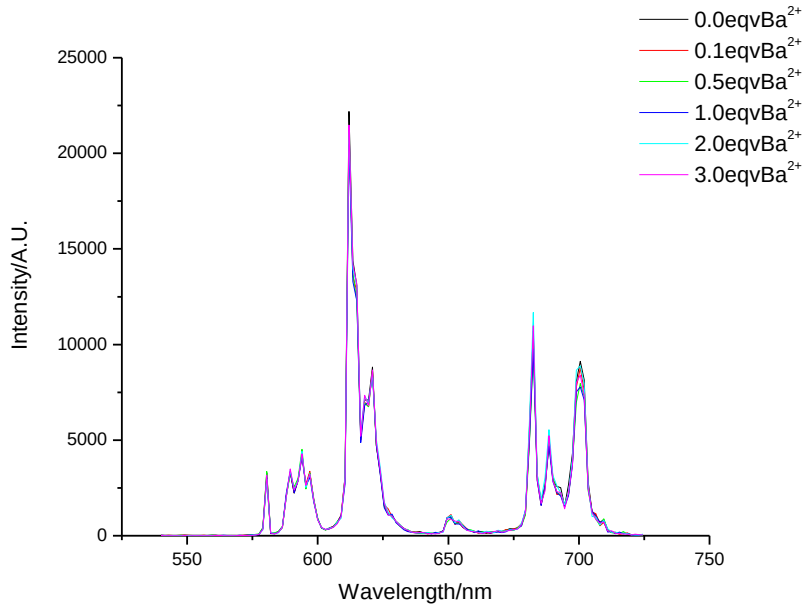

Figure 6.39 Emission spectra of 10 µM aqueous solution upon addition of aliquots of various equiv of Ba(II) ions with respect to **EuL7** (0.01M HEPES, pH=7.4, λ_{ex}=350nm).

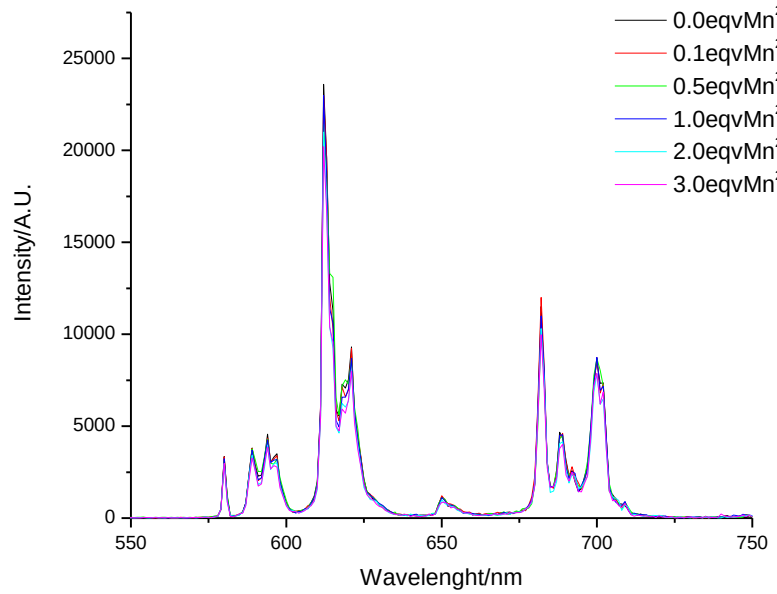

Figure 6.40 Emission spectra of 10 µM aqueous solution upon addition of aliquots of various equiv of Mn(II) ions with respect to **EuL7** (0.01M HEPES, pH=7.4, λ_{ex}=350nm).

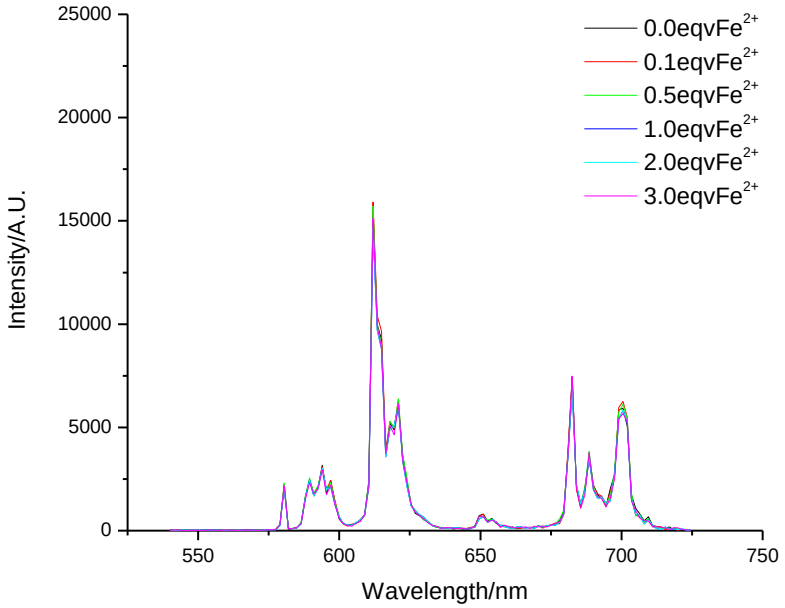

Figure 6.41 Emission spectra of 10 μM aqueous solution upon addition of aliquots of various equiv of Fe(II) ions with respect to **EuL7** (0.01M HEPES, pH=7.4, λ_{ex}=350nm).

CHAPTER 7

Experimental procedure

7.1 Materials

All starting materials and reagents were obtaind from commercial companies such as TCI, Meryer, Acros, Fisher Scientific, Sigma-Aldrich and used without further treatment unless otherwise specified. Solvents were purchased from Anaqua Chemical Supply, Duksan and LabScan. The dried solvents for organic synthese were prepared by using an appropriate drying agent, including drying triethylanime over moleucular sieves, drying dichloromethane (DCM) and acetonitrile (CH_3CN) over CaH_2, drying tetrahydrofuran (THF) over Na/benzophenone. Solvents for photophysical measurement were of spectrophotometric grade (CHROMASOLV®) and purchased from Sigma-Aldrich. All lanthanide(III) salts were purchased from Strem and Sigma-Aldrich with purity of 99.99 % or above. Any reactions requiring anhydrous conditions were performed in pre-dried glassware at 130°C with Schlenk line techniques under N_2 environment.

7.2 Chromatography

Thin-layer chromatography was performed using silica plates (Merck 100390) and each silica plate was visualised under UV irradiation (254 and 365 nm) or iodine staining, whichever was appropriate. Preparative column chromatography was done with Davisil® silica (Grace LC60A 40 – 63 Å)

7.3 ^{1}H NMR and ^{13}C NMR Measurements

^{1}H NMR spectra and ^{13}C NMR spectra were obtained on a Bruker Advance III 400 (^{1}H at frequency of 400.13 MHz and ^{13}C at frequency of 100.62 MHz) at room temperature. ^{1}H NMR and ^{13}C NMR chemical shifts were referenced to internal $CDCl_3$ and re-referenced to Tetramethylsilane (δ = 0.00 ppm).

7.4 ESI Measurements

Low resolution electrospray mass spectra were obtained from a LCQ Deca XP mass spectrometer. High resolution electrospray mass spectra were obtained from a

Micromass® Q-ToF 2 mass spectrometer.

7.5 Spectroscopic measurements

Unless otherwise noted, all photophysical measurements were averages of triplicates. UV-Vis absorption spectra were measured by a HP UV-8453 spectrophotometer. Single-photon luminescence was obtained using an Edinburgh Instrument FLSP920 equipped with a Hamamatsu R928P cooled at -20 °C, a xenon flashlamp (60W) and a Xe900 continuous xenon lamp (450W). Each sample was contained in a quartz cuvette with 1cm pathlength. Measurements were done at room temperature. Appropriate longpass filters were ultized to avoid the second order of the excitation light which could influence the emission and excitation spectra.The emission and excitation spectra were corrected for stray background light phosphorescence and detector response.

7.6 Lifetime Measurement

Lifetime spectra were recorded with FLSP290 (stop condition 10000 counts). The decay curves would have monoexponetial fitting to equation 7.1with Origin software.

$$I = I_0 + A_0 e^{-Ct} \tag{7.1}$$

where

I = intensity at time (t) after the flash

I_0 = intensity after the decay has completed

A_0 = pre-exponential factor

C = rate constant of excited state decay

7.7 Inner Sphere Hydration Number (q)

The hydration number of Eu(III) ion ,q , can be calculated by equations 7.2 and 7.3.[1][2]

$$q_{Eu} = 1.2(k_{H2O} - k_{D2O} - 0.25) \quad (7.2)$$

$$q_{Eu} = 1.2[(k_{H2O} - k_{D2O} - 0.25) - 0.075n] \quad (7.3)$$

7.8 Molar Absorption Coefficient Measurement

Five solutions with known concentration were prepared and their absorbances maximums of UV-vis spectra were recorded. A graph of absorbance against the concentration was then plotted and the molar absorption coefficient can be obtained through the gradient.

The molar absorption coefficient (ε) is calculated by equation 7.4.

$$A = \varepsilon l c \quad (7.4)$$

Where

A = absorbance at UV peak maximum

I = cuvette path length (1 cm)

c = concentration of sample

7.9 Low Temperature Measurements

Low temperature (77K) measurements were made on FLSP920 using Oxford Instruments optical cryostat. Samples were dissolved in appropriate solvent such as DMSO, mixture of methanol and ethanol, DMSO, mixture of H_2O and glycerol in ratios of 75 – 80% to 25 – 20% and 2-methyltetrahydrofuran in a special glass container and cooled down with liquid nitrogen. Spectra were recorded at 30 minute intervals.

7.10 Quantum Yield Determination

Quantum yield measurements were referenced to a standard quinine sulfate in 0.1 M sulfuric acid (λ_{ex} = 350 nm, Φ_r = 0.577).[3] In the study, five sample solutions of

known absorbances between 0.01 and 0.1 were obtained from UV-vis spectra. Then, the total integrated emission area of each emission spectrum was determined. A graph of total integrated emission against absorbance wass plotted and the slope would be determined. Using equation 7.5 the relative quantum yield would be calculated.

$$\Phi_x=\Phi_r \frac{\text{gradient}_x}{\text{gradient}_r} \cdot \left(\frac{n_x}{n_r}\right)^2 \quad (7.5)$$

7.11 Selectivity Test Measurements

The luminescence emission from Eu(III) complex (10 μM) was first measured in 10 mM HEPES buffer (pH 7.4, λ_{ex}=350 nm) with addition of various amounts of analytes with appropriate amount to solution of Eu(III) complex. Then other luminescence emission was measured when identical solutions were prepared with the addition of target analytes with appropriate amount to the solution of Eu(III) complex and other analytes.

7.12 Binding Constant Measurements

The binding constant was calculated from the emission intensity-titration curve based on equation 7.6.[4]

$$\frac{I_0}{I-I_0}=\left(\frac{1}{f}\right)\left(\frac{1}{K_s[M]}+1\right) \quad (7.6)$$

Here, I_0 was the intensity of the free Eu(III) complex, I was the intensity measured with addition of various amount of analyts, f was the fraction of initial luminescence, [M] was the concentraton of analyte and K was the intercept/slope ratio.

7.13 Kinetic Studies [5]

Kinetic studies of Eu(III) complex with analytes such as Cys, Hcy and GSH was monitored by measuring the fluorescence intensity at 612nm in 10 mM HEPES buffer (pH 7.4, λ_{ex}=350 nm) at room temperature, 37 ^{0}C and 45 ^{0}C. The pseudo first-order rate constant was calculated by fitting a plot of ln((I_{max}-I)/I_{max}) as a function of time where I

and I_{max} luminescent intensities at 612 nm at times t and the maximum value were obtained during reaction.

7.14 Synthetic Procedures and Characterizations

2A

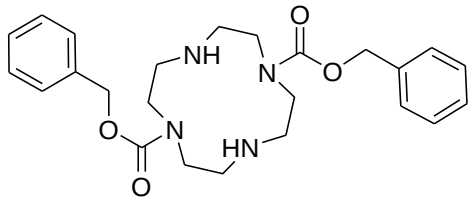

Cyclen (1g, 5.81mmol) was dissolved in D. I. water (5ml) and dioxane (4ml). Sodium phosphate dibasic (2.5g, 0.017mol) was added into the reaction mixture. pH was adjusted to pH 3. Then, benzyl chloroformate (1.65ml, 0.012mol) was added dropwise into the reaction mixture. The reaction was allowed to react for 8h. The crude product was washed by diethyl ether. Yield: 51%. ^{1}H NMR (400 MHz, $CDCl_3$) δ 2.86-3.11 (m, 8H, CH_2), 3.68-3.74 (m, 8H, CH_2), 5.18 (s, 2H, CH_2), 7.28-7.35 (m, 8H, ArH) ppm; ^{13}C NMR (100 MHz, $CDCl_3$) δ 48.85, 49.10, 49.48, 49.81, 50.01, 50.34, 50.41, 67.60, 67.68, 127.67, 127.85, 127.88, 128.23, 128.31, 128.51, 128.55, 135.66, 135.75, 155.99; MS (ESI). Calcd for $C_{24}H_{33}N_4O_4$ $[(M + 1)^+]$ m/z 441.25. Found: m/z 441.49.

2BE

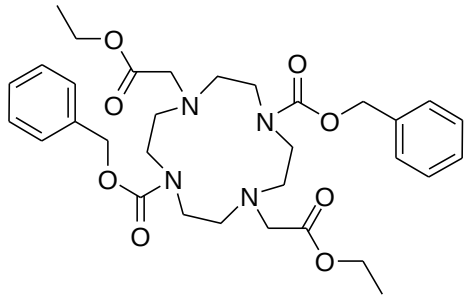

2A (510mg, 0.83mmol) and K_2CO_3 (230mg, 1.66mmol) were stirred in ACN (15mL). Ethyl bromoacetate (0.55g, 1.66mmol) was added dropwise into the reaction mixture. The reaction was stirred overnight at room temperature. The crude product was purified through silica column chromatography eluting with MeOH:DCM (1:40) to afford **2BE**

(Yield: 68%) ^{1}H NMR (400 MHz, $CDCl_3$) δ1.23 (t, J=6.4Hz, 6H, CH_3), 2.88 (s, br, 8H, CH_2), 3.42-3.43 (m, 12H, CH_2), 4.10 (s, br, 4H, CH_2), 5.12 (s, 2H, CH_2), 7.26-7.34 (m, 10H, ArH) ppm; ^{13}C NMR (100 MHz, $CDCl_3$) δ 28.15, 41.88, 46.64, 47.02, 54.36, 55.95, 66.91, 80.84, 127.84, 127.89, 128.42, 136.82, 156.39, 170.48. MS (ESI). Calcd for $C_{32}H_{45}N_4O_8$ $[(M + 1)^+]$ m/z 613.32. Found: m/z 613.87.

2BT

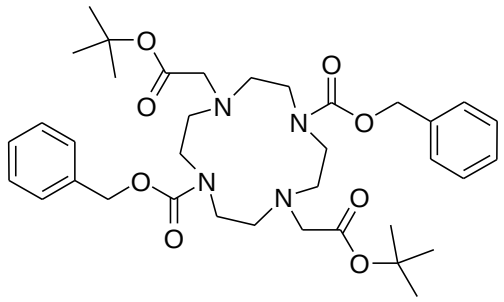

2A (510mg, 0.83mmol) and K_2CO_3 (230mg, 1.66mmol) were stirred in ACN (15mL). Tertbutyl bromoacetate (0.65g, 1.66mmol) was added dropwise into the reaction mixture. The reaction was stirred overnight at room temperature. The crude product was purified through silica column chromatography eluting with MeOH:DCM (1:40) to afford **2BE** (Yield: 73%) ^{1}H NMR (400 MHz, $CDCl_3$) δ 1.43 (s, 18H, CH_3), 2.88 (s, br, 8H, CH_2), 3.31-3.42 (m, 14H, CH_2), 5.12 (s, 4H, CH_2), 7.27-7.34 (m, 10H, ArH) ppm; ^{13}C NMR (100 MHz, $CDCl_3$) δ 28.15, 41.88, 46.64, 47.02, 54.36, 55.9, 66.91, 127.84, 127.89, 128.42, 136.82, 156.39, 170.48. MS (ESI). Calcd for $C_{36}H_{53}N_4O_8$ $[(M + 1)^+]$ m/z 669.39. Found: m/z 669.32.

2CE

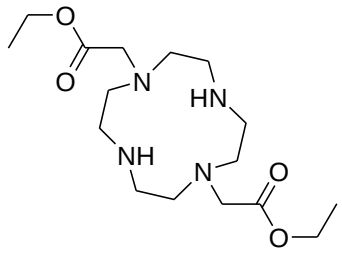

2BE (420mg, 1.22mmol) and Pd/C (50mg) was stirred under a hydrogen balloon for 8h. The reaction mixture was filtered by a pad of Celite and the solvent was removed in vacuo to obtain **2CE**. Yield was 82%.^{1}H NMR (400 MHz, MeOD) δ 1.30 (t, J=7.2Hz, 6H, CH_3), 2.92 (s, br, 4H, CH_2), 3.17-3.32 (m, 12H, CH_2), 3.60 (s, 4H, CH_2), 4.20-4.25 (m, 4H, CH_2) ppm; ^{13}C NMR (100 MHz, MeOD) δ 13.06, 42.57, 49.31, 53.31, 61.30, 172.44. MS (ESI). Calcd for $C_{16}H_{33}N_4O_4$ [$(M + 1)^+$] m/z 345.25. Found: m/z 345.27.

2CT

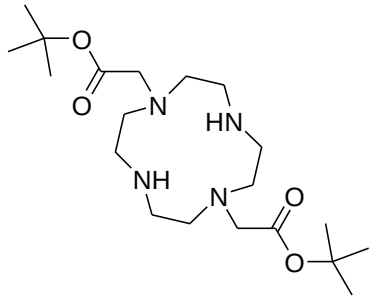

2BT (420mg, 1.22mmol) and PdC (50mg) was stirred under hydrogen balloon for 8h. The reaction mixture was filtered by a pad of Celite and the solvent is removed in vacuo to obtain **2CT**. Yield was 82%.^{1}H NMR (400 MHz, $CDCl_3$) δppm; ^{13}C NMR (100 MHz, MeOD) δ 1.48 (s, 18H, CH_3), 3.01 (s, 8H, CH_2), 3.14 (d, J=4.8Hz, 8H, CH_2), 3.50 (s, 4H, CH_2), 4.20-4.25 (m, 4H, CH_2) ppm; ^{13}C NMR (100 MHz, MeOD) δ 27.27, 43.79, 43.79, 55.27, 81.92, 171.59. Calcd for $C_{20}H_{41}N_4O_4$ [$(M + 1)^+$] m/z 401.31. Found: m/z 401.62.

Tert-butyl 2-(2-chloroethoxy)acetate

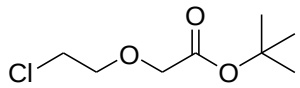

T-butyl bromoacetate (2.78g, 0.014mol) was dissolved in DMF (4ml) and chloroethanol (1.15ml, 0.017mol) was added dropwise. The reaction mixture was cooled to 0°C and sodium hydroxide (0.684 g, 0.017mmol) was added into the solution mixture. The reaction mixture was stirred at 0°C for 4 hours and then at room temperature overnight. Water (20ml) and haxane (50ml) were added. The organic phase was washed with water (50ml), dried over Mg_2SO_4, filtered and evaporated to afford the title compound as colourless liquid with yield: 72%. ^{1}H NMR (400 MHz, $CDCl_3$) δ 1.48 (s, 9H, CH_3), 3.67 (t, J=5.6Hz, 2H, CH_2), 3.82 (t, J=5.6Hz, 2H, CH_2), 4.04 (s, 2H, CH_2) ppm; ^{13}C NMR (100 MHz, $CDCl_3$) δ 28.04, 42.60, 68.92, 71.43, 81.80, 169.25.

2-(2-chloroethoxy)acetic acid

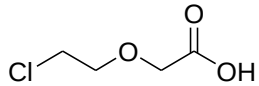

To the solution of tert-butyl 2-(2-chloroethoxy)acetate (2g, 0.01mol) THF (4mL) was added conc. H_2SO_4 (0.5mL). The reaction mixture was stirred for 6h. Water (50ml) and DCM (20ml) were added. The organic phases were obtained, dried over Mg_2SO_4, filtered and evaporated to afford the titled compound as a colourless liquid with yield: 84%.^{1}H NMR (400 MHz, $CDCl_3$) δ 3.70 (s, 2H, CH_2), 3.86 (s, 2H, CH_2),4.24 (s, 2H, CH_2), 9.60 (s, 1H, COOH) ppm; ^{13}C NMR (100 MHz, $CDCl_3$) δ 42.62, 67.97, 71.67, 175.05.

Ethyl 2-(2-chloroethoxy)acetate

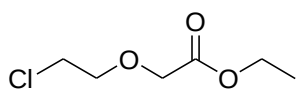

To the solution of 2-(2-chloroethoxy)acetic acid (1.5g, 0.01mol) in THF (4mL) was added absolute ethanol (4mL) and conc. H_2SO_4 (0.2mL). The reaction mixture was

refluxed for 18h. Water (20ml) and DCM (10ml) were added. The organic phases were obtained, dried over Mg_2SO_4, filtered and evaporated to afford the titled compound as a colourless liquid with yield: 70%.^{1}H NMR (400 MHz, $CDCl_3$) δ 1.29 (t, J=7.2Hz, 3H, CH_3), 3.68 (t, J=5.6Hz, 2H, CH_2), 3.84 (t, J=5.6Hz, 2H, CH_2), 4.22 (q, J=7.2Hz, 2H, CH_2) ppm; ^{13}C NMR (100 MHz, $CDCl_3$) δ 14.06, 42.55, 60.83, 68.45, 71.51, 169.97.

DO3A-ME

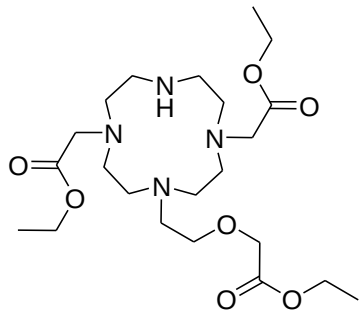

2CE (400mg, 1.16mmol) was dissolved in dry ACN, followed by the addition of K_2CO_3 (160mg, 1.16mmol). Then ethyl 2-(2-chloroethoxy)acetate (192mg, 1.16mmol) was added dropwise to the reaction mixture. The reaction was refluxed for 2 days. The reaction mixture was filtered and purified by silica column chromatography eluting with MeOH:DCM (1:20) to give **DO3A-ME**. (yield:56%) ^{1}H NMR (400 MHz, $CDCl_3$) δ 1.26-1.31(m, 9H, CH_3), 2.70 (s, 4H, CH_2), 2.83-2.84 (s, 6H, CH_2), 3.12-3.21 (m, 7H, CH_2), 3.55 (s, 4H, CH_2), 3.68-3.71 (m, 3H, CH_2), 4.10-4.25 (m, 8H, CH_2) ppm; ^{13}C NMR (100 MHz, $CDCl_3$) δ14.1, 14.2, 42.6, 44.8, 49.1, 49.9, 53.3, 4.7, 56.0, 60.5, 60.8, 61.1, 67.9, 68.4, 68.0, 169.9, 171.1. MS (ESI). Calcd for $C_{22}H_{42}N_4O_7$ [$(M + 1)^+$] m/z 475.31. Found: m/z 475.59.

DO3A-MT

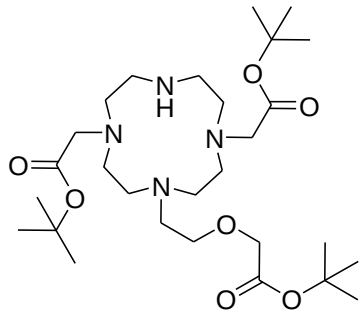

2CT (400mg, 1.16 mmol) was dissolved in dry ACN, followed by the addition of K_2CO_3 (160mg, 1.16mmol). Then tert-butyl 2-(2-chloroethoxy)acetate (225mg, 1.16mmol) was added dropwise to reaction mixture. The reaction was refluxed for 2 days. The reaction mixture was filtered and purified by silica column chromatography eluting with MeOH:DCM (1:20) to give **DO3A-MT**. (yield:61%) ^{1}H NMR (400 MHz, $CDCl_3$) δ 1.34 (s, 27H, CH_3), 2.58-2.70 (m, 10H, CH_2), 2.98-3.06 (m, 8H, CH_2), 3.32 (s, 4H, CH_2), 3.54-3.55 (m, 2H, CH_2), 3.99 (s, 2H, CH_2), ppm; ^{13}C NMR (100 MHz, $CDCl_3$) δ 27.85, 27.90, 44.68, 48.81, 49.66, 54.41, 56.48, 67.54, 68.92, 80.98, 81.98, 170.16. MS (ESI). Calcd for $C_{28}H_{55}N_4O_7$ [$(M + 1)^+$] m/z 559.41. Found: m/z 559.10.

3A

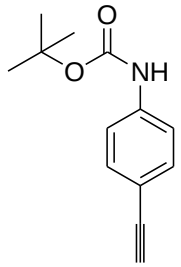

$(Boc)_2O$ (2.18g, 1.0mmol) and 4-Ethylaniline (936mg, 0.8mmol) were refluxed in THF (10ml) overnight. The reaction mixture was then purified by silica column chromatography eluting with EA:PE (1:15) to afford **3A**. (yield:62%) ^{1}H NMR (400 MHz, $CDCl_3$) δ 1.52 (m, 9H, OCH_3), 3.01 (s, 1H, CH), 6.51 (s, br, 1H, NH) , 7.32 (m, J=8.6, 1H, ArH), 7.41-7.43 (m, 2H, ArH), ppm; ^{13}C NMR (100 MHz, $CDCl_3$) δ 28.3, 80.9, 83.5, 116.2, 117.9, 132.9, 138.9, 152.3.MS (ESI). Calcd for $C_{13}H_{15}NO_2Na$ [(M +

22)$^+$] m/z 240.10. Found: m/z 240.13.

3B

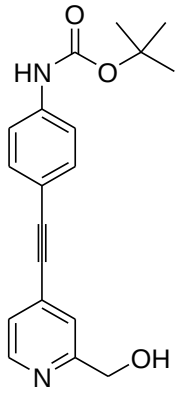

Dry triethylamine (8 mL) was first mixed with dry THF (4mL), followed by addition of **1** under an atmosphere of nitrogen. Triphenylphosphine (52mg, 0.02 mmol), dichlorobis(triphenylphosphine)palladium(II) (35mg, 0.005 mmol) and copper(I) iodide (9.8mg, 0.005 mmol) were added to the solution mixture. Finally, (4-bromopyridin-2-yl)methanol (752mg, 0.40 mmol) was added and reaction was allowed to be heated to 70^o C for 12 h. After cooling, the precipitate was filtered off and washed with THF. The crude product was purified by silica column chromatography eluting with EA:PE (1:10) to afford **3B**. (yield: 46%) ^{1}H NMR (400 MHz, $CDCl_3$) δ 1.52 (s, 9H, CH_3), δ 4.76 (s, 2H, CH_2), 6.77 (s, 1H, NH), 7.27-7.48 (m, 6H, ArH), 8.51 (d, J=4.5, 1H, ArH) ppm; ^{13}C NMR (100 MHz, $CDCl_3$) δ29.7, 65.4, 82.5, 87.5, 95.7, 117.5, 119.5, 123.7, 125.5, 133.9, 134.3, 140.9, 0149.8, 153.8, 160.7. MS (ESI). Calcd for $C_{19}H_{20}N_2O_3$ [(M + 1)$^+$] m/z 325.16. Found: m/z 325.07.

3C

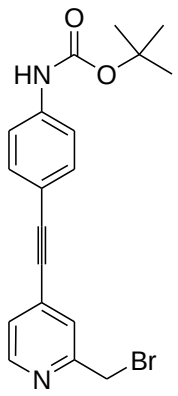

Triphenylphosphine (99.6mg, 0.38mmol) was added into the solution of **3C** (113mg, 0.35mmol) in DCM (20mL), followed by the addition of CBr_4 (132mg, 0.4mmol). The reaction was stirred for three hours. The crude product was purified by silica column chromatography eluting with EA:PE (1:20) to afford **3C**. (yield: 37%) ^{1}H NMR (400 MHz, $CDCl_3$) δ 1.52 (s, 9H, CH_3), δ 4.53 (s, 2H, CH_2), 7.09 (s, 1H, NH), 7.27 (d, J= 5.4Hz, 1H, ArH), 7.41-7.51 (m, 5H, ArH), 8.53 (d, J=5.1, 1H, ArH) ppm; ^{13}C NMR (100 MHz, $CDCl_3$) δ28.3, 33.3, 80.9, 85.7, 94.9, 115.8, 118.1, 124.6, 125.2, 132.9, 132.9, 139.7, 149.46, 152.4, 156.8. MS (ESI). Calcd for $C_{19}H_{19}BrN_2O_2$ [$(M + 1)^+$] m/z 387.06. Found: m/z 387.13.

3D

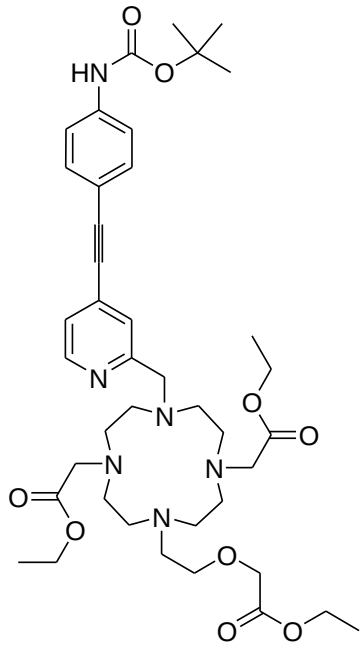

DO3A-ME (133mg, 0.28mmol) and **3C** (108mg, 0.28mmol) were first dissolved in dry

ACN (15ml) and K_2CO_3 (77mg, 0.56mmol) was added into the reaction mixture and refluxed overnight. Then, the reaction mixture was filtered and purified by silica column chromatography eluting with MeOH: DCM (1:20) to afford **3D**. (yield:37%) ^{1}H NMR (400 MHz, $CDCl_3$) δ 1.23-1.29 (m, 9H, CH_3), 1.52 (s, 9H, OCH_3), 2.40-2.98 (m, br, 22H, CH_2), 3.25-3.81 (m, 4H, CH_2), 4.12-4.18 (m, 8H, CH_2), 7.23 (d, J= 4.9Hz, 1H, ArH), 7.28 (s, 1H, ArH), 7.44-7.47 (m, 3H, ArH), 7.56-7.58 (m, 2H, ArH), 8.28 (d, J=5.04, 1H, ArH) ppm; ^{13}C NMR (100 MHz, $CDCl_3$) δ14.1, 28.3, 49.6, 50.3, 52.0, 55.9, 58.90, 60.9, 61.2, 67.6, 68.4, 80.6, 85.4, 95.5, 115.2, 118.3, 123.9, 125.4, 132.7, 132.9, 140.2, 149.1, 152.6, 158.3, 170.2, 172.9. MS (ESI). Calcd for $C_{41}H_{60}N_6O_9$ [(M + 1)+] m/z 781.44. Found: m/z 781.33.

3E

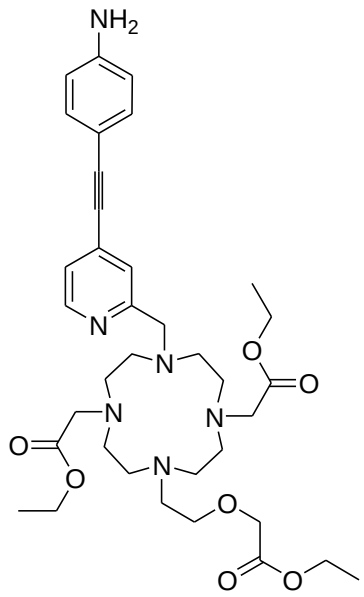

Trifluoroacetic acid (1mL) was added to the solution of **3D** (68mg, 0.1mmol) and stirred in DCM (2ml) overnight. The reaction mixture was purified by diethyl ether: DCM (1:1) to afford **3E**. (yield:80%) ^{1}H NMR (400 MHz, $CDCl_3$) δ 1.18-1.25 (m, 9H, CH_3), 2.15-2.90 (s, 22H, CH_2), 3.20-3.50 (m, 4H, CH_2), 4.07-4.18 (m, 8H, CH_2), 4.51 (s, br, 2H, NH_2),7.14 (ms, 1H, NH), 7.23-7.29 (m, 2H, ArH), 7.45-7.53 (m, 5H, ArH), 8.28 (d, 1H, ArH)ppm; ^{13}C NMR (100 MHz, $CDCl_3$) 14.1, 49.6, 50.3, 51.2, 52.8, 56.0,57.1, 60.7, 60.8, 61.2, 67.9, 80.74, 86.4, 95.9,114.6, 124.2, 125.2, 125.9, 133.4, 149.0, 158.1,

170.7. MS (ESI). Calcd for $C_{36}H_{52}N_6O_7$ [(M + 1)$^+$] m/z 681.39. Found: m/z 681.43.

3F

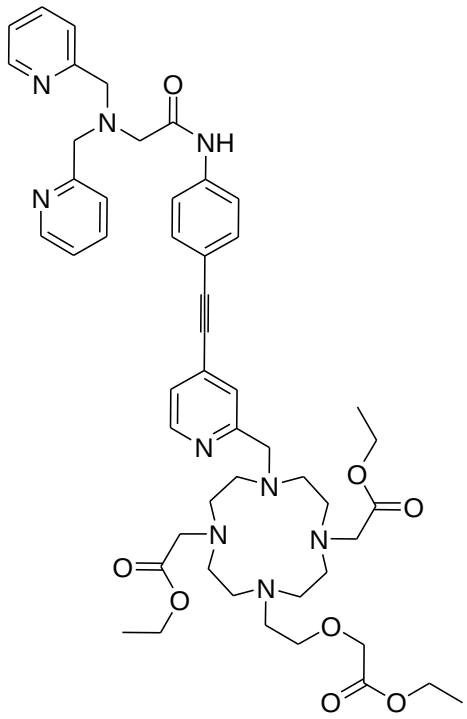

3E (50mg, 0.073mmol) was first dissolved in dry DCM (10ml). Then, triethylamine chloroacetylchloride (0.006ml, 0.073mmol) was added to the reaction mixture. The reaction was stirred for half a day at room temperature. The reaction mixture was filtered and combined filtrates evaporated under reduced pressure. Without further purification, the reaction mixture were reacted with K_2CO_3 and dipicolylamine (0.018ml, 0.1mmol) (20.7mg, 0.15mmo) and were refluxed in ACN (6ml) for three days. The reaction mixture was filtered and combined filtrates were evaporated under reduced pressure. The reaction mixture was then washed by water several times and purified by silica column chromatography eluting with gradient from DCM to MeOH:DCM (1:3) to afford **3F**. (yield:35%) ^{1}H NMR (400 MHz, $CDCl_3$) δ 1.26-1.30 (m, 9H, CH_3), 2.18-2.85 (m, br, 26H, CH_2), 3.77 (s, br,7H, CH_2), 4.14-4.20 (m, br, 7H, CH_2), 7.22-7.24 (m, 4H, ArH), 7.36-7.38 (m, 4H, ArH),7.61-7.68 (m, 4H, ArH), 8.35 (s, 1H, NH)ppm, 8.67-8.12 (m, 3H, ArH); ^{13}C NMR (100 MHz, $CDCl_3$) 14.3, 49.6, 50.3, 52.4, 55.9, 59.0, 60.2, 61.0, 65.4, 66.8, 67.6 68.5 69.31, 80.6, 85.6 95.5 114.3 118.4 120.9, 123.4,

124.2, 125.4 131.6, 132.7 136.2, 141.7 147.4 149.2 152.6, 155.3 158.4, 170.2 172.9. Elemental analysis calcd (%) for $C_{50}H_{65}N_9O_8$: C 65.27, H 7.13, N 13.71; found: C 65.91, H 7.85, N 14.38.MS (ESI).Calcd for $C_{50}H_{65}N_9O_8$ [$(M + 1)^+$] m/z 920.50. Found: m/z 920.53.

EuL1

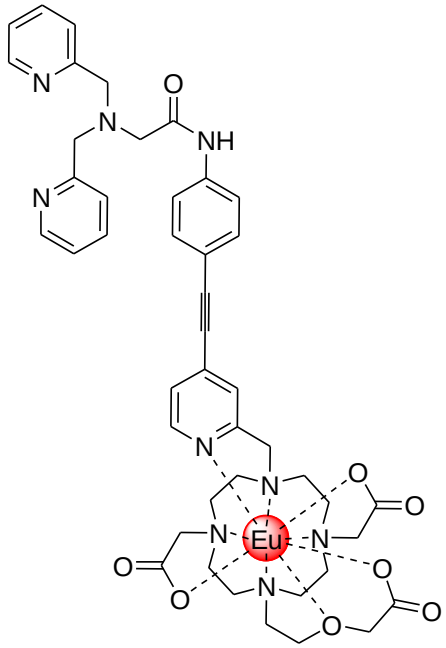

3F (10mg, 0.011mmol) was dissolved in THF and then mixed with in 0.05M NaOH (1ml). The reaction mixture was stirred at room temperature for half a day until the solution became clear. It was then filtered and neutralized to pH 7 and re-crystallized in a mixture of methanol and diethyl ether several times to afford deprotected **3F**, which was then refluxed with 1 eqv. of $EuCl_3 \cdot 6H_2O$ (4mg, 0.011mmol) in D.I. water overnight. The reaction mixture was adjusted to pH 6 and filtered and combined filtrates were evaporated under reduced pressure. The product was purified in chloroform to afford **EuL1**. (yield 41%) ^{1}H NMR (400 MHz, D_2O) δ 2.02-3.69 (m, 10H, CH_2), 4.23-4.33 (m, 10H, CH_2), 7.73-7.85 (m, 7H, ArH), 8.23 (s, 4H, ArH),8.30-8.57 (m, 3H, ArH), 9.44 (s, 1H, ArH) ppm, 8.67-8.12 (m, 3H, ArH). Elemental analysis calcd (%) for $C_{44}H_{52}EuN_9O_8$: C 53.55, H 5.31, N 12.77; found: C 53.89, H 5.61, N 13.08. HRMS (+):492.6581 $(M+2H)^{2+}$ $[C_{44}H_{52}EuN_9O_8]^{2+}$requires 492.6563.The isotopic distribution

matched closely with the simulated spectrum. Retention time (HPLC): = 7.35min.

4E

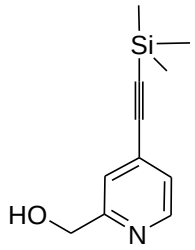

Dry triethylamine (10 mL) was first mixed with dry THF (5mL), followed by addition of (4-bromopyridin-2-yl)methanol (1.0 g, 5.4 mmol) under an atmosphere of nitrogen. Triphenylphosphine (52 mg, 0.02 mmol), dichlorobis(tripheny lphosphine)palladium(II) (35 mg, 0.005 mmol) and copper(I) iodide (9.8 mg, 0.005 mmol) were added to the reaction mixture and heated to 60^{o}C for 12 h. The reaction mixture was then filtered and evaporated under reduced pressure. The crude product was purified by silica column chromatography eluting with EA:PE (1:15) to afford **4E**. (yield: 46%) ^{1}H NMR (400 MHz, $CDCl_3$) δ 0.74 (s, 9H, CH_3), δ 5.20 (s, 2H, CH_2), 5.91 (s, br, 1H, OH), 7.66 (d, J=4.8, 1H, ArH), 7.92 (s, 1H, ArH), 8.88 (d, J=4.8, 1H, ArH) ppm; ^{13}C NMR (100 MHz, $CDCl_3$) δ0.19, 64.73, 100.54, 102.60, 123.52, 124.79, 132.44, 148.85, 161.07. MS (ESI). Calcd for $C_{11}H_{16}NOSi$ [$(M + 1)^{+}$] m/z 206.10. Found: m/z 206.12.

4F

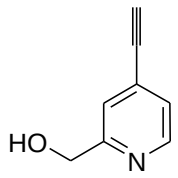

4E (0.6 g, 2.9 mmol) was dissolved in dry THF (8 mL) and then Tetra-n-butylammonium fluoride was added into the reaction mixture. The reaction was stirred for 5h. The crude product was purified by silica column chromatography eluting with EA: PE (1:12) to afford **4F**. (yield: 82 %) ^{1}H NMR (400 MHz, $CDCl_3$) δ 3.36 (s, 1H, CH), δ 4.74 (s, 2H, CH_2), 7.22 (d, J=5.2, 1H, ArH), 7.45 (s, 1H, ArH), 8.44 (d, J=4.8, 1H, ArH) ppm; ^{13}C NMR (100 MHz, $CDCl_3$) δ64.16, 80.95, 82.21, 123.18, 124.58, 128.61, 148.42, 160.51. MS (ESI). Calcd for C_8H_7NO [$(M + H)^{+}$] m/z 134.06.

Found: m/z 134.20.

4G

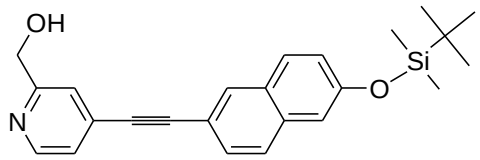

Dry triethylamine (8 mL) was first mixed with dry THF (5mL), followed by addition of **4F** (0.4 g, 0.30 mmol)under an atmosphere of nitrogen. Triphenylphosphine (50mg, 0.02 mmol), dichlorobis(triphenylphosphine)palladium(II) (30mg, 0.005 mmol) and copper(I) iodide (9.8mg, 0.005 mmol) were added to the solution mixture. Finally, (4-(2-(6-(tert-butyldimethylsilyloxy)naphthalen-2-yl)ethynyl)pyridin-2-yl)methanol (117 mg, 0.30 mmol) was added and the reaction was heated to 60^{o}C for 12 h. After cooling, the precipitate was filtered off and washed with THF. The crude product was purified by silica column chromatography eluting with EA:PE (1:5) to yield **4G**. (yield: 46 %) ^{1}H NMR (400 MHz, $CDCl_3$) δ 0.16 (s, 6H, CH_3), δ 0.92 (s, 9H, CH_3), 4.67 (s, 2H, CH_2), 7.27 (d, J= 7.2Hz, 2H, ArH), 7.07-7.18 (m, 2H, ArH), 7.39-7.40 (m, 1H, ArH), 7.88 (s, 1H, ArH), 8.38 (d, J= 5.2Hz, 1H, ArH) ppm; ^{13}C NMR (100 MHz, $CDCl_3$) δ-3.94, 18.62, 26.05, 64.54, 86.91,95.36, 115.30, 117.36, 122.92, 123.35, 124.50, 127.34, 128.90, 129.89, 132.47, 132.88, 135.00, 148.84, 155.15, 160.26. MS (ESI). Calcd for $C_{24}H_{27}NSiO_2$ [$(M + 1)^+$] m/z 390.19. Found: m/z 390.26.

4H

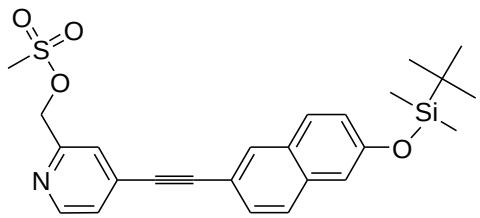

4G (0.2 g, 0.05 mmol) was dissolved in dry DCM, followed by the addition of triethylamine (0.14 ml, 1.03 mmol) and methanesulfonyl chloride (0.07 g, 0.68 mmol). The reaction was stiired under reflux overnight. The reaction mixture was filtered and

purified by silica column chromatography eluting with DCM:MeOH (30:1) to yield **4H**. (yield: 48 %) ^{1}H NMR (400 MHz, $CDCl_3$) δ 0.27 (s, 6H, CH_3), 1.03 (s, 9H, CH_3), 3.13 (s, 3H, CH_3), 5.36 (s, 2H, CH_2), 7.13 (d, J= 2.4Hz, 1H, ArH), 7.18-7.19 (m, 1H, ArH), 7.42 (d, J= 4Hz, 1H, ArH), 7.51-7.53 (m, 1H, ArH), 7.61 (s, 1H, ArH), 7.68-7.74 (m, 2H, ArH), 8.03 (s, J= 5.2 Hz, 1H, ArH) ppm; ^{13}C NMR (100 MHz, $CDCl_3$) δ 3.89, 18.68, 26.09, 38.51, 71.22, 86.44, 95.11, 115.36, 117.08, 123.49, 124.65, 125.87, 127.46, 128.88, 129.99, 132.76, 133.92, 135.23, 14.66, 154.01, 155.39. MS (ESI). Calcd for $C_{25}H_{29}NSSiO_4$ [(M + 1) $^{+}$] m/z 468.17. Found: m/z 468.56.

4I

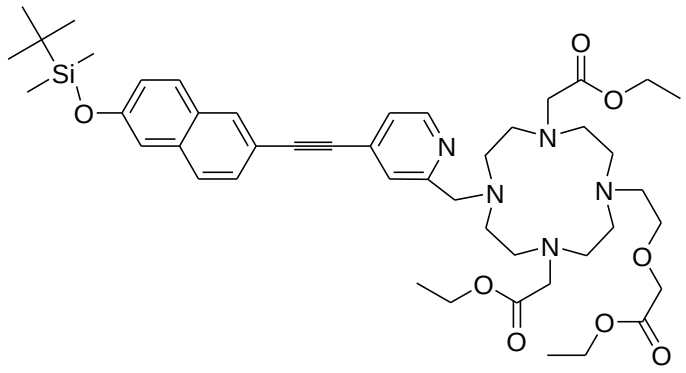

4H (0.12 g, 0.26 mmol) was dissolved in dry ACN (8 ml) under an atmosphere of nitrogen, followed by the addition of K_2CO_3 (35 mg, 0.26 mmol) and **DO3A-ME** (0.12 g, 0.26 mmol). The reaction mixture was stirred for 15 h. The reaction mixture was filtered and purified by silica column chromatography eluting with gradient from DCM to MeOH:DCM (1:5) to afford **4I**. (yield: 52 %) ^{1}H NMR (400 MHz, $CDCl_3$) δ 0.20 (s, 6H, CH_3), 0.95 (s, 9H, CH_3), 1.18-1.20 (m, 9H, OCH_3), 2.35-4.50 (m, 31H, CH_2), 7.04-7.11 (m, 3H, ArH), 7.27 (s, 1H, ArH), 7.42-7.45 (m, 1H, ArH), 7.60-7.67 (m, 3H, ArH), 7.94 (s, 1H, ArH), 8.25 (d, J=5.2, 1H, ArH) ppm; ^{13}C NMR (100 MHz, $CDCl_3$) δ 4.36, 14.10, 18.20, 25.62, 39.44, 49.60, 50.29, 52.05, 55.91, 58.91, 60.85, 61.12, 67.64, 68.38, 86.01, 95.65, 114.87, 123.01, 125.48, 127.00, 128.39, 128.54, 129.50, 132.15, 132.70, 134.69, 149.21, 154.88, 158.46, 170.28, 172.94. MS (ESI). Calcd for $C_{46}H_{67}N_5O_8Si$ [(M + 1)$^{+}$] m/z 846.48. Found: m/z 846.60. Elemental analysis calcd (%)

for $C_{46}H_{67}N_5O_8Si \cdot 2H_2O$: C,62.63;H,8.11;N,7.91; found: C,62.74; H,8.21;N,7.98.

4J

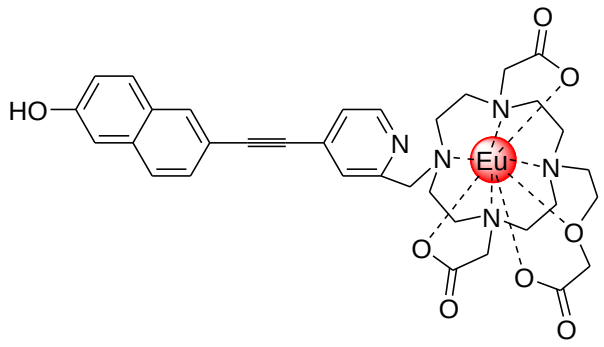

To the solution of **4I** (68 mg, 0.08 mmol) in THF was added LiOH (0.01 M). The reaction was stirred at room temperature overnight. The reaction mixture was filtered and purfied by washing with diethyl ether:DCM (1:1) to obtain a white solid which was then dissolved in D.I. water. The pH was adjusted to 7 and the reaction was refluxed with 1 eqv. of $EuCl_3 \cdot 6H_2O$ (4 mg, 0.008 mmol) overnight. The pH value of reaction mixture was adjusted to 6 and filtered and combined filtrates were evaporated under reduced pressure. The product was re-crystallized in MeOH: chloroform to yield **4J**. (yield 56 %) Elemental analysis calcd (%) for $C_{34}H_{46}N_5O_{12}Eu \cdot 4H_2O$:C,47.01;H,5.34;N,8.06; found:C,47.19; H,5.41;N,8.20.Retention time (HPLC): = 8.12min. HRMS (+):796.2006 $(M+H)^+$ $[C_{34}H_{39}EuN_5O_8]^+$ requires 796.1992.The isotopic distribution matched closely with the simulated spectrum.

EuL2

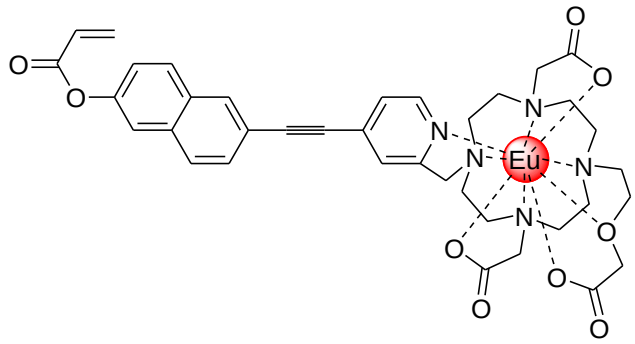

4J (20 mg, 0.025 mmol) was dissolved dry DCM (2 ml), followed by the addition of acryloyl chloride (20 mg, 0.025 mmol) in ice for half a day. The reaction was filtered

and then was washed by DCM and purified in a mixture of chloroform:MeOH to give **EuL2**. (yield:48%) Elemental analysis calcd (%) for $C_{37}H_{40}EuN_5O_9 \cdot 3H_2O$:C,49.12;H,5.12;N,7.74;found:C,49.20;H,5.26;N,7.82. Retention time (HPLC):= 8.41min.HRMS(+):850.2097$(M+H)^+$[$C_{37}H_{41}EuN_5O_9$]$^+$ requires 850.2072.The isotopic distribution matched closely with the simulated spectrum.

5E

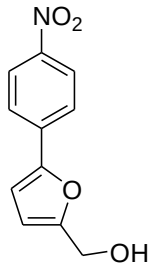

5-(4-nitrophenyl)furan-2-carbaldehyde (326mg, 1.5 mmol) was stirred in a mixture of DCM and MeOH in an ice bath and $NaBH_4$ (74mg, 2mmol) was added and stirred for overnight. The reaction mixture was quenched by addition of water and filtered to get a yellow solid and recrystalized in DCM to afford **5E**. (yield: 78%) ^{1}H NMR (400 MHz, $CDCl_3$) δ 1.84 (t, J=6.0, 6H, OH), 4.71 (d, 2H, CH_2), 6.46 (d, J=3.6, 1H, CH), 6.84 (d, J=3.6, 1H, CH), 7.80 (d, J=8.8, 2H, ArH), 8.25 (d, J=8.8, 2H, ArH) ppm; ^{13}C NMR (100 MHz, $CDCl_3$) δ 57.58, 109.71, 110.53, 123.91, 124.30, 136.21, 154.55. 155.80. MS (ESI). Calcd for $C_{11}H_{10}NO_4$ [$(M + 1)^+$] m/z 220.06. Found: m/z 220.56.

5F

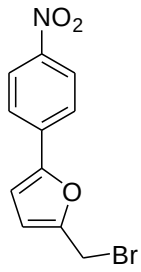

5E (263mg, 1.2 mmol) was stirred in DCM (10mL) and PBr_3 (0.12ml, 1.3mmol) was added slowly for 12 hours. Upon completion of the reaction (TLC), the reaction mixture was neutralized and extracted with DCM and evaporated under reduced pressure and

purified by the and the crude product was purified by silica column chromatography eluting with EA:hexane (1:9) to afford **5F**. (yield: 53%) ^{1}H NMR (400 MHz, $CDCl_3$) 4.58 (s, 2H, CH_2), 6.55 (d, J=3.2, H, CH), 6.82 (d, J=3.2, H, CH), 6.64 (d, J=8.4, 2H, ArH), 7.07-7.10 (m, 2H, ArH), 7.43 (d, J=8.4, 2H, ArH), 7.57-7.62 (m, 4H, ArH), 8.49 (d, J=4.8, 2H, ArH) ppm; ^{13}C NMR (100 MHz, $CDCl_3$) δ 50.62, 59.79, 102.96, 110.91, 113.18, 115.12, 121.90, 122.03, 122.90, 125.02, 136.43, 145.74, 148.95, 150.43, 154.05, 159.63. Calcd for $C_{11}H_9NO_3$ [(M + 1) $^{+}$] m/z 281.98. Found: m/z 282.22.

5H

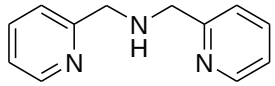

A solution of 2-pyridinecarboxaldehyde (1.03g, 9.6mmol) and 2-aminopyridine (752mg, 8mmol) was stirred under reflux in benzene (15mL) overnight. Then the solvent was evaporated under reduced pressure. EtOH (15mL) was added and $NaBH_4$ (10mmol) was then added and stirred overnight. The reaction mixture was quenched by addition of water and NH_4Cl and was extracted with EA. The crude product was purified by silica column chromatography eluting with DCM:MeOH (20:1) to afford **5H**.(yield: 32%) ^{1}H NMR (400 MHz, $CDCl_3$) δ2.67 (s, br, 1H, NH), 3.98 (s, 4H, CH_2), 7.14-7.17 (t, J= 6.8, 2H, ArH), 7.32 (d, J= 7.6, 2H, ArH), 7.62-7.66 (m,2H, ArH), 8.55-8.57 (m,2H, ArH) ppm. Calcd for $C_{12}H_{14}N_3$ [(M + 1) $^{+}$] m/z 200.12. Found: m/z 200.22.

5I

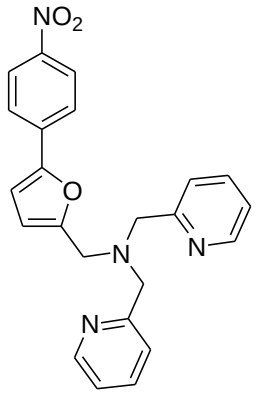

5F (226mg, 0.8mmol), K_2CO_3 (110mg, 0.8mmol) and **5H** (159mg, 0.8mmol) were stirred in ACN (10mL) and refluxed for 12 hours. Upon completion of the reaction (TLC), the reaction mixture was filtered and evaporated under reduced pressure and purified by the silica column chromatography eluting with MeOH:DCM (1:40) to afford **5I**. (yield: 45%) ^{1}H NMR (400 MHz, $CDCl_3$) 3.76-3.90 (m, 6H, CH_2), 6.22 (d, J=3.2, 2H, CH), 6.32 (d, J=3.2, 2H, CH), 7.77 (d, J=8.4, 2H, ArH), 8.22 (d, J=8.4, 2H, ArH) ppm; ^{13}C NMR (100 MHz, $CDCl_3$) δ 23.20, 110.21, 112.56, 123.57, 234.13, 124.28, 135.75, 146.62, 151.96, 152.33. Calcd for $C_{23}H_{21}N_4O_3$ [$(M + 1)^+$] m/z 401.16. Found: m/z 401.42.

5J

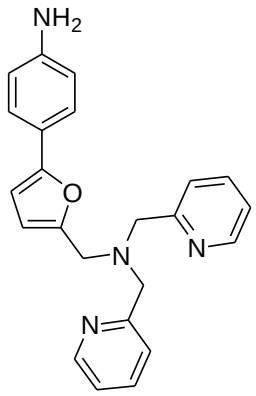

5I (176mg, 0.44 mmol) and zinc (29mg, 0.44mmol) were stirred in acetic acid (3mL) for 6 hours. Upon completion of the reaction (TLC), the reaction mixture was filtered and evaporated under reduced pressure and extracted with NaOH with DCM to afford **5J**. (yield: 45%) ^{1}H NMR (400 MHz, $CDCl_3$) δ 3.87 (s, 2H, CH_2), 3.91 (s, 4H, CH_2),

6.64 (d, J=7.6, 2H, ArH), 7.12-7.20 (m, 4H, ArH), 7.58 (d, J=7.6, 2H, ArH), 7.64-7.68 (m, 4H, ArH), 8.46-8.54 (m, 2H, ArH)ppm; ^{13}C NMR (100 MHz, $CDCl_3$) δ 50.40, 59.85, 109.85, 111.83, 122.03, 122.81, 123.59, 124.21, 136.41, 136.44, 146.05, 149.01, 151.02, 154.36, 159.16. Calcd for $C_{23}H_{23}N_4O$ [(M + 1) $^+$] m/z 371.19. Found: m/z 371.31.

5K

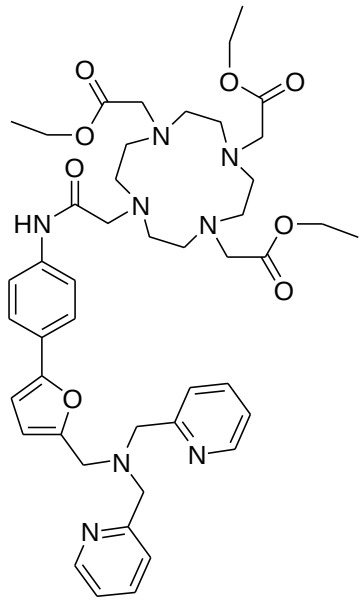

To the solution of **5J** (37mg, 0.1 mmol) and triethylamine (0.014mL, 0.1mmol) was added chloroacetyl chloride (7μL, 0.1 mmol). The reaction was stirred for 4h. The reaction mixture was filtered and combined filtrates were evaporated under reduced pressure. Without further purification, the reaction mixture was reacted with **DO3AE** (43mg, 0.1mmol) and K_2CO_3 (13mg, 0.1mmol) in dry ACN (5mL) for 12h. The reaction mixture was filtered and evaporated under reduced pressure and purified by the and the crude product was purified by silica column chromatography eluting with MeOH:DCM (1:20) to afford **5K**. (yield: 41%) ^{1}H NMR (400 MHz, $CDCl_3$) 1.23-1.29 (m, 9H, CH_3), 2.39-3.21 (m, 24H, CH_2), 3.92 (s, 2H, CH_2), 4.12-4.20 (m, 10H, CH_2), 6.34 (d, J=3.2, 1H, CH), 6.41 (d, J=3.2, 1H, CH), 7.29-7.32 (m, 2H, ArH), 7.40 (d, J=8.4, 2H, ArH), 7.47 (d, J=8.0, 2H, ArH), 7.60 (d, J=8.4, 2H, ArH), 7.60 (t, J=8.4, 2H, ArH), 8.27 (s, 1H, ArH), 8.59-8.61 (m, 1H, ArH) ppm; ^{13}C NMR (100 MHz, $CDCl_3$) δ 14.12, 50.94, 55.11, 58.10, 61.34, 105.11, 112.52, 120.17, 123.38, 123.64, 123.93, 126.24, 137.40, 139.04,

147.11, 153.66, 156.68, 170.70, 173.38. Calcd for $C_{45}H_{60}N_8O_8Na$ $[(M + Na)^+]$ m/z 863.44. Found: m/z 863.00.

EuL3

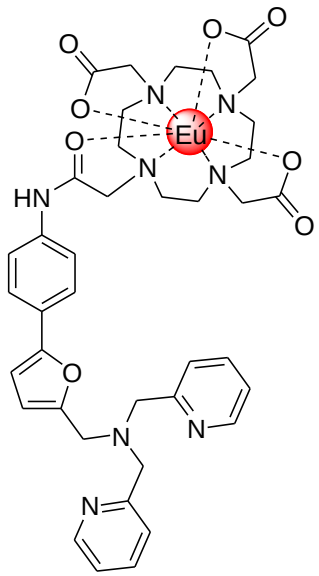

To the solution of **5K** (15mg, 0.02 mmol) in THF was added LiOH (0.01 M). The reaction was stirred at room temperature overnight. The reaction mixture was filtered and purfied by washing with diethyl ether:DCM (3:1) to obtain a yellow solid which was then dissolved in D.I. water. The pH was adjusted to 7 and the reaction was refluxed with 1 eqv. of $EuCl_3 \cdot 6H_2O$ (2 mg, 0.002 mmol) in overnight. The pH of the reaction mixture was adjusted to 6 and filtered and combined filtrates were evaporated under reduced pressure. The product was re-crystallized in MeOH: chloroform to yield **EuL3**. (yield:40%) Elemental analysis calcd (%) for $C_{39}H_{45}N_8O_8Eu \cdot 5H_2O$: C,47.04;H,5.57;N,11.25; found:C,47.71; H,5.87;N,11.60. HRMS (+):927.2451 $(M+Na)^+$ $[C_{39}H_{45}N_8O_8NaEu]^+$ requires 927.2451.The isotopic distribution matched closely with the simulated spectrum.

5L

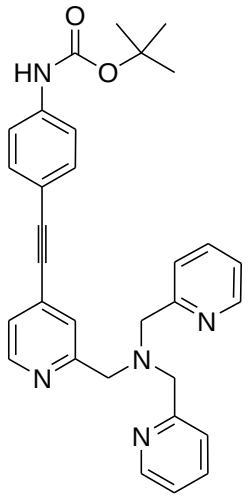

5H (55.8mg, 0.28 mmol), **3C** (108mg, 0.28 mmol) and K_2CO_3 (77mg, 0.56mmol) were stirred in dry ACN (10mL) overnight. Upon completion of the reaction (TLC), the reaction mixture was filtered and purified by silica column chromatography eluting with MeOH: DCM (1:15) to afford **5L**. (yield:49%) ^{1}H NMR (400 MHz, $CDCl_3$) δ 1.49 (s, 9H, CH_3), 3.89-3.92 (m 6H, CH_2), 4.06 (s, 2H, CH_2), 7.13-7.18 (m, 3H, ArH), 7.44-7.50 (m, 4H, ArH), 7.58-7.69 (m, 6H, ArH), 8.49-8.54 (m, 2H, ArH) ppm; ^{13}C NMR (100 MHz, $CDCl_3$) δ 28.24, 54.13, 59.94, 60.20, 80.69, 86.32, 93.98, 115.96, 118.09, 122.04, 122.16, 122.40, 123.01, 123.08, 124.57, 132.09, 132.73, 136.47, 136.56, 139.73, 148.95, 149. 05, 149.23, 152.55, 158.41, 159.05. Calcd for $C_{31}H_{32}N_5O_2$ [$(M + 1)^+$] m/z 506.26. Found: m/z 506.10.

5M

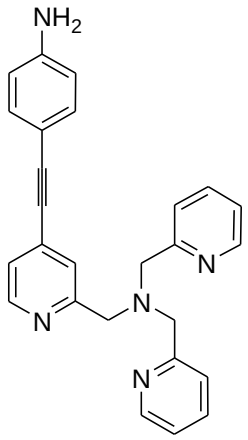

5H (40mg, 0.08mmol) was stirred in the solution of TFA and DCM (1:1) overnight.

Upon completion of the reaction (TLC), the reaction mixture was filtered and evaporated under reduced pressure. The crude product was washed by solution of diethyl ether and DCM. Yield: 60% ^{1}H NMR (400 MHz, $CDCl_3$) δ 3.87(s, 2H, CH_2), 3.91 (s, 4H, CH_2), 6.64 (d, J=8.4Hz, 2H, ArH), 7.12-7.29 (m, 4H, ArH), 7.57-7.68 (m, 4H, ArH), 8.46-8.54 (m, 2H, ArH) ppm; ^{13}C NMR (100 MHz, $CDCl_3$) δ 60.03, 60.25, 85.37, 95.06, 110.98, 114.60, 121.96, 122.02,122.78, 123.02, 123.69, 124.44, 130.44, 132.54, 133.37, 136.45, 147.70, 148.88, 149.04, 149.26, 159.17, 159.35. Calcd for $C_{26}H_{24}N_5$ [$(M + 1)^+$] m/z 406.20. Found: m/z 406.11.

5N

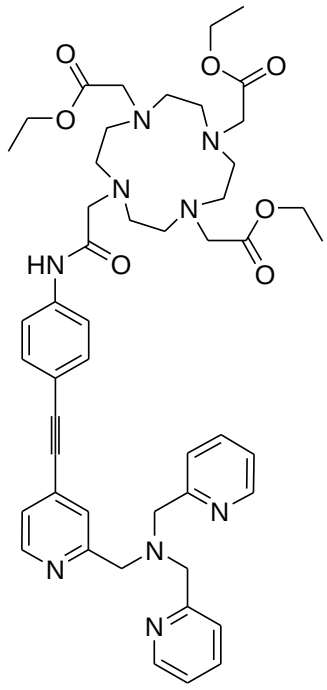

To the solution of **5M** (30mg, 0.07 mmol) and triethylamine (0.011mL, 0.07mmol) was added chloroacetyl chloride (6μL, 0.07 mmol). The reaction was stirred for 6h. The reaction mixture was filtered and combined filtrates were evaporated under reduced pressure. Without further purification, the reaction mixture was reacted with **DO3AE** (30mg, 0.07mmol) and K_2CO_3 (10mg, 0.07mmol) in dry ACN (5mL) for 12h. The reaction mixture was filtered and evaporated under reduced pressure and purified by the silica column chromatography eluting with MeOH:DCM (1:10) to afford **5N**. (yield:

57%) ^{1}H NMR (400 MHz, $CDCl_3$) δ 1.27 (t, J=6Hz, 9H, CH_3), 2.42-3.19 (s, 26H, CH_2), 3.78 (s, br, 4H, CH_2), 4.16-4.18 (m, 6H, CH_2), 7.22-7.38 (m, 8H, ArH), 7.61-7.68 (m, 4H, ArH), 8.36 (s, 1H, ArH), 8.55-8.70 (m, 2H, ArH) ppm; ^{13}C NMR (100 MHz, $CDCl_3$) δ 14.06, 14.12, 51.81, 54.97, 55.09, 55.21, 56.87, 58.91, 61.10, 61,.24, 61.33, 114.61, 116.82, 119.74, 122.08, 122.39, 122.64, 123.11, 124.67, 124.82, 125.18, 132.4, 13.52, 137.51, 150.50, 156.89, 171.14, 173.15, . Calcd for $C_{48}H_{61}N_9N_7Na$ [$(M + Na)^+$] m/z 898.46. Found: m/z 898.12.

EuL4

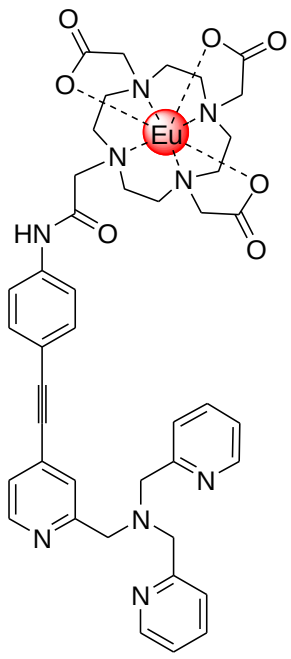

To the solution of **5N** (17mg, 0.02 mmol) in THF was added LiOH (0.01 M). The reaction was stirred at room temperature overnight. The reaction mixture was filtered and purfied by washing with DCM to obtain an oily product which was then dissolved in D.I. water. pH was adjusted to 7 and the reaction was refluxed with 1 eqv. of $EuCl_3 \cdot 6H_2O$ (2 mg, 0.002 mmol) in overnight. The pH of the reaction mixture was adjusted to 6 and filtered and combined filtrates were evaporated under reduced pressure. The product was re-crystallized in MeOH: chloroform to yield **EuL4**. (yield:52%) Elemental analysis calcd (%) for $C_{42}H_{46}N_9O_7Eu \cdot 4H_2O$:C,49.8;H,5.37;N,12.45; found:C,50.12;H,5.41; N,12.60. HRMS (+):481.6344 $(M+H+Na)^{2+}$

$[C_{42}H_{47}N_9O_7EuNa]^{2+}$ requires 481.6342. The isotopic distribution matched closely with the simulated spectrum.

5O

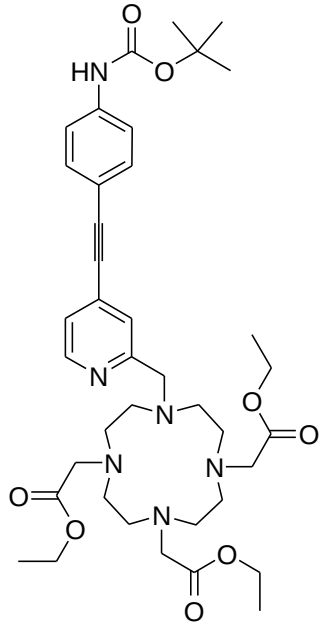

DO3AE (241mg, 0.56 mmol), **3C** (217mg, 0.56 mmol) and K_2CO_3 (154mg, 1.12mmol) were stirred in dry ACN (10mL) overnight. Upon completion of the reaction (TLC), the reaction mixture was filtered and purified by silica column chromatography eluting with MeOH: DCM (1:25) to afford **5O**. (yield:39%) ^{1}H NMR (400 MHz, $CDCl_3$) δ 1.24-1.33 (m, 9H, CH_3), 1.52 (s, 9H, CH_2), 2.38-3.22 (m, 26H, CH_2), 4.16-4.25 (m, 8H, CH_2), 7.23 (d, J=5.2Hz, 1H, ArH), 7.29 (s, 2H, NH) ,7.45-7.46 (m, 3H, ArH) , 7.56 (d, J=8Hz, 2H, ArH), 7.45-7.46 (m, J=5.2Hz, 3H, ArH) ppm; ^{13}C NMR (100 MHz, $CDCl_3$) δ 614.14, 28.27, 50.32, 55.25, 55.49, 58.88, 61.16, 61.27, 80.81, 85.42, 95.48, 118.22, 123.99, 125.55, 132.78, 132.96, 140.07, 148.89, 152.55, 158.75, 173.51. Calcd for $C_{39}H_{55}N_6O_8Na_2$ [(M-H + 2Na) $^+$] m/z 781.40. Found: m/z 781.33.

5P

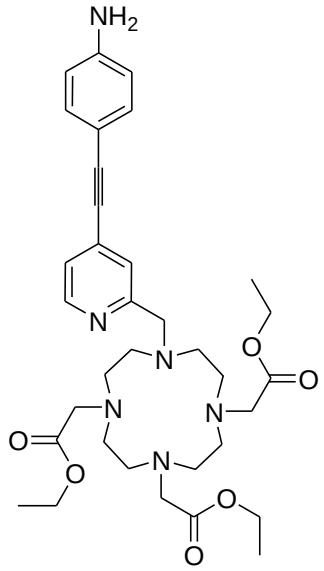

5O (60mg, 0.08mmol) was stirred in the solution of TFA and DCM (1:1) overnight. Upon completion of the reaction (TLC), the reaction mixture was filtered and evaporated under reduced pressure. The crude product was washed by solution of diethyl ether and DCM to obtain **5P**. Yield: 37% ^{1}H NMR (400 MHz, $CDCl_3$) δ 1.23-1.33 (m, 9H, CH_3), 2.36-3.41 (s, 26H, CH_2), 4.12-4.24 (m, 8H, CH_2), 6.73 (d, J=8.4Hz, 2H, ArH), 7.18 (d, J=5.2Hz, 1H, ArH) , 7.24 (s, 1H, ArH), 7.29 (d, J=8.4Hz, 2H, ArH), 8.13 (m, J=5.2Hz, 3H, ArH) ppm; ^{13}C NMR (100 MHz, $CDCl_3$) δ 14.07, 50.14, 55.11, 55.34, 58.75, 61.10, 61.23, 84.32, 97.33, 108.96, 114.53, 123.67, 125.17, 133.28, 133.50, 148.64, 149.10, 158.36, 173.36. Calcd for $C_{34}H_{47}N_6O_6Na_2$ $[(M-H+2Na)^+]$ m/z 680.34. Found: m/z 680.43.

5R

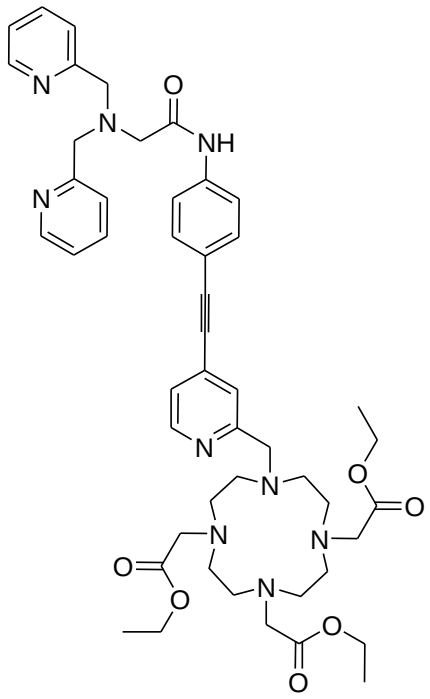

To the solution of **5P** (45mg, 0.07 mmol) and triethylamine (0.011mL, 0.07mmol) was added chloroacetyl chloride (7μL, 0.07 mmol). The reaction was stirred for 6h. The reaction mixture was filtered and combined filtrates were evaporated under reduced pressure. Without further purification, the reaction mixture was reacted with **DO3AE** (30mg, 0.07mmol) and K_2CO_3 (10mg, 0.07mmol) in dry ACN (5mL) for 12h. The reaction mixture was filtered and evaporated under reduced pressure and purified by silica column chromatography eluting with MeOH:DCM (1:15) to afford **5R**. (yield: 40%) ^{1}H NMR (400 MHz, $CDCl_3$)δ 1.23-1.33 (m, 9H, CH_3), 2.37-3.42 (s, 26H, CH_2), 3.49 (s, 2H, CH_2), 4.14 (s, 4H, CH_2), 4.22-4.24 (m, 8H, CH_2), 7.19-7.23 (m, 3H, ArH), 7.51-7.53 (m, 2H, ArH), 7.65-7.67 (m, 5H, ArH), 8.19-8.20 (m, 2H, ArH),8.61-8.40 (m, 2H, ArH) ppm; ^{13}C NMR (100 MHz, $CDCl_3$) δ14.12, 38.57, 40.28, 44.72, 50.11, 55.16, 55.16, 55.42, 58.79, 60.19, 61.24, 61.34, 119.52, 121.87, 122.22, 122.72, 123.40, 124.09, 125.62, 126.24, 132.40, 132.73, 136.79, 137.29, 146.79, 148.29, 148.89, 149.30, 149.47, 157.76, 158.71, 173.51. Calcd for $C_{48}H_{60}N_9O_7Na_2$ [(M-H + 2Na)$^+$] m/z 920.45. Found: m/z 920.65.

EuL5

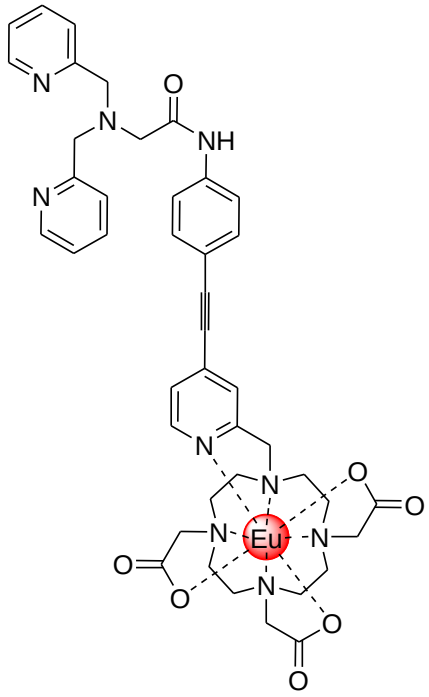

To the solution of **5R** (15mg, 0.02 mmol) in THF was added LiOH (0.01 M). The reaction was stirred at room temperature overnight. The reaction mixture was filtered and purfied by washing with DCM to obtain an oily product which was then dissolved in D.I. water. The pH was adjusted to 6 and reaction was refluxed with 1 eqv. of $EuCl_3 \cdot 6H_2O$ (2 mg, 0.002 mmol) overnight. The pH of the reaction mixture was adjusted to 6 and filtered and combined filtrates were evaporated under reduced pressure. The product was re-crystallized in MeOH: chloroform to yield **EuL5**. (yield:40%) Elemental analysis calcd (%) for Elemental analysis calcd (%) for $C_{42}H_{46}N_9O_7Eu \cdot 5H_2O$:C,49.8;H,5.37;N,12.45; found:C,50.01;H,5.65;N,12.50. HRMS (+):940.2786 $(M+H)^+$ $[C_{42}H_{47}N_9O_7Eu]^+$ requires 940.2791. The isotopic distribution matched closely with the simulated spectrum.

6A

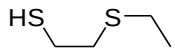

2-chloroethylethyl sulfide (1.6 g, 13 mmol) and thiourea (1.0 g, 13 mmol) were refluxed under N_2 atmosphere. After all thiourea had dissolved in a very viscous solution, the reaction mixture was cooled down and hydrolyzed by the addition of 2.5 mL of 10 M NaOH and then stirred overnight. The mixture was acidified with 12 M HCl to pH 2-3 and extracted with diethyl ether. The organic extract was dried (Mg_2SO_4) and concentrated in vacuo to obtain **6A** (yield:64%). ^{1}H NMR ($CDCl_3$, 400 MHz) δ 1.27 (t, J=7.6 Hz, 3H, CH_3), 1.71-1.75 (m, 1H, SH), 2.59 (dd, J=7.6Hz, 2H, CH_2), 2.69-2.86 (m, 4H, CH_2); 13C NMR ($CDCl_3$, 100 MHz) δ14.7, 24.6, 25.7, 35.6.

6B

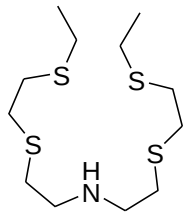

6a (1g, 8.20mmol), K_2CO_3 (1.13g, 8.20mmol) and bis(2-chloroethyl)amine (582mg, 4.10mmol) were refluxed in dry ACN (8mL) overnight. Upon completion of the reaction (TLC), the crude product was purified by silica column chromatography eluting with PE: EA (30:1) to obtain **6B** as a slightly yellow liquid (Yield: 52%). ^{1}H NMR ($CDCl_3$, 400 MHz) δ 1.27 (t, J=7.2 Hz, 3H, CH_3), 2.58 (dd, J=7.6Hz, 4H, CH_2), 2.71-2.74 (m, 12H, CH_2), 2.84 (t, J=6.8Hz, 4H, CH_2); ^{13}C NMR ($CDCl_3$, 100 MHz) δ 14.09, 26.33, 30.11, 47.16, 49.95.

6C

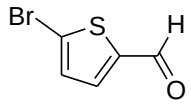

To the solution of $NaHCO_3$ (1.26 g, 0.015mol) and thiophene-2-carbaldehyde (1.62 g, 0.014 mol) in chloroform, bromine (0.74 mL, 0.014 mol) was added dropwise. The reaction mixture was stirred at room temperature overnight. Upon completion of the reaction (TLC), D.I. water was added into the reaction mixture. The water layer was extracted with DCM and the organic layers were combined and dried with $MgSO_4$. The crude product was purified by silica column chromatography eluting with PE:EA (20:1) to obtain **6C** as a yellow liquid (Yield: 87%).^{1}H NMR ($CDCl_3$, 400 MHz) δ 7.20 (d, J=4.0 Hz, 1H, CH), 7.53(d, J=4.0 Hz, 4H, CH), 9.78 (s, 1H, CHO); ^{13}C NMR ($CDCl_3$, 100 MHz) δ 128.29, 135.09, 136.27, 144.04, 182.96.

6D

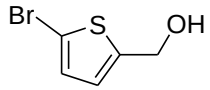

To the solution of **6C** (1.20 g, 6.28 mmol) in MeOH (10mL), $NaBH_4$ (237mg, 6.28mmol) was added portionwise. The reaction was stirred for 4h at room temperature. Upon completion of the reaction (TLC), the solvent was evaporated under reduced pressure. The crude product was purified by silica column chromatography eluting with PE: EA (15:1) to obtain **6D** as a yellow liquid (Yield: 80%).^{1}H NMR (400 MHz, $CDCl_3$) δ 4.72 (s, 1H, CH_2), 6.74 (d, J=3.6 Hz, 1H, CH), 6.91(d, J=3.6 Hz, 4H, CH); ^{13}C NMR ($CDCl_3$, 100 MHz) δ 60.05, 112.20, 125.66, 129.56, 145.68.

6E

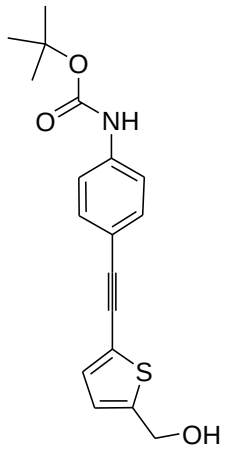

6D (729mg, 3.68 mmol) was dissolved in dry THF (5 mL) and triethylamine (10 mL) under an atmosphere of nitrogen. Copper(I) iodide (19mg,0.1mmol), triphenylphosphine (78.6mg, 0.3mmol) and dichlorobis(triphenylphosphine) palladium(II) (35mg, 0.05 mmol) were added to the solution. Tert-butyl 4-ethynylphenylcarbamate (798mg, 3.68 mmol) was added to the mixture which was then heated to 70 ^{0}C for 12 h. The crude product was purified by silica column chromatography eluting with PE:EA (10:1) to afford **6E**. (yield: 53%) ^{1}H NMR (400 MHz, $CDCl_3$) δ 1.52 (s, 9H, CH_3), 2.18 (s, br, 1H, OH), 4.77 (s, 2H, CH_2), 6.67 (s, 1H, ArH), 6.87 (s, 1H, ArH), , 7.10 (s, 1H, ArH), 7.33 (d, J=7.2 Hz,ArH), 7.42 (d, J=.7.2 Hz,ArH); ^{13}C NMR ($CDCl_3$, 100 MHz) δ 28.29, 60.04, 93.15, 117.06, 118.10, 123.55, 125.21, 131.53, 132.27, 138.0, 145.63, 152.45. Calcd for $C_{18}H_{20}NO_3S$ [$(M + H)^+$] m/z 330.12. Found: m/z.330.26.

6F

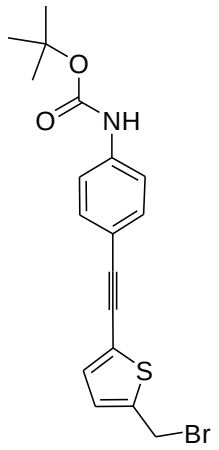

6E (510mg, 1.55mmol), triphenyl phosphine (487mg, 1.86mmol), tetrabromomethane (616mg, 1.86mmol) were stirred at room temperature overnight. Upon completion of the reaction (TLC), the solvent was evaporated under reduced pressure. The crude product was purified by silica column chromatography eluting with PE:EA (20:1) to obtain **6F** as a yellow liquid (Yield: 58%).^{1}H NMR (400 MHz, $CDCl_3$) δ 1.50 (s, 9H, CH_3), 4.55 (s, 2H, CH_2), 6.85 (d, J=3.6Hz, 1H, ArH), 7.09 (d, J=3.2Hz, 1H, ArH), 7.37 (dd, J=8.4Hz, 1H, ArH); ^{13}C NMR ($CDCl_3$, 100 MHz) δ 28.31, 57.74, 68.96,80.79, 81.91, 93.28, 116.93, 118.12, 123.87, 126.36, 131.37, 132.22, 138.82, 142.46, 152.54. Calcd for $C_{18}H_{19}NO_2SBr$ [$(M + H)^+$] m/z 394.03. Found: m/z.394.16.

6G

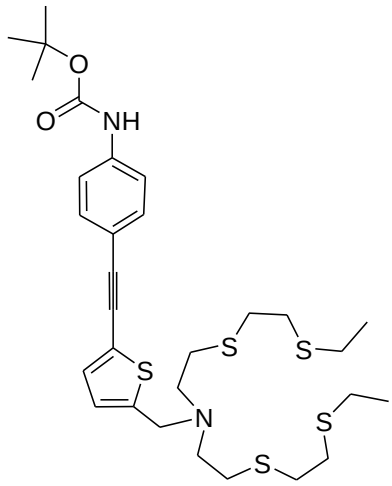

6F (300mg, 0.77mmol), K_2CO_3 (106mg 0.77mmol) and **6B** (239mg, 0.77mmol) were stirred at room temperature overnight. The reaction mixture was filtered and purified by silica column chromatography eluting with PE:EA (20:1) to obtain **6G** as a yellow liquid (yield: 49%) ^{1}H NMR (400 MHz, $CDCl_3$) δ 1.26 (t, J= 7.2, 6H, CH_3), 1.52 (s, 9H, CH_3), 2.57 (t, J= 7.2, 4H, CH_2), 2.67-2.77 (m, 16H, CH_2), 6.79 (d, J=3.2Hz, 1H, ArH), 7.08 (d, J=3.6Hz, 1H, ArH), 7.35 (d, J=8.4Hz, 2H, ArH) , 7.42 (d, J=8.4Hz, 2H, ArH); ^{13}C NMR ($CDCl_3$, 100 MHz) δ 14.82, 26.06, 28.29, 30.24, 31.79, 32.42, 53.21, 53.81, 80.91, 82.10, 92.96, 117.17, 11.02, 122.92, 125.55, 131.32, 132.21, 138.52, 144.46, 152.34. Calcd for $C_{30}H_{45}N_2O_2S_5$ $[(M + H)^+]$ m/z 625.21. Found: m/z.625.15.

6H

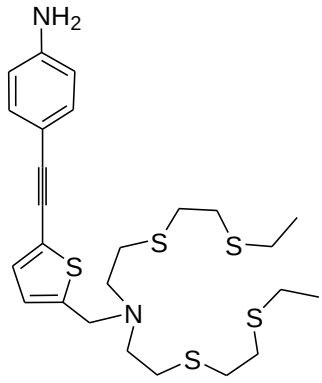

To the solution of **6G** (150mg, 0.24mmol) in THF, conc HCl (2mL) was added dropwise. The reaction was stirred at room temperature for 4h. Upon completion of the reaction (TLC), D.I. water (20mL) and DCM (20mL) were added. The organic layer

was extracted and evaporated under reduced pressure. The crude product was purified by silica column chromatography eluting with PE:EA (5:1) to obtain **6H** (Yield: 48%). ^{1}H NMR (400 MHz, $CDCl_3$) δ 1.26 (t, J= 7.6, 6H, CH_3), 2.58 (dd, J= 7.2, 4H, CH_2), 2.80 (s, 12H, CH_2), 3.04 (m, 4H, CH_2), 6.65 (d, J=8.4Hz, 2H, ArH), 7.30 (d, J=8.4Hz, 2H, ArH); ^{13}C NMR ($CDCl_3$, 100 MHz) δ 14.84, 26.06, 30.23, 31.81, 32.43, 53.18, 53.80, 80.73, 93.84, 112.10, 114.68, 123.49, 125.55, 130.76, 132.77, 143.77, 146.84. Calcd for $C_{25}H_{37}N_2S_5$ $[(M + H)^+]$ m/z 525.16. Found: m/z.525.05.

6J

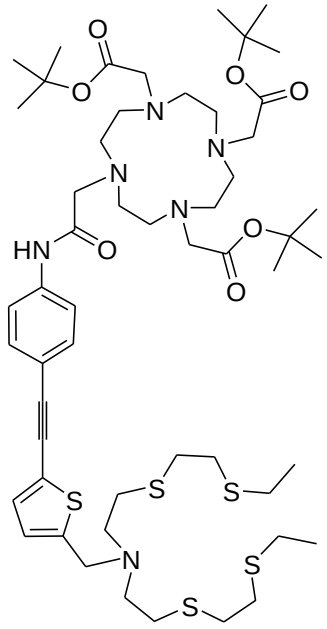

To the solution of **6H** (80mg, 0.15 mmol) and triethylamine (0.021mL, 0.15mmol) was added chloroacetyl chloride (11μL, 0.15 mmol). The reaction was stirred for 8h. The reaction mixture was filtered and combined filtrates were evaporated under reduced pressure. Without further purification, the reaction mixture was reacted with **DO3AE** (77mg, 0.15mmol) and K_2CO_3 (20mg, 0.15mmol) in dry ACN (5mL) overnight. The reaction mixture was filtered and evaporated under reduced pressure and purified by silica column chromatography eluting with MeOH:DCM (1:20) to afford **6J**. (yield: 30%) ^{1}H NMR (400 MHz, $CDCl_3$) δ 1.26 (t, J= 7.2, 6H, CH_3), 1.48 (m, 27H, CH_2), 2.54-2.78 (m, 42H, CH_2), 3.75-3.85 (m, 4H, CH_2), 6.78 (d, J=3.2Hz, 1H, ArH), 7.08 (d,

J=3.6Hz, 2H, ArH), 7.32 (d, J=8.8Hz, 2H, ArH), 7.93 (d, J=8.4Hz, 2H, ArH) ; ^{13}C NMR ($CDCl_3$, 100 MHz) δ16.22, 27.49, 29.32, 29.38, 29.53, 31.06, 31.65, 33.23, 33.89, 5447, 55.16, 56.41, 56.96, 57.05, 83.77, 121.18, 128.83, 133.19, 134.03, 143.25, 168.61, 172.43, 173.76. Calcd for $C_{53}H_{86}N_6O_7S_5Na$ [$(M + Na)^+$] m/z 1101.51. Found: m/z 1101.90.

EuL6

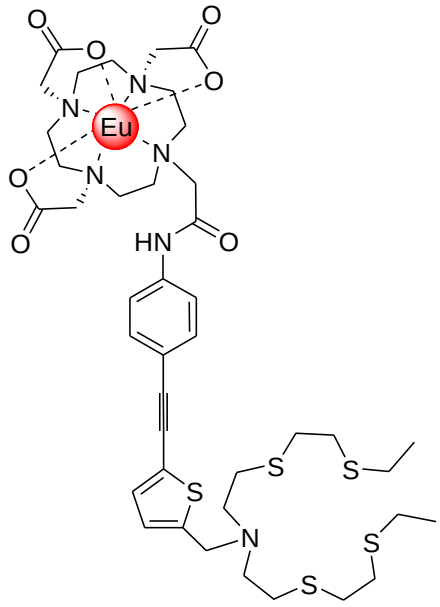

To the solution of **6J** (20mg, 0.02 mmol) in THF was added LiOH (0.01 M). The reaction was stirred at room temperature overnight. The reaction mixture was filtered and purfied by washing with DCM to obtain an oily product which was then dissolved in D.I. water. The pH was adjusted to 7 and reaction was refluxed with 1 eqv. of $EuCl_3 \cdot 6H_2O$ (2 mg, 0.002 mmol) overnight. The pH of the reaction mixture was adjusted to 6 and filtered and combined filtrates were evaporated under reduced pressure. The product was re-crystallized in DCM: MeOH: chloroform to yield **EuL6**. (yield:51%) Elemental analysis calcd (%) for $C_{41}H_{59}N_6O_7EuS_5 \cdot 3H_2O$:C,44.2;H,5.88;N,7.54; found: 44.59;H, 5.61;N,7.20. HRMS (+):552.1018 $(M+2Na)^{2+}$ $[C_{41}H_{59}N_6O_7S_5EuNa_2]^{2+}$ requires 552.1016. The isotopic distribution matched closely with the simulated spectrum.

6K

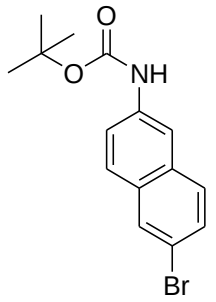

6-bromonaphthalen-2-amine (2g, 9.0mmol) and Boc_2O (1.96g, 9.0mmol) were refluxed in THF (6mL) for 24h. Upon completion of the reaction (TLC), the reaction mixture was filtered and purified through by silica column chromatography eluting with PE:EA (20:1) to obtain **6K**. (yield: 53%) ^1H NMR (400 MHz, $CDCl_3$) δ 1.55 (s, 9H, CH_3), 6.76 (s, 1H, NH), 7.32 (dd, J=2Hz, 1H, ArH), 7.46-7.49 (m, 1H, ArH), 7.57-7.63 (m, 2H, ArH), 7.88 (s, H, ArH), 7.98 (s, H, ArH); ^{13}C NMR ($CDCl_3$, 100 MHz) δ28.34, 80.91, 114.32, 118.08, 120.06, 127.82, 129.02, 129.51, 129.76, 130.94, 132.48, 136.20, 152.72. Calcd for $C_{15}H_{17}NO_2Br$ $[(M + H)^+]$ m/z 322.04. Found: m/z 322.16.

6L

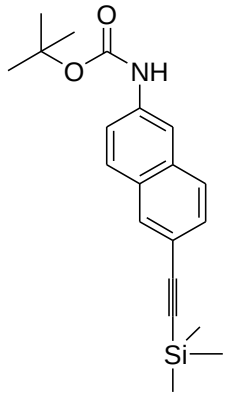

Dry triethylamine (10 mL) was first mixed with dry THF (5mL), followed by addition of **6K** (1.5 g, 4.66 mmol) under an atmosphere of nitrogen. Triphenylphosphine (104 mg, 0.04 mmol), dichlorobis(triphenylphosphine)palladium(II) (105 mg, 0.015 mmol) and copper(I) iodide (20 mg, 0.01 mmol) were added to the reaction mixture and heated to 70°C for 12 h. The reaction mixture was then filtered and evaporated under reduced pressure. The crude product was purified by silica column chromatography eluting with

EA:PE (1:30) to afford **6L**. (yield: 66%) ^{1}H NMR (400 MHz, $CDCl_3$) δ 0.69 (s, 9H, CH_3), 1.91 (s, 9H, CH_3), 7.48 (s, 1H, NH), 7.63-7.74 (m, 2H, ArH), 7.82-7.84 (m, 1H, ArH), 7.95-8.00 (m, 2H, ArH), 8.28-8.32 (m, 1H, ArH); ^{13}C NMR ($CDCl_3$, 100 MHz) δ0.09, 28.36, 80.80, 94.12, 105.75, 114.33, 118.86, 119.81, 127.32, 128.62, 129.18, 129.32, 131.66, 133.63, 136.79, 152.81.

6M

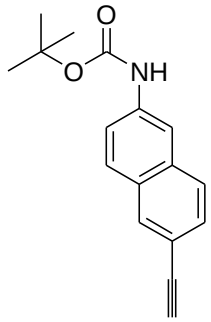

6L (1.0 g, 2.95 mmol) was dissolved in dry THF (10mL) and then Tetra-n-butylammonium fluoride (770mg, 2.95mmol) was added the reaction mixture. The reaction was stirred for 6h. Upon completion of the reaction (TLC), the crude product was purified by silica column chromatography eluting with EA: PE (1:25) to afford **6M**. (yield: 46 %) ^{1}H NMR (400 MHz, $CDCl_3$) δ 1.55 (s, 9H, CH_3), 3.12 (s, 1H, CH), 7.48 (s, 1H, NH), 6.66 (s, 1H, NH), 7.32-7.35 (m, 1H, ArH), 7.47-7.49 (m, 1H, ArH), 7.69-7.72 (m, 1H, ArH), 7.93 (s, 1H, ArH), 8.00 (s, 1H, ArH); ^{13}C NMR ($CDCl_3$, 100 MHz) δ28.35, 80.84, 84.22, 114.27, 117.79, 119.87, 127.45, 128.61,128.61, 129.14, 129.25, 131.9, 133.77, 136.93, 150.82. Calcd for $C_{17}H_{18}NO_2$ [$(M + H)^+$] m/z 268.13. Found: m/z 268.32.

6N

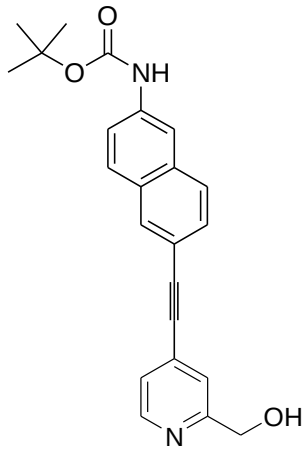

6M (800mg, 3.00 mmol) was dissolved in dry THF (8 mL)and triethylamine (15 mL) under an atmosphere of nitrogen. Copper(I) iodide (22.8mg, 0.12mmol), triphenylphosphine (94.3mg, 0.36mmol) and dichlorobis(triphenylphosphine) palladium(II) (42mg, 0.06 mmol) were added to the stirred solution. Tert-butyl (4-bromopyridin-2-yl)methanol (564mg, 3.00 mmol) was added to the mixture and the mixture was heated to 60 ^{0}C for 12 h. The crude product was purified by silica column chromatography eluting with PE:EA (10:1) to afford **6M**. (yield: 46%) ^{1}H NMR (400 MHz, $CDCl_3$) δ 1.56 (s, 9H, CH_3), 4.79 (s, 2H, CH_2), 6.84 (s, 1H, NH), 7.31-7.40 (m, 3H, ArH), 7.50-7.53 (m, 2H, ArH), 7.72-7.75 (m, 2H, ArH),7.79-8.03 (m, 2H, ArH), 8.54-8.55 (m, 2H, ArH); ^{13}C NMR ($CDCl_3$, 100 MHz) δ 28.36, 80.80, 94.12, 105.75, 114.33, 118.86, 119.81, 127.32, 128.62, 129.18, 129.32, 1311.66, 133.63, 136.79, 152.81. Calcd for $C_{23}H_{23}N_2O_3Br$ [$(M + H)^+$] m/z 375.17. Found: m/z 375.35.

6O

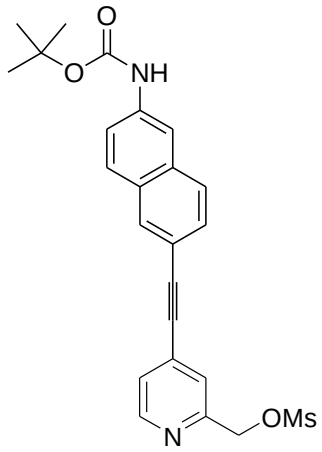

6N (509mg, 1.36mmol), MsCl (0.32mL, 4.08mmol), triethylamine (8ml) were stirred in DCM at room temperature for 8h. Upon completion of the reaction (TLC), D.I. water (10mL) was added to reaction mixture and the organic layer was extracted and evaporated under reduced pressure. The crude product was purified by silica column chromatography eluting with PE:EA (10:1) to obtain **6O** (Yield: 55%).^{1}H NMR (400 MHz, $CDCl_3$) δ 1.56 (s, 9H, CH_3), 3.12 (s, 3H, CH_3), 5.34 (s, 2H, CH_2), 6.73 (s, 1H, NH), 7.35-7.41 (m, 3H, ArH), 7.52-7.55 (m, 1H, ArH), 7.59 (s, 1H, ArH),7.75-7.77 (m, 2H, ArH), 8.60 (d, J=5.2Hz, 1H, ArH); ^{13}C NMR ($CDCl_3$, 100 MHz) δ 228.32, 38.08, 71.05, 81.03, 86.30, 95.66, 114.16, 117.42, 119.90, 124.08, 125.35, 127.71, 128.77, 128.90, 129.28, 132.09, 132.9, 13.13, 137.25, 149.61, 152.59.

6P

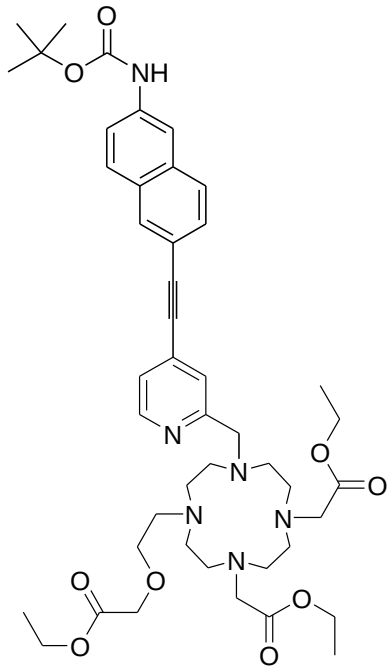

6O (100mg, 0.221mmol), K_2CO_3 (30mg, 0.221mmol) and **DO3A-ME** (105mg, 0.221mmol) were stirred in dry ACN (10mL) overnight. Upon completion of the reaction (TLC), the reaction mixture was filtered and evaporated under reduced pressure and purified by silica column chromatography eluting with MeOH:DCM (1:20) to afford **6P**. (yield: 45%).^{1}H NMR (400 MHz, $CDCl_3$) δ 1.17-1.18 (m, 9H, CH_3), 1.48 (s, 9H, CH_3), 2.06-2.88 (m, 20H, CH_2), 3.16-3.28 (m, 2H, CH_2), 3.61-3.72 (m, 4H, CH_2), 4.04 (s, 8H, CH_2), 7.13-7.22 (m, 2H, ArH), 7.42-7.44 (m, 2H, ArH), 7.67 (s, 3H, ArH), 7.92-8.03 (m, 2H, ArH), 8.23 (s, 1H, ArH); ^{13}C NMR ($CDCl_3$, 100 MHz) δ 14.12, 28.31, 49.65, 50.33, 51.99, 55.93, 58.91, 60.90, 61.21, 67.59, 68.40, 80.79, 86.19, 114.03, 117.12, 120.24, 124.03, 125.49, 127.69, 128.54, 128.74, 129.14, 132.03, 132.65, 149.15, 152.79, 158..39, 170.27, 172.92. Calcd for $C_{45}H_{62}N_6O_9Na$ [$(M + Na)^+$] m/z 853.45. Found: m/z 853.36.

6Q

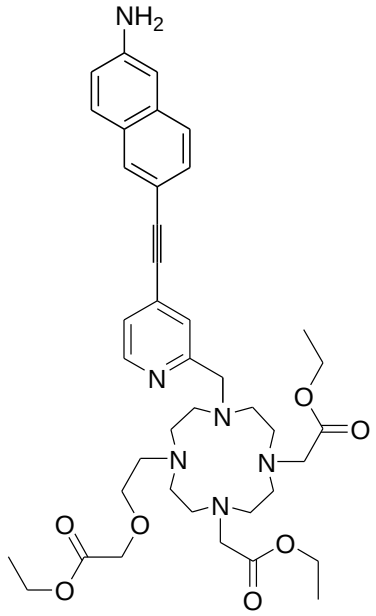

6P (82mg, 0.99mmol) was stirred in the solution of TFA and DCM (1:1) overnight. The reaction mixture was filtered and evaporated under reduced pressure. Upon completion of the reaction (TLC), the crude product was washed by solution of diethyl ether and DCM to obtain **6Q**. Yield: 80% ^{1}H NMR (400 MHz, $CDCl_3$) δ 1.07-1.16 (m, 9H, CH_3), 2.99-3.17 (m, 8H, CH_2), 3.41-3.56 (m, 12H, CH_2), 3.84-4.07 (m, 8H, CH_2), 7.34-7.36 (m, 1H, ArH), 7.45-746 (m, 1H, ArH), 7.53-7.67 (m, 3H, ArH), 7.67 (s, 1H, ArH), 7.67-7.80 (m, 1H, ArH), 7.88-7.90 (m, 1H, ArH), 8.40 (s, 1H, ArH); ^{13}C NMR ($CDCl_3$, 100 MHz) δ 13.08, 50.89, 51.78, 52.99, 54.16, 57.21, 60.84, 61.15, 65.32, 67.55, 121.11, 125.19, 125.40, 127.75, 129.11, 130.07, 132.02, 133.01, 133.56, 148.87, 150.83, 170.45, 171.89. Calcd for $C_{40}H_{54}N_6O_7Na$ [$(M + Na)^+$] m/z 753.40. Found: m/z 753.36.

6H

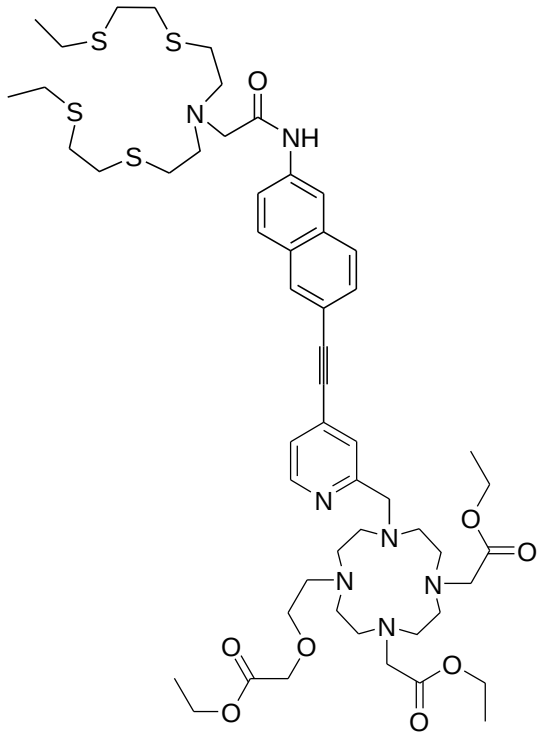

To the solution of **6Q** (61mg, 0.08 mmol) and triethylamine (0.011mL, 0.08mmol) was added chloroacetyl chloride (9μL, 0.08 mmol). The reaction was stirred for 8h. The reaction mixture was filtered and combined filtrates were evaporated under reduced pressure. Without further purification, the reaction mixture was reacted with **6B** (24mg, 0.05mmol) and K_2CO_3 (10mg, 0.7mmol) in dry ACN (5mL) overnight. The reaction mixture was filtered and evaporated under reduced pressure and purified by silica column chromatography eluting with MeOH:DCM (1:15) to afford **6H**. (yield: 54%)^{1}H NMR (400 MHz, $CDCl_3$) δ 1.15-1.26 (m, 15H, CH_3), 1.96-1.99 (m, 16H, CH_2), 2.43-2.96 (m, 26H, CH_2), 3.30-3.40 (m, 6H, CH_2), 4.04-4.21 (m, 8H, CH_2), 7.32-7.40(m, 2H, ArH), 7.54-7.56 (m, 1H, ArH), 7.75-7.78 (m, 3H, ArH), 8.03 (s, 1H, ArH), 8.03-8.31 (m, 2H, ArH), 8.40 (s, 1H, ArH); ^{13}C NMR (100 MHz, $CDCl_3$) δ 14.28, 26.10, 29.51, 32.86, 32.49, 43.91, 50.14, 52.23, 57.56, 60.99, 61.43, 64.73, 67.65, 68.51,122.27, 114.39, 114.46, 115.11, 115.34, 120.04, 125.81, 127.32, 127.97, 130.43, 139.22, 142.06, 146.10, 147.15, 155.49, 170.23, 170.87, 172.99. Calcd for $C_{54}H_{81}N_7O_8S_4$ [$(M + H)^+$] m/z 1084.51. Found: m/z 1084.67.

EuL7

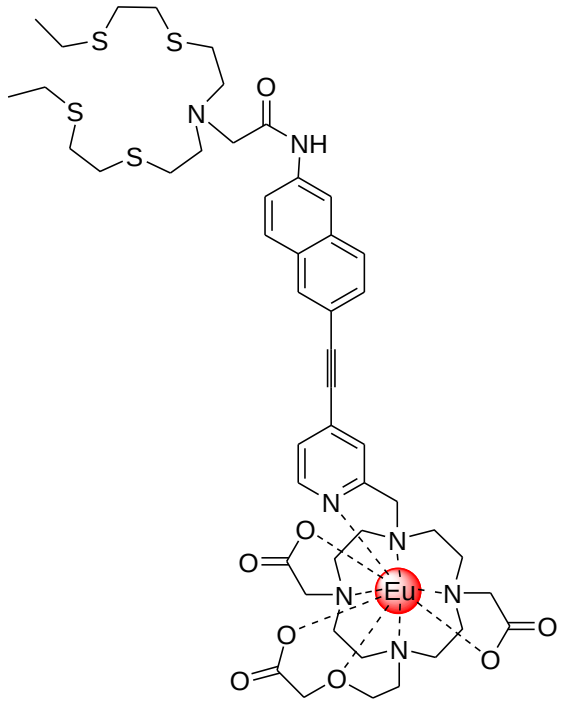

To the solution of **6J** (20mg, 0.02 mmol) in THF was added LiOH (0.01 M). The reaction was stirred at room temperature overnight. The reaction mixture was filtered and purfied by washing with DCM to obtain an oily product which was then dissolved in D.I. water. pH was adjusted to 7 and reaction was refluxed with 1 eqv. of $EuCl_3 \cdot 6H_2O$ (2 mg, 0.002 mmol) in overnight. The pH of the reaction mixture was adjusted to 6 and filtered and combined filtrates were evaporated under reduced pressure. The product was re-crystallized in DCM: MeOH: chloroform to yield **EuL6**. (yield:46%) Elemental analysis calcd (%) for $C_{48}H_{66}N_7O_8EuS_4 \cdot 5H_2O$:C,44.2.;H,5.88;N,7.54;found:C,44.11; H,5.79;N,7.20. HRMS (+):552.1018 $(M+2Na)^{2+}$ $[C_{41}H_{59}N_6O_7S_5EuNa_2]^{2+}$ requires 552.1016. The isotopic distribution matched closely with the simulated spectrum.

6I

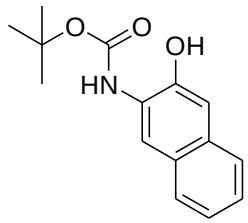

3-aminonaphthalen-2-ol (1g, 6.29mmol), Boc_2O (1.37, 6.29mmol) were refluxed in dry THF (10mL) for 18h. Upon completion of the reaction (TLC), the crude product was filter and purified by silica column chromatography eluting with MeOH:DCM (1:30) to afford **6I**. (yield: 80%)^{1}H NMR (400 MHz, $CDCl_3$) δ 1.56 (m, 9H, CH_3), 6.96-7.05 (m, 1H, ArH), 7.23(m, 1H, ArH), 7.30-7.35 (m, 2H, ArH), 7.62(d, J=8Hz, 1H, ArH), 7.68(d, J=7.6Hz, 1H, ArH), 7.95 (s, 1H, NH); ^{13}C NMR ($CDCl_3$, 100 MHz) δ 28.29, 117.07, 124.14, 125.11, 125.87, 126.55, 126.78, 127.06, 128.12, 129.22, 145.46, 156.22.

L8

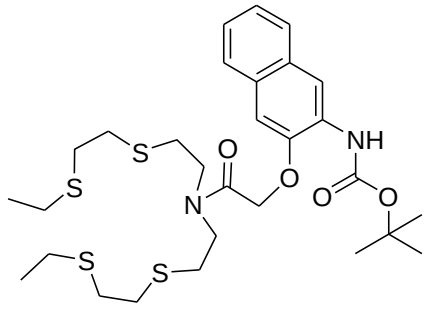

To the solution of **6I** (820mg, 2.62mmol) and triethylamine (0.36mL, 2.62mmol) was added chloroacetyl chloride (0.2mL, 2.62mmol). The reaction was stirred for 8h. The reaction mixture was filtered and combined filtrates were evaporated under reduced pressure. Without further purification, the reaction mixture was reacted with **6I** (679mg, 2.62mmol) and K_2CO_3 (362mg, 2.62mmol) in dry ACN (8mL) overnight. The reaction mixture was filtered and evaporated under reduced pressure and purified by silica column chromatography eluting with MeOH:DCM (1:50) to afford **L8**. (yield: 56%) ^{1}H NMR (400 MHz, $CDCl_3$) δ 1.20-1.25 (m, 6H, CH_3), 1.57 (s, 9H, CH_3), 2.52-2.55 (m, 4H, CH_2), 2.71-2.80 (m, 12H, CH_2), 3.57-3.59 (m, 4H, CH_2), 4.96 (s, 2H, CH_2), 7.15 (s,

1H, Ar), 7.30-7.34 (m, 2H, ArH), 7.63-7.65 (m, 1H, ArH), 7.73-7.75 (m, 2H, ArH), 8.54 (s, 1H, NH); ^{13}C NMR ($CDCl_3$, 100 MHz) δ14.72, 28.39, 31.20, 46.69, 47.69, 67.55, 80.55, 107.51, 115.11, 124.68, 124.72, 126.31, 127.32, 128.53, 129.37, 129.88, 146.47, 152.79, 167.33. Calcd for $C_{29}H_{45}N_2O_4S_4$ [$(M + H)^+$] m/z 613.23. Found: m/z 613.33.

6R

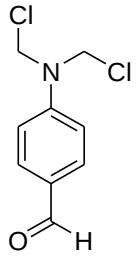

$POCl_3$ (0.35mL, 3.8mmol) in DMF (2ml) was stirred for half an hours in an ice bath and N-Phenyldiethanolamine (0.58g, 3.8mmol) in DMF (2ml) was added dropwise and stirred at 90^{o}C for 8 hours Upon completion of the reaction (TLC), the reaction mixture was neutralized by K_2CO_3 and filtered to give a yellow solid which was then recrystalizated in absolute ethanol to afford a white solid with a yield of 70%. ^{1}H NMR (400 MHz, $CDCl_3$) δ 3.61 (t, J= 6.8Hz, 4H, CH_2), 3.77 (t, J= 6.8Hz, 4H, CH_2), 6.67 (d, J= 8.8Hz, 2H, ArH), 7.70 (d, J= 8.8Hz, 2H, ArH), 9.71 (s, 1H, CHO); ^{13}C NMR ($CDCl_3$, 100 MHz) δ 40.01, 53.27, 111.28, 126.74, 132.30, 150.97, 190.18. Calcd for $C_9H_{10}NOCl_2$ [$(M + H)^+$] m/z 218.01. Found: m/z 218.33.

6S

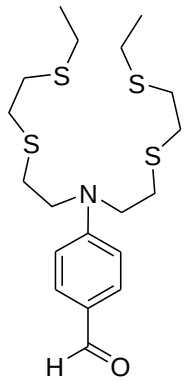

To the solution of **6A** (0.488g, 2.21mmol) and sodium ethoxide (340mg, 5mmol) in absolute ethanol, **6R** (0.1 mmol) was added. The reaction mixture was stirred at room temperature for overnight. Upon completion of the reaction (TLC), the solvent was evaporated under reduced pressure and the crude product was purified by silica column chromatography eluting with DCM:hexane (1:15) to afford **6S**. (yield: 46%) ^{1}H NMR (400 MHz, $CDCl_3$) δ 1.26 (t, J= 7.6Hz, 6H, CH_3), 2.58 (q, J= 7.2Hz, 4H, CH_2), 2.71-2.80 (m, 12H, CH_2), 3.65 (t, J= 7.2Hz, 4H, CH_2), 6.69 (d, J= 8.8Hz, 2H, ArH), 7.74 (d, J= 8.8Hz, 2H, ArH), 9.75 (s, 1H, CHO); ^{13}C NMR ($CDCl_3$, 100 MHz) δ 14.78, 2.16, 29.37, 31.86, 32.62, 51.50, 111.01, 126.01, 132.32, 151.35, 190.07. Calcd for $C_{19}H_{32}NOS_4$ $[(M + H)^+]$ m/z 418.14. Found: m/z 418.00.

6T

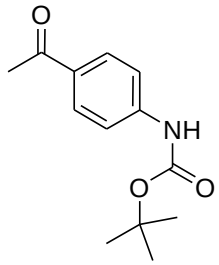

1-(4-aminophenyl)ethanone (2g, 0.015mmol) and Boc_2O (3.22g, 0.015mmol) were refluxed overnight. Upon completion of the reaction (TLC), the solvent was evaporated under reduced pressure and the crude product was purified by silica column chromatography eluting with DCM:hexane (1:15) to afford **6T**. (yield: 71%) ^{1}H NMR (400 MHz, $CDCl_3$) δ 1.36 (s, 9H, CH_3), 2.43 (s, 3H, CH_2), 7.49 (d, J= 8.8Hz, 2H, ArH),

7.78 (d, J= 8.8Hz, 2H, ArH), 8.01 (s, 1H, NH); ^{13}C NMR ($CDCl_3$, 100 MHz) δ 26.17, 28.12, 8064, 117.53, 129.70, 131.21, 143.80, 152.64.

6U

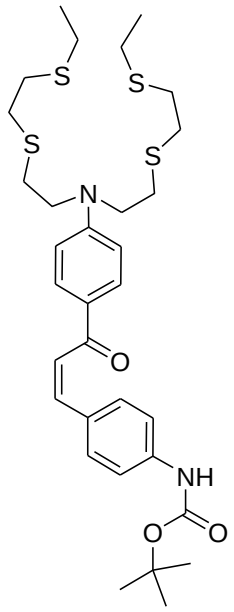

To the solution of **6S** (137mg, 0.33 mmol) and **6T** (77.6mg, 0.33 mmol) in ethanol (10ml), ethanolic potassium hydroxide solution (20 ml) was added. The reaction was stirred for 8 hrs. Upon completion of the reaction (TLC), the reaction mixture was filtered and the crude product was purified by silica column chromatography eluting with DCM:hexane (1:20) to afford **6U**. (yield: 52%) ^{1}H NMR (400 MHz, $CDCl_3$) δ 1.81 (t, J=7.2Hz, 6H, CH_3), 1.45 (s, 9H, CH_3), 2.47 (q, J= 7.2Hz, 4H, CH_2), 2.64-2.73 (d, 12H, CH_2), 3.54 (t, J= 7.2Hz, 4H, CH_2), 6.58 (d, J= 8.8Hz, 2H, ArH), 6.92 (s, 1H, NH), 7.28 (d, J=15.6Hz, 1H, CH), 7.42-7.48 (m, 4H, ArH), 7.68 (d, J=15.2Hz, 1H, CH), 7.91 (d, J=8.4, 2H, ArH); ^{13}C NMR ($CDCl_3$, 100 MHz) δ 14.81, 26.12, 28.28, 29.43, 31.84, 32.55, 51.50, 81.09, 111.64, 117.20, 117.51, 123.53, 129.8, 130.67, 133.24, 142.45, 144.62, 148.45, 152.30. Calcd for $C_{32}H_{47}N_2O_3S_4$ [$(M + H)^+$] m/z 635.25. Found: m/z 635.20.

6V

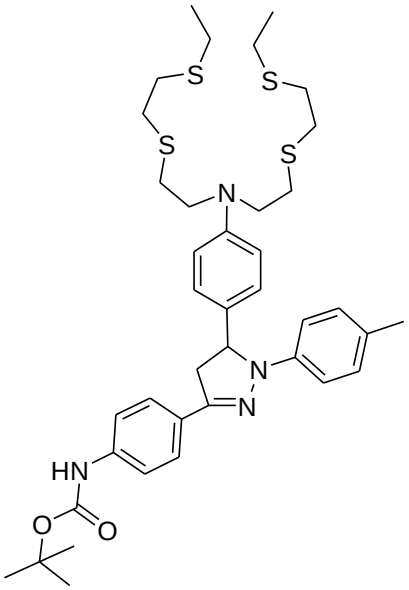

To the solution of **6U** (120mg 0.19mmol) and 1-phenylhydrazine (26mg, 0.24mmol.) in absolute ethanol, a few drops of hydrochloric acid were added. The reaction was stirred at 90^0C for 12 h. Upon completion of the reaction (TLC), the mixture was cooled down and diluted with D.I.water (10mL). The precipitated product was filtered off and washed consecutively with hydrochloric acid (1 M) and sodium hydroxide (0.03M). Then, the reaction mixture was extracted with EtOAc. The combined organic phases were washed with HCl (1 M) and dried (Mg_2SO_4) and concentrated under reduced pressure. The crude product was purified by silica column chromatography eluting with DCM:hexane (1:10) to afford **6V**. (yield: 52%) ^{1}H NMR (400 MHz, $CDCl_3$) δ 1.17 (t, J=7.2Hz, 6H, CH_3), 2.15 (s, 3H, CH_3), 2.46 (q, J= 8.0Hz, 4H, CH_2), 2.63-2.70 (m, 12H, CH_2), 2.96-2.98 (m, J= 7.2Hz, 1H, CH_2), 3.43 (t, J= 8.0Hz, 4H, CH_2), 3.51-3.61 (m, 1H, CH), 4.96-5.01 (m, 1H, CH), 6.51 (m, J= 8.4Hz, 2H, ArH), 6.60 (m, J= 8.4Hz, 2H, ArH), 6.90 (s, 4H, ArH), 7.10 (d, J=8.4Hz, 2H, ArH), 7.45 (m, 8.4H, ArH); ^{13}C NMR ($CDCl_3$, 100 MHz) δ 14.80, 15.93, 20.47, 26.09, 29.47, 31.84, 32.48, 43.89, 51.65, 64.16, 112.27, 113.32, 113.71, 114.83, 123.52, 127.10, 127.33, 127.59, 129.30, 130.78, 131.20, 143.52, 145.85, 146.87, 146.99. Calcd for $C_{39}H_{55}N_4O_2S_4$ [$(M + H)^+$] m/z 739.32. Found: m/z 739.11.

6W

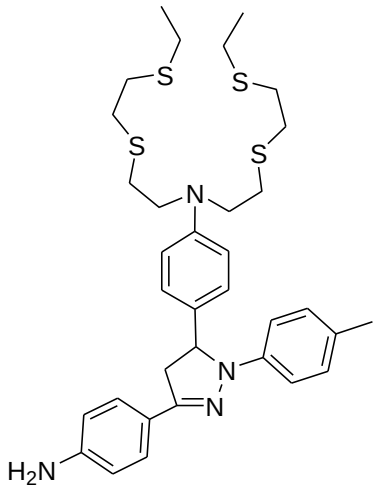

6V (148mg, 0.2mmol) was stirred with HCl (2mL) in THF (3mL). Upon completion of the reaction (TLC), the reaction mixture was extracted with D.I. water and DCM. The organic layer was dried (Mg_2SO_4) and concentrated under reduced pressure. The crude product was purified by silica column chromatography eluting with DCM:hexane (1:3) to afford **6W**. ^{1}H NMR (400 MHz, $CDCl_3$) δ 1.19 (t, J=7.2Hz, 6H, CH_3), 2.47 (s, 3H, CH_3), 2.50 (q, J= 7.6Hz, 4H, CH_2), 2.66-2.69 (m, 12H, CH_2), 3.44-3.48 (m, 6H, CH_2), 4.60 (s, br, 2H, NH_2), 5.04-5.08 (m, 1H, CH), 6.52 (d, J= 8.8Hz, 2H, ArH), 6.63-6.64 (m, 2H, ArH), 6.94 (m, J= 8.4Hz, 2H, ArH), 7.94 (d, J=6.4Hz, 1H, ArH); ^{13}C NMR ($CDCl_3$, 100 MHz) δ 14.78, 16.01, 26.13, 29.47, 31.85, 32.52, 47.96, 51.49, 62.16, 62.55, 94.04, 104.13, 106.28, 122.40, 126.75, 127.53, 145.61, 146.64, 147.25, 151.22, 156.49. Calcd for $C_{34}H_{47}N_4S_4$ [$(M + H)^+$] m/z 639.27. Found: m/z 639.27.

6X

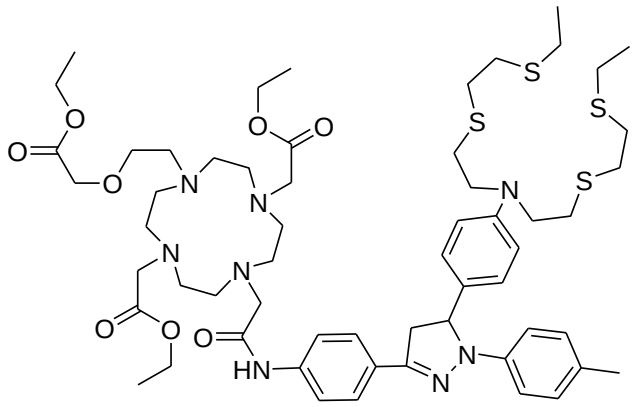

To the solution of **6W** (81mg, 0.13 mmol) and triethylamine (0.011mL, 0.13mmol) was added chloroacetyl chloride (10μL, 0.13 mmol). The reaction was stirred for 8h. The reaction mixture was filtered and combined filtrates were evaporated under reduced pressure. Without further purification, the reaction mixture was reacted with **DO3A-ME** (56mg, 0.13mmol) and K_2CO_3 (17.9mg, 0.13mmol) in dry ACN (10mL) overnight. The reaction mixture was filtered and evaporated under reduced pressure and purified by silica column chromatography eluting with MeOH:DCM (1:20) to afford **6X**. (yield: 39%) ^{1}H NMR (400 MHz, $CDCl_3$) δ 1.16-1.21 (m, 15H, CH_3), 2.45-3.67(m, 48H, CH_2), 4.00-4.16 (m, 9H, CH_2), 4.9-5.01 (m, 1H, CH), 6.54 (d, J= 8.8Hz, 2H, ArH), 6.79 (t, J= 8.8Hz, 2H, ArH), 6.91-6.94 (m, 2H, CH), 7.09 (d, J= 8.8Hz, 2H, ArH), 7.49 (d, J= 8.8Hz, 2H, ArH), 7.87 (m, J= 8.8Hz, 2H, ArH); ^{13}C NMR ($CDCl_3$, 100 MHz) δ 14.11, 14.14, 14.78, 26.10, 29.51, 32.86, 32.49, 43.91, 49.78, 50.04, 51.60, 52.14, 55.52, 57.56, 60.99, 61.43, 64.73, 67.65, 68.51, 112.27, 114.39, 114.46, 115.11, 115.34, 120.04, 125.81, 127.32, 127.97, 130.43, 139.22, 142.06, 146.10, 147.15, 170.23, 172.99. Calcd for $C_{58}H_{89}N_8O_8S_4$ [$(M + H)^+$] m/z 1153.53. Found: m/z 1153.49.

EuL9

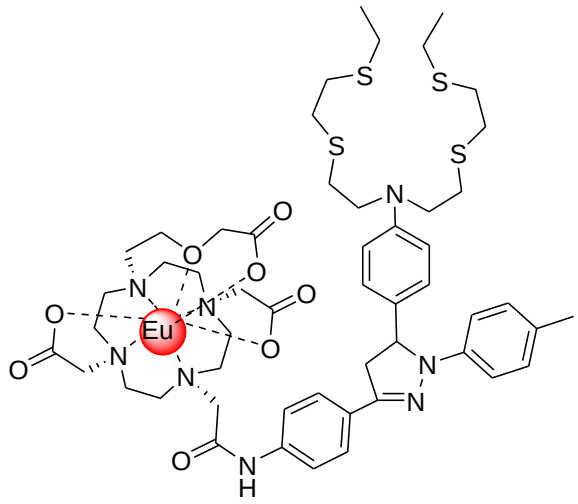

To the solution of **6X** (30mg, 0.03 mmol) in THF was added LiOH (0.01 M). The reaction was stirred at room temperature overnight. The reaction mixture was filtered and purfied by washing with DCM to obtain an oily product which was then dissolved in D.I. water. The pH was adjusted to 6 and the reaction was refluxed with 1 eqv. of $EuCl_3 \cdot 6H_2O$ (3mg, 0.003 mmol) in overnight. The pH of the reaction mixture was adjusted to 6 and filtered and combined filtrates were evaporated under reduced pressure. The product was re-crystallized in DCM: MeOH to yield **EuL9**. (yield:69%) Elemental analysis calcd (%) for $C_{52}H_{73}N_8O_8S_4Eu \cdot 4H_2O$:C,44.2;H,5.88;N,7.54;found:C,44.65;H,5.99;N,7.39. HRMS (+):631.1678 $(M+2Na)^{2+}$ $[C_{52}H_{73}EuN_8O_8S_4Na_2]^{2+}$ requires 631.1709. The isotopic distribution matched closely with the simulated spectrum.

7.15 General conclusion

The development of new class of responsive Eu(III) based probes for detection of Cu(II) ion, H_2S, cysteine, Cu(I) ion, Zn(II) ion is reported. Generally, they are thermodynamically stable under physiological condition and water soluble in aqueous solution for detection. They demonstrated good selectivity for the desired analytes. For instance, **EuL1Cu** showed high selectivity response to H_2S. Therefore, it is believe that the works in this thesis are beneficial to the development of future Eu(III) based probe for selective monitoring of desired analytes, such as Cu(II) ion or H_2S or cysteine or Cu(I) ion or Zn(II) ion for potential disease evaluation.

7.16 Future work

H_2S sensor

The work has clearly demonstrated the high selective and reversible sensing of complexes **EuL1** towards Cu(II) ion and **EuL1Cu** towards H_2S. Future work will be study of the sensing of Cu(II) or H_2S in physiological conditions to have further exploration of their biology. For instance, visualization of how H_2S modulates physiological condtions and therefore has further understands of their biological role. To study their toxicity is important to assess whether they are applicable to do biological study. For instance, MTT assay will be performed to assess the toxicity.

Cys sensor

The behavior of the complexes **EuL2** showed promising selectivity towards Cys. Although **EuL2** is turn-off sensor and has not good contrast than turn-on sensor, it is worth doing some cellular imaging of cellular Cys in future due to its high selectivity and stability of complex. To study their toxicity is crucial to realize whether they are applicable to do biological study. For instance, MTT assay will be done to assess the toxicity.

The long term is related to the structural modification of chromophore of **EuL2** in

order to obtain the turn-on probe for detection of Cys and they still use the same acrylate functional group as selective reaction site for Cys. Further titration, photophysical study will be followed.

Zinc sensor

Although zinc sensor developed in this thesis generally showed good selectivity towards Zn(II) ion and had higher binding constants towards Zn(II) ion, their responses are found to be influenced by other cations in some cases such as Cd(II) ion. Therefore, the structural modification of receptor will be done in future. For instance, change of receptor into other common selective Zn(II) receptor such as quinoline. Moreover, they have one water molecule in inner coordination environment and lead to non-radiative process, so the metal chelator will be changed to **DO3A-ME** which provides nine coordination environment for Eu(III) ion and will not have inner coordination water molecule.

7.17 References

[1] Y. Haas and G. Stein, *J. Phys. Chem. A.*, 1972, **76**, 1093-1104.

[2] V. Alexander, *Chem. Rev*., 1995, **95**, 273-342.

[3] J. W. Eastman, *Photochem. Photobiol*., 1967, **6**, 55-72.

[4] F. Hou, J. Cheng, P. Xi, F. Chen, L. Huang, G. Xie, Y. Shi, H. Liu, D. Bai and Z. Zeng, *Dalton Trans*., 2012, **41**, 5799-5804.

[5] B. H. Shankar, D. T. Jayaram, and D. Ramaiah, *Chem. Asian J*., 2014, **9**, 1636–1642.